

ISSN 2312-4334

MINISTRY OF EDUCATION AND SCIENCE OF UKRAINE

# **East European Journal of Physics**

No 1. 2023

2023

# East European Journal of Physics

EEJP is an international peer-reviewed journal devoted to experimental and theoretical research on the nuclear physics, cosmic rays and particles, high-energy physics, solid state physics, plasma physics, physics of charged particle beams, plasma electronics, radiation materials science, physics of thin films, condensed matter physics, functional materials and coatings, medical physics and physical technologies in an interdisciplinary context.

Published quarterly in hard copy and online by V.N. Karazin Kharkiv National University Publishing  
ISSN 2312-4334 (Print), ISSN 2312-4539 (Online)

The editorial policy is to maintain the quality of published papers at the highest level by strict peer review.

Approved for publication by the Academic Council of the V.N. Karazin Kharkiv National University (27.02.2023, Protocol no. 4).

EEJP registered by the order of Ministry of Education and Science of Ukraine No. 1643 of 28.12.2019, and included in the list of scientific professional editions of Ukraine (category "A", specialty: 104, 105), in which can be published results of dissertations for obtaining Ph.D. and Dr. Sci. degrees in physical and mathematical sciences.

The Journal is a part of the Web of Science Core Collection (ESCI) scientometric platform and indexed by SCOPUS.

## Editor-in-Chief

☛ Azarenkov M.O., *Academician of NAS of Ukraine, Professor, NSC Kharkiv Institute of Physics and Technology, Kharkiv, Ukraine*

## Deputy editor

☛ Girka I.O., *Corresponding Member of NAS of Ukraine, Professor, V.N. Karazin Kharkiv National University, Kharkiv, Ukraine*

## Editorial Board

☛ Adamenko I.M., *Professor, V.N. Karazin Kharkiv National University, Ukraine*

☛ Antonov A.N., *D.Sc., Professor, Institute of Nuclear Research and Nuclear Energy, Sofia, Bulgaria*

☛ Afanasev A.V., *D.Sc., George Washington University, Washington, District of Columbia, United States*

☛ Barannik E.O., *D.Sc., Professor, V.N. Karazin Kharkiv National University, Ukraine*

☛ Beresnev V.M., *D.Sc., Professor, V.N. Karazin Kharkiv National University, Ukraine*

☛ Berezhnoy Yu.A., *D.Sc., Professor, V.N. Karazin Kharkiv National University, Ukraine*

☛ Bizyukov A.A., *D.Sc., Professor, V.N. Karazin Kharkiv National University, Ukraine*

☛ Bragina L.L., *D.Sc., Professor, STU "Kharkiv Polytechnic Institute", Ukraine*

☛ Broda B., *D.Sc., University of Lodz, Poland*

☛ Dragovich B.G., *D.Sc., University of Belgrade, Serbia*

☛ Duplij S.A., *D.Sc., Center für Information Technology (ZIV), Westfälische Wilhelms-Universität Münster, Münster, Germany*

☛ Garkusha I.E., *Corresponding Member of NAS of Ukraine, NSC Kharkiv Institute of Physics and Technology, Ukraine*

☛ Grekov D.L., *D.Sc., NSC Kharkiv Institute of Physics and Technology, Ukraine*

☛ Karnaukhov I.M., *Academician of NAS of Ukraine, NSC Kharkiv Institute of Physics and Technology, Ukraine*

☛ Korchin A.Yu., *Corresponding Member of NAS of Ukraine, NSC Kharkiv Institute of Physics and Technology, Ukraine*

☛ Kryshchal O.P., *Dr. hab., AGH University of Science and Technology in Kraków, Poland*

☛ Lazurik V.T., *D.Sc., Professor, V.N. Karazin Kharkiv National University, Ukraine*

☛ Lytovchenko S.V., *D.Sc., Professor, V.N. Karazin Kharkiv National University, Ukraine*

☛ Maliyov I.L., *Ph.D., Postdoctoral Researcher at Caltech, Pasadena, California, United States*

☛ Mel'nik V.N., *D.Sc., Institute of Radio Astronomy, Kharkiv, Ukraine*

☛ Merenkov N.P., *D.Sc., NSC Kharkiv Institute of Physics and Technology, Ukraine*

☛ Neklyudov I.M., *Academician of NAS of Ukraine, NSC Kharkiv Institute of Physics and Technology, Ukraine*

☛ Noterdaeme J.-M., *D.Sc., Max Planck Institute for Plasma Physics, Garching, Germany*

☛ Nurmagambetov A.Yu., *D.Sc., Professor, NSC Kharkiv Institute of Physics and Technology, Ukraine*

☛ Ostrikov K.N., *D.Sc., Plasma Nanoscience Centre Australia, Clayton, Australia*

☛ Pershin Yu.V., *D.Sc., University of South Carolina, Columbia, USA*

☛ Pilipenko M.M., *D.Sc. in Technical Sciences, NSC Kharkiv Institute of Physics and Technology, Ukraine*

☛ Radinschi I., *D.Sc., Gheorghe Asachi Technical University, Iasi, Romania*

☛ Slipko V.A., *Institute of Physics, Opole University, Opole, Poland*

☛ Slyusarenko Yu.V., *Academician of NAS of Ukraine, NSC Kharkiv Institute of Physics and Technology, Ukraine*

☛ Smolyakov A.I., *University of Saskatchewan, Saskatoon, Canada*

☛ Shul'ga M.F., *Academician of NAS of Ukraine, NSC Kharkiv Institute of Physics and Technology, Ukraine*

☛ Sorokin D.P., *D.Sc., Istituto Nazionale di Fisica Nucleare, Italy*

☛ Styervoyedov A.M., *D.Sc., Max Planck Institute of Microstructure Physics, Halle, Germany*

☛ Tkachenko V.I., *D.Sc., NSC Kharkiv Institute of Physics and Technology, Ukraine*

## Executive Secretary

☛ Hirnyk S.A., *Ph.D., V.N. Karazin Kharkiv National University, Kharkiv, Ukraine*

## Editorial office

Department of Physics and Technologies, V.N. Karazin Kharkiv National University

Kurchatov av., 31, office 402, Kharkiv, 61108, Ukraine

Tel: +38-057-335-18-33,

E-mail: [eejp@karazin.ua](mailto:eejp@karazin.ua),

Web-pages: <http://periodicals.karazin.ua/eejp> (Open Journal System)

Certificate of State registration No.20644-10464P, 21.02.2014

# Східно-європейський фізичний журнал

Східно-європейський фізичний журнал – міжнародний рецензований журнал, присвячений експериментальним і теоретичним дослідженням ядерної фізики, космічних променів і частинок, фізики високих енергій, фізики твердого тіла, фізики плазми, фізики пучків заряджених частинок, плазмової електроніки, радіаційного матеріалознавства, фізики тонких плівок, фізики конденсованої речовини, функціональних матеріалів та покриттів, медичної фізики та фізичних технологій у міждисциплінарному контексті.

Видається щоквартально в друкованому вигляді та в Інтернеті видавництвом Харківського національного університету імені В.Н. Каразіна

ISSN 2312-4334 (Друкована версія), ISSN 2312-4539 (Онлайн)

Редакційна політика полягає у підтримуванні якості опублікованих статей на найвищому рівні шляхом суворої експертної оцінки. Схвалено до друку Вченою радою Харківський національний університет імені В.Н. Каразіна (27.02.2023 р., Протокол № 4).

Східно-європейський фізичний журнал зареєстровано наказом Міністерства освіти і науки України № 1643 від 28.12.2019 та включено до Переліку наукових фахових видань України (категорія «А», спеціальність: 104, 105), у яких може публікуватися результати дисертацій на здобуття ступенів кандидата та доктора фізико-математичних наук.

Журнал є частиною наукометричної платформи Web of Science Core Collection (ESCI) і індексується SCOPUS.

## Головний редактор

● Азаренков Н.А., академік НАН України, професор, Харківський національний університет імені В.Н. Каразіна, Харків, Україна

## Заступник редактора

● Гірка І.О., член-кореспондент НАН України, професор, Харківський національний університет імені В.Н. Каразіна, Харків, Україна

## Editorial Board

● Адаменко І.Н., професор, Харківський національний університет імені В.Н. Каразіна, Україна

● Антонов А.Н., д.ф.-м.н., професор, Інститут ядерних досліджень та ядерної енергії, Софія, Болгарія

● Афанасьєв А.В., д.ф.-м.н., Університет Джорджа Вашингтона, Вашингтон, округ Колумбія, США

● Баранник С.А., д.ф.-м.н., професор, Харківський національний університет імені В.Н. Каразіна, Україна

● Береснев В.М., д.ф.-м.н., професор, Харківський національний університет імені В.Н. Каразіна, Україна

● Бережной Ю.А., д.ф.-м.н., професор, Харківський національний університет імені В.Н. Каразіна, Україна

● Бізюков А.А., д.ф.-м.н., професор, Харківський національний університет імені В.Н. Каразіна, Україна

● Брагіна Л.Л., д.ф.-м.н., професор, ДТУ «Харківський політехнічний інститут», Україна

● Брода Б., д.ф.-м.н., Лодзинський університет, Польща

● Драгович Б.Г., д.ф.-м.н., Белградський університет, Сербія

● Дуплій С.А., д.ф.-м.н., Центр інформаційних технологій (ZIV), Університет Мюнстера, Мюнстер, Німеччина

● Гаркуша І.Є., член-кореспондент НАН України, ННЦ Харківський фізико-технічний інститут, Україна

● Греков Д.Л., д.ф.-м.н., ННЦ Харківський фізико-технічний інститут, Україна

● Карнаухов І.М., академік НАН України, ННЦ Харківський фізико-технічний інститут, Україна

● Корчин А.Ю., д.ф.-м.н., ННЦ Харківський фізико-технічний інститут, Україна

● Кришталь О.П., доктор habilit., Науково-технічний університет АГН у Кракові, Польща

● Лазурка В.Т., д.ф.-м.н., професор, Харківський національний університет імені В.Н. Каразіна, Україна

● Литовченко С.В., д.т.н., наук, професор, Харківський національний університет імені В.Н. Каразіна, Україна

● Малійов І.Л., PhD, постдокторант, науковий співробітник Каліфорнійського технологічного інституту, Пасадена, США

● Мельник В.Н., д.ф.-м.н., Інститут радіоастрономії, Харків, Україна

● Меренков Н.П., д.ф.-м.н., ННЦ Харківський фізико-технічний інститут, Україна

● Неклюдов І.М., академік НАН України, ННЦ Харківський фізико-технічний інститут, Україна

● Нотердам Ж.-М., доктор наук, Інститут фізики плазми Макса Планка, Гархінг, Німеччина

● Нурмагамбетов А.Ю., д.ф.-м.н., професор, ННЦ Харківський фізико-технічний інститут, Україна

● Остріков К.Н., д.ф.-м.н., Центр нанонауки плазми, Австралія, Клейтон, Австралія

● Першин Ю.В., д.ф.-м.н., Університет Південної Кароліни, Колумбія, США

● Сліпко В.А., Інститут фізики, Опольський університет, Ополь, Польща

● Сорокін Д.П., д.ф.-м.н., Національний інститут ядерної фізики, Італія

● Стервоєдов А.М., д.ф.-м.н., Інститут фізики мікроструктури Макса Планка, Галле, Німеччина

● Пилипенко М.М., д.т.н., ННЦ Харківський фізико-технічний інститут, Україна

● Радінчі І., д.ф.-м.н., Технічний університет Георга Асачі, Ясси, Румунія

● Слюсаренко Ю.В., академік НАН України, ННЦ Харківський фізико-технічний інститут, Україна

● Смоляков А.І., Саскачеванський університет, Саскатун, Канада

● Шульга Н.Ф., академік НАН України, ННЦ Харківський фізико-технічний інститут, Україна

● Ткаченко В.І., д.ф.-м.н., ННЦ Харківський фізико-технічний інститут, Україна

## Відповідальний секретар

● Гірник С.А., к.ф.-м.н., Харківський національний університет імені В.Н. Каразіна, Харків, Україна

## Редакція

Науково-навчальний інститут «ФТФ», Харківський національний університет імені В.Н. Каразіна

пр. Курчатова, 31, офіс 402, Харків, 61108, Україна

Тел: +38-057-335-18-33,

Електронна пошта: eejr@karazin.ua,

Веб-сторінка: <http://periodicals.karazin.ua/eejr> (система журналів з відкритим доступом)

Свідоцтво про державну реєстрацію №20644-10464П від 21.02.2014р.

ORIGINAL ARTICLES

- MHD Flow and Heat Transfer of a Ternary Hybrid Ferrofluid Over a Stretching/Shrinking Porous Sheet with the Effects of Brownian Diffusion and Thermophoresis** 7  
Michael I. Kopp, Volodymyr V. Yanovsky, Thippeswamy Anusha, Ulavathi S. Mahabaleshwar  
*МГД течія і теплопередача потрійної гібридної ферорідини над пористим листом, що розтягується/стискається, з ефектами броунівської дифузії та термофорезу*  
Михайло Й. Копп, Володимир В. Яновський, Тіпсвами Ануша, Улаваті С. Махабалешвар
- Structural Variations of Dust Acoustic Solitary Waves (DASWs) Propagating in an Inhomogeneous Plasma** 19  
Hirak Jyoti Dehingia, P.N. Deka  
*Структурні варіації пилових акустичних солітонних хвиль (ПАСХ), які поширюються в неоднорідній плазмі*  
Хірак Джіоті Дехінгія, П.Н. Дека
- The Influence of Deformation Phase-Space on Spectra of Heavy Quarkonia in Improved Energy Potential at Finite Temperature Model of Schrodinger Equation Via the Generalized Bopp's Shift Method and Standard Perturbation Theory** 28  
Abdelmadjid Maireche  
*Вплив деформації фазового простору на спектри важкого кварконію в покращеному енергетичному потенціалі за скінченної температурної моделі рівняння Шредінгера через метод узагальненого зсуву Боппа та стандартну теорію збурень*  
Абдельмаджид Маїреш
- Bianchi Type V Universe with Time Varying Cosmological Constant and Quadratic Equation of State in  $f(R, T)$  Theory of Gravity** 44  
Chandra Rekha Mahanta, Shayanika Deka, Manash Pratim Das  
*Всесвіт Б'янчі типу V зі змінною в часі космологічною сталою та квадратичним рівнянням стану в теорії гравітації  $f(R, T)$*   
Чандра Рекха Маханта, Шаяніка Дека, Манаши Пратім Дас
- Theoretical Investigation of Meson Spectrum Using Exact Quantization Rule Technique** 53  
Etido P. Inyang, Fina O. Faithpraise, Joseph Amajama, Eddy S. William, Effiong O. Obisung, Joseph E. Ntibi  
*Теоретичне дослідження спектру мезонів за методикою правила точного квантування*  
Етідо П. Іньянг, Фіна О. Фейтпрайз, Джозеф Амаджама, Едді С. Вільям, Еффіонг О. Обісунг, Джозеф Е. Нтібі
- The Fractional Schrödinger Equation with the Generalized Woods-Saxon Potential** 63  
Mohamed Abu-Shady, Etido P. Inyang  
*Дробове рівняння Шредінгера з узагальненим потенціалом Вудса-Саксона*  
Мохамед Абу-Шаді, Етідо П. Іньянг
- Nuclear Energy Levels in  $^{44}\text{Ca}$  using FPD6pn Interaction** 69  
Maryam K. Hassan, Firas Z. Majeed  
*Рівні ядерної енергії в  $^{44}\text{Ca}$  за використання FPD6PN взаємодії*  
Мар'ям К. Хассан, Фірас З. Маджид
- Theoretical Study of Proton Halo Structure and Elastic Electron Scattering Form Factor For  $^{23}\text{Al}$  and  $^{27}\text{P}$  Nuclei by Using Full Correlation Functions (Tensor Force and Short Range)** 75  
Abeer A.M. Hussein, Ghaith N. Flaiyh  
*Теоретичне дослідження структури протонного гало та форм-фактора пружного розсіяння електронів для ядер  $^{23}\text{Al}$  та  $^{27}\text{P}$  за використання повних кореляційних функцій (тензорна сила і короткодія)*  
Абір А.М. Хусейн, Гейт Н. Флей
- Theoretical Study of Matter Density Distributions, and Elastic Electron Scattering Form Factors of Exotic Nuclei ( $^{26}\text{F}$  and  $^9\text{C}$ )** 82  
Abeer A.M. Hussein, Ghaith N. Flaiyh  
*Теоретичне дослідження розподілу густини матерії та форм-факторів пружного розсіювання електронів екзотичних ядер ( $^{26}\text{F}$  та  $^9\text{C}$ )*  
Абір А.М. Хусейн, Гейт Н. Флей
- FP Shell Effective Interactions and Nuclear Shell Structure of  $^{44}\text{Sc}$**  89  
Maryam K. Hassan, Firas Z. Majeed  
*Ефективні взаємодії оболонки FP та структура ядерної оболонки  $^{44}\text{Sc}$*   
Мар'ям К. Хассан, Фірас З. Маджид
- Vitrification of a Simulator of Vat Residues from Liquid Radioactive Waste** 94  
Sergii Sayenko, Volodymyr Shkuropatenko, Yevhenii Svitlychnyi, Anna Zykova, Svitlana Karsim, Dmytro Kutnii, Volodymyr Morgunov  
*Осклування імітатора кубових залишків рідких радіоактивних відходів*  
Сергій Ю. Сасенко, Володимир А. Шкурпатенко, Євгеній О. Світличний, Ганна В. Зикова, Світлана О. Карсім, Дмитро В. Кутній, Володимир В. Моргунов
- Investigation of the Impact of Glass Waste in Reactive Powder Concrete on Attenuation Properties for Bremsstrahlung Ray** 102  
Wasan Z. Majeed, Rawaa K. Aboud, Nesreen B. Naji, Shatha D. Mohammed  
*Дослідження впливу скляних відходів у реактивному порошковому бетоні на властивості ослаблення гальмівного випромінювання*  
Васан З. Маджид, Раваа К. Абуд, Несрін Б. Наджі, Шата Д. Мохаммед

- The Electronic and Thermodynamic Properties of Ternary Rare Earth Metal Alloys** 109  
Aman Kumar, Anuj Kumar, Kamal Kumar, Rishi Pal Singh, Ritu Singh, Rajesh Kumar  
*Електронні та термодинамічні властивості трійних рідкісноземельних сплавів*  
Аман Кумар, Анудж Кумар, Камал Кумар, Ріші Пал Сінгх, Ріту Сінгх, Раджеш Кумар
- A Qualitative Theoretical Study of Inorganic HTM-Free RbGeI<sub>3</sub> Based Perovskite Solar Cells Using SCAPS-1D as a Pathway Towards 3.601% Efficiency** 118  
Mary T. Ekwu, Eli Danladi, Nicholas N. Tasiе, Idoko S. Haruna, Osaretin E. Okoro, Philibus M. Gyuk, Olayinka M. Jimoh, Rita C. Obasi  
*Якісне теоретичне дослідження неорганічних сонячних елементів на основі RbGeI<sub>3</sub> перовскіту без НТМ, з використанням SCAPS-1D як шляху до 3,601% ефективності*  
Мері Т. Екву, Елі Данладі, Ніколас Н. Тасі, Ідоко С. Харуна, Осаретін Е. Окоро, Філібус М. Гюк, Олайнка М. Джімох, Ріта К. Обасі
- Effect of Competing Ions on Multisorption (Cs<sup>+</sup>, Sr<sup>2+</sup>) by Composite Sorbents Based on Natural and Synthetic Zeolites** 125  
Oleksii Yu. Lonin, Volodymyr V. Levenets, Oleksandr P. Omelnyk, Andriy O. Shchur  
*Вплив конкуруючих іонів на мультисорбцію (Cs<sup>+</sup>, Sr<sup>2+</sup>) композиційними сорбентами на основі природного та синтетичних цеолітів*  
Олексій Ю. Лонін, Володимир В. Левенець, Олександр П. Омельник, Андрій О. Щур
- Monitoring of Radiation Defects Recovery in MgAl<sub>2</sub>O<sub>4</sub> During Annealing by Optical Spectroscopy** 130  
Yurii H. Kazarinov, Ivan G. Megela, Oksana M. Pop  
*Моніторинг відновлення радіаційних дефектів в MgAl<sub>2</sub>O<sub>4</sub> при відпалі методом оптичної спектроскопії*  
Юрій Г. Казарінов, Іван Г. Мегела, Оксана М. Поп
- Insinuation of Arrhenius Energy and Solar Radiation on Electrical Conducting Williamson Nanofluids Flow with Swimming Microorganism: Completion of Buongiorno's Model** 135  
Muhammad Jawad  
*Вплив енергії Арреніуса та сонячного випромінювання на електропровідність нанорідини Вільямсона з плаваючим мікроорганізмом: завершення моделі Буонджорно*  
Мухаммад Джавад
- Structural, Electrical and Optical Studies of Ni<sub>x</sub>Cd<sub>1-x</sub>S (x = 0.8, 0.6, 0.4 and 0.2) Nanoparticle System** 146  
Moly M. Rose, R. Sheela Christy, T. Asenath Benitta, J. Thampi Thanka Kumaran  
*Структурні, електричні та оптичні дослідження системи наночастинок Ni<sub>x</sub>Cd<sub>1-x</sub>S (x = 0,8, 0,6, 0,4 і 0,2)*  
Молі М. Роуз, Р. Шіла Крісті, Т. Асенат Бенітта, Дж. Тампі Танка Кумаран
- Synthesis of SnS/SnO Nanostructure Material for Photovoltaic Application** 154  
Egwunyenga N. Josephine, Okunzuwa S. Ikponmwosa, Imosobomeh L. Ikhioya  
*Синтез наноструктурного матеріалу SnS/SnO для фотоелектричного застосування*  
Егвуньєнга Н. Джозефін, Окунзува С. Ікпонмоса, Імособоме Л. Іхіоя
- The Green Synthesis of Copper Oxide Nanoparticles Using the Moringa Oleifera Plant and Its Subsequent Characterization for Use in Energy Storage Applications** 162  
Imosobomeh L. Ikhioya, Edwin U. Onoh, Agnes C. Nkele, Bonaventure C. Abor, B.C.N. Obitte, M. Maaza, Fabian I. Ezema  
*Зелений синтез наночастинок оксиду міді з використанням рослини moringa oleifera та його подальша характеристика для використання у накопичувачах енергії*  
Імособоме Л. Іхіоя, Едвін У. Оно, Агнес К. Нкеле, Бонавентура К. Абор, В.С.Н. Обітте, М. Мааза, Фабіан І. Езема
- Preparation and Properties of ZrO<sub>2</sub>/SiC-H<sub>2</sub>O Nanofluids to Use for Energy Storage Application** 173  
Ahmed Hashim, Farhan Lafta Rashid, Noor Al-Huda Al-Aaraji, Bahaa H. Rabee  
*Отримання та властивості нанорідин ZrO<sub>2</sub>/SiC-H<sub>2</sub>O для використання у накопичувачах енергії*  
Ахмед Хашім, Фархан Лафта Рашид, Нур Аль-Худа Аль-Аараджі, Бахаа Х. Рабі
- Nanofluids of PEG/MGO/SiC-H<sub>2</sub>O as Excellent Heat Transfer Medium: Synthesis, Properties and Application** 177  
Farhan Lafta Rashid, Ahmed Hashim, Noor Al-Huda Al-Aaraji, Aseel Hadi  
*Нанорідини PEG/MgO/SiC-H<sub>2</sub>O як чудове теплопередаюче середовище: синтез, властивості та застосування*  
Фархан Лафта Рашид, Ахмед Хашім, Нур Аль-Худа Аль-Аараджі, Асіль Хаді
- Exploring the Optical and Electrical Characteristics of MgO/SiC-H<sub>2</sub>O Nanofluids for Thermal Energy Storage** 181  
Farhan Lafta Rashid, Ahmed Hashim, M.H. Abbas, Aseel Hadi  
*Дослідження оптичних та електричних характеристик нанорідини MgO/SiC-H<sub>2</sub>O для зберігання теплової енергії*  
Фархан Лафта Рашид, Ахмед Хашім, М.Х. Аббас, Асіль Хаді
- Preparation of Nanofluids from Inorganic Nanostructures Doped PEG: Characteristics and Energy Storage Applications** 185  
Ahmed Hashim, Farhan Lafta Rashid, M.H. Abbas, Bahaa H. Rabee  
*Приготування нанорідин з неорганічних наноструктур легованих ПЕГ: характеристики та застосування для зберігання енергії*  
Ахмед Хашім, Фархан Лафта Рашид, М.Х. Аббас, Бахаа Х. Рабі
- Influence of Deposition Voltage on Strontium Sulphide Doped Silver for Optoelectronic Application** 189  
Shaka O. Samuel, M. Lagbegha-ebi Frank, E.P. Ogherohwo, Arthur Ekpekpо, J.T. Zhimwang, Imosobomeh L. Ikhioya  
*Вплив напруги осадження на легований сріблом сульфід стронцію для оптоелектронного застосування*  
Шака О. Самуель, М. Лагбегха-ебі Франк, Е.П. Огерохво, Артур Екпекпо, Дж.Т. Джимванг, Імособоме Л. Іхіоя

- Computational Investigation of IR and UV-Vis Spectra of 2-isopropyl-5-methyl-1,4-benzoquinone Using DFT and HF Methods** 197  
Salah M.A. Ridha, Zahraa Talib Ghaleb, Abdulhadi Mirdan Ghaleb  
*Обчислювальне дослідження IR та UV-Vis спектрів 2-ізопропіл-5-метил-1,4-бензохінону за допомогою методів DFT та HF Салах М.А. Рідха, Захра Таліб Галєб, Абдулхаді Мірдан Галєб*
- Molecular Geometry, Homo-Lumo Analysis and Mulliken Charge Distribution of 2,6-Dichloro-4-Fluoro Phenol Using DFT and HF Method** 205  
Surbhi, Deeya Shalya, Sarvendra Kumar  
*Молекулярна геометрія, homo-lumo аналіз та розподіл заряду маллікена 2,6-діхлор-4-фторфенола за допомогою DFT та HF методів Сурбхі, Дія Шаля, Сарвендра Кумар*
- Semi-Empirical Investigation of Electronic, Vibrational and Thermodynamic Properties of Perylene Molecule (C<sub>20</sub>H<sub>12</sub>)** 210  
Abdul Hakim Sh. Mohammed, Issa Z. Hassan, Hassan A. Kadhem, Rosure Borhanalden Abdulrahman  
*Напівемпіричне дослідження електронних, коливальних та термодинамічних властивостей молекули перилєну (C<sub>20</sub>H<sub>12</sub>) Абдул Хакім Ш. Мохаммед, Ісса З. Хасан, Хасан А. Кадхем, Росуре Борханалден Абдулрахман*
- Semi-Empirical Predictions for Hardness of Rare Earth Pyrochlores; High-Permittivity Dielectrics and Thermal Barrier Coating Materials** 222  
Rekha Bhati, Dheerendra Singh Yadav, Preeti Varshney, Rajesh Chandra Gupta, Ajay Singh Verma  
*Напівемпіричні передбачення твердості рідкісноземельних пірохлорів; діелектрики з високою проникністю та матеріали для термозахисних покриттів Рекха Бхаті, Дірендра Сінх Ядав, Пріті Варшні, Раджеш Чандра Гупта, Аджай Сінх Верма*
- Structural, Electrical and Optical Studies of Zn<sub>x</sub>Cu<sub>1-x</sub>S (x = 0.8, 0.6, 0.4 and 0.2) Nanoparticles** 228  
Moly M. Rose, R. Sheela Christy, T. Asenath Benitta, J. Thampi Thanka Kumaran  
*Структурні, електричні та оптичні дослідження наночастинок Zn<sub>x</sub>Cu<sub>1-x</sub>S (x = 0,8, 0,6, 0,4 та 0,2) Молі М. Роз, Р. Шіла Крісті, Т. Асенат Бенітта, Дж. Тампі Танка Кумаран*
- Interactions of Fibrillar Proteins with Lipids: A Molecular Docking Insight** 236  
Valeriya Trusova, Uliana Tarabara, Olga Zhytniakivska, Kateryna Vus, Galyna Gorbenko  
*Взаємодія фібрилярних білків з ліпідами: дослідження методом молекулярного докінгу Валерія Трусова, Уляна Тарабара, Ольга Житняківська, Катерина Вус, Галина Горбенко*
- Evaluation of the Influence of Body Mass Index and Signal-to-Noise Ratio on the PET/CT Image Quality in Iraqi Patients with Liver Cancer** 241  
Aya B. Hade, Samar I. Essa  
*Оцінка впливу індексу маси тіла та співвідношення сигнал-шум на якість PET/CT - зображень у пацієнтів Іраку з раком печінки Ая Б. Хаде, Самар І. Есса*
- Enhancement of the TPD/AgO NPs Hybrid Photodetector by Adding PEDOT PSS** 246  
Majid J. Shahlaa, Omar Adnan  
*Покращення гібридного фотодетектора TPD/AgO NPs шляхом додавання PEDOT PSS Шахлаа Маджид Дж., Омар Аднан*
- Synthesis of Graphene via ARC Discharge and Its Characterization: A Comparative Approach** 252  
Michael O. Awoji, Audu D. Onoja, Mathias I. Echi  
*Синтез графєну дуговим розрядом та його характеристика: порівняльний підхід Міхаєл О. Аводжі, Ауду Д. Оноджа, Матіас І. Ечі*

# MHD FLOW AND HEAT TRANSFER OF A TERNARY HYBRID FERROFLUID OVER A STRETCHING/SHRINKING POROUS SHEET WITH THE EFFECTS OF BROWNIAN DIFFUSION AND THERMOPHORESIS<sup>†</sup>

Michael I. Kopp<sup>a\*</sup>, Volodymyr V. Yanovsky<sup>a,b</sup>, Thippeswamy Anusha<sup>c</sup>,  
Ulavathi S. Mahabaleshwar<sup>c</sup>

<sup>a</sup>Institute for Single Crystals, Nat. Academy of Science Ukraine, Nauky Ave. 60, Kharkiv 31001, Ukraine

<sup>b</sup>V.N. Karazin Kharkiv National University, 4, Svoboda Sq., Kharkiv, 61022, Ukraine

<sup>c</sup>Department of Mathematics, Shivangotri, Davangere University, Davangere, India 577 007

\*E-mail: michaelkopp0165@gmail.com

Received December 9, 2022; revised December 30, 2022; accepted December 31, 2022

In this paper, the magnetohydrodynamic (MHD) flow of a ternary hybrid ferrofluid over a stretching/shrinking porous sheet in the presence of radiation and mass transpiration is studied. The ternary hybrid ferrofluid is formed by suspending three types of nanoparticles for enhancing heat transfer. The nanoparticles of copper (Cu), iron oxide ( $Fe_3O_4$ ), and cobalt ferrite ( $CoFe_2O_4$ ) are suspended in water in this study, producing in the combination  $Cu - Fe_3O_4 - CoFe_2O_4 - H_2O$ . Brownian motion and thermophoresis are integrated into the ternary hybrid ferrofluid model. Similarity transformations convert the governing partial differential equations into ordinary differential equations. The boundary value problem (bvp) is used in the Maple computer software to solve transformed equations numerically. The computed results for relevant parameters such as velocity profile, temperature profile, skin friction coefficient, local Nusselt and Sherwood numbers are visually shown and explained in detail.

**Keywords:** ternary hybrid ferrofluid; stretching/shrinking; heat and mass transfer; mass transpiration; magnetic field

**PACS:** 44.10.+i, 44.30.+v, 44.05.+e

## 1. INTRODUCTION

For several decades, interest in studying the flow and heat transfer of the boundary layer on a stretching/shrinking sheet has not waned due to a wide range of technical applications such as medical, industrial, and mechanical engineering applications. Maxwell [1] was the first to try to improve the heat transfer rate of ordinary fluids by suspending micro-sized particles, but his experiment failed due to sedimentation and blocking of the flow patterns. Choi [2], Sakiadis [3]-[4], and Crane [5] initially researched nanofluids and stretching sheets. Following this, many researchers were interested in the topic and performed significant research in it. Nanofluids have a greater thermal conductivity than regular fluids, which is needed for the efficient transfer of thermal energy. According to studies, the thermal conductivity coefficient of nanofluids rises dramatically when compared to ordinary base fluids, even at extremely low nanoparticle concentrations [2]. Existing refrigerants in several industries, including energy, electronics, transportation, and manufacturing, can be replaced by nanofluids. In relation to this, researchers have been very interested in the applications of nanofluid since the discovery of this innovative idea.

Recently, a new type of nanofluid known as hybrid nanofluid has been created, which is formed by the suspension of several nanoparticles in the base fluid. MHD flow of hybrid nanofluid and heat transfer over a stretching/shrinking sheet was introduced by Aly and Pop [6]. Khan et al. [7] and Jamaludin et al. [8] examined hybrid nanofluids in different flow scenarios. Mahabaleshwar et al. [9] developed a hybrid nanofluid algebraically decaying approach. Mahabaleshwar et al. recently researched couple stress hybrid nanofluid [10], MHD flow micro polar fluid [11], and an MHD nanofluid through a penetrable and also stretching/shrinking surface, a horizontal surface with a radiated effect, and mass transpiration [12]. Heat transmission is enhanced by increasing the volume fraction of nanoparticles, according to the researchers.

Among the various hybrid nanofluids, we focus on hybrid ferrofluids. The study of ferrofluids is of great interest due to its wide application in biomedicine and technology, namely for drug delivery, real-time chemical monitoring of human brain activity, destruction of tumors, etc. Ferrofluids are colloidal liquids made of magnetic nanoparticles like cobalt ferrite  $CoFe_2O_4$ , hematite  $Fe_2O_3$ , magnetite  $Fe_3O_4$ , and many other nanometersized particles containing iron in the base fluid [13].

Chu et al. [14] investigated the thermal performance and flow properties of a hybridized nanofluid ( $MWCNT - Fe_3O_4$ -water) in a cavity. Kumar et al. [15] studied the flow characteristics of hybrid ferrofluids ( $Fe_3O_4 - CoFe_2O_4$ ) using water-ethylene glycol combination (50% -50%) as a basis fluid in thin film flow and found that hybrid ferrofluid enhances rate of heat transfer than ferrofluid. Tlili et al. [16] studied the stream and energy transport in magnetohydrodynamic dissipative ferro and hybrid ferrofluids by considering an uneven heat rise/fall and radiation

<sup>†</sup> Cite as: M.I. Kopp, V.V. Yanovsky, T. Anusha, and U.S. Mahabaleshwar, East Eur. J. Phys. 1, 7 (2023), <https://doi.org/10.26565/2312-4334-2023-1-01>  
© M.I. Kopp, V.V. Yanovsky, T. Anusha, U.S. Mahabaleshwar, 2023

effects. They found that the magnetic oxide and cobalt iron oxide suspended in  $H_2O-EG$  (ethylene glycol) (50% -50%) mixture effectively reduces the heat transfer rate under specific conditions. Anuar et al. [17] investigated MHD hybrid ferrofluid flow on exponentially stretching/shrinking surfaces with heat source/sink effects under stagnation point region. They found that hybrid ferrofluid increases the rate of heat transfer compared to ferrofluid and for a stronger heat source, heat absorption is more likely to occur in the sheet. The effects of MHD and viscous dissipation have been studied by Lund et al, [18] considering  $(Cu-Fe_3O_4-H_2O)$  hybrid nanofluid in a porous medium.

In recent years, a new class of nanofluids has emerged, consisting of three solid nanoparticles distributed in an ordinary liquid. The term ternary hybrid nanofluid is commonly used to describe these liquids [19]. Khan and Mahmood [20] presented a study of MHD ternary hybrid nanofluid flow into a stretching/shrinking cylinder with mass suction and either Joule heating. The combination of copper nanoparticles ( $Cu$ ), iron oxide ( $Fe_3O_4$ ), and silicon dioxide ( $SiO_2$ ) with polymer as the base fluid has been chosen as an example of a ternary hybrid nanofluid. They showed that the heat transfer rate could be increased. Ramesh et al. [21] studied the increase of heat transfer in ternary nanofluid flows caused by stretched convergent or divergent channels. Temperature was reduced when the solid volume-fraction of both stretched and shrunk channels increased. It has also been found that ternary nanofluids have a stronger influence than hybrid and mono-nanofluids. Animasau et al. [22] investigated the dynamics of stagnant ternary-hybrid nanofluid (i. e. water conveying spherical silver nanoparticles, cylindrical aluminum oxide nanoparticles, and platelet aluminum nanoparticles) when induced magnetic field and convective heating surface are significant. In [22], it was concluded that the increase in convective heating of the wall is a factor that can accelerate temperature dispersion in both the case of a heat source and a heat sink. It was shown that the growing effects of an inclined magnetic field can cause the distance between the shear stress turning points and the gradient of magnetic flux density to be placed near the domain's centre. Manjunatha et al. [23] presented a new theoretical ternary nanofluid model for enhancing heat transfer. The ternary hybrid nanofluid was formed by suspending the nanoparticles  $TiO_2$ ,  $Al_2O_3$ , and  $SiO_2$  in water thus forming the combination  $TiO_2-SiO_2-Al_2O_3-H_2O$ . They showed that the ternary nanofluid flowing past a stretching sheet has better thermal conductivity than the hybrid nanofluid.

In the current study, we propose a new kind of ternary hybrid ferrofluid formed by suspending metallic nanoparticles of copper ( $Cu$ ), iron oxide ( $Fe_3O_4$ ), and cobalt ferrite ( $CoFe_2O_4$ ) in water ( $H_2O$ ). Copper nanoparticles have rather high values of thermal and electrical conductivity coefficients; therefore, their use in ternary hybrid ferrofluids will enhance heat transfer, which is very important for solving some medical problems.

The purpose of the present investigation is to study the boundary layer flow and heat transfer past a stretching/shrinking sheet in a porous medium saturated by a ternary hybrid ferrofluid. The governing partial differential equations are transformed into a set of ordinary differential equations using a similarity transformation, before being solved numerically by the *bvp* method. The results obtained are presented graphically and discussed. This theoretical study will be useful to engineers conducting experiments with ternary hybrid ferrofluid.

**2. STATEMENT OF THE PROBLEM AND MATHEMATICAL MODEL**

We consider the two-dimensional steady flow and heat transfer of MHD ternary hybrid ferrofluid past a permeable stretching/shrinking sheet of a porous medium. The  $x$ -axis is chosen to run parallel to the horizontal surface, whereas the  $y$ -axis is chosen to run perpendicular to it. The surface velocity is assumed to be  $u_w(x)$ , and the mass flux velocity is  $v_0$ , with  $v_0 < 0$  for suction and  $v_0 > 0$  for fluid injection. The applied magnetic field  $B_0$  is determined along the sheet's normal. It is also assumed that the constant temperature and constant nanofluid volume fraction of the sheet's surface are  $T_w$  and  $C_w$ , respectively, whereas the ambient fluid's are  $T_\infty$  and  $C_\infty$ . This physical model is shown in Fig.1.

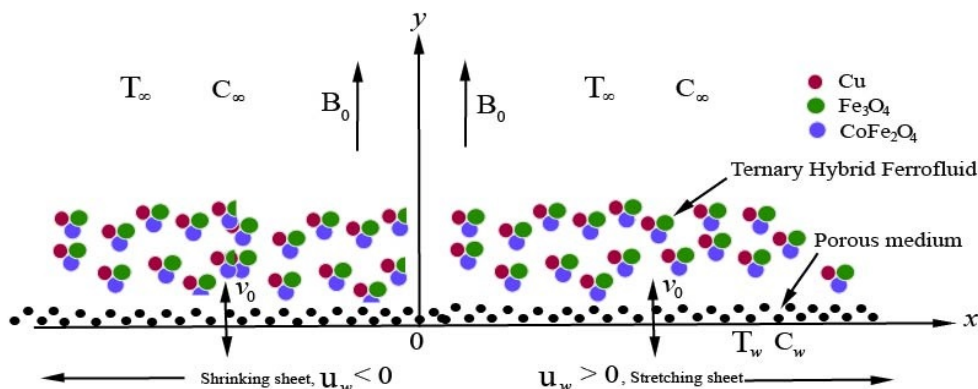


**Figure 1.** Coordinate system and physical model: stretching and shrinking sheet.

The investigating physical model's basic equations can be written as

$$\frac{\partial u}{\partial x} + \frac{\partial v}{\partial y} = 0 \tag{1}$$

$$u \frac{\partial u}{\partial x} + v \frac{\partial u}{\partial y} = \frac{\mu_{thf}}{\rho_{thf}} \frac{\partial^2 u}{\partial y^2} - \frac{\mu_{thf}}{K \rho_{thf}} u - \frac{\sigma_{thf}}{\rho_{thf}} B_0^2 u \tag{2}$$

$$u \frac{\partial T}{\partial x} + v \frac{\partial T}{\partial y} = \frac{k_{thf}}{(\rho C_p)_{thf}} \frac{\partial^2 T}{\partial y^2} + \tag{3}$$

$$+ \delta \left[ D_B \frac{\partial C}{\partial y} \frac{\partial T}{\partial y} + \frac{D_T}{T_\infty} \left( \frac{\partial T}{\partial y} \right)^2 \right] - \frac{1}{(\rho C_p)_{thf}} \frac{\partial q_r}{\partial y}$$

$$u \frac{\partial C}{\partial x} + v \frac{\partial C}{\partial y} = D_B \frac{\partial^2 C}{\partial y^2} + \frac{D_T}{T_\infty} \frac{\partial^2 T}{\partial y^2} \tag{4}$$

The following are the boundary conditions for the investigated model:

$$u = u_w = U_w(x)\lambda, v = v_0, T = T_w, C = C_w, \text{ at } y = 0 \tag{5}$$

$$u \rightarrow 0, T = T_\infty, C = C_\infty, \text{ at } y \rightarrow \infty \tag{6}$$

Here  $K$  is the permeability of a porous medium,  $T$  denotes the temperature of the ternary hybrid nanofluid,  $C$  the concentration of nanoparticles,  $D_B$  the Brownian diffusion coefficient,  $D_T$  the thermophoretic diffusion coefficient, and  $\delta = (\rho C_p)_s / (\rho C_p)_f$  the ratio of nanoparticle heat capacity to base fluid heat capacity. Further,  $\mu_{thf}$  is the dynamic viscosity of the ternary hybrid nanofluids,  $\rho_{thf}$  is the density of the ternary hybrid nanofluids, and  $k_{thf}$  is the ternary hybrid nanofluid's thermal conductivity,  $\sigma_{thf}$  the electrical conductivity,  $(\rho C_p)_{thf}$  is the ternary hybrid nanofluid's heat capacity,  $\lambda$  is the constant stretching/shrinking parameter, with  $\lambda > 0$  for a stretching sheet,  $\lambda < 0$  for a shrinking sheet, and  $\lambda = 0$  for a static sheet. Furthermore, we assume that  $U_w(x) = ax$ , where  $a$  is a positive constant.

In this study, the physical quantities of interest are the local skin friction coefficient  $C_{fx}$ , the local Nusselt number  $Nu_x$ , and the local Sherwood number  $Sh_x$ , which are defined as follows [24]:

$$C_{fx} = \frac{\mu_{thf}}{\rho_f a^2 x^2} \left( \frac{\partial u}{\partial y} \right)_{y=0},$$

$$Nu_x = - \frac{x k_{thf}}{k_f (T_w - T_\infty)} \left( \frac{\partial T}{\partial y} \right)_{y=0}, \tag{7}$$

$$Sh_x = - \frac{D_B x}{D_B (C_w - C_\infty)} \left( \frac{\partial C}{\partial y} \right)_{y=0}.$$

Let the ternary hybrid ferrofluid be composed of three sorts of nanoparticles, denoted by indices 1,2, and 3. The nanofluid is formed by first adding copper nanoparticles ( $Cu$ ) to water-based base fluid. Then a hybrid nanofluid is prepared by adding iron oxide ( $Fe_3O_4$ ) nanoparticles to the nanofluid. Finally, a ternary hybrid nanofluid is formed by adding cobalt iron oxide ( $CoFe_2O_4$ ) nanoparticles to the hybrid nanofluid. The overall volume fraction is the summation of the volume concentration of two dissimilar kinds of nanoparticles:  $\phi = \phi_1 + \phi_2 + \phi_3$ .

The thermophysical properties of the  $Cu - H_2O$  nanofluid have been studied in many works. For example, Raza et al. [25] obtained several solutions for the rheology of the  $Cu - H_2O$  nanofluid in a porous heat transfer channel. Lund et al. [18] identified the thermophysical properties of hybrid ferrofluid ( $Fe_3O_4 - CoFe_2O_4 - H_2O$ ). Takabi and

Salehi [26], Gorla et al. [27], and Anuar et al. [17] describe the thermophysical properties of hybrid ferrofluid ( $Fe_3O_4 - CoFe_2O_4 - H_2O$ ). The thermophysical properties of  $Cu - Fe_3O_4 - CoFe_2O_4 - H_2O$  ternary hybrid nanofluid are

- Density

$$\rho_{thf} = (1 - \phi_3) \{ (1 - \phi_2) [(1 - \phi_1) \rho_f + \phi_1 \rho_{s1}] + \phi_2 \rho_{s2} \} + \phi_3 \rho_{s3} \tag{8}$$

- Thermal conductivity

$$\frac{k_{thf}}{k_{hmf}} = \frac{k_{s3} + 2k_{hmf} - 2\phi_3(k_{hmf} - k_{s3})}{k_{s3} + 2k_{hmf} + \phi_3(k_{hmf} - k_{s3})}, \text{ where} \tag{9}$$

$$\frac{k_{hmf}}{k_{nf}} = \frac{k_{s2} + 2k_{nf} - 2\phi_2(k_{nf} - k_{s2})}{k_{s2} + 2k_{nf} + \phi_2(k_{nf} - k_{s2})}, \text{ and}$$

$$\frac{k_{nf}}{k_f} = \frac{k_{s1} + 2k_f - 2\phi_1(k_f - k_{s1})}{k_{s1} + 2k_f + \phi_1(k_f - k_{s1})}.$$

- Heat capacity

$$(\rho C_p)_{thf} = (1 - \phi_3) \{ (1 - \phi_2) [(1 - \phi_1) (\rho C_p)_f + \phi_1 (\rho C_p)_{s1}] + \phi_2 (\rho C_p)_{s2} \} + \phi_3 (\rho C_p)_{s3} \tag{10}$$

- Dynamic viscosity

$$\frac{\mu_{thf}}{\mu_f} = \frac{1}{(1 - \phi_1)^{2.5} (1 - \phi_2)^{2.5} (1 - \phi_3)^{2.5}} \tag{11}$$

- Electrical conductivity

$$\frac{\sigma_{thf}}{\sigma_{hf}} = \frac{(1 + 2\phi_3)\sigma_{s3} + (1 - 2\phi_3)\sigma_{hmf}}{(1 - \phi_3)\sigma_{s3} + (1 + \phi_3)\sigma_{hmf}}, \text{ where} \tag{12}$$

$$\frac{\sigma_{hmf}}{\sigma_{nf}} = \frac{(1 + 2\phi_2)\sigma_{s2} + (1 - 2\phi_2)\sigma_{nf}}{(1 - \phi_2)\sigma_{s2} + (1 + \phi_2)\sigma_{nf}}, \text{ and}$$

$$\frac{\sigma_{nf}}{\sigma_f} = \frac{(1 + 2\phi_1)\sigma_{s1} + (1 - 2\phi_1)\sigma_f}{(1 - \phi_1)\sigma_{s1} + (1 + \phi_1)\sigma_f}.$$

Here,  $\rho_f$  is the density of the base fluid,  $\sigma_f, k_f$  is the electrical and thermal conductivity of the base fluid.  $(\rho C_p)_f$  is the heat capacity of the base fluid, and  $C_p$  is the heat capacity at the constant pressure of the base fluid. The subscripts  $s1, s2$ , and  $s3$  denote the characteristics of nanoparticles  $Cu$ ,  $Fe_3O_4$ , and  $CoFe_2O_4$ , respectively. Table 1 shows the thermophysical constants for nanoparticles and base fluid.

**Table1.** Thermophysical properties of the nanoparticles and base fluid [18],[27]

	$\rho[kg \cdot m^{-3}]$	$C_p[J \cdot kg^{-1} \cdot K^{-1}]$	$k[W \cdot m^{-1} \cdot K^{-1}]$	$\sigma[S \cdot m^{-1}]$
$H_2O$	997.1	4179	0.613	0.05
$Cu$	8933	385	401	$5.96 \cdot 10^7$
$Fe_3O_4$	5180	670	9.7	$7.4 \cdot 10^5$
$CoFe_2O_4$	4907	700	3.7	$1.1 \cdot 10^7$

### 3. SIMILARITY TRANSFORMATION AND PHYSICAL QUANTITIES

The partial differential equations (1)-(4) are transformed into ordinary differential equations through similarity transformation (see, for example, [28]):

$$u = \frac{xv_f}{L^2} \frac{\partial f(\eta)}{\partial \eta}, v = -\frac{v_f}{L} f(\eta), \eta = \frac{y}{L}, \theta(\eta) = \frac{T - T_\infty}{T_w - T_\infty}, \varphi(\eta) = \frac{C - C_\infty}{C_w - C_\infty}, \tag{13}$$

where  $\nu_f$  is the kinematic viscosity of the base fluid,  $f, \theta, \varphi$  are the dimensionless functions.  $L$  is a reference length that will be found further below. Furthermore, the radiant heat flow  $q_r$  is given by using the Rosseland approximation for radiation (see [29]):

$$\frac{1}{(\rho C_p)_{hf}} \frac{\partial q_r}{\partial y} \approx -\frac{16\kappa T_\infty^3}{3(\rho C_p)_{hf} k^*} \frac{\partial T}{\partial y} \quad (14)$$

where  $\sigma^*, k^*$  is the Stefan-Boltzmann constant and the mean absorption coefficient, respectively. It is interesting to note that, according to the definitions of  $u$  and  $v$ , equation (1) is automatically satisfied. Equations (2)-(4), as well as the boundary conditions (5)-(6), are transformed into the ordinary (similarity) differential equations shown below:

$$A_1 f''' + ff'' - f'^2 - (A_2 + A_3 \cdot M) f' = 0 \quad (15)$$

$$A_4 \theta'' + N_B \varphi' \theta' + N_T \theta'^2 + f \theta' = 0 \quad (16)$$

$$\varphi'' + Le f \varphi' + \frac{N_T}{N_B} \theta'' = 0 \quad (17)$$

$$f(0) = s, f'(0) = \lambda, \theta(0) = 1, \varphi(0) = 1, \text{ at } \eta = 0 \quad (18)$$

$$f''(\eta) \rightarrow 0, \theta(\eta) \rightarrow 0, \varphi(\eta) \rightarrow 0, \text{ at } \eta \rightarrow \infty \quad (19)$$

Primes denote differentiation with regard to  $\eta$  in this context. Using the boundary conditions (18)-(19), we find expressions for  $L$  and  $v_0$

$$L = \sqrt{\frac{\nu_f}{a}}, v_0 = -\sqrt{a\nu_f} s \quad (20)$$

The following ratios are used in Equations (15)-(16):

$$A_1 = \frac{\mu_{thf} / \mu_f}{\rho_{thf} / \rho_f}, A_2 = A_1 \cdot \frac{\nu_f}{aK}, A_3 = \frac{\sigma_{thf} / \sigma_f}{\rho_{thf} / \rho_f}, \quad (21)$$

$$A_4 = \frac{1}{Pr} \cdot \frac{k_{thf} / k_f}{(\rho C_p)_{thf} / (\rho C_p)_f} + \frac{(\rho C_p)_f}{(\rho C_p)_{thf}} \cdot \frac{Nr}{Pr}.$$

Where  $M, Pr, Nr, Le, N_B$  and  $N_T$  denote the magnetic parameter, Prandtl number, radiation parameter, Lewis number, Brownian motion parameter and thermophoresis parameter, respectively, where

$$M = \frac{B_0^2 \sigma_f}{a \rho_f}, Pr = \frac{\nu_f (\rho C_p)_f}{k_f}, Nr = \frac{16 \sigma^* T_\infty^3}{3 k_f k^*}, Le = \frac{\nu_f}{D_B}, \quad (22)$$

$$N_B = \frac{\delta D_B (C_w - C_\infty)}{\nu_f}, N_T = \frac{\delta D_T (T_w - T_\infty)}{\nu_f T_\infty}.$$

Using the similarity variables (13), one can easily obtain the expressions for physical quantities (7):

$$C_{fx} \sqrt{Re_x} = \frac{\mu_{thf}}{\mu_f} f''(0), Nu_x (\sqrt{Re_x})^{-1} = -\frac{k_{thf}}{k_f} \theta'(0), \quad (23)$$

$$Sh_x (\sqrt{Re_x})^{-1} = -\varphi'(0),$$

where  $Re_x = U_w x / \nu_f$  is the local Reynolds number.

#### 4. MODIFIED SYSTEM OF EQUATIONS

The exact analytical solution to the equation for the dimensionless stream function is represented as (see, for example, [5])

$$f(\eta) = \alpha_1 + \alpha_2 \exp(-\beta\eta) \quad (24)$$

Applying boundary conditions (18) to the solution (24), we find expressions for the constants  $\alpha_1$  and  $\alpha_2$ . As a result, solution (24) takes the following form

$$f(\eta) = s + \frac{\lambda}{\beta}(1 - \exp(-\beta\eta)) \tag{25}$$

Clearly,  $\beta$  may be found by substituting the relation (25) in Eq. (15):

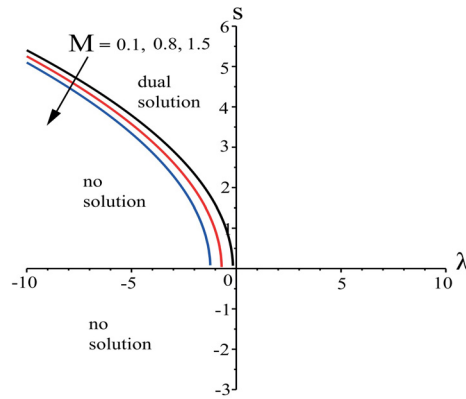


Figure 2. Regions of solutions of  $s$  as a function of  $\lambda$  for stretching/shrinking sheet when  $\phi_1 = 0.1$ ,  $\phi_2 = 0.01$  and  $\phi_3 = 0.02$ .

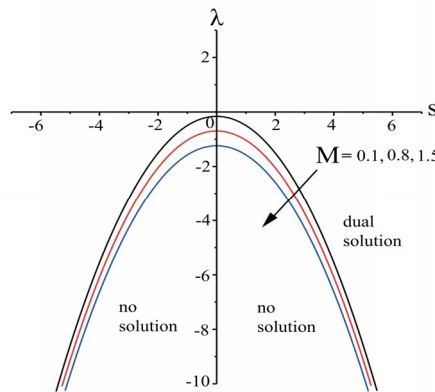


Figure 3. Regions of solutions of  $\lambda$  as a function of  $s$  for stretching/shrinking sheet when  $\phi_1 = 0.1$ ,  $\phi_2 = 0.01$  and  $\phi_3 = 0.02$ .

$$\beta = \frac{s}{2A_1} \pm \sqrt{\frac{s^2}{4A_1^2} + \frac{A_2 + A_3 \cdot M + \lambda}{A_1}} \tag{26}$$

It's obvious that physical solution correspond to a positive value of  $\beta$ , when  $\lambda > 0$  (stretched sheet) for any value of  $s$ . Fig. 2 depicts the influence of the external magnetic field on the region of no, unique and dual solutions  $s$  depending on  $\lambda$  for a stretching/shrinking sheet. With an increase in the magnetic field, the curve of critical values  $s$  shifts towards negative parameters  $\lambda$ . Similarly, in Fig. 3, curves are plotted for the critical  $\lambda$  depending on the magnitude of the magnetic field. We see that as the magnetic field increases, the regions of no, unique, and dual solutions shift towards negative  $\lambda$ .

After calculating  $\beta$ , we find an analytical solution for  $f(\eta)$  (25). Then the skin friction coefficient ( $Sr$ ) is given by:

$$Sr = C_{fx} \sqrt{Re_x} = \frac{\mu_{thf}}{\mu_f} \lambda \beta \tag{27}$$

By substituting this solution into equations (16)-(17), we obtain the modified system of equations shown below:

$$A_4 \theta'' + N_B \phi' \theta' + N_T \theta'^2 + \left( s + \frac{\lambda}{\beta}(1 - \exp(-\beta\eta)) \right) \theta' = 0 \tag{28}$$

$$\varphi'' + Le \left( s + \frac{\lambda}{\beta} (1 - \exp(-\beta\eta)) \right) \varphi' + \frac{N_T}{N_B} \theta'' = 0 \tag{29}$$

Equations (28)-(29) are supplemented by boundary conditions (18)-(19).

### 5. RESULTS AND DISCUSSIONS

The *bvp* method in Maple computer software is used to solve dimensionless ordinary differential equations (28)-(29) with boundary conditions (18)-(19). The results for the velocity profile are found analytically from expression (25), and as can be seen from expression (26), two analytical solutions are possible corresponding to the values of  $\beta$ . Similarity solutions exist when the mass suction parameter  $s > 0$  and the parameter  $\lambda < 0$  (shrinking sheet) (see Figs. 2 and 3).

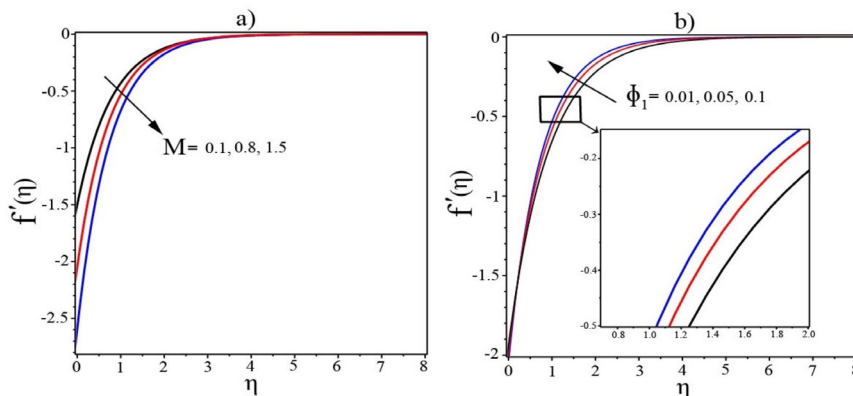


Figure 4. a) Effect of magnetic field on velocity profiles for  $\phi_{mf} = 0.13$ ; b) effect of volume fraction on velocity profiles for  $M = 0.8$ .

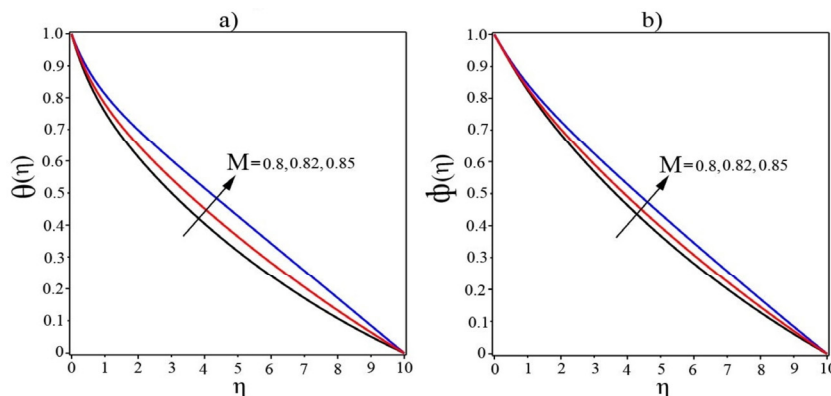
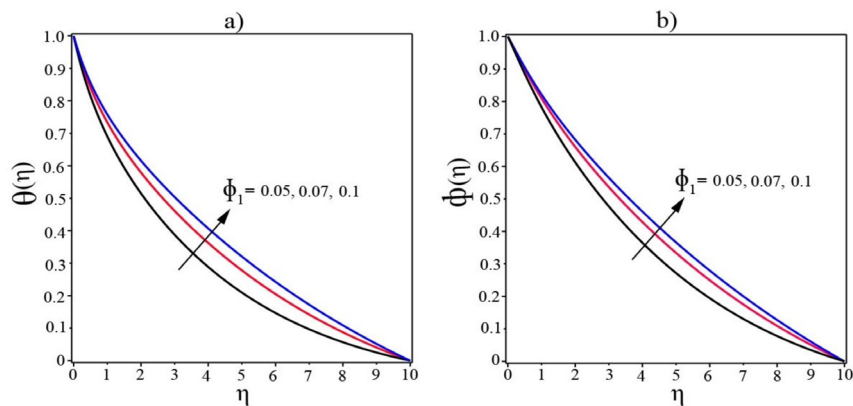


Figure 5. a) Effect of magnetic field on temperature for  $\phi_{mf} = 0.13$ ; b) effect of magnetic field on concentration profile for  $\phi_{mf} = 0.13$ .

Figs. 4a and 4b show the influence of a magnetic field and a volume fraction on the velocity profile of a ternary hybrid nanofluid for shrinking case  $\lambda = -2$  when the suction is presented as  $s = 2$ . Due to the very small difference between the solutions of the upper and lower branches for the velocity profile, Figs. 4a and 4b show graphs for the upper branch solutions. It can be seen from these figures that the boundary conditions at  $\eta \rightarrow \infty$  (19) are achieved asymptotically. The calculations are performed out with an accuracy of  $10^{-5}$  by setting  $\eta_{\infty} = 10$  for the far field boundary conditions. The presence of a magnetic field produces a force known as the Lorentz force, which resists fluid flow. This force's magnitude is directly proportional to  $M$  value. As a result, increasing  $M$  increases the Lorentz force. As seen in Fig. 4a, the thickness of the boundary layer grows as  $M$  increases. From Fig. 4b, we observe that the fluid flow rate increases with an increase in the volume fraction of  $Cu$ -nanoparticles ( $\phi$ ).

The decrease in flow rate due to the increase in the magnetic field  $M$  allows the nanoparticles to conduct more heat, and hence an increase in temperature is observed as shown in Fig. 5a. Due to the effect of thermophoresis, an increase in the temperature profile also causes an increase in the concentration profile, as seen in Fig. 5b.

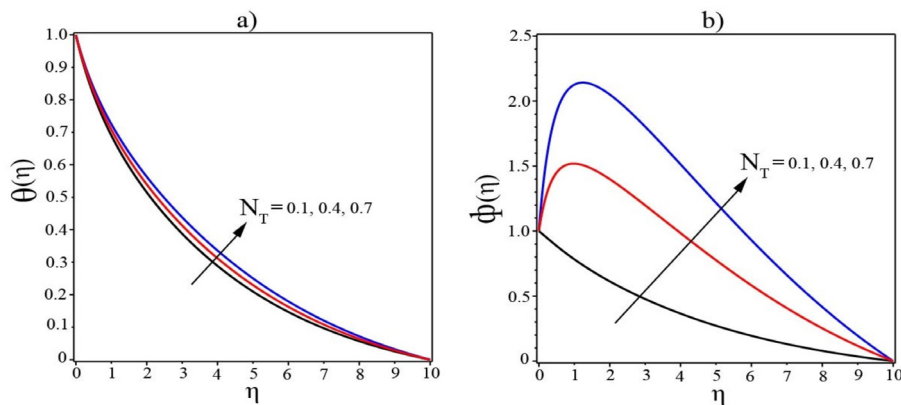
Figs. 6a and 6b show the effect of volume fraction on temperature and concentration profiles. As a result, with an increase in the volume fraction of  $Cu$  nanoparticles, new possibilities for increasing thermal conductivity appear, as shown in Fig. 6a. In addition, with an increase in the volume fraction of  $Cu$  nanoparticles, the concentration profile of the nanofluid increases (see Fig. 6b). This effect has applications in medicine when it is necessary to heat up soft tissues with the help of hybrid ferrofluids in the treatment of cancer. The results shown in Figs. 4-6 are in good agreement with the conclusions of the paper [23].



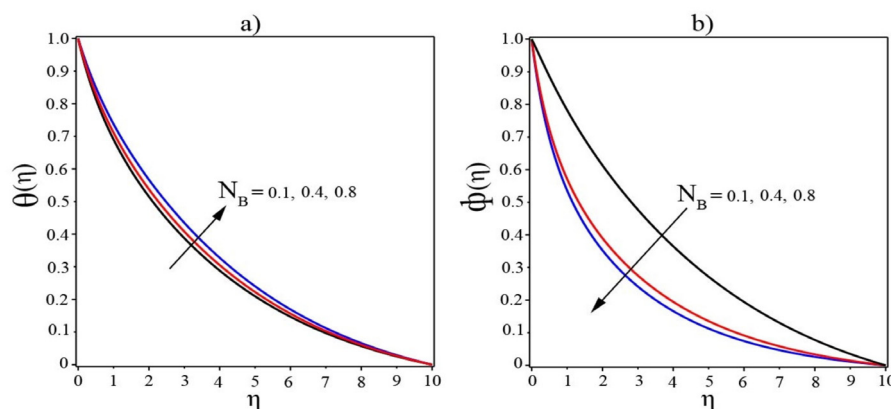
**Figure 6.** a) Effect of volume fraction  $\phi_1$  on temperature profile for  $M = 0.8$ ; b) effect of volume fraction  $\phi_1$  on concentration profile for  $M = 0.8$ .

Fig. 7a and Fig. 7b show the temperature and concentration profiles for various  $N_T$  values. As shown in Fig. 7a, any small increase in the thermophoresis force ( $N_T$ ) effectively increases the temperature profile. Due to the dependency of the concentration on the temperature field, we observe that higher thermophoresis parameters increase the concentration profile sharply (see Fig. 7b).

Adding more nanoparticles to the base fluid changed the behavior of the temperature and concentration profiles, as shown in Figs. 8a and 8b. The Brownian motion of nanoparticles plays a significant role in the distribution of heat, which is noticeable in the graph in Fig. 8a, where we observe an increase in the temperature profile with  $N_B$ . The concentration profile decreases as the Brownian motion parameter  $N_B$  increases, as shown in Fig. 8b.



**Figure 7.** a) Temperature profiles for different values of  $N_T$ ; b) concentration profiles for different values of  $N_T$ .



**Figure 8.** a) Temperature profiles for different values of  $N_B$ ; b) concentration profiles for different values of  $N_B$ .

Figs. 9a and 9b show that both temperature and concentration profiles decrease with increasing  $Le$ . For analysis, we chose small values of  $Le$ , which correspond to the slightly viscous base fluid. The results shown in Figs. 7-9 are in good agreement with the conclusions of the paper [30].

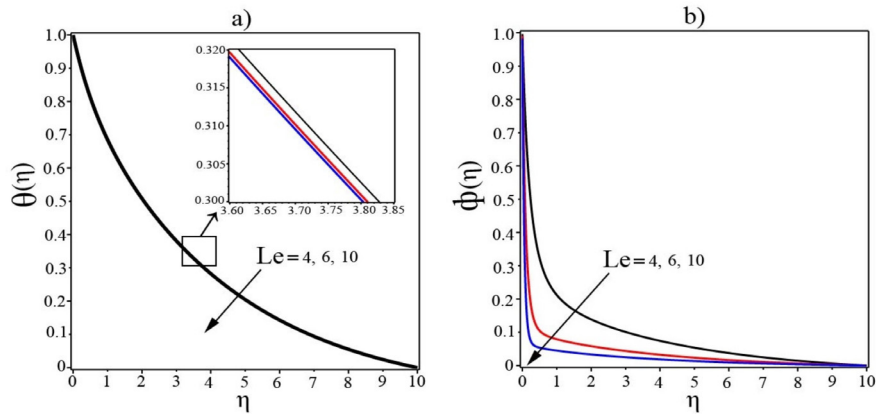


Figure 9. a) Effect of  $Le$  number on temperature distribution; b) effect of  $Le$  number on concentration distribution.

Fig. 10a depicts the variation of the skin friction coefficient  $Sr$  with the stretching/shrinking parameter  $\lambda$  for several values of the suction parameter  $s$ . When the shrinking parameter is changed from  $-2.046$  to  $-6.090$ , the value of the suction parameter increases from  $s = 2$  to  $s = 4$ . The double solution regions also expand with an increase in the suction parameter  $s$  at fixed values parameters of magnetic field  $M = 0.8$  and volume fraction  $\phi_{mf} = 0.13$ . Increasing the magnetic field parameter increases the coefficient of skin friction  $Sr$ , as shown in Fig. 10b. However, with an increase in  $\phi_1$ , the coefficient of surface friction  $Sr$  decreases because thermal conductivity increases at a higher concentration of nanoparticles. Due to the fact that thermal conductivity is enhanced by increasing the concentration of copper particles, the Nusselt number (heat transfer rate) decreases (see Fig. 11a). As the magnetic field  $M$  increases, the rate of heat transfer and concentration decreases, but the rate of concentration increases with increasing  $\phi_1$ , as shown in Fig. 11b.

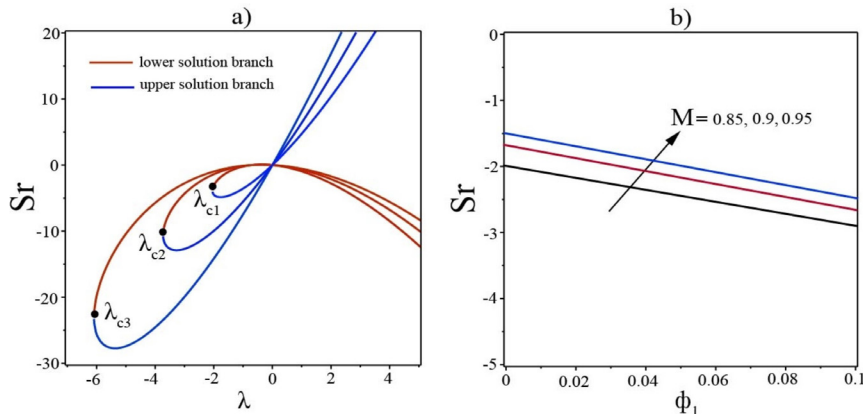


Figure 10. a) Variation of  $Sr$  as a function of  $\lambda$  for several values of  $s$  ( $s = 2, \lambda_{c1} = -2.046, s = 3, \lambda_{c2} = -3.731, s = 4, \lambda_{c3} = -6.090$ ) for  $\phi_{mf} = 0.13$ ; b) effect of magnetic field and volume fraction on skin friction coefficient  $Sr$ .

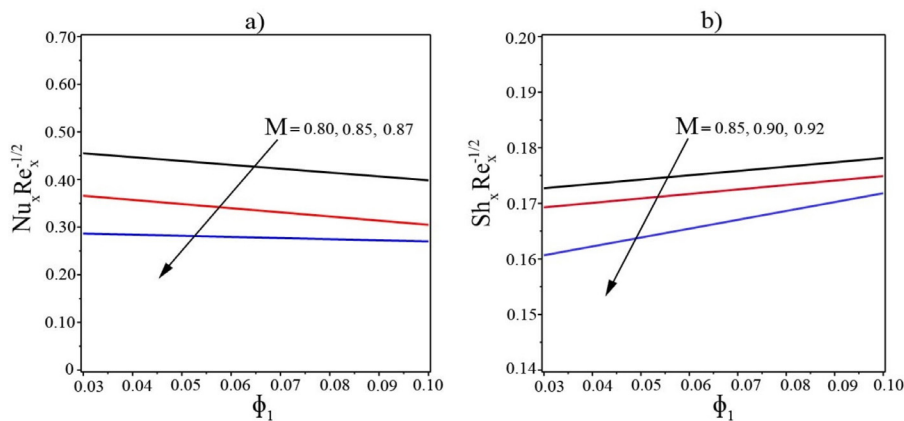
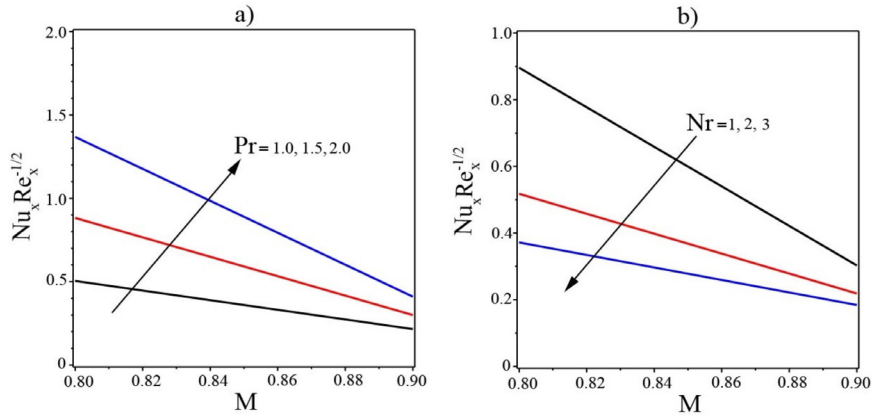


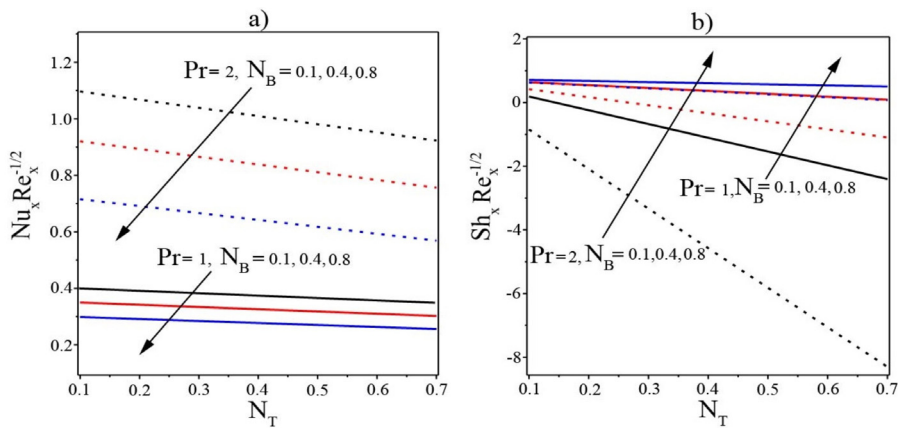
Figure 11. a) The influence of the magnetic field and volume fraction  $\phi_1$  on the local Nusselt number; b) the influence of the magnetic field and volume fraction  $\phi_1$  on the local Sherwood number.

Fig. 12a displayed the impact of Prandtl number  $Pr$  on the rate of heat transfer. An increase in the Prandtl number is associated with a decrease in the thermal conductivity of the base fluid  $k_f$ , which leads to an increase in heat transfer. Figure 12b depicts the influences of  $Nu_x$  as a function of  $M$  for various  $Nr$ . This graphic shows that  $Nu_x$  decreases as the examined two parameters ( $M$  and  $Nr$ ) increase.

The change in the local heat and concentration transfer rates depending on the parameter  $N_T$  is shown in Figs. 13 and 14.



**Figure 12.** a) Effect of Prandtl number  $Pr$  and magnetic field on the local Nusselt number; b) effect of the radiation parameter  $Nr$  and magnetic field on the local Nusselt number.



**Figure 13.** a) Effects of  $N_B$  and  $Pr$  numbers are seen on heat transfer rates; b) effects of  $N_B$  and  $Pr$  numbers are seen on dimensionless concentration rates.

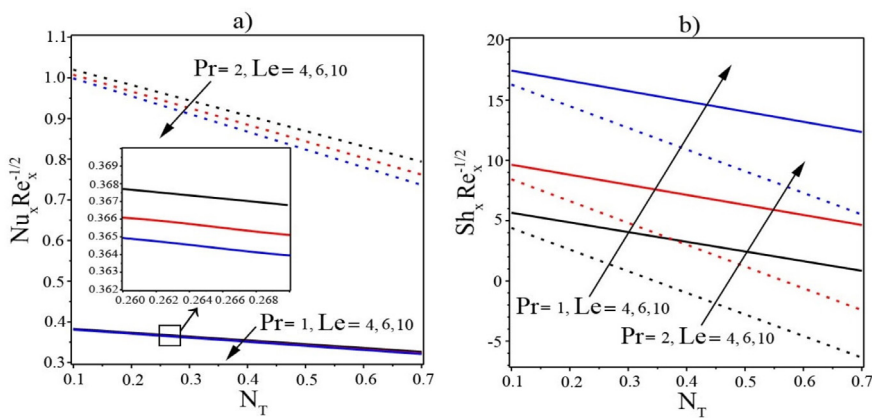


**Figure 14.** a) Effects of  $Le$  and  $Pr$  numbers are seen on heat transfer rates; b) effects of  $Le$  and  $Pr$  numbers are seen on dimensionless concentration rates.

Graphs in Fig. 13 show the effect of the  $N_B$  parameters and  $Pr$  Prandtl number on the local heat and concentration transfer rate for a fixed  $Le$  number. As can be seen from Fig. 13, the dimensionless heat transfer rate

decreases with increasing parameters  $N_B$  and  $N_T$  but increases with increasing  $Pr$ . The local Sherwood number  $Sh_x$ , on the other hand, increases as the Brownian motion parameter  $N_B$  increases but decreases as the Prandtl number increases. However, with an increase in the  $Le$  number, a decrease in the local heat transfer rates was observed. As shown in Fig. 14a, the change in local heat transfer rates increases with an increase in the Prandtl number. In contrast, the local Sherwood number increases with the Lewis parameter  $Le$ , but decreases with the  $Pr$  number, as shown in Fig. 14b. These results are in good agreement with the conclusions of the papers[24],[30].

## 6. CONCLUSIONS

An analysis was made of the diffusion characteristics of heat and nanoparticles in a ternary hybrid ferrofluid flow over a linearly stretching/shrinking porous sheet under conditions of mass transpiration and radiation heating. Using the similarity transformation, a system of nonlinearly coupled ODEs was obtained, which was numerically solved in the Maple software application using the *bvp* technique. Numerical results are interpreted using graphs. We have found the boundaries of the existence of unique and double solutions depending on the magnitude of the magnetic field for the shrinking case ( $\lambda < 0$ ). The main research results are:

- An increase in the magnetic field resists the flow of the trihybrid ferrofluid, while an increase in the volume fraction of nanoparticles increases the momentum of the flow.
- The skin friction coefficient increases with an increase in the suction rate  $s > 0$  and the magnitude of the Lorentz force.
- The rates of heat and mass transfer decrease as the Lorentz force increases.
- The local Nusselt number (rate of heat transfer) decreases when the values of the parameters  $Pr$ ,  $Le$ ,  $N_B$ ,  $N_T$  and  $N_r$  are increased.
- The local Sherwood number (rate of mass transfer) increases as the Brownian motion parameter increases and decreases as the thermophoresis parameter increases.

The results obtained can be generalized to other types of ternary hybrid nanofluids that are used in various practical problems.

## ORCID IDs

-  Michael I. Kopp, <https://orcid.org/0000-0001-7457-3272>, 
  Volodymyr V. Yanovsky, <https://orcid.org/0000-0003-0461-749X>  
 Thippeswamy Anusha, <https://orcid.org/0000-0003-0950-6481>; 
  Ulavathi S. Mahabaleshwar, <https://orcid.org/0000-0003-1380-6057>

## REFERENCES

- [1] J. C. Maxwell, *A Treatise on Electricity and Magnetism* (Clarendon, Oxford, 1873)
- [2] S. Choi, Enhancing thermal conductivity of fluids with nanoparticles, in: *Development and applications of Non-Newtonian flows*, edited by D.A. Signier and H.P. Wang, Vol. 66, (ASME, New York, 1995) pp. 99-105.
- [3] B.C. Sakiadis, "Boundary layer behaviour on continuous solid surfaces: I. boundary layer equations for two-dimensional and axisymmetric flow", *AIChE J.* **7**, 26-28 (1961). <https://doi.org/10.1002/aic.690070108>
- [4] B.C. Sakiadis, "Boundary layer behaviour on continuous solid surfaces: II. the boundary layer on a continuous flat surface", *AIChE J.* **7**, 221-225 (1961), <https://doi.org/10.1002/aic.690070211>
- [5] L.J. Crane, "Flow past a Stretching Plate", *Z. Angrew. Math. Phys.* **21**, 645-647 (1970). <https://doi.org/10.1007/BF01587695>
- [6] E.H. Aly, and I. Pop, "MHD flow and heat transfer near stagnation point over a stretching/shrinking surface with partial slip and viscous dissipation: Hybrid nanofluid versus nanofluid", *Powder Technol.* **367**, 192-205 (2020). <https://doi.org/10.1016/j.powtec.2020.03.030>
- [7] U. Khan, A. Shafiq, A. Zaib, and D. Baleanu, "Hybrid nanofluid on mixed convective radiative flow from an irregular variably thick moving surface with convex and concave effects", *Case stud. Therm. Eng.* **21**, 100660 (2020). <https://doi.org/10.1016/j.csite.2020.100660>
- [8] A. Jamaludin, K. Naganthran, R. Nazar, and I. Pop, "MHD mixed convection stagnation-point flow of Cu-Al<sub>2</sub>O<sub>3</sub>/water hybrid nanofluid over a permeable stretching/shrinking surface with heat source/sink", *Euro. J. Mech. B/Fluids*, **84**, 71-80 (2020). <https://doi.org/10.1016/j.euromechflu.2020.05.017>
- [9] U.S. Mahabaleshwar, A.B. Vishalakshi, and H.I. Andersson, "Hybrid nanofluid flow past a stretching/shrinking sheet with thermal radiation and mass transpiration", *Chinese Jour. Phys.* **75**, 152-168 (2022). <https://doi.org/10.1016/J.CJPH.2021.12.014>
- [10] T. Anush, U.S. Mahabaleshwar, and Y. Sheikhejad, "An MHD of Nanofluid Flow Over a Porous Stretching/Shrinking Plate with Mass Transpiration and Brinkman Ratio", *Transp. Porous Med.* **142**, 333-352 (2021). <https://doi.org/10.1007/s11242-021-01695-y>
- [11] K.E. Aslani, U.S. Mahabaleshwar, J. Singh, I.E. Sarris, "Combined effect of radiation and inclined MHD flow of a micro polar fluid over a porous stretching/shrinking sheet with mass transpiration", *Int. J. Appl. Comput. Math.* **7**, 1-21 (2021). <https://doi.org/10.1007/s40819-021-00987-7>
- [12] U.S. Mahabaleshwar, K.N. Sneha, and H.N. Haug, "An effect of MHD and radiation on CNTs-water based nanofluids due to a stretching sheet in a Newtonian fluid", *Case Stud. Therm. Eng.* **28**, 101462 (2021). <https://doi.org/10.1016/j.csite.2021.101462>
- [13] R.E. Rosensweig, *Ferrohydrodynamics*, (Cambridge University Press, Cambridge, 1985)
- [14] Y.M. Chu, S. Bilal, and M.R. Hajizadeh, "Hybrid ferrofluid along with MWCNT for augmentation of thermal behavior of fluid during natural convection in a cavity", *Math. Methods Appl. Sci.* **2020**, 1-12 (2020). <https://doi.org/10.1002/mma.6937>
- [15] K.A. Kumar, N. Sandeep, V. Sugunamma, and I.L. Animasaun, "Effect of irregular heat source/sink on the radiative thin film flow of MHD hybrid ferrofluid", *J. Therm. Anal. Calorim.* **139**, 2145-2153 (2020). <https://doi.org/10.1007/s10973-019-08628-4>

- [16] I. Tlili, M.T. Mustafa, K.A. Kumar, and N. Sandeep, "Effect of asymmetrical heat rise/fall on the film flow of magnetohydrodynamic hybrid ferrofluid", *Sci. Rep.* **10**, 6677 (2020). <https://doi.org/10.1038/s41598-020-63708-y>
- [17] N.S. Anuar, N. Bachok, and I. Pop, "Influence of MHD Hybrid Ferrofluid Flow on Exponentially Stretching/Shrinking Surface with Heat Source/Sink under Stagnation Point Region", *Mathematics*, **9**, 2932 (2021). <https://doi.org/10.3390/math9222932>
- [18] L.A. Lund, Z. Omar, J. Raza, and I. Khan, "Magnetohydrodynamic flow of Cu-Fe<sub>3</sub>O<sub>4</sub>/H<sub>2</sub>O hybrid nanofluid with effect of viscous dissipation: Dual similarity solutions", *J. Therm. Anal. Calorim.* **143**, 915-927 (2021). <https://doi.org/10.1007/s10973-020-09602-1>
- [19] L.S. Sundar, K.V.V.C. Mouli, Z. Said, and A.C.M. Sousa, "Heat transfer and second law analysis of ethylene glycol-based ternary hybrid nanofluid under laminar flow", *J. Therm. Sci. Eng. Appl.* **13**, 1-15 (2021). <https://doi.org/10.1115/1.4050228>
- [20] U. Khan, and Z. Mahmood, "MHD Stagnation Point Flow of Ternary Hybrid Nanofluid Flow over a Stretching/Shrinking Cylinder with Suction and Ohmic Heating", Preprint, (2022). <https://www.authorea.com/doi/full/10.22541/au.164873383.38887373>
- [21] G.K. Ramesh, J.K. Madhukesh, S.A. Shehzad, and A. Rauf, "Ternary nanofluid with heat source/sink and porous medium effects in stretchable convergent/divergent channel", *Proc. Inst. Mech. Eng. E: J. Process Mech. Eng.* **2022**, 1-10 (2022). <https://doi.org/10.1177/09544089221081344>
- [22] I.L. Animasau, S.J. Yook, T. Muhammad, and A. Mathew, "Dynamics of ternary-hybrid nanofluid subject to magnetic flux density and heat source or sink on a convectively heated surface", *Surf. Interfaces* **28**, 101654 (2022). <https://doi.org/10.1016/j.surf.2021.101654>
- [23] S. Manjunatha, V. Puneeth, B.J. Gireesha, and A.J. Chamkha, "Theoretical Study of Convective Heat Transfer in Ternary Nanofluid Flowing past a Stretching Sheet." *J. Appl. Comput. Mech.* **8**, 1279-1286 (2022). <https://doi.org/10.22055/JACM.2021.37698.3067>
- [24] N.L. Aleng, N. Bachok, and N.M. Arifin, "Flow and Heat Transfer of a Nanofluid over an Exponentially Shrinking Sheet", *Indian J. Sci. Technol.* **8**, 1-6 (2015). <https://doi.org/10.17485/ijst/2015/v8i31/87246>
- [25] J. Raza, A.M. Rohni, Z. Omar, and M. Awais, "Rheology of the Cu-H<sub>2</sub>O nanofluid in porous channel with heat transfer: Multiple solutions" *Phys. E: Low-Dimens. Syst. Nanostructures*, **86**, 248-252 (2017). <https://doi.org/10.1016/j.physe.2016.10.038>
- [26] B. Takabi, and S. Salehi, "Augmentation of the heat transfer performance of a sinusoidal corrugated enclosure by employing hybrid nanofluid." *Adv. Mech. Eng.* **6**, 147059 (2014). <https://doi.org/10.1155/2014/147059>
- [27] R.S.R. Gorla, S. Siddiqua, M.A. Mansour, A.M. Rashad, and T. Salah, "Heat source/sink effects on a hybrid nanofluid-filled porous cavity", *J. Thermophys. Heat Transf.* **31**, 847-857 (2017). <https://doi.org/10.2514/1.T5085>
- [28] E. Magyari, and A.J. Chamkha, "Exact analytical results for the thermosolutal mhd marangoni boundary layers", *Int. J. Therm. Sci.* **47**, 848-857 (2008). <https://doi.org/10.1016/j.ijthermalsci.2007.07.004>
- [29] P.G. Siddheshwar, and U.S. Mahabaleswar, "Effects of radiation and heat source on MHD flow of a viscoelastic liquid and heat transfer over a stretching sheet", *Int. J. Non-Linear Mech.* **40**, 807-820 (2005). <https://doi.org/10.1016/j.ijnonlinmec.2004.04.006>
- [30] A. Alam, D.N.K. Marwat, and A. Ali, "Flow of nano-fluid over a sheet of variable thickness with non-uniform stretching (shrinking) and porous velocities", *Adv. Mech. Eng.* **13**, 1-16 (2021). <https://doi.org/10.1177/16878140211012913>

### МГД ТЕЧІЯ І ТЕПЛОПЕРЕДАЧА ПОТРІЙНОЇ ГІБРИДНОЇ ФЕРОРІДИНИ НАД ПОРИСТИМ ЛИСТОМ, ЩО РОЗТЯГУЄТЬСЯ/СТИСКАЄТЬСЯ, З ЕФЕКТАМИ БРОУНІВСЬКОЇ ДИФУЗІЇ ТА ТЕРМОФОРЕЗУ

Михайло Й. Копп<sup>a</sup>, Володимир В. Яновський<sup>a,b</sup>, Тіпсвамї Ануша<sup>c</sup>, Улаватї С. Махабалешвар<sup>c</sup>

<sup>a</sup>Інститут монокристалів, Національна Академія Наук України  
пр. Науки 60, 61001 Харків, Україна

<sup>b</sup>Харківський національний університет імені В.Н. Каразіна  
майдан Свободи, 4, 61022, Харків, Україна

<sup>c</sup>Факультет математики, Шіваганготрі, Університет Давангере, Давангере, Індія 577 007

В даній роботі досліджується магнітогідродинамічна (МГД) течія потрійної гібридної ферорідини над пористим листом, що розтягується/стискається, в присутності випромінювання і масової транспірації. Потрійна гібридна нанорідина утворюється шляхом суспендування трьох типів наночастинок для покращення теплопередачі. Наночастинки міді ( $Cu$ ), оксиду заліза ( $Fe_3O_4$ ) та фериту кобальту ( $CoFe_2O_4$ ) суспендовані у воді та утворюють комбінацію  $Cu - Fe_3O_4 - CoFe_2O_4 - H_2O$ . Броунівський рух та термофорез інтегровані в модель потрійної гібридної ферорідини. Перетворення подібності конвертують основні диференціальні рівняння в приватних похідних у звичайні диференціальні рівняння. Метод розв'язання крайової задачі використовується в програмному забезпеченні Maple для чисельного розв'язання перетворених рівнянь. Результати обчислень для відповідних параметрів, таких як профіль швидкості, температурний профіль, коефіцієнт поверхневого тертя, локальні числа Нуссельта та Шервуда, наочно показані і докладно пояснені.

**Ключові слова:** потрійна гібридна ферорідина; розтягнення/стиск; тепло- та масообмін; масова транспірація; магнітне поле

## STRUCTURAL VARIATIONS OF DUST ACOUSTIC SOLITARY WAVES (DASWs) PROPAGATING IN AN INHOMOGENEOUS PLASMA<sup>†</sup>

 **Hirak Jyoti Dehingia\***,  **P.N. Deka<sup>§</sup>**

*Department of Mathematics, Dibrugarh University, Assam, India*

*\*Corresponding Author e-mail: [hirakjyotidehingia11@gmail.com](mailto:hirakjyotidehingia11@gmail.com); <sup>§</sup>E-mail: [pndeka@dibru.ac.in](mailto:pndeka@dibru.ac.in)*

*Received January 6, 2023; revised January 28, 2023; accepted February 1, 2023*

This paper presents our theoretical investigations on the structural variations of dust acoustic solitary waves (DASWs) in inhomogeneous unmagnetized plasmas. To study the structural variations of DASWs, we have considered collisionless, hot isothermal, and Boltzmannian distribution for electrons-ions with negatively charged dust grains in weakly inhomogeneous plasmas. We have used the reductive perturbation technique (RPT) in the governing equations of plasmas, derived the modified Korteweg-de-Vries (m-KdV) equation, and obtained the solitary wave solution. We have considered the appropriate stretched coordinates for space and time variables for the inhomogeneous plasma. This paper investigates the effects of dust particles on ion-acoustic solitary waves' propagation in the inhomogeneous plasma model. We have also included the effect of inhomogeneity parameters on the soliton structures.

**Keywords:** *Dusty plasma; reductive perturbation technique (RPT); isothermal electrons; inhomogeneous plasma*

**PACS:** 52.35.Mw, 52.27.Lw

### I. INTRODUCTION

Plasma and charged dusts or dust grains are the two fundamental ubiquities of the universe. Dusty plasma is a relatively new branch of the research area in plasma physics. In dusty plasmas, the interaction of dust grains and plasma particles are studied. Plasma particles consist of hot and electrically conductive electrons and ions, but the dusty plasma particles consist of both plasma particles and dust grains, i.e., dusty plasma particles are comprised of three fundamental ingredients ions, electrons, and charged dust particles or dust charged grains. The dust particles show more complex behaviours when added to the plasma particles. So, the dusty plasmas are also known as complex plasmas or multi-component plasmas. Investigations on these complex or multi-component plasmas are abundant throughout the universe. The majority of extant solid matter is thought to be made up of dust grains that are frequently contained by plasma particles. Planetary magnetospheres, cometary environments, nebulae, etc. [1], are some examples of dusty plasmas. These complex plasmas are enormous important to understand the theories of geophysics better, complete some space missions, advancements of knowledge in astrophysical environments like the formation of stars, galaxies, and nebulae, and manufacture some new materials in the semiconductor industries, etc. Dusty plasmas are one of the significant fields for working in Controlled Thermonuclear Research (CTR). In 1982, Voyager spacecraft [2] discovered the radial spokes of the Saturn's B ring. Apart from the wide range of applications of dusty plasmas in the astrophysical problems, researchers have observed the wide use of dusty plasmas and their related issues during the use of dusty plasmas in the manufacturing of new materials in the semiconductor industries [3]. Later, a number of authors have worked in the both theoretical and experimental works on the dusty plasmas. In the early eighties of last century, the concept of dusty plasma could not be developed convincingly. However, to understand the fundamental properties of dusty plasmas, some devices are introduced in dusty plasma laboratories like the rotating drum system [4] and dust shaker systems [5]. Subsequently, in the review literature of Goertz [6] and Northrop [7], we have some details of works carried out in dusty plasma for astrophysical cases. Basically, for unmagnetized plasmas, dusty plasma waves are characterized by three different modes such as dust-acoustic waves [9] (DAW), dust ion-acoustic waves [8] (DIAW), and dust lattice waves [10] (DLW). Several theoretical [8-10] and experimental [11,12] studies have been done to achieve more understanding on the complex behaviours of DAWs, DIAWs, and DLWs. Apart from the above, large number of literatures could be found on the various nonlinear wave phenomena and instabilities for homogeneous dusty plasmas, inhomogeneous dusty plasmas [13-20] and nonlinear wave excitation in nonequilibrium plasmas. For studying the linear wave theories in plasmas, the nonlinearities for small amplitude waves are not considered, but in the case of large amplitude waves, the nonlinearities cannot be neglected. Due to the existence of nonlinearities in the plasma waves, the various physical parameters and their effects can be studied. The nonlinearities are also indicated in the experimental and theoretical behaviours of some nonlinear plasma wave structures such as solitons or solitary waves, supersolitons, rouge waves, shock waves, etc. In inhomogeneous plasmas, few more researchers have done their works on the properties and effects of dust ion-acoustic (DIA) solitary waves [21,22], dust acoustic (DA) solitary waves [8,27,28,32], shock waves [23-26], and dust lattice (DL) solitary waves [10,29], etc. Apart from the broad applications of complex or dusty plasmas in astrophysical systems and space science, the wide applications of dusty plasmas have also been seen in the fusion sciences and laboratory environments [30,31]. Gogoi and Deka also studied the propagation of dust acoustic (DA) solitary wave propagations in

<sup>†</sup> *Cite as:* H.J. Dehingia, and P.N. Deka, East Eur. J. Phys. 1, 19 (2023), <https://doi.org/10.26565/2312-4334-2023-1-02>

© H.J. Dehingia, P.N. Deka, 2023

inhomogeneous plasmas [32]. Some more basic properties and the effects on dust-acoustic waves (DAWs) have been studied theoretically in the presence of both positively and negatively dust particles with negatively charged ion fluids and  $\kappa$ -distributed superthermal electrons [33]. Dusty plasmas are basically studied in inhomogeneous plasma systems to understand the advanced use of plasmas in astrophysical environments and in laboratory discharges [34]. The modulational instability and dust-cyclotron wave for DAWs in three-component plasmas have been explored in the presence of ions, electrons, and dust particles under the influence of a magnetic field [35]. In the presence of pair-ion fullerene plasma, magneto-acoustic wave propagation was also studied in both the linear and nonlinear plasma environments [36]. Pakzad and Nobahar [39] studied the properties of dust ion-acoustic (DIA) solitary waves in inhomogeneous unmagnetized plasmas in the presence of stationary dust grains, super thermal electrons, and inertial ions. They have also studied the behaviours of DIAWs propagating in the various astrophysical environments like Solar winds, Venus's ionosphere, and the Earth's atmosphere. Dehingia and Deka [41] have recently studied ion-acoustic solitons' variations in an inhomogeneous plasma. They have observed how the ion-acoustic solitary wave bends in some critical points due to the inhomogeneity present in the plasma system. Though many investigations on the effect of dust particles on plasma properties have been done till date, there are still many scopes to study the role of dust particles in affecting the nonlinear structures of plasmas, in particular for the case of inhomogeneous plasmas. In this paper, we will extend the investigations of Gogoi and Deka [32], to understand the structural variations of dust-acoustic solitary waves in inhomogeneous plasma under the following considered physical situations.

Here, we present our investigations on the structural variations of dust acoustic solitary waves in inhomogeneous plasma in the presence of hot isothermal electrons with Boltzmannean electron-ion distribution. This model consists of unmagnetized, collisionless, hot isothermal electrons and weakly inhomogeneous plasmas in the presence of negatively charged dust grains. Using the governing equations of plasmas and the reductive perturbation method or technique (RPT), we have derived the modified Korteweg-de-Vries (mKdV) equation with the help of appropriate stretched coordinates for space and time variables for the inhomogeneous plasmas. The solution of the above mKdV equation also indicates the various nonlinear effects of dust grains propagating in inhomogeneous, unmagnetized plasmas in the presence of negatively charged dust particles. We have also presented our results and investigated the effect of dust particles on ion-acoustic solitary waves' propagation due to the inhomogeneity parameters in the inhomogeneous above-considered plasma model.

## II. GOVERNING EQUATIONS

We have considered an unmagnetized, collisionless, hot isothermal, Boltzmannean distributed electrons and ions, in the presence negatively charged dust particles in weakly inhomogeneous plasma. With the variable density gradient and along the x-direction only, the system is considered to be inhomogeneous. The set of dimensionless and nonlinear governing fluid equations for slowly moving dust acoustic waves along the x- direction is taken as follows:

Continuity equation:

$$\frac{\partial n_d}{\partial t} + \frac{\partial}{\partial x}(n_d v_d) = 0. \quad (1)$$

Momentum equation:

$$\frac{\partial v_d}{\partial t} + v_d \left( \frac{\partial v_d}{\partial x} \right) + q \left( \frac{\partial \phi}{\partial x} \right) = 0. \quad (2)$$

Poisson equation :

$$\frac{\partial^2 \phi}{\partial x^2} - n_e - q n_d + n_i = 0. \quad (3)$$

Boltzmannean distribution of electrons:

$$n_e = n_{e0} e^{k\phi}. \quad (4)$$

Boltzmannean distribution of ions:

$$n_i = n_{i0} e^{-\phi}. \quad (5)$$

In the above equations,  $n_d$  represents the number density of dust grains which is normalized by  $n_{d0}$  at an equilibrium condition. Here,  $v_d$  represents the fluid velocity of dust grains which is normalized by dust acoustic speed (DAS)  $C_{ds} = \left( Z_{d0} \frac{T_i}{m_d} \right)^{1/2}$  where ion temperature is  $T_i$  and mass of the charged dust particles is  $m_d$ . Here, we assume  $\phi$  as the electrostatic potential with the charge neutrality at equilibrium state  $n_{i0} = n_{e0} + Z_{d0} n_{d0}$ . The quantities  $n_d, v_d, \phi, n_e, n_i$  are reduced to the dimensionless form with the help of Debye length  $\lambda_D = \sqrt{\frac{T_e}{4\pi n_{i0} e^2}}$ , DAS  $C_{ds}$  and thermal electrostatic potential  $\phi = \frac{T_e}{e}$  where  $T_e$  is the electron temperature and  $e$  is the electron charge. For

charged dust grains  $q = Z_d e$ , the balanced current equation is given by [6]  $q_t + v_d q_x = I_e + I_i$  where  $q_t$  and  $q_x$  are dust currents,  $I_i$  and  $I_e$  are the ion and electron currents respectively.

Due to slow motion of the dust fluid its velocity  $v_{d0}$  is small at equilibrium state, the dust current is balanced by both the ion and electron currents together. Then we have the balanced current equation is given by [10]  $I_e + I_i \approx 0$  where  $I_e$  and  $I_i$  are respectively given by [40]

$$\left. \begin{aligned} I_e &= -\pi r^2 e \left( \frac{8T_e}{\pi m_e} \right)^{1/2} n_{e0} e^{k\phi} \\ I_i &= -\pi r^2 e \left( \frac{8T_i}{\pi m_i} \right)^{1/2} n_{i0} \left( 1 - \frac{e\phi}{T_i} \right) \end{aligned} \right\}, \quad (6)$$

where  $r$  denotes the radius of charged dust grains and  $k = T_i/T_e$ .

### III. DERIVATION OF MODIFIED K-dV (m-KdV) EQUATION

To study the structural variations of dust acoustic (DA) solitary wave propagations in inhomogeneous plasmas, we use the reductive perturbation technique (RPT). To apply the RPT for some small amplitude wave, we use an appropriate one-dimensional space-time stretched coordinate which is given by [37]

$$\left. \begin{aligned} \xi &= \epsilon^{1/2} \left( \frac{x}{M} - t \right) \\ \tau &= \epsilon^{3/2} x \end{aligned} \right\}, \quad (7)$$

where  $\epsilon$  is a smallness parameter,  $M$  is the phase velocity of the DA soliton, normalized by  $C_{ds}$ .

Now, using Eq. (7) in Eqs. (1) – (5) we get the following set of equations are as follows:

$$-\epsilon^{1/2} \frac{\partial n_d}{\partial \xi} + \frac{\epsilon^{3/2}}{M} \frac{\partial}{\partial \xi} (n_d v_d) + \epsilon^{3/2} \frac{\partial}{\partial \tau} (n_d v_d) = 0, \quad (8)$$

$$-\epsilon^{1/2} \frac{\partial v_d}{\partial \xi} + \frac{\epsilon^{3/2} v_d}{M} \left( \frac{\partial v_d}{\partial \xi} \right) + \frac{\epsilon^{3/2} v_d}{M} \left( \frac{\partial v_d}{\partial \tau} \right) + \frac{\epsilon^{3/2} Z_d}{M} \left( \frac{\partial \phi}{\partial \xi} \right) + \frac{\epsilon^{3/2} Z_d}{M} \left( \frac{\partial \phi}{\partial \tau} \right) = 0, \quad (9)$$

$$\frac{\epsilon}{M^2} \frac{\partial^2 \phi}{\partial \xi^2} + 2 \frac{\epsilon^2}{M} \frac{\partial^2 \phi}{\partial \xi \partial \tau} + \epsilon^3 \frac{\partial^2 \phi}{\partial \tau^2} - n_{e0} e^{k\phi} n - n_d Z_d + n_{i0} e^{-\phi} = 0. \quad (10)$$

Expanding the dependent variables  $n_d, v_d, Z_d$  and  $\phi$  about the equilibrium parts in terms of power series of  $\epsilon$  as follows:

$$\begin{bmatrix} n_d \\ v_d \\ \phi \\ Z_d \end{bmatrix} = \begin{bmatrix} n_{d0} \\ 0 \\ 0 \\ Z_{d0} \end{bmatrix} + \epsilon \begin{bmatrix} n_{d1} \\ v_{d1} \\ \phi_1 \\ Z_{d1} \end{bmatrix} + \epsilon^2 \begin{bmatrix} n_{d2} \\ v_{d2} \\ \phi_2 \\ Z_{d2} \end{bmatrix} + \dots \quad (11)$$

Using the Eq. (11) in Eq. (8), (9) and (10) respectively we get the following set of equations as follows: (Neglecting the higher terms having powers of  $\epsilon$  more than  $\frac{5}{2}$ )

$$\left. \begin{aligned} & -\epsilon^{1/2} \frac{\partial n_{d0}}{\partial \xi} + \epsilon^{3/2} \left[ -\frac{\partial n_{d1}}{\partial \xi} + \frac{1}{M} \frac{\partial}{\partial \xi} (n_{d0} v_{d1}) \right] \\ & + \epsilon^{5/2} \left[ -\frac{\partial n_{d2}}{\partial \xi} + \frac{1}{M} \frac{\partial}{\partial \xi} (n_{d0} v_{d2}) + \frac{1}{M} \frac{\partial}{\partial \xi} (n_{d1} v_{d1}) + \frac{1}{M} \frac{\partial}{\partial \tau} (n_{d0} v_{d1}) \right] = 0 \end{aligned} \right\}, \quad (12)$$

$$\left. \begin{aligned} & \epsilon^{3/2} \left[ -\frac{\partial v_{d1}}{\partial \xi} + \frac{Z_{d0}}{M} \left( \frac{\partial \phi_1}{\partial \xi} \right) \right] \\ & + \epsilon^{5/2} \left[ -\frac{\partial v_{d2}}{\partial \xi} + \frac{v_{d1}}{M} \left( \frac{\partial v_{d1}}{\partial \xi} \right) + \frac{Z_{d0}}{M} \left( \frac{\partial \phi_2}{\partial \xi} \right) + \frac{Z_{d1}}{M} \left( \frac{\partial \phi_1}{\partial \xi} \right) + Z_{d0} \left( \frac{\partial \phi_1}{\partial \tau} \right) \right] = 0 \end{aligned} \right\}, \quad (13)$$

$$\left. \begin{aligned} & (n_{e0} + n_{d0} Z_{d0} - n_{i0}) + \epsilon \{ Z_{d0} n_{d1} + n_{d0} Z_{d1} + (n_{e0} k + n_{i0}) \phi_1 \} \\ & + \epsilon^2 \left[ \frac{1}{M^2} \frac{\partial^2 \phi_1}{\partial \xi^2} - (n_{e0} k + n_{i0}) \phi_2 - \left( \frac{n_{e0}}{2} k^2 + \frac{n_{i0}}{2} \right) \phi_1^2 \right] = 0 \end{aligned} \right\}. \quad (14)$$

Now we compare the coefficients of  $\epsilon$  from lower to the highest powers in the Eq. (12) – (14), we get At  $\epsilon^{1/2}$ , we get,

$$\frac{\partial n_{d0}}{\partial \xi} = 0. \tag{15}$$

At  $\epsilon^{\frac{3}{2}}$ , we get,

$$\frac{1}{M} \frac{\partial}{\partial \xi} (n_{d0} v_{d1}) = \frac{\partial n_{d1}}{\partial \xi}. \tag{16}$$

$$\frac{\partial v_{d1}}{\partial \xi} = \frac{Z_{d0}}{M} \left( \frac{\partial \phi_1}{\partial \xi} \right). \tag{17}$$

At  $\epsilon$ , we get,

$$(n_{e0}k + n_{i0})\phi_1 + n_{d0}Z_{d1} + n_{d1}Z_{d0} = 0. \tag{18}$$

So, using the boundary conditions  $n_{d1}, v_{d1}, \phi_1 \rightarrow 0$  as  $|\xi| \rightarrow \infty$ , we get from (16) – (18)

$$v_{d1} = \frac{Z_{d0}}{M} \phi_1, \tag{19}$$

$$n_{d1} = \frac{n_{d0}Z_{d0}}{M^2} \phi_1, \tag{20}$$

$$Z_{d1} = L\phi_1, \tag{21}$$

where

$$L = - \left[ \frac{(n_{e0}k + n_{i0})}{n_{d0}} + \left( \frac{Z_{d0}}{M} \right)^2 \right], \tag{22}$$

and

$$M = \sqrt{\frac{n_{d0}}{n_{e0}k + n_{i0}}} Z_{d0}, \tag{23}$$

where  $M$  determines the phase velocity of DAW.

At the highest order coefficients of  $\epsilon$  we get,

$$-\frac{\partial n_{d2}}{\partial \xi} + \frac{1}{M} \frac{\partial}{\partial \xi} (n_{d0} v_{d2}) + 2 \frac{n_{d0} Z_{d0}^2}{M^4} \phi_1 \frac{\partial \phi_1}{\partial \xi} + \frac{1}{M} \frac{\partial}{\partial \tau} (n_{d0} v_{d1} \phi_1) = 0, \tag{24}$$

$$-\frac{\partial v_{d2}}{\partial \xi} + \frac{Z_{d0}}{M} \left( \frac{\partial \phi_2}{\partial \xi} \right) + \frac{Z_{d0}^2}{M^3} \phi_1 \left( \frac{\partial \phi_1}{\partial \xi} \right) + \frac{Z_{d1}}{M} \left( \frac{\partial \phi_1}{\partial \xi} \right) + Z_{d0} \left( \frac{\partial \phi_1}{\partial \tau} \right) = 0, \tag{25}$$

$$\frac{1}{M^2} \left( \frac{\partial^2 \phi_1}{\partial \xi^2} \right) - (n_{e0}k + n_{i0})\phi_2 - \left( \frac{n_{e0}}{2} k^2 - \frac{n_{i0}}{2} \right) \phi_1^2 - (n_{d0}Z_{d2} + n_{d1}Z_{d1} + n_{d0}Z_{d2}) = 0. \tag{26}$$

Now, differentiating Eq. (26) w.r.t.  $\xi$  we get,

$$\begin{aligned} & \frac{1}{M^2} \left( \frac{\partial^3 \phi_1}{\partial \xi^3} \right) - (n_{e0}k + n_{i0}) \left( \frac{\partial \phi_2}{\partial \xi} \right) - (n_{e0}k^2 - n_{i0}) \phi_1 \left( \frac{\partial \phi_1}{\partial \xi} \right) - n_{d0} \left( \frac{\partial Z_{d2}}{\partial \xi} \right) \\ & - n_{d1} \left( \frac{\partial Z_{d1}}{\partial \xi} \right) - Z_{d1} \left( \frac{\partial n_{d1}}{\partial \xi} \right) - Z_{d0} \left( \frac{\partial n_{d2}}{\partial \xi} \right) = 0 \end{aligned} \tag{27}$$

Now, eliminating all the 2<sup>nd</sup> order quantities from Eqs. from (24), (25) and (27) and adding all of them we get a nonlinear PDE with variable coefficient is of the form:

$$\left( \frac{\partial \phi_1}{\partial \tau} \right) + A\phi_1 \left( \frac{\partial \phi_1}{\partial \xi} \right) + B \left( \frac{\partial^3 \phi_1}{\partial \xi^3} \right) + C\phi_1 \left( \frac{\partial n_{d0}}{\partial \tau} \right) = 0, \tag{28}$$

where

$$\begin{aligned} A &= \frac{M}{(Z_{d0}M + Z_{d0}n_{d0})} \left[ \frac{Z_{d0}^2}{M} - \frac{1}{M} \left\{ \left( \frac{Z_{d0}}{M} \right)^2 + \left( \frac{n_{e0}k + n_{i0}}{n_{d0}} \right) \right\} + 2 \frac{Z_{d0}n_{d0}}{M^4} + (n_{e0}k - n_{i0}) \right] \\ &+ \frac{M}{(Z_{d0}M + Z_{d0}n_{d0})} \left[ \left( \frac{n_{e0}k + n_{i0}}{n_{d0}} \right) - 2 \frac{Z_{d0}n_{d0}}{M^2} \left\{ \left( \frac{Z_{d0}}{M} \right)^2 \right\} \right], \\ B &= \frac{-1}{M^3 Z_{d0} (n_{d0} + M)}, \\ C &= \left[ \frac{1}{Z_{d0}} + \frac{R^2}{MZ_{d0}} \right]. \end{aligned}$$

The above Eq. (28) is in the new form of the KdV equation known as mKdV equation, as there is an additional term due to the plasma inhomogeneity of number density. The solution of the above modified K-dV (mKdV) equation i.e., Eq. (28) represents the structural variations of nonlinear dust acoustic (DA) solitary waves propagating in inhomogeneous plasma. The nonlinear constant coefficient  $A$  and the dispersion coefficient  $B$  depend on the inhomogeneous number density. The extra term in the above considered inhomogeneous plasma model appears with the coefficient  $C$  due to the inhomogeneous number density gradient.

#### IV. SOLUTION OF MODIFIED K-dV (mKdV) EQUATION

We have considered the transformation<sup>38</sup>  $\phi_1 = \mu e^{-cn_{d0}}$  to get the solitary wave solution of the Eq. (28) for the KdV equation is of the form

$$\frac{\partial \mu}{\partial \tau} + P\mu \frac{\partial \mu}{\partial \xi} + Q \frac{\partial^3 \mu}{\partial \xi^3} = 0, \quad (29)$$

where  $P = Ae^{-cn_{d0}}$  and  $Q = B$ .

The above nonlinear coefficients  $P$  and  $Q$  functionally depends on the environment of the chosen plasma system. To reduce the complexities of the calculations, the variations are considered relatively small compared to the locally constants parameters. Now, we have considered a new frame of reference  $U = \xi - V\tau$  w.r.t. velocity  $V$  to solve the Eq. (29). After using this new frame of reference and the Kodama - Taniuti method [38], we have obtained the solution of Eq. (29) is as follows:

$$\mu = A_m \left[ \operatorname{sech}^2 \left( \frac{U}{W} \right) \right], \quad (30)$$

where  $W = \sqrt{\frac{4Q}{V}}$  and  $A_m = \frac{3V}{P}$  are the width and amplitude of the DA solitary wave respectively.

#### V. RESULTS AND DISCUSSION

In this paper, we have studied the nonlinear DA solitary waves to understand the structural variations of DA solitary wave while propagating in inhomogeneous, unmagnetized plasmas consisting of negatively charged dust grains. We have used the RPT method to derive an mKdV equation with the variable coefficients. We have considered appropriate stretched coordinates for both space and time to employ the RPT method. Then the Kodama-Taniuti method [38] is applied to get the DA solitary wave solution, and the numerical results for DA solitary wave propagation are obtained in Eq. (30). We have focused on the issues of structural variations of DA solitary waves in the above-considered plasma environment.

It is clear from the Eq.(23), the phase velocity  $M$  depends on the various choices of  $n_{e0}, n_{i0}, Z_{d0}$ , and  $k$ . Figures 1 to 4 shows the dependency of the phase velocity  $M$  with the inhomogeneous number density  $n_{d0}$  and with the various choices of parameters  $n_{e0}, Z_{d0}, k$ , and  $n_{i0}$ . Here, we have introduced the various figures of phase velocity depending on the various choices of parameters  $n_{e0}, Z_{d0}, k$ , and  $n_{i0}$  respectively. From Fig. 1, we have seen that the phase velocity of the DA solitary wave i.e.,  $M$  increases with the increase in the number density  $n_{d0}$ , with the less significance of  $n_{e0}$ . But in Fig. 2, the phase velocity  $M$  increases uniformly with the increasing values of  $Z_{d0}$  and  $n_{d0}$ . Similarly, Figs. 3 and 4 show the expanding rate of  $M$  w.r.t.  $n_{d0}$ , where the phase velocity  $M$  decreases with the increase in  $k$ . Also Figs. 3 and 4 also indicates the rapid decrease of the phase velocity with the increasing values of  $n_{i0}$ .

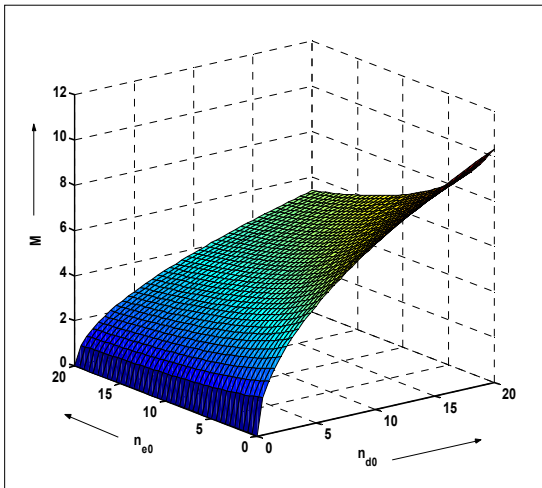


**Figure 1.** Dependency of phase velocity  $M$  with  $n_{d0}$  and  $n_{e0}$  and  $Z_{d0}$  at  $n_{i0} = 0.75, Z_{d0} = 2$ , and  $k = 0.1$

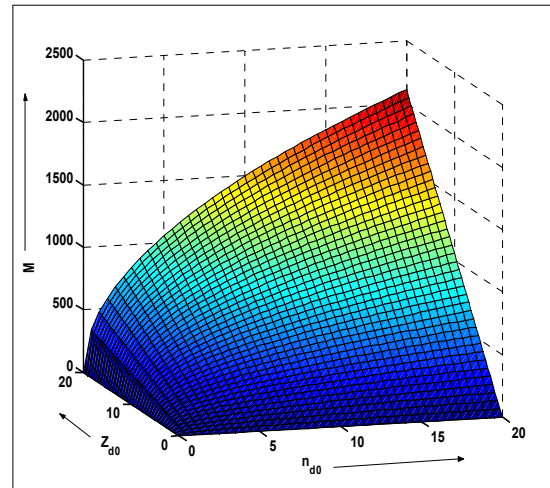


**Figure 2.** Dependency of phase velocity  $M$  at  $n_{e0} = 2, n_{i0} = 0.008$  and  $k = 1.5$

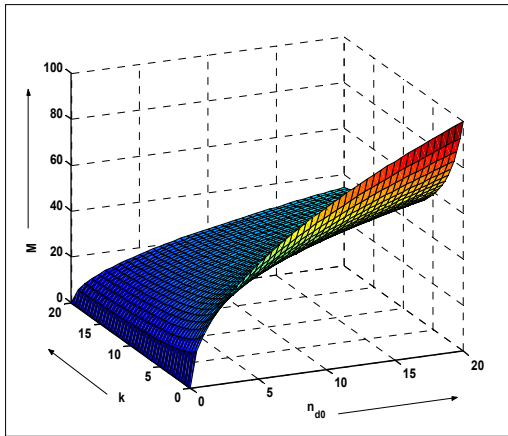


**Figure 3.** Dependency of phase velocity  $M$  with  $n_{d0}$  and  $k$  at  $n_{i0} = 0.008, n_{e0} = 0.003,$  and  $Z_{d0} = 2$

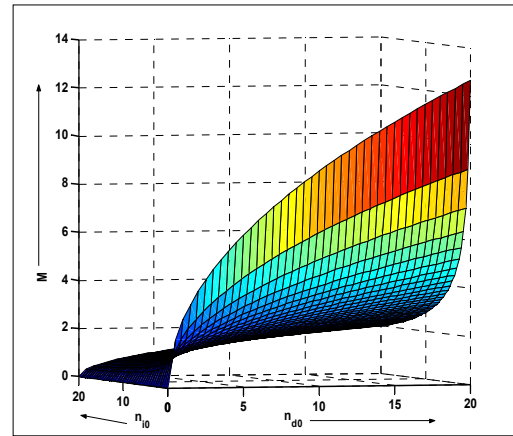


**Figure 4.** Dependency of phase velocity  $M$  with  $k = 1, n_{e0} = 0.03,$  and  $Z_{d0} = 2$

We have observed the coefficients  $A$  and  $P$  in the above Eqs. (28) and (29), which indicates the dependency of the amplitude  $A_m$  of the DA solitary waves on the parameters  $n_{e0}, n_{i0}, n_{d0}, Z_{d0},$  and  $k$ . Depending on the various choices of the values of  $n_{e0}, n_{i0}, n_{d0}, Z_{d0},$  and  $k$ , the structural variations in the amplitude of the DA solitary wave  $A_m$  w.r.t. the density gradient  $n_{d0}$  will be seen in Figs. 5, 6 and 7. Here, the Figs. 6 and 7 shows the variations in the amplitude of DA solitary wave  $A_m$  w.r.t.  $n_{d0}$ , which is increasing with the increasing values of  $k$  and  $n_{e0}$ , respectively.

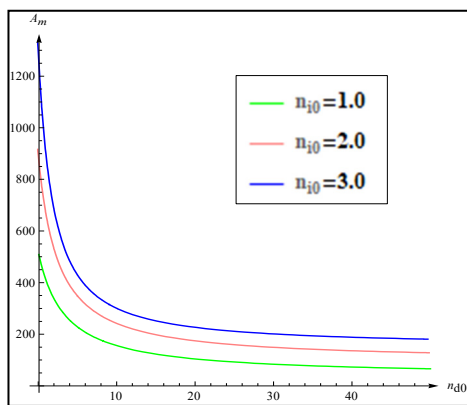


**Figure 5.** Structural variations of soliton amplitude  $A_m$  w.r.t  $n_{d0}$  for various choices of  $n_{i0} = 1, 2$  and  $3$  with  $n_{e0} = 2, Z_{d0} = 1.0$  and  $k = 0.2$

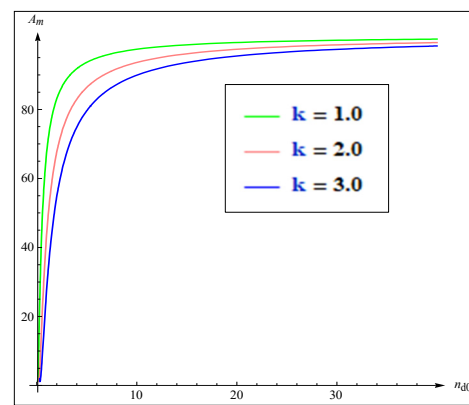


**Figure 6.** Structural variations of soliton amplitude  $A_m$  w.r.t  $n_{d0}$  for various choices of  $k = 1, 2$  and  $3$  with  $n_{e0} = 0.1, Z_{d0} = 1.0$  and  $n_{i0} = 0.001$

Based on the above results, it can be observed that with the increasing/decreasing of values of  $k$  and  $n_{e0}$ , the shape variations of the soliton amplitude will also be seen. With the increasing/decreasing of values of  $k$  and  $n_{e0}$ , the solitary wave amplitude will be increased/decreased, while on the other hand, in Fig. 5, the amplitude of the solitary wave will be decreased/increased with the increasing/decreasing values of  $n_{i0}$  simultaneously.

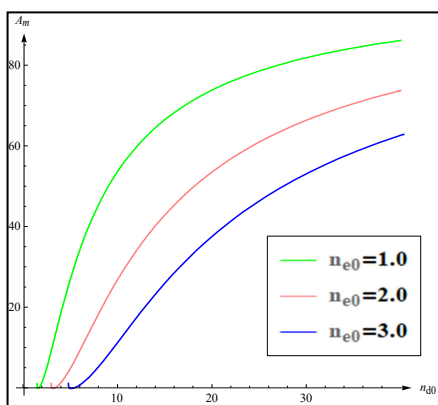


**Figure 7.** Structural variations of soliton amplitude  $A_m$  w.r.t  $n_{d0}$  for various choices of  $n_{e0} = 1, 2$  and  $3$  with  $n_{i0} = 0.01, Z_{d0} = 1.0$  and  $k = 1.5$

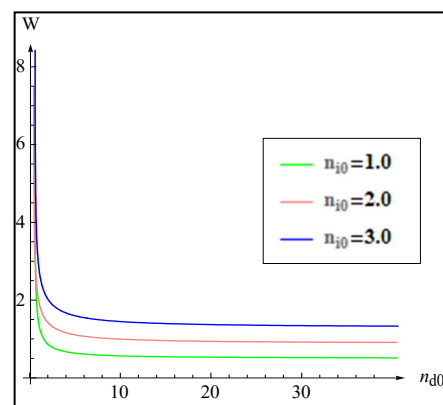


**Figure 8.** Structural variations of soliton width  $W$  w.r.t  $n_{d0}$  for various choices of  $n_{i0} = 1, 2$  and  $3$  with  $n_{e0} = 0.01, Z_{d0} = 1.0$  and  $k = 1.5$

We have also observed the coefficients  $B = Q$  in the above Eqs. (28) and (29), which indicates the dependency of the DA soliton width  $W$  on the parameters  $n_{e0}, n_{i0}, n_{d0}, Z_{d0}$ , and  $k$ . Figs. 8, 9, and 10 shows the shape variations of DA solitons and their width with inhomogeneous density gradient  $n_{d0}$  for the various choices of the parameters  $n_{i0}$  (Fig. 8),  $n_{e0}$  (Fig. 9) and  $k$  (Fig. 10) respectively. So, from Figs. 9 and 10, it can be observed that the width of the solitary wave  $W$  increases with the increasing values of  $n_{e0}$ , and  $k$ , respectively, while the fig. 8 indicates the decreasing of soliton width with the increase of  $n_{i0}$ . Thus, based on the above results and discussions, it can be observed that phase velocity  $M$  of the DA solitary wave depends on the various choices of the parameters  $n_{e0}, n_{i0}, Z_{d0}$ , and  $k$ . Figures 1 to 4 show the dependency of the phase velocity  $M$  with the inhomogeneous number density  $n_{d0}$  and the other parameters  $n_{e0}, Z_{d0}, k$ , and  $n_{i0}$ . It can be ensured from figures 1 to 4 that due to the increase in the dust number density  $n_{d0}$ , the phase velocity of the solitary wave becomes larger during the propagation of the solitary waves in the plasma.

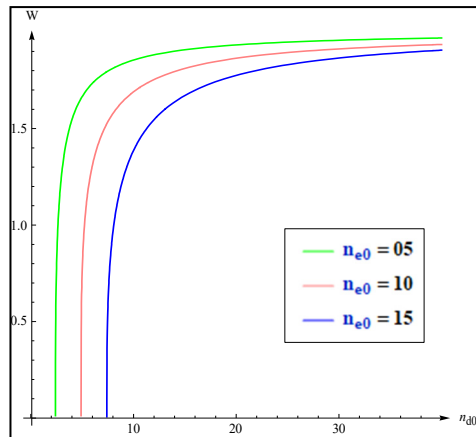


**Figure 9.** Structural variations of soliton width  $W$  w.r.t  $n_{d0}$  for various choices of  $n_{e0} = 5, 10$  and  $15$  with  $k = 0.5$ , and  $n_{i0} = 2$

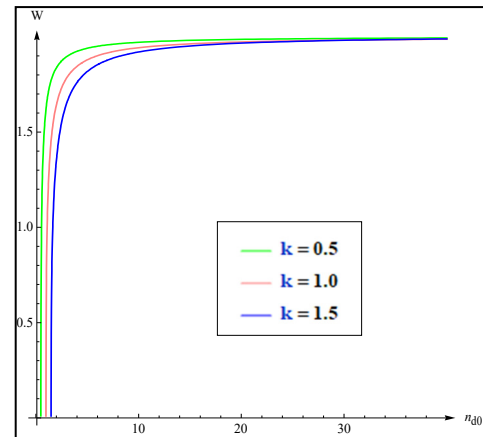


**Figure 10.** Structural variations of soliton width  $W$  w.r.t  $n_{d0}$  for various choices of  $k = 0.5, 1.0$  and  $1.5$  with  $n_{e0} = 0.01$ , and  $n_{i0} = 0.1$

Also, the solitary waves experience more deformation due to the faster compression and vibrations of intermolecular interactions in ions, electrons, and dust particles in the plasma system. So, the DA solitary waves produce variations in the soliton structures while propagating in an inhomogeneous plasma. The variations of structures in the amplitude  $A_m$  and width  $W$  of the DA solitary waves also occur with the increasing/decreasing of number density  $n_{d0}$ . While the DA soliton propagates in inhomogeneous plasma, it gets deflected due to plasma inhomogeneity i.e., the number density  $n_{d0}$ . From the above figures (Fig. 5), it can be observed that with the increase in number density and ion density profile, the smaller the soliton amplitude. Also, the higher the number density, electron density, and ratio of temperature difference, the higher the soliton amplitude which is shown in Fig (6, 7). Similarly, when the number density and ion density increase, the width of the solitary wave decreases (Fig. 8) Also, when the number density and electron density increase, the width of the solitary wave is increased Fig (9, 10). Thus, it can be ensured that the structure of the solitary waves varies with the variations of amplitude and width of the DA solitary waves. From the above observations, it is observed that the amplitude with the width of the solitary waves slightly deforms during the propagations in inhomogeneous plasma. So, it ensures the shape conservation of solitary structures as the first principle of K-dV soliton.

## VI. CONCLUSION

In this work, theoretically, we have studied variations in the structures of DA solitary wave propagations in inhomogeneous unmagnetized dusty plasma. We have considered collisionless, hot isothermal and Boltzmannian distributed ions and electrons, with negatively charged dust grains in weakly inhomogeneous plasmas. In our problem, the basic governing fluid equations are considered and the reductive perturbation technique (RPT) is employed to solve the modified KdV (mKdV) equation. We have used an appropriate set of stretched variable to use the RPT in the governing fluid equations of plasmas. Due to inhomogeneity in the plasma system, an extra term arises in the modified KdV (mKdV) equation associated with charged dust particles and the inhomogeneous density gradient. During the investigations, we have also studied the structural variations of amplitude and width of the DA solitary waves depending on the various choices of the parameters i.e., number density of the dust grains ( $n_{d0}$ ), electron number density ( $n_{e0}$ ), temperature ratio of ion to electron ( $k$ ), and the ion number density ( $n_{i0}$ ).

In this paper, primarily, we have studied the variations in soliton structures of DA solitary wave propagation in inhomogeneous plasmas. But during the investigations, we have also observed and established a relation between amplitude  $A_m$  and width  $W$  of the dust acoustic (DA) solitons shown in the eq. (30). The Eq. (30) implies that if the plasma inhomogeneity is neglected, the soliton amplitude  $A_m$  will increase with the decrease in soliton width  $W$ . But based on the various choices of the parameters  $n_{e0}$  and  $n_{i0}$ , the relation between the amplitude  $A_m$  and width  $W$ , shown in the eq. (30), has been changed captiously. Also, from the above results, it is clear that  $A_m$  and  $W$  increase with the

increase in  $n_{e0}$  (Figs. 7 and 9). Similarly,  $A_m$  and  $W$  decrease with the increase in  $n_{d0}$  (Figs. 5 and 8). Thus, from all the results and discussion, it can be concluded that the variations in the soliton structures are modified proportionately due to the presence of plasma inhomogeneity. Features like reflection, refraction, transmission, etc., i.e., variations in soliton structure, are also vital and relevant features in the inhomogeneous plasma systems.

**Data Availability.** There is no data associated with it.

#### ORCID IDs

✉ **Hirak Jyoti Dehingia**, <https://orcid.org/0000-0002-3119-0842>; ✉ **P.N. Deka**, <https://orcid.org/0000-0001-9485-9294>

#### REFERENCES

- [1] L. Spitzer Jr., "Review of Publications: Physical Processes in the Interstellar Medium", *Journal of the Royal Astronomical Society of Canada*, **72**, 349 (1978).
- [2] B.A. Smith, L. Soderblom, R. Batson, P. Bridges, J.A.Y. Inge, H. Masursky, E. Shoemaker, et al., "A new look at the Saturn system: The Voyager 2 images", *Science*, **215**(4532), 504-537 (1982). <https://doi.org/10.1126/science.215.4532.504>
- [3] K.G. Spears, T.J. Robinson, and R.M. Roth, "Particle distributions and laser-particle interactions in an RF discharge of silane", *IEEE transactions on plasma science*, **14**(2), 179-187 (1986). <https://doi.org/10.1109/TPS.1986.4316521>
- [4] W. Xu, B. Song, R.L. Merlino, and N. D'Angelo, "A dusty plasma device for producing extended, steady state, magnetized, dusty plasma columns", *Review of scientific instruments*, **63**(11), 5266 (1992). <https://doi.org/10.1063/1.1143438>
- [5] D.P. Sheehan, M. Carillo, and W. Heidbrink, "Device for dispersal of micrometer- and submicrometer-sized particles in vacuum", *Review of scientific instruments*, **61**(12), 3871-3875 (1990). <https://doi.org/10.1063/1.1141515>
- [6] C.K. Goertz, "Dusty plasmas in the solar system", *Reviews of Geophysics*, **27**(2), 271-292 (1989). <https://doi.org/10.1029/RG027i002p00271>
- [7] T.G. Northrop, "Dusty plasmas", *Physica Scripta*, **45**(5), 475 (1992). <https://doi.org/10.1088/0031-8949/45/5/011>
- [8] N.N. Rao, P.K. Shukla, and M.Y. Yu, "Dust-acoustic waves in dusty plasmas", *Planetary and space science*, **38**(4), 543 (1990). [https://doi.org/10.1016/0032-0633\(90\)90147-1](https://doi.org/10.1016/0032-0633(90)90147-1)
- [9] P.K. Shukla, and V.P. Silin, "Dust ion-acoustic wave", *Physica Scripta*, **45**(5), 508. <https://doi.org/10.1088/0031-8949/45/5/015>
- [10] F. Melandso, "Lattice waves in dust plasma crystals", *Physics of Plasmas*, **3**(11), 3890 (1996). <https://doi.org/10.1063/1.871577>
- [11] A. Barkan, N. D'Angelo, and R.L. Merlino, "Experiments on ion-acoustic waves in dusty plasmas", *Planetary and Space Science*, **44**(3), 239 (1996). [https://doi.org/10.1016/0032-0633\(95\)00109-3](https://doi.org/10.1016/0032-0633(95)00109-3)
- [12] A. Barkan, R.L. Merlino, and N. D'Angelo, "Laboratory observation of the dust-acoustic wave mode", *Physics of Plasmas*, **2**(10), 3563-3565 (1995). <https://doi.org/10.1063/1.871121>
- [13] F. Verheest, "Waves and instabilities in dusty space plasmas", *Space Science Reviews*, **77**(3), 267 (1996). <https://doi.org/10.1007/BF00226225>
- [14] P.K. Shukla, "A survey of dusty plasma physics", *Physics of Plasmas*, **8**(5), 1791 (2001). <https://doi.org/10.1063/1.1343087>
- [15] F. Verheest, *Waves in dusty space plasmas*, Vol. 245, (Springer Science, Business Media, 2000).
- [16] P.K. Shukla, and A.A. Mamun, *Introduction to dusty plasma physics*, (Institute of Physics Publishing Ltd, Bristol, 2015), pp. 450. ISBN 9781420034103.
- [17] M.G.M. Anowar, and A.A. Mamun, "Effects of two-temperature electrons and trapped ions on multidimensional instability of dust-acoustic solitary waves", *IEEE Transactions on plasma science*, **37**(8), 1638 (2009). <https://doi.org/10.1109/TPS.2009.2024668>
- [18] T.K. Baluku, and M.A. Hellberg, "Kinetic theory of dust ion acoustic waves in a kappa-distributed plasma", *Physics of Plasmas*, **22**(8), 083701 (2015). <https://doi.org/10.1063/1.4927581>
- [19] H. Alinejad, and V. Khorrami, "Effects of Polarized Debye Sheath and Trapped Ions on Solitary Structures in a Strongly Coupled Inhomogeneous Dusty Plasma", *IEEE Transactions on Plasma Science*, **46**(4), 755 (2017). <https://doi.org/10.1109/TPS.2017.2749382>
- [20] A. Atteya, M.A. El-Borie, G.D. Roston, and A.S. El-Helbawy, "Nonlinear dust acoustic waves in an inhomogeneous magnetized quantum dusty plasma", *Waves in Random and Complex Media*, **31**, 1 (2021). <https://doi.org/10.1080/17455030.2021.1880030>
- [21] R. Bharuthram, and P.K. Shukla, "Large amplitude ion-acoustic solitons in a dusty plasma", *Planetary and space science*, **40**(7), 973 (1992). [https://doi.org/10.1016/0032-0633\(92\)90137-D](https://doi.org/10.1016/0032-0633(92)90137-D)
- [22] A.A. Mamun, and P.K. Shukla, "Cylindrical and spherical dust ion-acoustic solitary waves", *Physics of Plasmas*, **9**(4), 1468 (2002). <https://doi.org/10.1063/1.1458030>
- [23] P.K. Shukla, "Dust ion-acoustic shocks and holes", *Physics of Plasmas*, **7**(3), 1044 (2000). <https://doi.org/10.1063/1.873905>
- [24] S.I. Popel, M.Y. Yu, and V.N. Tsytovich, "Shock waves in plasmas containing variable-charge impurities", *Physics of Plasmas*, **3**(12), 4313 (1996). <https://doi.org/10.1063/1.872048>
- [25] F. Melandso, and P.K. Shukla, "Theory of dust-acoustic shocks", *Planetary and Space Science*, **43**(5), 635 (1995). [https://doi.org/10.1016/0032-0633\(94\)00200-B](https://doi.org/10.1016/0032-0633(94)00200-B)
- [26] P.K. Shukla, and A.A. Mamun, "Dust-acoustic shocks in a strongly coupled dusty plasma", *IEEE transactions on plasma science*, **29**(2), 221 (2001). <https://doi.org/10.1109/27.923698>
- [27] A.A. Mamun, R.A. Cairns, and P.K. Shukla, "Solitary potentials in dusty plasmas", *Physics of Plasmas*, **3**(2), 702-704 (1996). <https://doi.org/10.1063/1.871905>
- [28] J.X. Ma, and J. Liu, "Dust-acoustic soliton in a dusty plasma", *Physics of plasmas*, **4**(2), 253 (1997). <https://doi.org/10.1063/1.872086>
- [29] B. Farokhi, P.K. Shukla, N.L. Tsintsadze, and D.D. Tskhakaya, "Linear and nonlinear dust lattice waves in plasma crystals", *Physics Letters A*, **264**(4), 318 (1999). [https://doi.org/10.1016/S0375-9601\(99\)00820-8](https://doi.org/10.1016/S0375-9601(99)00820-8)
- [30] H.U. Rehman, "Electrostatic dust acoustic solitons in pair-ion-electron plasmas", *Chinese Physics Letters*, **29**(6), 065201 (2012). <https://doi.org/10.1088/0256-307X/29/6/065201>

- [31] S.K. El-Labany, W.F. El-Taibany, A.E. El-Samahy, A.M. Hafez, and A. Atteya, “Higher-order corrections to nonlinear dust-ion-acoustic shock waves in a degenerate dense space plasma”, *Astrophysics and Space Science*, **354**(2), 385 (2014). <https://doi.org/10.1007/s10509-014-2096-3>
- [32] L.B. Gogoi, and P.N. Deka, “Propagation of dust acoustic solitary waves in inhomogeneous plasma with dust charge fluctuations”, *Physics of Plasmas*, **24**(3), 033708 (2017). <https://doi.org/10.1063/1.4977988>
- [33] A. Atteya, S. Sultana, and R. Schlickeiser, “Dust-ion-acoustic solitary waves in magnetized plasmas with positive and negative ions: The role of electrons superthermality”, *Chinese journal of physics*, **56**(5), 1931 (2018). <https://doi.org/10.1016/j.cjph.2018.09.002>
- [34] W.F. El-Taibany, W.M. Moslem, M. Wadati, and P.K. Shukla, “On the instability of electrostatic waves in a nonuniform electron–positron magnetoplasma”, *Physics Letters A*, **372**(22), 4067 (2008). <https://doi.org/10.1016/j.physleta.2008.03.024>
- [35] N. Akhtar, S.A. El-Tantawy, S. Mahmood, and A.M. Wazwaz, “On the dynamics of dust-acoustic and dust-cyclotron freak waves in a magnetized dusty plasma”, *Romanian Reports in Physics*, **71**, 403 (2019). <https://rrp.nipne.ro/2019/AN71403.pdf>
- [36] H. Ur-Rehman, S. Mahmood, and S. Hussain, “Magneto-acoustic solitons in pair-ion fullerene plasma”, *Waves in Random and Complex Media*, **30**(4), 632 (2020). <https://doi.org/10.1080/17455030.2018.1549762>
- [37] H. Washimi, and T. Taniuti, “Propagation of ion-acoustic solitary waves of small amplitude”, *Physical Review Letters*, **17**(19), 996 (1966). <https://doi.org/10.1103/PhysRevLett.17.996>
- [38] Y. Kodama, and T. Taniuti, “Higher order approximation in the reductive perturbation method. I. The weakly dispersive system”, *Journal of the Physical Society of Japan*, **45**(1), 298 (1978). <https://doi.org/10.1143/JPSJ.45.298>
- [39] H.R. Pakzad, and D. Nobahar, “Dust-ion acoustic solitons in superthermal dusty plasmas”, *New Astronomy*, **93**, 101752 (2022). <https://doi.org/10.1016/j.newast.2021.101752>
- [40] N.N. Rao, and P.K. Shukla, “Nonlinear dust-acoustic waves with dust charge fluctuations”, *Planetary and Space Science*, **42**(3), 221 (1994). [https://doi.org/10.1016/0032-0633\(94\)90084-1](https://doi.org/10.1016/0032-0633(94)90084-1)
- [41] H.J. Dehingia, and P.N. Deka, *Structural Variations of Ion-Acoustic Solitons, in Nonlinear Dynamics and Applications*, (Springer, Cham., 2022), pp. 97-104. [https://doi.org/10.1007/978-3-030-99792-2\\_8](https://doi.org/10.1007/978-3-030-99792-2_8)

### СТРУКТУРНІ ВАРІАЦІЇ ПИЛОВИХ АКУСТИЧНИХ СОЛІТОННИХ ХВИЛЬ (ПАСХ), ЯКІ ПОШИРЮЮТЬСЯ В НЕОДНОРІДНІЙ ПЛАЗМІ

Хірак Джіоті Дехінгія, П.Н. Дека

Факультет математики, Університет Дібругарх, Ассам, Індія

Ця стаття представляє наші теоретичні дослідження структурних варіацій пилових акустичних солітонних хвиль (DASW) у неоднорідній ненамагніченій плазмі. Для вивчення структурних варіацій DASW ми розглянули беззіткнівний, гарячий ізотермічний і больцманівський розподіл електронів-іонів з негативно зарядженими порошинками в слабо неоднорідній плазмі. Ми використали метод редукованих збурень (RPT) у керуючих рівняннях плазми, вивели модифіковане рівняння Кортевега-де-Фріза (m-KdV) і отримали розв'язок із самотньою хвилею. Ми розглянули відповідні розтягнуті координати для просторових і часових змінних для неоднорідної плазми. У цій статті досліджено вплив частинок пилу на поширення іонно-акустичних солітонних хвиль у моделі неоднорідної плазми. Ми також включили вплив параметрів неоднорідності на солітонні структури.

**Ключові слова:** пилова плазма; метод редукованих збурень (RPT); ізотермічні електрони; неоднорідна плазма

# THE INFLUENCE OF DEFORMATION PHASE-SPACE ON SPECTRA OF HEAVY QUARKONIA IN IMPROVED ENERGY POTENTIAL AT FINITE TEMPERATURE MODEL OF SHRODINGER EQUATION VIA THE GENERALIZED BOPP'S SHIFT METHOD AND STANDARD PERTURBATION THEORY<sup>†</sup>

 **Abdelmadjid Maireche**

*Department of Physics, M'sila University, PMC Laboratory, M'sila University, Algeria*

*Corresponding Author e-mail: [abdelmadjid.maireche@univ-msila.dz](mailto:abdelmadjid.maireche@univ-msila.dz)*

Received November 20, 2022; revised December 13, 2022; accepted December 15, 2022

In this work, we obtain solutions of the deformed Schrödinger equation (DSE) with improved internal energy potential at a finite temperature model in a 3-dimensional nonrelativistic noncommutative phase-space (3D-NRNCPS) symmetries framework, using the generalized Bopp's shift method in the case of perturbed nonrelativistic quantum chromodynamics (pNRQCD). The modified bound state energy spectra are obtained for the heavy quarkonium system such as charmonium  $c\bar{c}$  and bottomonium  $b\bar{b}$  at finite temperature. It is found that the perturbative solutions of the discrete spectrum are sensible to the discrete atomic quantum numbers  $(j, l, s, m)$  of the  $Q\bar{Q}$  ( $Q = c, b$ ) state, the parameters of internal energy potential  $(T, \alpha_s(T), m_D(T), \beta, c)$ , which are the Debye screening mass  $m_D(T)$ , the running coupling constant  $\alpha_s(T)$ , the critical temperature  $\beta$ , the free parameter  $c$  in addition to noncommutativity parameters  $(\theta, \bar{\theta})$ . The new Hamiltonian operator in 3D-NRNCPS symmetries is composed of the corresponding operator in commutative phase-space and three additive parts for spin-orbit interaction, the new magnetic interaction, and the rotational Fermi-term. The obtained energy eigenvalues are applied to obtain the mass spectra of heavy quarkonium systems ( $c\bar{c}$  and  $b\bar{b}$ ). The total complete degeneracy of the new energy levels of the improved internal energy potential changed to become equal to the new value  $3n^2$  in 3D-NRNCPS symmetries instead of the value  $n^2$  in the symmetries of 3D-NRQM. Our non-relativistic results obtained from DSE will possibly be compared with the Dirac equation in high-energy physics.

**Keywords:** *Schrödinger equation; noncommutative phase-space; internal energy potential at finite temperature; Bopp shift method; heavy quarkonium systems*

**PACS:** 03.65.-w; 03.65. Ge; 03.65. Ca; 12.39. Jh

## 1. INTRODUCTION

It is well known that the ordinary Schrödinger equation (SE) describes the dynamics of quantum systems at low energy without considering the temperature effect. Recently, the finite temperature SE allows us to study quantum systems such as superconductivity mechanisms and Bose-Einstein condensates at an arbitrary temperature, and when the temperature is equal to zero, it becomes identical to the SE [1]. Very recently, many authors have studied the finite-temperature SE for hot quark-gluon plasma, heavy quarkonia in quark-gluon plasma, (electron and proton systems), and so on [2-5]. The problem of calculating the energy spectra of the SE with various types of potentials such as the internal energy potential and the Cornell potential at finite temperature has been attracting interest in recent years [2-8]. Abu-Shady has studied heavy-quarkonium mesons (HLM) using an internal energy potential and obtained wave function and energy spectra by solving SE using AEIM when the finite temperature is included [7]. The main objective is to develop the research article [7] and expand it to the large symmetry known by nonrelativistic noncommutative phase-space (NRNCPS) to achieve a more accurate physical vision so that this study becomes valid in the field of nanotechnology. Noncommutative quantum mechanics is an old idea that has been extensively discussed in the literature. It should be noted that noncommutativity (NC) was first introduced by Heisenberg in 1930 [9] and then by Snyder in 1947 [10]. It has appeared since the beginning of ordinary quantum mechanics. There has been a growing interest in this field since the discovery of string theory and the modified uncertainty principle. In addition, the NC idea is suggested as a result of the production of quantum gravity. It would provide a natural background for finding a suitable solution for a possible regularization of QFT [11-23]. During the past three decades, the NC theory has been the focus of extensive investigation and has produced a very interesting new class of quantum field theories with intriguing and occasionally unexpected properties [24]. Thus, the topographical properties of the NC space-space and phase-phase have a clear effect on the various physical properties of quantum systems and this has been a very interesting field in many fields of physics. The idea of noncommutativity has been studied in many articles, such as [24-36]. On the other hand, we explore the possibility of creating new applications and more profound interpretations in the sub-atomics and nanoscales using a new version of the improved internal energy potential, which has the following form:

$$V_{ip}(r) = F_1(r, T) - T \frac{\partial F_1(r, T)}{\partial T} \rightarrow V_{ip}(\hat{r}) = V_{ip}(r) + \left( \frac{A_1}{2r} - \frac{A_2}{2r^2} + \frac{D_3}{2r^3} - \frac{A_4}{2} r - \frac{A_3}{2} \right) \exp(-m_D(T)r) \vec{\mathbf{L}} \vec{\mathbf{\theta}} \quad (1)$$

<sup>†</sup> **Cite as:** A. Maireche, East Eur. J. Phys. 1, 28 (2023), <https://doi.org/10.26565/2312-4334-2023-1-03>

© A. Maireche, 2023

We refer to this term  $\vec{L}\vec{\theta}$  and the parameters  $(\mathbf{A}_1, \mathbf{A}_1, \mathbf{A}_1, \mathbf{A}_1, \mathbf{D}_3, \mathbf{m}_D(T))$  in the materials and methods section. The new structure of 3D-NRNCPS is based on new canonical commutation relations in both Schrödinger SP and Heisenberg HP, respectively, as follows (Throughout this paper, the natural units  $\mathbf{c} = \mathbf{h} = \mathbf{1}$  will be used) [36-46]:

$$[x_\mu, p_\nu] = i\delta_{\mu\nu}\hbar \rightarrow [\hat{x}_\mu^*, \hat{p}_\nu] = [\hat{x}_\mu(t)^*, \hat{p}_\nu(t)] = i\delta_{\mu\nu}\hbar_{eff} \Rightarrow |\Delta\hat{x}_\mu\Delta\hat{p}_\nu| \geq \frac{\hbar_{eff}\delta_{\mu\nu}}{2}, \quad (2.1)$$

and

$$[x_\mu, x_\nu] = 0 \rightarrow [\hat{x}_\mu^*, \hat{x}_\nu] = [\hat{x}_\mu(t)^*, \hat{x}_\nu(t)] = i\theta_{\mu\nu} \Rightarrow |\Delta\hat{x}_\mu\Delta\hat{x}_\nu| \geq \left|\frac{\theta_{\mu\nu}}{2}\right|, \quad (2.2)$$

and

$$[p_\mu, p_\nu] = 0 \rightarrow [\hat{p}_\mu^*, \hat{p}_\nu] = [\hat{p}_\mu(t)^*, \hat{p}_\nu(t)] = i\bar{\theta}_{\mu\nu} \Rightarrow |\Delta\hat{p}_\mu\Delta\hat{p}_\nu| \geq \left|\frac{\bar{\theta}_{\mu\nu}}{2}\right|, \quad (2.3)$$

the indices  $\mu, \nu \equiv \overline{1,3}$ ,  $\hbar_{eff}$  equal  $\hbar\left(1 + \frac{\theta\bar{\theta}}{4}\right)$  denote the effective Planck constant. This means that the principle of uncertainty of Heisenberg is generalized to include another two new uncertainties related to the positions  $(\hat{x}_\mu, \hat{x}_\nu)$  and the momenta  $(\hat{p}_\mu, \hat{p}_\nu)$ , in addition to the ordinary uncertainty  $(\hat{x}_\mu, \hat{p}_\nu)$ . The non-commutativity of the phase-space is based on the deformed Heisenberg–Weyl algebra, which is represented by the above commutation relations. here  $\theta_{\mu\nu}$  and  $\bar{\theta}_{\mu\nu}$  are invertible antisymmetric real constant  $(3 \times 3)$  matrices which satisfied  $\theta_{\mu\nu} = \varepsilon_{\mu\nu}\theta$  and  $\bar{\theta}_{\mu\nu} = \varepsilon_{\mu\nu}\bar{\theta}$ , with  $\varepsilon_{\mu\nu} = -\varepsilon_{\nu\mu}$  and  $\varepsilon_{\mu\mu} = 0$ , here  $(\theta, \bar{\theta})$  are interpreted as being new constants in the quantum theory. The very small two parameters  $(\theta^{\mu\nu}$  and  $\bar{\theta}^{\mu\nu})$  (compared to the energy) are elements of two antisymmetric real matrixes, parameters of non-commutativity, and  $(*)$  denote the Weyl Moyal star product, which is generalized between two arbitrary functions  $(f, g)(x, p)$  to the new form  $\hat{f}(\hat{x}, \hat{p})\hat{g}(\hat{x}, \hat{p}) \equiv (f * g)(x, p)$  in the 3D-NRNCPS symmetries as follows [47-55]:

$$(fg)(x, p) \rightarrow (f * g)(x, p) = \left(fg - \frac{i}{2}\theta^{\mu\nu}\partial_\mu^x f \partial_\nu^x g - \frac{i}{2}\bar{\theta}^{\mu\nu}\partial_\mu^p f \partial_\nu^p g\right)(x, p). \quad (3)$$

The second and third terms in the above equation are the present effects of (space-space) and (phase-phase) noncommutativity properties. However, the new operators  $\hat{\xi}(t) = (\hat{x}_\mu \vee \hat{p}_\mu)(t)$  in HP are depending on the corresponding new operators  $\hat{\xi} = \hat{x}_\mu \vee \hat{p}_\nu$  in SP from the following projection relations:

$$\chi(t) = \exp\left(\frac{i}{\hbar}\hat{H}_{ip}(t-t_0)\right)\chi \exp\left(-\frac{i}{\hbar}\hat{H}_{ip}(t-t_0)\right) \Rightarrow \hat{\chi}(t) = \exp\left(\frac{i}{\hbar_{eff}}\hat{H}_{nc}^{ip}(t-t_0)\right) * \hat{\chi} * \exp\left(-\frac{i}{\hbar_{eff}}\hat{H}_{nc}^{ip}(t-t_0)\right), \quad (4)$$

Here  $\chi = x_\mu \vee p_\nu$  and  $\chi(t) = (x_\mu \vee p_\nu)(t)$ . The dynamics of the new systems  $\frac{d\hat{\chi}(t)}{dt}$  are described by the following motion equations in 3D-NRNCPS symmetries:

$$\frac{d\chi(t)}{dt} = \frac{i}{\hbar}[\chi(t), \hat{H}_{ip}] + \frac{\partial\chi(t)}{\partial t} \Rightarrow \frac{d\hat{\chi}(t)}{dt} = \frac{i}{\hbar_{eff}}[\hat{\xi}(t)^*, \hat{H}_{nc}^{ip}] + \frac{\partial\hat{\chi}(t)}{\partial t}. \quad (5)$$

The two operators  $(\hat{H}_{nc}^{ip}$  and  $\hat{H}_{ip})$  are present as the quantum Hamiltonian operators for the internal energy potential and the improved internal energy potential in the 3D-NRNCPS symmetries and their extension. This paper consists of five sections and the organization scheme is given as follows: In the next section, the theory part, we briefly review the SE with internal energy potential at finite temperature based on refs. [7-8]. Section 3 is devoted to studying the DSE by applying the generalized Bopp's shift method and obtaining the improved internal energy potential and the modified spin-orbit operator at finite temperature. Then, we applied the standard perturbation theory to find the quantum spectrum of the ground state, the first excited state, and the  $(n, l, m)^{th}$  excited state produced by the effects of modified spin-orbit and newly modified Zeeman interactions. In the fourth section, a discussion of the main results is presented in addition to determining the new formula for determining the mass spectra of the quarkonium system in the 3D-NRNCPS symmetries framework. Finally, in the last section, a summary and conclusions are presented.

## 2. THEORY

### 2.1. Overview of the eigenfunctions and energy eigenvalues for the internal energy potential at finite temperature in the 3D-NRNCPS symmetries framework

As already mentioned, our objective was to obtain the spectrum of the improved internal energy potential at finite temperatures. To achieve this goal, it is useful to summarize the time-independent Schrödinger equation for the internal energy potential at a finite temperature [7-8]:

$$V_{ip}(r) = F_1(r, T) - T \frac{\partial F_1(r, T)}{\partial T}, \quad (6)$$

where  $F_1(r, T)$  is determined from:

$$F_1(r, T) = \left(cr - \frac{4}{3}\frac{\alpha_s(T)}{r}\right) \exp(-m_D(T)r),$$

and  $m_D(T)$  is the Debye screening mass,  $c$  is a free parameter, the running coupling constant

$$\alpha_s(T) = \frac{2\Pi}{11-2/3n_f \ln(T/\beta T_c)}$$

Here  $n_f$ ,  $T_c$  and  $\beta$  are the number of quark flavors, the critical temperature, and  $(0,104 \pm 0.009)$ , respectively, the relative spatial coordinate between the two quarks is  $r$ . By substituting  $F_1(r, T)$  into Eq. (6), we obtain the internal energy potential that satisfies the following equation at a finite temperature [7-8]:

$$V_{ip}(r) = \left(D_2 + \frac{D_3}{r} + D_4 r + D_5 r^2\right) \exp(-m_D(T)r), \tag{7}$$

where

$$\begin{aligned} d_2 &= -2\mu D_2 = \frac{8\mu T}{3} \alpha_s(T) \frac{dm_D(T)}{dT}, \\ d_3 &= -2\mu D_3 = \frac{8\mu}{3} \alpha_s(T) + \frac{16\mu\Pi(11-2/3n_f)}{3[11-2/3n_f \ln(T/\beta T_c)]^2}, \\ d_4 &= -2\mu D_4 = -2\mu c, \end{aligned}$$

and

$$d_5 = -2\mu D_5 = 2\mu c T \frac{dm_D(T)}{dT}.$$

If we insert this potential into the Schrödinger equation, the radial part function  $U_{nl}(r) = \frac{R_{nl}(r)}{r}$  is given as:

$$\frac{d^2 U_{nl}(r)}{dr^2} + \frac{2}{r} \frac{dU_{nl}(r)}{dr} + 2\mu \left\{ E - \left( D_2 + \frac{D_3}{r} + D_4 r + D_5 r^2 \right) \exp(-m_D(T)r) - \frac{l(l+1)}{2\mu r^2} \right\} U_{nl}(r) = 0, \tag{8}$$

and

$$\frac{d^2 R_{nl}(r)}{dr^2} + 2\mu \left[ E - \left( D_2 + \frac{D_3}{r} + D_4 r + D_5 r^2 \right) \exp(-m_D(T)r) - \frac{l(l+1)}{2\mu r^2} \right] R_{nl}(r) = 0. \tag{9}$$

The reduced mass  $\mu$  for the quarkonium particle for example  $(c\bar{c}$  and  $b\bar{b})$  equal  $\frac{m_q m_{\bar{q}}}{m_q + m_{\bar{q}}}$ . The complete wave function

$\Psi_{nlm}(r, \theta, \phi) = \frac{R_{nl}(r)}{r} Y_l^m(\theta, \phi)$  is given by [7]:

$$\Psi_{nlm}(r, \theta, \phi) = N_{nl} \prod_{i=1}^n (r - \alpha_i) r^{\delta-1} \exp(-1/2\alpha r^2 - \beta r) Y_l^m(\theta, \phi). \tag{10}$$

Also, the energy  $E_{nl}$  of the potential in Eq. (7) is determined from the following equation:

$$E_{nl} = \frac{1}{2\mu} [\alpha(1 + 2(\delta + n) - \beta^2 - d_2 + m_D(T)d_3)], \tag{11}$$

where  $N_{nl}$  is a normalizing constant,  $n$  is a natural number accounting for the radial excitation, while  $l$  is a non-negative integer number that represents the orbital angular momentum,

$$\left. \begin{aligned} \alpha &= \sqrt{d_4 m_D - d_5 - \frac{d_2}{2} m_D^2} \\ \beta &= \frac{d_2 m_D - d_4 - d_3 m_D^2}{2\sqrt{d_4 m_D - d_5 - \frac{d_2}{2} m_D^2}} \\ \delta &= \frac{1}{2} \left( 1 \pm \sqrt{1 + 4(l + 1/2)^2 - 1/4} \right) \end{aligned} \right\}$$

### 3. MATERIALS AND METHODS

#### 3.1. DSE solution for an improved new internal energy potential at finite temperature in pNRQCD

In this subsection, we shall give an overview of a brief preliminary investigation of the improved internal energy potential in 3D-NRNCPS symmetries. To perform this task, the physical form of DSE, it is necessary to replace the ordinary three-dimensional Hamiltonian operators  $\hat{H}_{ip}(x_\mu, p_\mu)$ , the complex wave function  $\Psi(\vec{r})$ , and energy  $E_{nl}$  with the new three Hamiltonian operators  $\hat{H}_{nc}^{ip}(\hat{x}_\mu, \hat{p}_\mu)$ , the new complex wave function  $\Psi(\hat{r})$ , and new values  $E_{nc}^{ip}$ , respectively. In addition to replacing the ordinary product with the Weyl-Moyal star product, which allows us to construct the DSE in the 3D-NRNCPS symmetries framework as [55-60]:

$$\frac{d^2 R_{nl}(r)}{dr^2} + 2\mu \left[ E_{nl} - \left( D_2 + \frac{D_3}{r} + D_4 r + D_5 r^2 \right) \exp(-m_D(T)r) - \frac{l(l+1)}{2\mu r^2} \right] * R_{nl}(r) = 0. \tag{12}$$

Bopp's shift method [70-72] has been successfully applied to relativistic and nonrelativistic noncommutative quantum mechanical problems using the modified Dirac equation (MDE) [73-81], the modified Klein-Gordon equation (MKGE) [36-38, 48-61] and DSE [46, 64-69]. This method has produced very promising results for several situations of physical and chemical interest. The method reduces MDE, MKGE, and DSE to the Dirac equation, Klein-Gordon equation, and Schrödinger equation, respectively, under two simultaneous translations in space and phase. It is based on the following new commutators [46, 64-72]:

$$\begin{cases} [\hat{x}_\mu(t), \hat{p}_\nu(t)] = i\delta_{\mu\nu}\hbar_{eff} \\ [\hat{x}_\mu, \hat{x}_\nu] = [\hat{x}_\mu(t), \hat{x}_\nu(t)] = i\theta_{\mu\nu} \\ [\hat{p}_\mu, \hat{p}_\nu] = [\hat{p}_\mu(t), \hat{p}_\nu(t)] = i\bar{\theta}_{\mu\nu} \end{cases} \quad (13)$$

The new generalized positions and momentum coordinates  $(\hat{x}_\mu, \hat{p}_\nu)$  in 3D-NRNCPS are defined in terms of the commutative counterparts  $(x_\mu, p_\nu)$  in ordinary quantum mechanics via, respectively [46, 55-60]:

$$(x_\mu, p_\nu) \Rightarrow (\hat{x}_\mu, \hat{p}_\nu) = \left( x_\mu - \frac{\theta_{\mu\nu}}{2} p_\nu, p_\mu + \frac{\bar{\theta}_{\mu\nu}}{2} x_\nu \right). \quad (14)$$

The above equation allows us to obtain the two operators  $(\hat{r}^2, \hat{p}^2)$  in the 3D-NRNCPS symmetries framework [28-31]:

$$(r^2, p^2) \Rightarrow (\hat{r}^2, \hat{p}^2) = \left( r^2 - \vec{\mathbf{L}}\vec{\boldsymbol{\theta}}, p^2 + \vec{\mathbf{L}}\vec{\bar{\boldsymbol{\theta}}} \right). \quad (15)$$

The two couplings  $\vec{\mathbf{L}}\vec{\boldsymbol{\theta}}$  and  $\vec{\mathbf{L}}\vec{\bar{\boldsymbol{\theta}}}$  are  $(L_x\theta_{12} + L_y\theta_{23} + L_z\theta_{13})$  and  $(L_x\bar{\theta}_{12} + L_y\bar{\theta}_{23} + L_z\bar{\theta}_{13})$ , respectively, and  $(L_x, L_y, \text{ and } L_z)$  are the three components of the angular momentum operator  $\vec{\mathbf{L}}$  while  $\theta_{\mu\nu}$  equal  $\theta_{\mu\nu}/2$ . Thus, the reduced Schrödinger equation (without star product) can be written as:

$$\frac{d^2 R_{nl}(r)}{dr^2} + 2\mu \left( E - V_{ip}^{eff}(\hat{r}) \right) R_{nl}(r) = 0. \quad (16)$$

The new operator of Hamiltonian  $H_{nc}^{ip}(\hat{x}_\mu, \hat{p}_\nu)$  can be expressed as:

$$H_{nc}^{ip}(\hat{x}_\mu, \hat{p}_\mu) = \frac{\hat{p}^2}{2\mu} + V_{ip}(\hat{r}), \quad (17)$$

here  $\hat{r}$  equal  $\sqrt{\left(x_\mu - \frac{\theta_{\mu\nu}}{2} p_\nu\right)\left(x^\mu - \frac{\theta^{\mu\alpha}}{2} p_\alpha\right)}$ . The effectively improved internal energy potential  $V_{ip}^{eff}(\hat{r})$  can be expressed in 3D-NRNCPS symmetries:

$$V_{ip}^{eff}(\hat{r}) = \left( D_2 + \frac{D_3}{\hat{r}} + D_4\hat{r} + D_5\hat{r}^2 \right) \exp(-m_D(T)\hat{r}) + \frac{l(l+1)}{2\mu\hat{r}^2}. \quad (18)$$

Again, apply Eq. (15) to find the three terms  $\left(\frac{D_3}{\hat{r}}, D_4\hat{r}, D_5\hat{r}^2 \text{ and } \exp(-m_D(T)\hat{r})\right)$ , which will be used to determine the effective improved internal energy potential  $V_{ip}^{eff}(\hat{r})$ , as follows:

$$\frac{D_3}{r} \rightarrow \frac{D_3}{\hat{r}} = \frac{D_3}{r} + \frac{D_3}{2r^3} \vec{\mathbf{L}}\vec{\boldsymbol{\theta}} + O(\theta^2), \quad (19.1)$$

$$D_4 r \rightarrow D_4 \hat{r} = D_4 r - \frac{D_4}{2r} \vec{\mathbf{L}}\vec{\boldsymbol{\theta}} + O(\theta^2), \quad (19.2)$$

$$D_5 r^2 \rightarrow D_5 \hat{r}^2 = D_5 r^2 - D_5 \vec{\mathbf{L}}\vec{\boldsymbol{\theta}} + O(\theta^2), \quad (19.3)$$

$$\frac{l(l+1)}{r^2} \rightarrow \frac{l(l+1)}{\hat{r}^2} = \frac{l(l+1)}{r^2} + \frac{l(l+1)}{r^4} \vec{\mathbf{L}}\vec{\boldsymbol{\theta}} + O(\theta^2), \quad (19.4)$$

and

$$\exp(-m_D(T)r) \rightarrow \exp(-m_D(T)\hat{r}) = \exp(-m_D(T)r) - \frac{m_D(T)}{2r} \vec{\mathbf{L}}\vec{\boldsymbol{\theta}} \exp(-m_D(T)r). \quad (19.5)$$

Thus, we have the following.

$$\frac{D_3}{r} \exp(-m_D(T)r) \rightarrow \frac{D_3}{\hat{r}} \exp(-m_D(T)\hat{r}) = \left( \frac{D_3}{r} + \frac{D_3}{2r^3} \vec{\mathbf{L}}\vec{\boldsymbol{\theta}} \right) \left( 1 - \frac{m_D(T)}{2r} \vec{\mathbf{L}}\vec{\boldsymbol{\theta}} \right) \exp(-m_D(T)r), \quad (20.1)$$

$$D_4 r \exp(-m_D(T)r) \rightarrow D_4 \hat{r} \exp(-m_D(T)\hat{r}) = \left( D_4 r - \frac{D_4}{2r} \vec{\mathbf{L}}\vec{\boldsymbol{\theta}} \right) \left( 1 - \frac{m_D(T)}{2r} \vec{\mathbf{L}}\vec{\boldsymbol{\theta}} \right) \exp(-m_D(T)r), \quad (20.2)$$

$$D_5 r^2 \exp(-m_D(T)r) \rightarrow D_5 \hat{r}^2 \exp(-m_D(T)\hat{r}) = \left( D_5 r^2 - D_5 \vec{\mathbf{L}}\vec{\boldsymbol{\theta}} \right) \left( 1 - \frac{m_D(T)}{2r} \vec{\mathbf{L}}\vec{\boldsymbol{\theta}} \right) \exp(-m_D(T)r), \quad (20.3)$$

and

$$D_1 \exp(-m_D(T)r) \rightarrow D_1 \exp(-m_D(T)\hat{r}) = D_1 \exp(-m_D(T)r) - D_1 \frac{m_D(T) \exp(-m_D(T)r)}{2r} \vec{\mathbf{L}}\vec{\boldsymbol{\theta}}. \quad (20.4)$$

which gives immediately at the first order of the infinitesimal vector parameter  $\vec{\boldsymbol{\theta}}$  as follows:

$$\frac{D_3}{\hat{r}} \exp(-m_D(T)\hat{r}) = \frac{D_3}{r} \exp(-m_D(T)r) - \left( \frac{m_D(T)D_3}{2r^2} \exp(-m_D(T)r) + \frac{D_3 \exp(-m_D(T)r)}{2r^3} \right) \vec{\mathbf{L}}\vec{\boldsymbol{\theta}} + O(\theta^2), \quad (21.1)$$

$$D_4 \hat{r} \exp(-m_D(T)\hat{r}) = D_4 r \exp(-m_D(T)r) - \left( \frac{m_D(T)D_4}{2} \exp(-m_D(T)r) - \frac{D_4 \exp(-m_D(T)r)}{2r} \right) \vec{\mathbf{L}}\vec{\boldsymbol{\theta}} + O(\theta^2), \quad (21.2)$$

$$D_4 \hat{r} \exp(-m_D(T)\hat{r}) = D_4 r \exp(-m_D(T)r) - \left( \frac{m_D(T)D_4}{2} \exp(-m_D(T)r) - \frac{D_4 \exp(-m_D(T)r)}{2r} \right) \vec{\mathbf{L}}\vec{\boldsymbol{\theta}} + O(\theta^2), \quad (213)$$

and

$$D_1 \exp(-m_D(T)\hat{r}) = D_1 \exp(-m_D(T)r) - D_1 \frac{m_D(T) \exp(-m_D(T)r)}{2r} \vec{\mathbf{L}}\vec{\boldsymbol{\theta}} + O(\theta^2). \quad (214)$$

Substituting, Eq. (21) in Eq. (18), gives the new improved internal energy potential, we obtain the effective improved internal energy potential  $V_{ip}^{eff}(\hat{r})$  in 3D-NRNCPS symmetries as follows:

$$V_{ip}^{eff}(\hat{r}) = V_{ip}(r) + \frac{l(l+1)}{2\mu r^2} + \left[ \left( \frac{A_1}{2r} - \frac{A_2}{2r^2} + \frac{D_3}{2r^3} - \frac{A_4}{2} r - \frac{A_3}{2} \right) \exp(-m_D(T)r) + \frac{l(l+1)}{r^4} \right] \vec{\mathbf{L}}\vec{\boldsymbol{\theta}} + O(\theta^2), \quad (22)$$

with

$$\left. \begin{aligned} A_1 &= m_D(T)D_5 - D_1 m_D(T) - D_4, \\ A_2 &= m_D(T)D_3, \\ A_3 &= m_D(T)D_4, \\ A_4 &= m_D(T)D_5. \end{aligned} \right\}$$

By making the above substitution equation in Eq. (17), we find the global our working new modified Hamiltonian operator  $H_{nc}^{ip}(\hat{r})$  in 3D-NRNCPS symmetries:

$$H_{nc}^{ip}(\hat{r}) = H_{ip}(x_\mu, p_\nu) + H_{pert}^{ip}(r, \theta, \bar{\theta}), \quad (23)$$

here  $H_{ip}(x_\mu, p_\nu)$  is just the ordinary Hamiltonian operator with internal energy potential in 3D-NR quantum mechanics symmetries:

$$H_{ip}(x_\mu, p_\nu) = \frac{p^2}{2\mu} + \left( D_2 + \frac{D_3}{r} + D_4 r + D_5 r^2 \right) \exp(-m_D(T)r), \quad (24)$$

while the rest part  $H_{pert}^{ip}(r, \theta, \bar{\theta})$ , which we called the perturbative Hamiltonian operator, is proportional to two infinitesimals couplings  $\vec{\mathbf{L}}\vec{\boldsymbol{\theta}}$  and  $\vec{\mathbf{L}}\vec{\bar{\boldsymbol{\theta}}}$ :

$$H_{pert}^{ip}(r, \theta, \bar{\theta}) = \left[ f(r, A_i, D_3) + \frac{l(l+1)}{r^4} \right] \vec{\mathbf{L}}\vec{\boldsymbol{\theta}} + \frac{\vec{\bar{\boldsymbol{\theta}}}}{2\mu}, \quad (25)$$

here  $f(r, A_i, D_3)$  is determined by:

$$f(r, A_i, D_3) = \left( \frac{A_1}{2r} - \frac{A_2}{2r^2} + \frac{D_3}{2r^3} - \frac{A_4}{2} r - \frac{A_3}{2} \right) \exp(-m_D(T)r).$$

Thus, we can consider  $H_{pert}^{ip}(r)$  it as a perturbation term compared with the principal Hamiltonian operator  $H_{ip}(x_\mu, p_\mu)$  in 3D-NRPS symmetries.

### 3.2. The exact modified spin-orbit operator for heavy-quarkonium systems with improved internal energy potential in the pNRQCD system:

In this subsection, we apply the same strategy that we have seen exclusively in some of our published scientific works [46, 55-60, 73-76]. Under such a particular choice, one can easily reproduce both couplings  $\vec{\mathbf{L}}\vec{\boldsymbol{\theta}}$  and  $\vec{\mathbf{L}}\vec{\bar{\boldsymbol{\theta}}}$  to the new physical forms  $(g_s \vec{\boldsymbol{\theta}}\vec{\mathbf{L}}\vec{\boldsymbol{\theta}}$  and  $g_s \vec{\bar{\boldsymbol{\theta}}}\vec{\mathbf{L}}\vec{\boldsymbol{\theta}}$ ), respectively. Thus, the perturbative Hamiltonian operator  $H_{pert}^{ip}(r, \theta, \bar{\theta})$  for the heavy quarkonium systems will be transformed into a modified spin-orbit operator  $H_{so}^{ip}(r, \theta, \bar{\theta})$ , under the improved internal energy potential at a finite temperature as follows:

$$H_{so}^{ip}(r, \theta, \bar{\theta}) \equiv g_s \left\{ f(r, A_i, D_3) \boldsymbol{\theta} + \frac{l(l+1)}{r^4} \boldsymbol{\theta} + \frac{\bar{\boldsymbol{\theta}}}{2\mu} \right\} \vec{\mathbf{L}}\vec{\boldsymbol{\theta}}, \quad (26)$$

here  $\boldsymbol{\theta}$  and  $\bar{\boldsymbol{\theta}}$  are equals  $\sqrt{\theta_{12}^2 + \theta_{23}^2 + \theta_{13}^2}$  and  $\sqrt{\bar{\theta}_{12}^2 + \bar{\theta}_{23}^2 + \bar{\theta}_{13}^2}$ , respectively, and  $g_s$  is a new constant, which plays the role of strong coupling in quantum chromodynamics or QCD theory, we have chosen two vectors  $(\vec{\boldsymbol{\theta}}$  and  $\vec{\bar{\boldsymbol{\theta}}}$ ) parallel to the spin-s of the heavy quarkonium system. Furthermore, the above perturbative terms  $H_{pert}^{ip}(r)$  can be rewritten to the following new form:

$$H_{so}^{ip}(r, \theta, \bar{\theta}) = \frac{g_s}{2} \left[ f(r, A_i, D_3) \boldsymbol{\theta} + \frac{l(l+1)}{r^4} \boldsymbol{\theta} + \frac{\bar{\boldsymbol{\theta}}}{2\mu} \right] G^2, \quad (27)$$

where  $G^2 \equiv \vec{\mathbf{J}}^2 - \vec{\mathbf{L}}^2 - \vec{\mathbf{S}}^2$  while  $\vec{\mathbf{J}}$  and  $\vec{\mathbf{S}}$  are the defined operators of the total angular momentum and spin of quarkonium systems. The operator  $H_{so}^{iq}(r, \theta, \bar{\theta})$  traduces the coupling between spin-orbit interaction  $\vec{\mathbf{L}}\vec{\boldsymbol{\theta}}$ . The set  $(H_{so}^{ip}(r, \theta, \bar{\theta}), J^2, L^2,$

$S^2$  and  $J_z$ ) forms a complete set of conserved physics quantities. For spin-1, the eigenvalues of the spin-orbit coupling operator are

$$k(l) \equiv \frac{1}{2}(j(j+1) - l(l+1) - 2)$$

corresponding  $j = l + 1$  (spin great),  $j = l$  (spin middle), and  $j = l - 1$  (spin little), respectively, then, one can form a diagonal  $(3 \times 3)$  matrix for the improved internal energy potential in 3D-NRNCPS symmetries, with diagonal elements  $(H_{so}^{ip})_{11}$ ,  $(H_{so}^{ip})_{22}$  and  $(H_{so}^{ip})_{33}$  are given by:

$$(H_{so}^{ip})_{11} = g_s k_1(l) \left\{ f(r, A_i, D_3) \theta + \frac{l(l+1)}{r^4} \theta + \frac{\bar{\theta}}{2\mu} \right\} \text{ if } j = l + 1, \quad (28.1)$$

$$(H_{so}^{ip})_{22} = g_s k_2(l) \left\{ f(r, A_i, D_3) \theta + \frac{l(l+1)}{r^4} \theta + \frac{\bar{\theta}}{2\mu} \right\} \text{ if } j = l, \quad (28.2)$$

and

$$(H_{so}^{ip})_{33} = g_s k_3(l) \left\{ f(r, A_i, D_3) \theta + \frac{l(l+1)}{r^4} \theta + \frac{\bar{\theta}}{2\mu} \right\} \text{ if } j = l - 1. \quad (28.3)$$

Here  $(k_1(l), k_2(l), k_3(l))$  are equals  $\frac{1}{2}(l, -2, -2l - 2)$ , respectively, and  $j$  is the total quantum number. The non-null diagonal elements  $((H_{so}^{ip})_{11}, (H_{so}^{ip})_{22}, (H_{so}^{ip})_{33})$  for the modified Hamiltonian operator  $H_{nc}^{ip}(\hat{r})$  will change the energy values  $E_{nl}$  by creating three new values:

$$E_g^{ip} = \langle \Psi(r, \theta, \phi) | (H_{so}^{ip})_{11} | \Psi(r, \theta, \phi) \rangle, \quad (29.1)$$

$$E_m^{ip} = \langle \Psi(r, \theta, \phi) | (H_{so}^{ip})_{22} | \Psi(r, \theta, \phi) \rangle, \quad (29.2)$$

and

$$E_l^{ip} = \langle \Psi(r, \theta, \phi) | (H_{so}^{ip})_{33} | \Psi(r, \theta, \phi) \rangle. \quad (29.3)$$

We will see them in detail in the next subsection. After profound calculation, one can show that the new radial function  $R_{nl}(r)$  satisfies the following differential equation for the improved internal energy potential:

$$\frac{d^2 R_{nl}(r)}{dr^2} + 2\mu \left[ E_{nl} - V_{ip}(r) - \frac{l(l+1)}{2\mu r^2} - [f(r, A_i, D_3) + l(l+1)r^{-4}] \vec{\mathbf{L}} \vec{\boldsymbol{\theta}} - \frac{l(l+1)}{r^4} \vec{\mathbf{L}} \vec{\boldsymbol{\theta}} - \frac{\vec{\mathbf{L}} \vec{\boldsymbol{\theta}}}{2\mu} \right] R_{nl}(r) = 0. \quad (30)$$

Through our observation of the expression of  $H_{pert}^{ip}(r, \theta, \bar{\theta})$ , which appears in equation (25), we see it as proportionate to the two infinitesimals parameters  $(\theta$  and  $\bar{\theta})$ , thus, in what follows, we proceed to solve the modified radial part of the DSE that is, equation (30) by applying standard perturbation theory to find an acceptable solution at the first order of two parameters  $\theta$  and  $\bar{\theta}$ . The proposed solutions for DSE under improved internal energy potential include energy corrections, which are produced automatically from two principal physical phonemes', the first one is the effect of modified spin-orbit interaction and the second is the modified Zeeman effect while the stark effect can appear in the linear part of improved internal energy potential at finite temperature model.

### 3.3. The exact modified spin-orbit spectrum for a heavy-quarkonium system under improved internal energy potential in pNRQCD

The purpose here is to give a complete prescription for determining the energy levels of the ground state, the first excited state, and  $(n, l, m)^{th}$  the excited state, of heavy quarkonium systems. We first find the corrections  $(E_{so}^{gip}(k_1(l), j, l, n), E_{so}^{mip}(k_2(l), j, l, n)$  and  $E_{so}^{lip}(k_3(l), j, l, n))$  for heavy quarkonium systems such as (charmonium and bottomonium) mesons that have the quark and antiquark flavor under a new improved internal energy potential at finite temperature, which have three polarities up and down  $j = l + 1$  (spin great),  $j = l$  (spin middle) and  $j = l - 1$  (spin little), respectively, at the first order of two parameters  $(\theta$  and  $\bar{\theta})$ . Moreover, by applying the perturbative theory, in the case of perturbed non-relativistic quantum chromodynamics pNRQCD framework, we obtained the following results:

$$E_{so}^{gip} = g_s N_{nl}^2 k_1(l) \int_0^{+\infty} \left\{ \prod_{i=1}^n (r - \alpha_i) r^{\delta-1} \right\}^2 \exp(-\alpha r^2 - 2\beta r) \left( f(r, A_i, D_3) \theta + \frac{l(l+1)}{r^4} \theta + \frac{\bar{\theta}}{2\mu} \right) r^2 dr, \quad (31.1)$$

$$E_{so}^{mip} = g_s N_{nl}^2 k_2(l) \int_0^{+\infty} \left\{ \prod_{i=1}^n (r - \alpha_i) r^{\delta-1} \right\}^2 \exp(-\alpha r^2 - 2\beta r) \left( f(r, A_i, D_3) \theta + \frac{l(l+1)}{r^4} \theta + \frac{\bar{\theta}}{2\mu} \right) r^2 dr, \quad (31.2)$$

$$E_{so}^{lip} = g_s N_{nl}^2 k_3(l) \int_0^{+\infty} \left\{ \prod_{i=1}^n (r - \alpha_i) r^{\delta-1} \right\}^2 \exp(-\alpha r^2 - 2\beta r) \left( f(r, A_i, D_3) \theta + \frac{l(l+1)}{r^4} \theta + \frac{\bar{\theta}}{2\mu} \right) r^2 dr. \quad (31.3)$$

We have used the standard identity:

$$\int Y_l^m(\theta, \phi) Y_l^{m'}(\theta, \phi) \sin(\theta) d\theta d\phi = \delta_{ll'} \delta_{mm'}$$

Now, we can rewrite the above equations to a simplified new form:

$$E_{so}^{mip}(k_1, j, n, l) = g_s N_{nl}^2 k_1(l) \left( \theta \sum_{i=1}^6 T_i^n + \frac{\bar{\theta}}{2\mu} \right), \tag{32.1}$$

$$E_{so}^{mip}(k_2, j, n, l) = g_s N_{nl}^2 k_2(l) \left( \theta \sum_{i=1}^6 T_i^n + \frac{\bar{\theta}}{2\mu} \right), \tag{32.2}$$

and

$$E_{so}^{lip}(k_3, j, n, l) = g_s N_{nl}^2 k_3(l) \left( \theta \sum_{i=1}^6 T_i^n + \frac{\bar{\theta}}{2\mu} \right). \tag{32.3}$$

Moreover, the expressions of the 6-factors  $T_i^n (i = \overline{1,6})$  are given by:

$$T_1^n = \frac{A_1}{2} \int_0^{+\infty} \left( \prod_{i=1}^n (r - \alpha_i) r^{\delta-1} \right)^2 \exp(-ar^2 - (2\beta + m_D(T))r) r dr, \tag{33.1}$$

$$T_2^n = -\frac{A_2}{2} \int_0^{+\infty} \left( \prod_{i=1}^n (r - \alpha_i) r^{\delta-1} \right)^2 \exp(-ar^2 - (2\beta + m_D(T))r) dr, \tag{33.2}$$

$$T_3^n = \frac{D_3}{2} \int_0^{+\infty} \left( \prod_{i=1}^n (r - \alpha_i) r^{\delta-1} \right)^2 \exp(-ar^2 - (2\beta + m_D(T))r) r^{-1} dr, \tag{33.3}$$

$$T_4^n = -\frac{A_4}{2} \int_0^{+\infty} \left( \prod_{i=1}^n (r - \alpha_i) r^{\delta-1} \right)^2 \exp(-ar^2 - (2\beta + m_D(T))r) r^3 dr, \tag{33.4}$$

$$T_5^n = -\frac{A_3}{2} \int_0^{+\infty} \left( \prod_{i=1}^n (r - \alpha_i) r^{\delta-1} \right)^2 \exp(-ar^2 - (2\beta + m_D(T))r) r^2 dr, \tag{33.5}$$

and

$$T_6^n = \int_0^{+\infty} \left( \prod_{i=1}^n (r - \alpha_i) r^{\delta-1} \right)^2 \exp(-ar^2 - 2\beta r) \frac{l(l+1)}{r^4} r^2 dr. \tag{33.6}$$

For the ground state  $n = 0$ , the expressions of the 6-factors  $T_i^0 (i = \overline{1,6})$  will be simplified to the following form:

$$T_1^0 = \frac{A_1}{2} \int_0^{+\infty} r^{2\delta-1} \exp(-ar^2 - \epsilon r) dr, \tag{34.1}$$

$$T_2^0 = -\frac{A_2}{2} \int_0^{+\infty} r^{2\delta-1-1} \exp(-ar^2 - \epsilon r) dr, \tag{34.2}$$

$$T_3^0 = \frac{D_3}{2} \int_0^{+\infty} r^{2\delta-2-1} \exp(-ar^2 - \epsilon r) dr, \tag{34.3}$$

$$T_4^0 = -\frac{A_4}{2} \int_0^{+\infty} r^{2\delta+2-1} \exp(-ar^2 - \epsilon r) r^3 dr, \tag{34.4}$$

$$T_5^0 = -\frac{A_3}{2} \int_0^{+\infty} r^{2\delta+1-1} \exp(-ar^2 - \epsilon r) dr, \tag{34.5}$$

$$T_6^0 = l(l+1) \int_0^{+\infty} r^{2\delta-3-1} \exp(-ar^2 - 2\beta r) dr, \tag{34.6}$$

where  $\epsilon = 2\beta + m_D(T)$ . It is convenient to apply the following special integral [82]:

$$\int_0^{+\infty} x^{\nu-1} \exp(-\lambda x^2 - \gamma x) dx = (2\lambda)^{-\frac{\nu}{2}} \Gamma(\nu) \exp\left(\frac{\gamma^2}{8\lambda}\right) D_{-\nu}\left(\frac{\gamma}{\sqrt{2\lambda}}\right), \tag{35}$$

where  $D_{-\nu}\left(\frac{\gamma}{\sqrt{2\lambda}}\right)$  and  $\Gamma(\nu)$  denote the parabolic cylinder functions and the Gamma function. After straightforward calculations, we can obtain the explicit results:

$$T_1^0 = \frac{A_1}{2} (2\alpha)^{-\frac{2\delta}{2}} \Gamma(2\delta) \exp\left(\frac{\epsilon^2}{8\alpha}\right) D_{-2\delta}\left(\frac{\epsilon}{\sqrt{2\alpha}}\right), \tag{36.1}$$

$$T_2^0 = -\frac{A_2}{2} (2\alpha)^{-\frac{2\delta-1}{2}} \Gamma(2\delta - 1) \exp\left(\frac{\epsilon^2}{8\alpha}\right) D_{-(2\delta-1)}\left(\frac{\epsilon}{\sqrt{2\alpha}}\right), \tag{36.2}$$

$$T_3^0 = \frac{D_3}{2} (2\alpha)^{-\frac{2\delta-2}{2}} \Gamma(2\delta - 2) \exp\left(\frac{\epsilon^2}{8\alpha}\right) D_{-(2\delta-2)}\left(\frac{\epsilon}{\sqrt{2\alpha}}\right), \tag{36.3}$$

$$T_4^0 = -\frac{A_4}{2} (2\alpha)^{-\frac{2\delta+2}{2}} \Gamma(2\delta + 2) \exp\left(\frac{\epsilon^2}{8\alpha}\right) D_{-(2\delta+2)}\left(\frac{\epsilon}{\sqrt{2\alpha}}\right), \tag{36.4}$$

$$T_5^0 = -\frac{A_3}{2} (2\alpha)^{-\frac{2\delta+1}{2}} \Gamma(2\delta + 1) \exp\left(\frac{\epsilon^2}{8\alpha}\right) D_{-(2\delta+1)}\left(\frac{\epsilon}{\sqrt{2\alpha}}\right), \tag{36.5}$$

and

$$T_6^0 = l(l+1)(2\alpha)^{-\frac{2\delta-3}{2}} \Gamma(2\delta - 3) \exp\left(\frac{4\beta^2}{8\alpha}\right) D_{-(2\delta-3)}\left(\frac{2\beta}{\sqrt{2\alpha}}\right). \tag{36.6}$$

Let us second to obtain the exact modifications ( $E_{so}^{gip}(k_1(l), j, l, n = 0)$ ,  $E_{so}^{mip}(k_2(l), j, l, n = 0)$  and  $E_{so}^{lip}(k_3(l), j, l, n = 0)$ ) of the ground state as:

$$E_{so}^{gip}(k_1(l), j, l, n = 0) = g_s \frac{(2\alpha)^{\frac{2\delta+1}{2}} \exp(-\beta^2/2\alpha)}{\Gamma(2\delta+1) D_{-(2\delta+1)}(\beta\sqrt{2/\alpha})} k_1(l) \left( \theta T_{00} + \frac{\bar{\theta}}{2\mu} \right), \tag{37.1}$$

$$E_{so}^{mip}(k_2(l), j, l, n = 0) = g_s \frac{(2\alpha)^{\frac{2\delta+1}{2}} \exp(-\beta^2/2\alpha)}{\Gamma(2\delta+1) D_{-(2\delta+1)}(\beta\sqrt{2/\alpha})} k_2(l) \left( \theta T_{00} + \frac{\bar{\theta}}{2\mu} \right), \tag{37.2}$$

and

$$E_{so}^{lip}(k_3(l), j, l, n = 0) = g_s \frac{(2\alpha)^{\frac{2\delta+1}{2}} \exp(-\beta^2/2\alpha)}{\Gamma(2\delta+1) D_{-(2\delta+1)}(\beta\sqrt{2/\alpha})} k_3(l) \left( \theta T_{00} + \frac{\bar{\theta}}{2\mu} \right). \tag{37.3}$$

with  $T_{00} = \sum_{i=1}^6 T_i^0$ . For the first excited state  $n = 1$ , we replace  $(\prod_{i=1}^n (r - \alpha_i) r^{\delta-1})^2$  by  $(r^{2\delta} - \alpha_1^2 r^{2\delta-2} - 2\alpha_1 r^{2\delta-1})$ , with  $\alpha_1 = \frac{d_3 - 2\beta(\delta+1)}{2\alpha}$ , the expressions of the 6-factors  $T_i^1 (i = \overline{1,6})$  will be simplified to the following form:

$$T_1^1 = \frac{A_1}{2} \int_0^{+\infty} (r^{2\delta+2-1} - \alpha_1^2 r^{2\delta-1} - 2\alpha_1 r^{2\delta+1-1}) \exp(-ar^2 - \epsilon r) dr, \tag{38.1}$$

$$T_2^1 = -\frac{A_2}{2} \int_0^{+\infty} r^{2\delta+1-1} - \alpha_1^2 r^{2\delta-1-1} - 2\alpha_1 r^{2\delta-1} \exp(-ar^2 - \epsilon r) dr, \tag{38.2}$$

$$T_3^1 = \frac{D_3}{2} \int_0^{+\infty} (r^{2\delta-1} - \alpha_1^2 r^{2\delta-2-1} - 2\alpha_1 r^{2\delta-1-1}) \exp(-ar^2 - \epsilon r) dr, \tag{38.3}$$

$$T_4^1 = -\frac{A_4}{2} \int_0^{+\infty} (r^{2\delta+4-1} - \alpha_1^2 r^{2\delta+2-1} - 2\alpha_1 r^{2\delta+3-1}) \exp(-ar^2 - \epsilon r) dr, \tag{38.4}$$

$$T_5^1 = -\frac{A_3}{2} \int_0^{+\infty} (r^{2\delta+3-1} - \alpha_1^2 r^{2\delta+1-1} - 2\alpha_1 r^{2\delta+2-1}) \exp(-ar^2 - \epsilon r) dr, \tag{38.5}$$

and

$$T_6^1 = l(l+1) \int_0^{+\infty} (r^{2\delta-1-1} - \alpha_1^2 r^{2\delta-3-1} - 2\alpha_1 r^{2\delta-2-1}) \exp(-ar^2 - 2\beta r) dr. \tag{38.6}$$

Evaluating the integral in Eq. (38) and applying the special integration, which is given by Eq. (33), we obtain the following results:

$$T_2^1 = -\frac{A_2}{2} \left\{ (2\alpha)^{-\frac{2\delta+1}{2}} \Gamma(2\delta+1) \exp\left(\frac{\epsilon^2}{8\alpha}\right) D_{-(2\delta+1)}\left(\frac{\epsilon}{\sqrt{2\alpha}}\right) + \alpha_1^2 (2\alpha)^{-\frac{2\delta-1}{2}} \Gamma(2\delta-1) \exp\left(\frac{\epsilon^2}{8\alpha}\right) D_{-(2\delta-1)}\left(\frac{\epsilon}{\sqrt{2\alpha}}\right) - 2\alpha_1 (2\alpha)^{-\frac{2\delta}{2}} \Gamma(2\delta) \exp\left(\frac{\epsilon^2}{8\alpha}\right) D_{-(2\delta)}\left(\frac{\epsilon}{\sqrt{2\alpha}}\right) \right\}, \tag{39.1}$$

$$T_3^1 = -\frac{A_2}{2} \left\{ (2\alpha)^{-\frac{2\delta+1}{2}} \Gamma(2\delta+1) \exp\left(\frac{\epsilon^2}{8\alpha}\right) D_{-(2\delta+1)}\left(\frac{\epsilon}{\sqrt{2\alpha}}\right) + \alpha_1^2 (2\alpha)^{-\frac{2\delta-1}{2}} \Gamma(2\delta-1) \exp\left(\frac{\epsilon^2}{8\alpha}\right) D_{-(2\delta-1)}\left(\frac{\epsilon}{\sqrt{2\alpha}}\right) - 2\alpha_1 (2\alpha)^{-\frac{2\delta}{2}} \Gamma(2\delta) \exp\left(\frac{\epsilon^2}{8\alpha}\right) D_{-(2\delta)}\left(\frac{\epsilon}{\sqrt{2\alpha}}\right) \right\}, \tag{39.2}$$

$$T_3^1 = \frac{D_3}{2} \left\{ (2\alpha)^{-\frac{2\delta-1}{2}} \Gamma(2\delta-1) \exp\left(\frac{\epsilon^2}{8\alpha}\right) D_{-(2\delta-1)}\left(\frac{\epsilon}{\sqrt{2\alpha}}\right) + \alpha_1^2 (2\alpha)^{-\frac{2\delta-2}{2}} \Gamma(2\delta-2) \exp\left(\frac{\epsilon^2}{8\alpha}\right) D_{-(2\delta-2)}\left(\frac{\epsilon}{\sqrt{2\alpha}}\right) - 2\alpha_1 (2\alpha)^{-\frac{2\delta-1}{2}} \Gamma(2\delta-1) \exp\left(\frac{\epsilon^2}{8\alpha}\right) D_{-(2\delta-1)}\left(\frac{\epsilon}{\sqrt{2\alpha}}\right) \right\}, \tag{39.3}$$

$$T_4^1 = -\frac{A_4}{2} \left\{ (2\alpha)^{-\frac{2\delta+4}{2}} \Gamma(2\delta+4) \exp\left(\frac{\epsilon^2}{8\alpha}\right) D_{-(2\delta+4)}\left(\frac{\epsilon}{\sqrt{2\alpha}}\right) + \alpha_1^2 (2\alpha)^{-\frac{2\delta+2}{2}} \Gamma(2\delta+2) \exp\left(\frac{\epsilon^2}{8\alpha}\right) D_{-(2\delta+2)}\left(\frac{\epsilon}{\sqrt{2\alpha}}\right) - 2\alpha_1 (2\alpha)^{-\frac{2\delta+3}{2}} \Gamma(2\delta+3) \exp\left(\frac{\epsilon^2}{8\alpha}\right) D_{-(2\delta+3)}\left(\frac{\epsilon}{\sqrt{2\alpha}}\right) \right\}, \tag{39.4}$$

$$T_5^1 = -\frac{A_3}{2} \left\{ (2\alpha)^{-\frac{2\delta+3}{2}} \Gamma(2\delta+3) \exp\left(\frac{\epsilon^2}{8\alpha}\right) D_{-(2\delta+3)}\left(\frac{\epsilon}{\sqrt{2\alpha}}\right) - \alpha_1^2 (2\alpha)^{-\frac{2\delta+1}{2}} \Gamma(2\delta+1) \exp\left(\frac{\epsilon^2}{8\alpha}\right) D_{-(2\delta+1)}\left(\frac{\epsilon}{\sqrt{2\alpha}}\right) - 2\alpha_1 (2\alpha)^{-\frac{2\delta+2}{2}} \Gamma(2\delta+2) \exp\left(\frac{\epsilon^2}{8\alpha}\right) D_{-(2\delta+2)}\left(\frac{\epsilon}{\sqrt{2\alpha}}\right) \right\}, \tag{39.5}$$

and

$$T_6^1 = l(l+1) (2\alpha)^{-\frac{2\delta+3}{2}} \Gamma(2\delta-1) \exp\left(\frac{4\beta^2}{8\alpha}\right) D_{-(2\delta-1)}\left(\frac{2\beta}{\sqrt{2\alpha}}\right) - l(l+1) \alpha_1^2 (2\alpha)^{-\frac{2\delta+1}{2}} \Gamma(2\delta-3) \exp\left(\frac{4\beta^2}{8\alpha}\right) D_{-(2\delta-3)}\left(\frac{2\beta}{\sqrt{2\alpha}}\right) - 2l(l+1) \alpha_1 (2\alpha)^{-\frac{2\delta+2}{2}} \Gamma(2\delta-2) \exp\left(\frac{4\beta^2}{8\alpha}\right) D_{-(2\delta-2)}\left(\frac{2\beta}{\sqrt{2\alpha}}\right). \tag{39.6}$$

Allow us to obtain the exact modifications ( $E_{so}^{gip}(k_1(l), j, l, n = 1)$ ,  $E_{so}^{mip}(k_2(l), j, l, n = 1)$  and  $E_{so}^{lip}(k_3(l), j, l, n = 1)$ ) of the first excited state as follows.

$$E_{so}^{gip}(k_1(l), j, l, n = 1) = \frac{g_s k_1(l)}{l_1 - 2\alpha_1 l_2 + \alpha_1^2 l_3} \left( \theta T_{11} + \frac{\tilde{\theta}}{2\mu} \right), \tag{40.1}$$

$$E_{so}^{mip}(k_2(l), j, l, n = 1) = \frac{g_s k_2(l)}{l_1 - 2\alpha_1 l_2 + \alpha_1^2 l_3} \left( \theta T_{11} + \frac{\tilde{\theta}}{2\mu} \right), \tag{40.2}$$

and

$$E_{so}^{lip}(k_3(l), j, l, n = 1) = \frac{g_s k_3(l)}{l_1 - 2\alpha_1 l_2 + \alpha_1^2 l_3} \left( \theta T_{11} + \frac{\tilde{\theta}}{2\mu} \right), \tag{40.3}$$

with

$$\left. \begin{aligned} I_1 &= \frac{\Gamma(2\delta+3)D_{-(2\delta+3)}(\beta\sqrt{2/\alpha})}{(2\alpha)^{(\delta+3/2)} \exp(-\beta^2/2\alpha)} \\ I_2 &= \frac{\Gamma(2\delta+1)D_{-(2\delta+1)}(\beta\sqrt{2/\alpha})}{(2\alpha)^{(\delta+1/2)} \exp(-\beta^2/2\alpha)} \\ I_3 &= \frac{\Gamma(2\delta+3)D_{-(2\delta+3)}(\beta\sqrt{2/\alpha})}{(2\alpha)^{\frac{2\delta+3}{2}} \exp(-\beta^2/2\alpha)} \end{aligned} \right\}$$

and  $T_{11} = \sum_{i=1}^6 T_1^i$ . In addition, in the same way, we find the exact modifications ( $E_{so}^{gip}(k_1(l), j, l, n), E_{so}^{mip}(k_2(l), j, l, n)$  and  $E_{so}^{lip}(k_3(l), j, l, n)$ ) for the excited states  $(n, l, m)^{th}$  of the heavy quarkonium system under the new improved internal energy potential in the global quantum group symmetry 3D-NRQM:

$$E_{so}^{gip}(k_1(l), j, l, n = 1) = g_s k_1(l) N_{1l}^2 \left( \theta T_{1n} + \frac{\bar{\theta}}{2\mu} \right), \tag{41.1}$$

$$E_{so}^{mip}(k_2(l), j, l, n = 1) = \gamma k_2(l) N_{1l}^2 \left( \theta T_{1n} + \frac{\bar{\theta}}{2\mu} \right), \tag{41.2}$$

and

$$E_{so}^{lip}(k_3(l), j, l, n = 1) = \gamma k_3(l) N_{1l}^2 \left( \theta T_{1n} + \frac{\bar{\theta}}{2\mu} \right), \tag{41.3}$$

with  $T_{1n} = \sum_{i=1}^6 T_n^i$ .

### 3.4. The exact modified magnetic spectrum for heavy quarkonium systems under improved internal energy potential in pNRQCD

In addition to the important results obtained previously, now we consider another important physically meaningful phenomenon produced by the effect of the improved internal energy potential at finite temperature on the perturbative NRQCD related to the influence of an external uniform magnetic field  $\vec{B}$ . To avoid repetition in the theoretical calculations, it is sufficient to apply the following replacements:

$$\vec{\theta} \rightarrow \vec{\sigma B} \text{ and } \frac{\vec{\theta}}{2\mu} \rightarrow \frac{\vec{\sigma B}}{2\mu}. \tag{42}$$

Allows us to replace the physical quantities  $f(r, A_i, D_3) \vec{L}\vec{\theta}$ ,  $\frac{l(l+1)}{r^4} \vec{L}\vec{\theta}$  and  $\frac{\vec{L}\vec{\theta}}{2\mu}$  with corresponding new physical quantities  $\sigma f(r) \vec{L}\vec{B}$ ,  $\sigma \frac{l(l+1)}{r^4} \vec{L}\vec{B}$  and  $\bar{\sigma} \frac{\vec{L}\vec{B}}{2\mu}$ , respectively, here  $(\sigma \text{ and } \bar{\sigma})$  are two infinitesimal real proportional constants, and we choose the arbitrary uniform external magnetic field  $\vec{B}$  parallel to the (Oz) axis, which allows us to introduce the new modified magnetic Hamiltonian  $H_m^{ip}(r, \sigma, \bar{\sigma})$  in 3D-NRNCPS symmetries as:

$$H_m^{ip}(r, \chi, \bar{\sigma}) = - \left( f(r, A_i, D_3) \chi + \frac{l(l+1)}{r^4} \chi - \frac{\bar{\sigma}}{2\mu} \right) \{ \vec{B}\vec{J} - \aleph_z \}, \tag{43}$$

here  $\aleph_z \equiv -\vec{S}\vec{B}$  denote to Zeeman effect in commutative quantum mechanics, while  $(\aleph_{mod}^z = \vec{B}\vec{J} - \aleph_z)$  is the new Zeeman effect. To obtain the exact NC magnetic modifications of energy for the ground state, the first excited state, and  $(n, l, m)^{th}$  excited states of the heavy quarkonium system  $E_{mag}^{ip}(m = 0, l = 0, n = 0)$ ,  $E_{mag}^{ip}(m = -l, +l, l, n = 1)$  and  $E_{mag}^{ip}(m = -l, +l, l, n)$  we just replace  $k_1(l)$  and  $\theta(\bar{\theta})$  in the Eqs. (37), (40), and (41) with the following parameters  $m$  and  $\sigma(\bar{\sigma})$ , respectively:

$$E_{mag}^{ip}(m = 0, l = 0, n = 0) = g_s \frac{(2\alpha)^{\frac{2\delta+1}{2}} \exp(-\beta^2/2\alpha)}{\Gamma(2\delta+1)D_{-(2\delta+1)}(\beta\sqrt{2/\alpha})} B \left( \sigma T_{00} + \frac{\bar{\sigma}}{2\mu} \right) m, \tag{44.1}$$

$$E_{mag}^{ip}(m = -l, +l, l, n = 1) = \frac{g_s B}{l_1 - 2\alpha_1 l_2 + \alpha_1^2 l_3} \left( \sigma T_{11} + \frac{\bar{\sigma}}{2\mu} \right) m, \tag{44.2}$$

and

$$E_{mag}^{ip}(m = -l, +l, l, n) = g_s N_{nl}^2 B \left( \sigma T_{1n} + \frac{\bar{\sigma}}{2\mu} \right) m. \tag{44.3}$$

We have  $-l \leq m \leq +l$ , which allows us to fix  $(2l + 1)$  values for discrete numbers  $m$ . It should be noted that the results obtained in Eq. (44) we could find by direct calculation:

$$E_{mag}^{ip} = \langle \Psi(r, \theta, \phi) | H_m^{ip}(r, \sigma, \bar{\sigma}) | \Psi(r, \theta, \phi) \rangle$$

that takes the following explicit relation:

$$E_{mag}^{ip} = N_{nl}^2 m B \int_0^{+\infty} \left( \prod_{i=1}^n (r - \alpha_i) r^{\delta-1} \right)^2 \exp(-\alpha r^2 - 2\beta r) \left\{ f(r, A_i, D_3) \sigma + \frac{l(l+1)}{r^4} \sigma + \frac{\bar{\sigma}}{2\mu} \right\} r^2 dr. \tag{45}$$

Eq. (45) can be rewritten as follows:

$$E_{mag}^{ip} = g_s N_{nl}^2 B \left( \sigma \sum_{i=1}^6 T_i^n + \frac{\bar{\sigma}}{2\mu} \right) m. \tag{46}$$

The 6-factors  $T_i^n (i = \overline{1,6})$  are given by Eq. (33). Then we find the magnetic specters of energy produced by the operator  $H_m^{ip}(r, \chi, \bar{\sigma})$  for the ground state and first excited states repeating the same calculations in the previous subsection.

Having completed the first and second-induced perturbed both spin-orbit interaction and self-magnetic phenomena, now, for our purposes, we are interested in finding a new third automatically important symmetry for improved internal energy potential at zero temperature in RNCQM symmetries. This physical phenomenon is induced automatically by the influence of the perturbative Hamiltonian operator  $H_{pert}^{ip-rot}(r, \chi, \bar{\chi})$ , which we can obtain from the initial perturbed Hamiltonian operator in Eq. (25). We discover these important physical phenomena when our studied system the quarkonium particle such as  $(c\bar{c}$  and  $b\bar{b})$  undergoing rotation with angular velocity  $\vec{\Omega}$  if we make the following two transformations to ensure that previous calculations are not repeated:

$$\vec{\theta} \rightarrow \chi \vec{\Omega} \quad \text{and} \quad \vec{\bar{\theta}} \rightarrow \bar{\chi} \vec{\Omega}. \tag{47}$$

Here  $(\chi, \bar{\chi})$  are just two infinitesimal real proportional constants. We can express the perturbative Hamiltonian operator  $H_{pert}^{ip-rot}(r, \chi, \bar{\chi})$  which induced the rotational movements of the quarkonium particle as follows:

$$H_{pert}^{ip-rot}(r, \chi, \bar{\chi}) = [f(r, A_i, D_3) \chi + \frac{l(l+1)}{r^4} \chi + \frac{\bar{\chi}}{2\mu}] \vec{\mathbf{L}} \vec{\Omega}. \tag{48}$$

To simplify the calculations without compromising physical content, we choose the rotational velocity  $\vec{\Omega} = \Omega e_z$ . Then we transform the spin-orbit coupling to the new physical phenomena as follows:

$$\left[ f(r, A_i, D_3) \chi + \frac{l(l+1)}{r^4} \chi + \frac{\bar{\chi}}{2\mu} \right] \vec{\mathbf{L}} \vec{\Omega} \rightarrow \left[ f(r, A_i, D_3) \chi + \frac{l(l+1)}{r^4} \chi + \frac{\bar{\chi}}{2\mu} \right] \Omega \mathbf{L}_z. \tag{49}$$

To obtain the exact NC modifications of energy for the ground state, the first excited state, and  $(n, l, m)^{th}$  excited states of the heavy quarkonium system  $E_{rot}^{ip}(m = 0, l = 0, n = 0)$ ,  $E_{rot}^{ip}(m = \overline{-l, +l}, l, n = 1)$ , and  $E_{rot}^{ip}(m = \overline{-l, +l}, l, n)$  we just replace  $k_1(l)$  and  $\theta(\bar{\theta})$  in Eqs. (37), (40), and (41) with the following parameters  $m$  and  $\chi(\bar{\chi})$ , respectively:

$$E_{rot}^{ip}(m = 0, l = 0, n = 0) = g_s \frac{(2\alpha)^{\frac{2\delta+1}{2}} \exp(-\beta^2/2\alpha)}{\Gamma(2\delta+1) D_{-(2\delta+1)}(\beta\sqrt{2/\alpha})} \Omega \left( \chi T_{00} + \frac{\bar{\chi}}{2\mu} \right) m, \tag{50.1}$$

$$E_{rot}^{ip}(m = \overline{-l, +l}, l, n = 1) = \frac{g_s \Omega}{l_1 - 2\alpha_1 l_2 + \alpha_1^2 l_3} \left( \chi T_{11} + \frac{\bar{\chi}}{2\mu} \right) m, \tag{50.2}$$

and

$$E_{rot}^{ip}(m = \overline{-l, +l}, l, n) = g_s N_{nl}^2 \Omega \left( \chi T_{1n} + \frac{\bar{\chi}}{2\mu} \right) m. \tag{50.3}$$

It is important to note that in Ref. [83], rotating isotropic and anisotropic harmonically confined ultra-cold Fermi gases were studied in two and three dimensions at absolute zero, but in that study, the rotational term had to be manually added to the Hamiltonian operator. In contrast, in our study, the rotation operator appears automatically because of the phase-space deformation caused by the improved internal energy potential models in the 3D-NRNCPS symmetries. It is crucial to note that perturbation theory cannot be utilized to find corrections of the second order ( $\theta^2$  and  $\bar{\theta}^2$ ) because we have only employed corrections of the first order of infinitesimal noncommutative parameters ( $\theta$  and  $\bar{\theta}$ ).

#### 4. MAIN RESULTS

In the previous subsections, we obtained the solution of the modified Schrödinger equation for new improved internal energy potential, which is given in Eq. (25) by using the generalized Bopp's shift method and standard perturbation theory in pNRQCD by the feature of 3D-NRNCPS symmetries. The modified eigenenergies  $(E_{nc}^{gip}, E_{nc}^{mip}, E_{nc}^{lip}) (T, c, n = 0, m = 0, l)$ ,  $(E_{nc}^{gip}, E_{nc}^{mip}, E_{nc}^{lip}) (T, c, j, n = 1, (m = \overline{-l, +l}), l)$  and  $(E_{nc}^{gip}, E_{nc}^{mip}, E_{nc}^{lip}) (T, c, j, n, (m = \overline{-l, +l}), l)$  with spin-1 for heavy quarkonium systems  $Q\bar{Q}$  ( $Q = c, b$ ) with improved internal energy potential at finite temperature are obtained in this paper based on our original results presented in Eqs. (37), (40), (41), (44), and (50) in addition to the ordinary energy  $E_{nl}$  for the improved internal energy potential at a finite temperature which is presented in Eq. (11):

➤ For the ground state:

$$E_{nc}^{gip}(T, c, n = 0, m = 0, l) = E_{0l} + g_s \frac{(2\alpha)^{\frac{2\delta+1}{2}} \exp(-\beta^2/2\alpha)}{\Gamma(2\delta+1) D_{-(2\delta+1)}(\beta\sqrt{2/\alpha})} \left\{ (\theta k_1(l) + B\sigma m + \Omega \chi m) T_{00} + \frac{1}{2\mu} (k_1(l) \bar{\theta} + B\bar{\sigma} m + \Omega \bar{\chi} m) \right\}, \tag{51.1}$$

$$E_{nc}^{mip}(T, c, n = 0, m = 0, l) = E_{0l} + g_s \frac{(2\alpha)^{\frac{2\delta+1}{2}} \exp(-\beta^2/2\alpha)}{\Gamma(2\delta+1) D_{-(2\delta+1)}(\beta\sqrt{2/\alpha})} \left\{ (\theta k_2(l) + B\sigma m + \Omega \chi m) T_{00} + \frac{1}{2\mu} (k_2(l) \bar{\theta} + B\bar{\sigma} m + \Omega \bar{\chi} m) \right\}, \tag{51.2}$$

$$E_{nc}^{lip}(T, c, n = 0, m = 0, l) = E_{0l} + g_s \frac{(2\alpha)^{\frac{2\delta+1}{2}} \exp(-\beta^2/2\alpha)}{\Gamma(2\delta+1)D_{-(2\delta+1)}(\beta\sqrt{2/\alpha})} \left\{ (\Theta k_3(l) + B\sigma m + \Omega\chi m)T_{00} \right\} + \frac{1}{2\mu} (k_3(l)\bar{\theta} + B\bar{\sigma}m + \Omega\bar{\chi}m), \quad (51.3)$$

➤ For the first excited state:

$$E_{nc}^{gip}(T, c, j, n = 1, (m = \overline{-l, +l}), l) = E_{1l} + \frac{g_s}{I_1 - 2\alpha_1 I_2 + \alpha_1^2 I_3} \left\{ (\Theta k_1(l) + B\sigma m + \Omega\chi)T_{01} \right\} + \frac{1}{2\mu} (k_1(l)\bar{\theta} + B\bar{\sigma}m + \Omega\bar{\chi}m), \quad (52.1)$$

$$E_{nc}^{mip}(T, c, j, n = 1, (m = \overline{-l, +l}), l) = E_{1l} + \frac{g_s B}{I_1 - 2\alpha_1 I_2 + \alpha_1^2 I_3} \left\{ (\Theta k_2(l) + B\sigma m + \Omega\chi)T_{01} \right\} + \frac{1}{2\mu} (k_2(l)\bar{\theta} + B\bar{\sigma}m + \Omega\bar{\chi}m), \quad (52.2)$$

$$E_{nc}^{lip}(T, c, j, n = 1, (m = \overline{-l, +l}), l) = E_{1l} + \frac{g_s B}{I_1 - 2\alpha_1 I_2 + \alpha_1^2 I_3} \left\{ (\Theta k_3(l) + B\sigma m + \Omega\chi m)T_{01} \right\} + \frac{1}{2\mu} (k_3(l)\bar{\theta} + B\bar{\sigma}m + \Omega\bar{\chi}m), \quad (52.3)$$

➤ For any  $(n, l, m)^{th}$  excited state:

$$E_{nc}^{gip}(T, c, j, n, (m = \overline{-l, +l}), l) = E_{nl} + g_s N_{nl}^2 \left\{ (\Theta k_1(l) + B\sigma m + \Omega\chi m)T_{1n} + \frac{1}{2\mu} (k_1(l)\bar{\theta} + B\bar{\sigma}m + \Omega\bar{\chi}m) \right\}, \quad (53.1)$$

$$E_{nc}^{mip}(T, c, j, n, (m = \overline{-l, +l}), l) = E_{nl} + g_s N_{nl}^2 \left\{ (\Theta k_2(l) + B\sigma m + \Omega\chi m)T_{1n} + \frac{1}{2\mu} (k_2(l)\bar{\theta} + B\bar{\sigma}m + \Omega\bar{\chi}m) \right\}, \quad (53.2)$$

$$E_{nc}^{lip}(T, c, j, n, (m = \overline{-l, +l}), l) = E_{nl} + g_s N_{nl}^2 \left\{ (\Theta k_3(l) + B\sigma m + \Omega\chi m)T_{1n} + \frac{1}{2\mu} (k_3(l)\bar{\theta} + B\bar{\sigma}m + \Omega\bar{\chi}m) \right\}, \quad (53.3)$$

where  $E_{0l}$  and  $E_{1l}$  are the energy of the ground state and the first excited state of heavy quarkonium systems in the symmetries of quantum mechanics under internal energy potential at finite temperature:

$$E_{0l} = \frac{\alpha(1+2\delta-\beta^2-d_2+m_D(T)d_3)}{2\mu}, \quad (54.1)$$

and

$$E_{1l} = \frac{\alpha(1+2(\delta+1)-\beta^2-d_2+m_D(T)d_3)}{2\mu}. \quad (54.2)$$

This is one of the main objectives of our research and by noting that the obtained eigenvalues of energy are real's and then the NC diagonal Hamiltonian  $H_{nc}^{ip}(x_\mu, p_\mu)$  is Hermitian. Furthermore, it's possible to write the three elements  $(H_{nc}^{ip})_{11}$ ,  $(H_{nc}^{ip})_{22}$  and  $(H_{nc}^{ip})_{33}$  as follows:

$$H_{ip}(x_\mu, p_\mu) \rightarrow H_{nc}^{ip}(x_\mu, p_\mu) \equiv \text{diag} \left( (H_{nc}^{ip})_{11}, (H_{nc}^{ip})_{22}, (H_{nc}^{ip})_{33} \right), \quad (55)$$

where

$$\left. \begin{aligned} (H_{nc}^{ip})_{11} &= -\frac{\Delta_{nc}}{2\mu} + H_{int}^{gip} \\ (H_{nc}^{ip})_{22} &= -\frac{\Delta_{nc}}{2\mu} + H_{int}^{mip} \\ (H_{nc}^{ip})_{33} &= -\frac{\Delta_{nc}}{2\mu} + H_{int}^{lip} \end{aligned} \right\}$$

In the symmetries of 3D-NRNCPS, the new kinetic term  $\frac{\Delta_{nc}}{2\mu}$  can be expressed as:

$$\frac{\Delta_{nc}}{2\mu} = \frac{\Delta - \vec{\mathbf{L}}\vec{\boldsymbol{\theta}} - \vec{\mathbf{L}}\vec{\boldsymbol{\sigma}} - \vec{\mathbf{L}}\vec{\boldsymbol{\chi}}}{2\mu}$$

The three modified interaction elements  $(H_{int}^{gip}, H_{int}^{mip}, H_{int}^{lip})$  are given by the following expressions:

$$H_{int}^{gip} = \left( D_2 + \frac{D_3}{r} + D_4 r + D_5 r^2 \right) \exp(-m_D(T)r) {}_s(k_1(l)\theta + \sigma \mathfrak{N}_{mod}^{zz})(r, A_i, D_3), \quad (56.1)$$

$$H_{int}^{mip} = \left( D_2 + \frac{D_3}{r} + D_4 r + D_5 r^2 \right) \exp(-m_D(T)r) {}_s(k_2(l)\theta + \sigma \mathfrak{N}_{mod}^{zz})(r, A_i, D_3), \quad (56.2)$$

and

$$H_{int}^{lip} = \left( D_2 + \frac{D_3}{r} + D_4 r + D_5 r^2 \right) \exp(-m_D(T)r) {}_s(k_3(l)\theta + \sigma \mathfrak{N}_{mod}^{zz})(r, A_i, D_3). \quad (56.3)$$

Thus, the ordinary kinetic term for the internal energy potential  $(-\frac{\Delta}{2\mu})$  and ordinary interaction

$\left( D_2 + \frac{D_3}{r} + D_4 r + D_5 r^2 \right) \exp(-m_D(T)r)$  are replaced by a new modified form of the kinetic term  $(\frac{\Delta_{nc}}{2\mu})$  and new modified

interactions modified to the new form  $(H_{int}^{gip}, H_{int}^{mip}, H_{int}^{lip})$  in 3D-NRNCPS symmetries. On the other hand, it is evident consider the quantum number  $m$  takes  $(2l + 1)$  values and we have also three values for  $(j = l \pm 1, l)$ , thus every state in the usually three-dimensional space of energy for a heavy quarkonium system under improved internal energy potential

will be  $3(2l + 1)$  sub-states. To obtain the complete total degeneracy of the energy level of the improved internal energy potential in 3D-NRNCPS symmetries, we need to sum all allowed values  $l$ . Total degeneracy is thus,

$$\underbrace{\sum_{l=0}^{n-1} (2l + 1)}_{3\text{D-NRQM}} = n^2 \rightarrow \underbrace{3(\sum_{l=0}^{n-1} (2l + 1))}_{3\text{D-NRNCPS}} \equiv 3n^2. \quad (57)$$

Note that the obtained new energy eigenvalues  $(E_{nc}^{gip}, E_{nc}^{mip}, E_{nc}^{lip})(T, c, j, n, (m = \overline{-l, +l}), l)$  now depend on new discrete atomic quantum numbers  $(n, j, l, s)$  and  $m$  in addition to the parameters of the internal energy potential. It is pertinent to note that when the atoms have spin-0, the total operator can be obtained from the interval  $|l - s| \leq j \leq |l + s|$ , which allows us to obtain the eigenvalues of the operator  $G^2$  as  $k(j, l, s) \equiv 0$  and then the nonrelativistic energy spectrum  $(E_{nc}^{gip}, E_{nc}^{mip}, E_{nc}^{lip})(T, j, n, (m = \overline{-l, +l}), l)$  reads [68, 69]:

$$(E_{nc}^{gip}, E_{nc}^{mip}, E_{nc}^{lip})(T, c, j, n, (m = \overline{-l, +l}), l) = E_{nl} + g_s N_{nl}^2 \left\{ \sigma T_{1n} + \frac{\bar{\sigma}}{2\mu} \right\} Bm. \quad (58)$$

It is important to apply the present results (53) and (58) to quarkonium mesons. One of the most important applications in the extended model of pNRQCD is to calculate the modified mass spectra of the heavy quarkonium systems (the mass of the quarkonium bound state), such as charmonium and bottomonium mesons, which have the quark and antiquark flavor in the symmetries of NCQM under improved internal energy potential at finite temperature. To achieve this goal, we generalize the traditional formula [84-91],

$$M = 2m_q + E_{nl}$$

which defines the total mass of the different quarkonium states (resonance masses), to the new form:

$$M = 2m_q + E_{nl} \rightarrow M_{nc}^{ip} = 2m_q + \frac{1}{3} (E_{nc}^{gip} + E_{nc}^{mip} + E_{nc}^{lip})(T, c, j, n, (m = \overline{-l, +l}), l). \quad (59)$$

Here  $m_q$  is the bare mass of quarkonium or twice the reduced mass of the system. Moreover,  $\frac{1}{3} (E_{nc}^{gip} + E_{nc}^{mip} + E_{nc}^{lip})(T, c, j, n, (m = \overline{-l, +l}), l)$  is the non-polarized energies, which can determine from Eqs. (49) and (54). Thus, at finite temperature, the modified mass of the quarkonium system  $M_{nc}^{ip}$  obtain:

$$M_{nc}^{ip} = M - g_s N_{nl}^2 \begin{cases} \left\{ (\sigma Bm + \chi \Omega m - \frac{l+4}{6} \theta +) T_{1n} + \frac{m}{2\mu} (B\bar{\sigma} + \Omega \bar{\chi}) - \frac{\bar{\theta}(l+4)}{12\mu} \right\} & \text{for spin-1} \\ \left\{ (\sigma B + \chi \Omega) T_{1n} m + \frac{1}{2} (B\bar{\sigma} + \Omega \bar{\chi}) m \right\} & \text{for spin-0} \end{cases}. \quad (60)$$

Here  $M$  is the heavy quarkonium system at a finite temperature with improved internal energy potential in commutative quantum mechanics, which is defined in ref. [7]. If we consider  $(\theta, \sigma, \chi) \rightarrow (0, 0, 0)$ , we recover the results of the commutative space of ref. [7] for the improved internal energy potential, which means that our calculations are correct. The novelty in this work is that the generalized Bopp shift method is successfully applied to find the solution of the 3-radial DSE at finite temperature in the symmetries of the 3D-NRNCPS framework. The automatic appearance of the spin in the term of improved energy as a quantum number clearly shows that the deformed Schrödinger equation under the influence of the improved energy potential model at finite temperature rises to the descriptor of the Dirac equation, meaning that this system can be valid in the field of high energies.

## 5. CONCLUSION

In the present work, the 3-dimensional deformed Schrodinger equation is analytically solved using the generalized Bopp's shift method and standard perturbation theory by the feature of 3D-NRNCPS symmetries. The improved internal energy potential at finite temperature is extended to include the effect of the non-commutativity space phase based on ref. [7]; we resume the main results:

➤ The ordinary Hamiltonian operator at finite temperature  $H_{ip}(x_\mu, p_\mu)$  in 3D-NRNCPS symmetries was replaced by a new modified operator  $H_{nc}^{ip}(x_\mu, p_\mu)$  which equals  $diag((H_{nc}^{ip})_{11}, (H_{nc}^{ip})_{22}, (H_{nc}^{ip})_{33})$  in the 3D-NRNCPS symmetries framework for the heavy quarkonium system such as  $Q\bar{Q}$  ( $Q = c, b$ ),

➤ The ordinary kinetic term  $-\frac{\Delta}{2\mu}$  in 3D-NRNCPS symmetries is modified to the new form  $\frac{\Delta_{nc}}{2\mu}$  which is equal  $(\frac{\Delta - \vec{L}\vec{\theta} - \vec{L}\vec{\sigma} - \vec{L}\vec{\chi}}{2\mu})$  to a heavy quarkonium system under the influence of the improved internal energy potential at the finite-temperature model.

➤ We have obtained the perturbative corrections  $((E_{nc}^{gip}, E_{nc}^{mip}, E_{nc}^{lip})(T, c, j, n, (m = \overline{-l, +l}), l), (E_{nc}^{gip}, E_{nc}^{mip}, E_{nc}^{lip})(T, c, j, n = 1, (m = \overline{-l, +l}), l)$  and  $(E_{nc}^{gip}, E_{nc}^{mip}, E_{nc}^{lip})(T, c, j, n, (m = \overline{-l, +l}), l)$  for the ground state, the first excited state,

and the  $(n, l, m)^{th}$  excited state with (spin-1 and spin-0) for the heavy quarkonium system under the influence of the improved internal energy potential model at finite temperature are obtained.

➤ We have obtained, at finite temperature, the modified mass of the quarkonium system  $M_{nc}^{ip}$  which equals the sum of the corresponding values  $M$  in the 3D-NRNCPSsymmetries, and two perturbative terms proportional with two parameters ( $\theta$  and  $\bar{\theta}$ ).

➤ Since the main quantum number, spin, appears clearly and automatically in the expression of the global Hamiltonian and its eigenvalues, this is an indication that our results are valid in the field of high energies where the Dirac equation is applied.

Through high-value results, which we have achieved in the present work, we hope to extend our recent work for further investigations of particle physics and other characteristics of quarkonium at finite temperatures.

#### Acknowledgments

The author would like to express gratitude to the General Directorate for Scientific Research and Technological Development for the financial assistance they provided throughout the execution of this work. The author would like to acknowledge the reviewers for their kind recommendations that lead to several improvements in the article.

**Competing interests.** The author declares that they have no competing interests.

#### ORCID IDs

Abdelmajid Maireche, <https://orcid.org/0000-0002-8743-9926>

#### REFERENCES

- [1] X.Y. Wu, B.J. Zhang, X.J. Liu, Y.H. Wu, Q.C. Wang, and Y. Wang, "Finite temperature Schrödinger equation", *Int. J. Theor. Phys.*, **50**(8), 2546 (2017). <https://doi.org/10.1007/s10773-011-0745-7>
- [2] C.Y. Wong, "Heavy quarkonia in quark-gluon plasma", *Phys. Rev. C.*, **72**(3), 034906 (2005). <https://doi.org/10.1103/PhysRevC.72.034906>
- [3] T. Matsui, and H. Satz, "J/ψ suppression by quark-gluon plasma formation", *Phys. Lett. B*, **178**(4), 416 (1986). [https://doi.org/10.1016/0370-2693\(86\)91404-8](https://doi.org/10.1016/0370-2693(86)91404-8)
- [4] V. Mateu, P. G. Ortega, D. R. Entem, and F. Fernández, "Calibrating the naïve Cornell model with NRQCD", *Eur. Phys. J. C*, **79** (4), 323 (2019). <https://doi.org/10.1140/epjc/s10052-019-6808-2>
- [5] J. Fingberg, "Heavy quarkonia at high temperature", *Physics Letters B*, **424**(3-4), 343 (1998). [https://doi.org/10.1016/s0370-2693\(98\)00205-6](https://doi.org/10.1016/s0370-2693(98)00205-6)
- [6] A.I. Ahmadov, C. Aydin, and O. Uzun, "Bound state solution of the Schrödinger equation at finite temperature", *Journal of Physics: Conference Series*, **1194**, 012001 (2019). <https://doi.org/10.1088/1742-6596/1194/1/012001>
- [7] M. Abu-Shady, "Multidimensional Schrödinger Equation and Spectral Properties of Heavy-Quarkonium Mesons at Finite Temperature", *Advances in Mathematical Physics*, **2016**, 1 (2016). <https://doi.org/10.1155/2016/4935940>
- [8] M.E. Naggar, N.I. Abou Salem, L.G. A. Shalaby, and A.M. Bourham, "The Equation of State for Non-ideal Quark Gluon Plasma", *Physical Science International Journal*, **4**(7), 912 (2014). <https://doi.org/10.9734/PSIJ/2014/10296>
- [9] W. Heisenberg, *Letter to R. Peierls*, in: *Wolfgang Pauli, Scientific Correspondence*, edited by K. von Meyenn – 1985. (Springer Verlag, 1930), Vol. III, p. 15.
- [10] H.S. Snyder, "Quantized Space-Time", *Phys. Rev.*, **71**, 38 (1947). <https://doi.org/10.1103/PhysRev.71.38>, "The Electromagnetic Field in Quantized Space-Time", *Phys. Rev.*, **72**, 68 (1947). <https://doi.org/10.1103/PhysRev.72.68>
- [11] A. Connes, M.R. Douglas, and A. Schwarz, "Noncommutative geometry and Matrix theory", *Journal of High Energy Physics*, **02**, 003 (1998). <https://doi.org/10.1088/1126-6708/1998/02/003>
- [12] N. Seiberg, and E. Witten, "String theory and noncommutative geometry", *Journal of High Energy Physics*, **1999**(09) 032 (1999). <https://doi.org/10.1088/1126-6708/1999/09/032>
- [13] S. Capozziello, G. Lambiase, and G. Scarpetta, "Generalized Uncertainty Principle from Quantum Geometry", *Int. J. Theor. Phys.*, **39**, 15 (2000). <https://doi.org/10.1023/A:1003634814685>
- [14] S.K. Doplicher, and J.E. Fredenhagen, "Spacetime quantization induced by classical gravity, Roberts", *Phys. Lett. B*, **331**(1-2), 39 (1994). [https://doi.org/10.1016/0370-2693\(94\)90940-7](https://doi.org/10.1016/0370-2693(94)90940-7)
- [15] E. Witten, "Reflections on the Fate of Spacetime", *Phys. Today*, **49**(4), 24 (1996). <https://doi.org/10.1063/1.881493>
- [16] A. Kempf, G. Mangano, and R.B. Mann, "Hilbert space representation of the minimal length uncertainty relation", *Phys. Rev. D*, **52**(2), 1108 (1995). <https://doi.org/10.1103/physrevd.52.1108>
- [17] F. Scardigli, "Some Heuristic Semi-Classical Derivations of the Planck the Hawking effect and the Unruh effect. Il Nuovo Cimento B Series, 11 B (9), 1029 (1995). <https://doi.org/10.1007/bf02726152>
- [18] R.J. Adler, and D.I. Santiago, "On gravity and the uncertainty principal", *Mod. Phys. Lett. A*, **14**(20), 1371 (1999). <https://doi.org/10.1142/s0217732399001462>
- [19] H. Benzaira, M. Merad, T. Boudjedaad, and A. Makhlof "Relativistic Oscillators in a Noncommutative Space: a Path Integral Approach", *Z. Naturforsch.* **67a**, 77 (2012). <https://doi.org/10.5560/ZNA.2011-0060>
- [20] F. Scardigli, "Generalized uncertainty principle in quantum gravity from micro-black hole gedanken experiment", *Phys. Lett. B*, **452**(1-2), 39 (1999). [https://doi.org/10.1016/s0370-2693\(99\)00167-7](https://doi.org/10.1016/s0370-2693(99)00167-7)
- [21] P.M. Ho and H.C. Kao, "Noncommutative Quantum Mechanics from Noncommutative Quantum Field Theory", *Phys. Rev. Lett.*, **88**(15), 151602-1(2002). <https://doi.org/10.1103/physrevlett.88.151602>
- [22] O. Bertolami, G.J. Rosa, C.M.L. Dearagao, P. Castorina, and D. Zappala, "Scaling variables and the relation between noncommutative parameters in noncommutative quantum mechanics", *Mod. Phys. Lett. A*, **21**(10), 795 (2006). <https://doi.org/10.1142/s0217732306019840>

- [23] P. Gnatenko, “Parameters of noncommutativity in Lie-algebraic noncommutative space”, *Phys. Rev. D.*, **99**(2), 026009-1(2019). <https://doi.org/10.1103/physrevd.99.026009>
- [24] E.E. N’Dolo, D.O. Samary, B. Ezinvi, and M.N. Hounkonnou, Noncommutative Dirac and Klein–Gordon oscillators in the background of cosmic string: Spectrum and dynamics. *International Journal of Geometric Methods in Modern Physics*, 17(05), 2050078 (2020). <https://doi.org/10.1142/S0219887820500784>
- [25] O. Bertolami, and P. Leal, Aspects of phase-space noncommutative quantum mechanics”, *Phys. Lett. B.*, **750**, 6 (2015). <https://doi.org/10.1016/j.physletb.2015.08.024>
- [26] M.A. De Andrade, and C. Neves, “Noncommutative mapping from the symplectic formalism”, *J. Math. Phys.*, **59**(1), 012105 (2018). <https://doi.org/10.1063/1.4986964>
- [27] K.P. Gnatenko, and V.M. Tkachuk, “Upper bound on the momentum scale in noncommutative phase space of canonical type”, *EPL*, **127**(2), 20008 (2019). <https://doi.org/10.1209/0295-5075/127/20008>
- [28] K.P. Gnatenko, and V.M. Tkachuk, “Composite system in rotationally invariant noncommutative phase space”, *Int. J. Mod. Phys. A.*, **33**(07), 1850037(2018). <https://doi.org/10.1142/s0217751x18500379>
- [29] A. Maireche, “Bound-state solutions of the modified Klein-Gordon and Schrödinger for arbitrary noncommutative quantum mechanics”, *J. Phys. Stud.* **25**(1), 1002 (2021). <https://doi.org/10.30970/jps.25.1002>
- [30] A. Maireche, “A Theoretical Model of Deformed Klein-Gordon Equation with Generalized Modified Screened Coulomb Plus Inversely Quadratic Yukawa Potential in RNCQM Symmetries”, *Few-Body Syst.* **62**, 12 (2021). <https://doi.org/10.1007/s00601-021-01596-2>
- [31] A. Maireche, “The Relativistic and Nonrelativistic Solutions for the Modified Unequal Mixture of Scalar and Time-Like Vector Cornell Potentials in the Symmetries of Noncommutative Quantum Mechanics”, *Jordan Journal of Physics*, **14**(1), 59 (2021). <https://doi.org/10.47011/14.1.6>
- [32] J. Gamboa, M. Loewe, and J.C. Rojas, Noncommutative quantum mechanics *Phys. Rev. D.*, **64**, 067901(2001). .
- [33] E.F. Djemai, and H. Smail, “On Quantum Mechanics on Noncommutative Quantum Phase Space”, *Commun. Theor. Phys.* (Beijing, China), **41**(6), 837 (2004). <https://doi.org/10.1088/0253-6102/41/6/837>
- [34] Y. Yi, K. Kang, W. Jian-Hua, and C. Chi-Yi, Spin-1/2 relativistic particle in a magnetic field in NC phase space”, *Chin. Phys. C.*, **34**(5), 543 (2010). <https://doi.org/10.1088/1674-1137/34/5/005G>.
- [35] G. Valencia-Ortega, and L.A. Arias-Hernandez, “Thermodynamic properties of diatomic molecule systems under SO (2,1)-anharmonic Eckart potential International”, *Journal of Quantum Chemistry*, **118**(14), e25589(2018). <https://doi.org/10.1002/qua.25589>
- [36] A. Maireche, “Solutions of Klein-Gordon equation for the modified central complex potential in the symmetries of noncommutative quantum mechanics”, *Sri Lankan Journal of Physics*, **22**(1), 1 (2021). <http://doi.org/10.4038/sljp.v22i1.8079>
- [37] A. Maireche, “Theoretical Investigation of the Modified Screened cosine Kratzer potential via Relativistic and nonrelativistic treatment in the NCQM symmetries”, *Lat. Am. J. Phys. Educ.* **14** (3), 3310-1 (2020). <https://dialnet.unirioja.es/descarga/articulo/7803865.pdf>
- [38] A. Maireche, “Modified Unequal Mixture Scalar Vector Hulthén–Yukawa Potentials Model as a Quark–Antiquark Interaction and Neutral Atoms via Relativistic Treatment Using the Improved Approximation of the Centrifugal Term and Bopp’s Shift Method”, *Few-Body Syst.*, **61**, 30 (2020). <https://doi.org/10.1007/s00601-020-01559-z>
- [39] O. Bertolami, J.G. Rosa, C.M.L. De Aragão, P. Castorina, and D. Zappalà, “Noncommutative gravitational quantum well Phys”, *Rev. D.*, **72**(2), 025010-1(2005). <https://doi.org/10.1103/PhysRevD.72.025010>
- [40] J. Zhang, “Coherent states of the deformed Heisenberg–Weyl algebra in non-commutative space”, *Phys. Lett. B*, **584**(1-2), 204 (2004). <https://doi.org/10.1016/j.physletb.2005.03.040>
- [41] J.F.G. Santos, “Heat flow and noncommutative quantum mechanics in phase-space,” *J. Math. Phys.*, **61**, 122101, (2020). <https://doi.org/10.1063/5.0010076>.
- [42] E.M.C. Abreu, C. Neves, and O.W. liveira, “Noncommutativity from the symplectic point of view”, *Int. J. Mod. Phys. A.*, **21**, 5359 (2006). <https://doi.org/10.1142/S0217751X06034094>.
- [43] E.M.C. Abreu, J.A. Neto, A.C.R. Mendes, C. Neves, W. Oliveira, and M.V. Marcial, “Lagrangian formulation for noncommutative nonlinear systems *Int. J. Mod. Phys. A*, **27**, 1250053(2012). <https://doi.org/10.1142/S0217751X12500534>
- [44] J. Wang, and K. Li, “The HMW effect in noncommutative quantum mechanics”, *J. Phys. A Math. Theor.*, **40**(9), 2197 (2007). <https://doi.org/10.1088/1751-8113/40/9/021>
- [45] K. Lin, and J. Wang, “The topological AC effect on non-commutative phase space”, *Eur. Phys. J. C*, **50**(4), 1007 (2007). <https://doi.org/10.1140/epjc/s10052-007-0256-0>
- [46] A. Maireche, A theoretical investigation of nonrelativistic bound state solution at finite temperature using the sum of modified Cornell plus inverse quadratic potential”, *Sri Lankan Journal of Physics*, **21**, 11-35(2020). <http://doi.org/10.4038/sljp.v21i1.8069>
- [47] A. Maireche, “Extended of the Schrödinger equation with new Coulomb potentials plus linear and Harmonic radial terms in the symmetries of noncommutative quantum mechanics”, *J. Nano-Electron. Phys.*, **10**(6), 06015-1 (2018). [https://doi.org/10.21272/jnep.10\(6\).06015](https://doi.org/10.21272/jnep.10(6).06015)
- [48] A. Maireche, “The Klein-Gordon equation with modified Coulomb plus inverse-square potential in the noncommutative three-dimensional space”, *Mod. Phys. Lett. A*, **35**(5), 052050015 (2020). <https://doi.org/10.1142/s0217732320500157>
- [49] A. Maireche, “The Klein–Gordon equation with modified Coulomb potential plus inverse-square–root potential in three-dimensional noncommutative space”, *To Physics Journal*, **3**, 186 (2019). <https://www.purkh.com/articles/the-kleingordon-equation-with-modified-coulomb-potential-plus-inversesquareroot-potential-in-three-dimensional-non-commut.pdf>
- [50] A. Maireche, “Bound-state solutions of Klein-Gordon and Schrödinger equations for arbitrary  $l$ -state with combination of Hulthén and Kratzer potentials”, *Afr. Rev Phys.* **15**(0003), 19 (2020). <http://lamp.ictp.it/index.php/aphysrev/article/download/1779/620>
- [51] H. Motavalli, and A.R. Akbarieh, “Klien-Gordon equation for the Coulomb potential in noncommutative space”, *Phys. Lett. A*, **25**(29), 2523 (2010). <https://doi.org/10.1142/s0217732310033529>
- [52] M. Darroodi, H. Mehraban, and H. Hassanabadi, “The Klein–Gordon equation with the Kratzer potential in the noncommutative space”, *Mod. Phys. Lett. A*, **33** (35), 1850203 (2018). <https://doi.org/10.1142/s0217732318502036>
- [53] A. Maireche, “A New Theoretical Investigation of the Modified Equal Scalar and Vector Manning–Rosen Plus Quadratic Yukawa Potential Within the Deformed Klein-Gordon and Schrödinger Equations Using the Improved Approximation of the Centrifugal

- Term and Bopp's Shift Method in RNCQM and NRNCQM Symmetries", *Spin J.* **11**, No. 4, 2150029 (2021). <https://doi.org/10.1142/S2010324721500296>
- [54] A. Maireche, "Heavy quarkonium systems for the deformed unequal scalar and vector Coulomb–Hulthén potential within the deformed effective mass Klein–Gordon equation using the improved approximation of the centrifugal term and Bopp's shift method in RNCQM symmetries", *International Journal of Geometric Methods in Modern Physics*, **18**(13), 2150214 (2021). <https://doi.org/10.1142/S0219887821502133>
- [55] A. Maireche, "A new theoretical study of the deformed unequal scalar and vector Hellmann plus modified Kratzer potentials within the deformed Klein–Gordon equation in RNCQM symmetries", *Modern Physics Letters A*, **36**(33), 2150232. (2021). <https://doi.org/10.1142/S0217732321502321>
- [56] A. Maireche, "A theoretical study of the modified equal scalar and vector Manning–Rosen potential within the deformed Klein–Gordon and Schrödinger in RNCQM and NRNCQM symmetries", *Rev. Mex. Fis.*, **67**, no. 5 050702 1–18, (2021). <https://doi.org/10.31349/revmexfis.67.050702>
- [57] A. Maireche, "The Investigation of Approximate Solutions of Deformed Klein–Gordon and Schrödinger Equations Under Modified More General Exponential Screened Coulomb Potential Plus Yukawa Potential in NCQM Symmetries", *Few-Body Syst* **62**, 66 (2021). <https://doi.org/10.1007/s00601-021-01639-8>
- [58] A. Maireche, "The Relativistic and Nonrelativistic Solutions for the Modified Unequal Mixture of Scalar and Time-Like Vector Cornell Potentials in the Symmetries of Noncommutative Quantum Mechanics", *Jordan Journal of Physics*, **14**(1), 59 (2021). <https://doi.org/10.47011/14.1.6>
- [59] A. Maireche, "A Theoretical Model of Deformed Klein–Gordon Equation with Generalized Modified Screened Coulomb Plus Inversely Quadratic Yukawa Potential in RNCQM Symmetries", *Few-Body Syst*, **62**, 12 (2021). <https://doi.org/10.1007/s00601-021-01596-2>
- [60] A. Maireche, "New bound-state solutions of the deformed Klien–Gordon and Schrödinger equations for arbitrary  $l$ -state with modified equal vector and scalar Manning–Rosen plus a class of Yukawa potential in RNCQM and NRNCQM symmetries", *Journal of Physical Studies*, **25**(4). 4301 (2021). <https://doi.org/10.30970/jps.25.4301>
- [61] A. Maireche, "Bound-state solutions of the modified Klein–Gordon and Schrödinger equations for arbitrary  $l$ -state with the modified morse potential in the symmetries of noncommutative quantum mechanics", *Journal of Physical Studies*, **25**(1), 1002 (2021). <https://doi.org/10.30970/jps.25.1002>
- [62] A. Saidi, and M.B. Sedra, "Spin-one (1 + 3)-dimensional DKP equation with modified Kratzer potential in the non-commutative space", *Phys. Lett. A*, **35**(5), 2050014 (2020). <https://doi.org/10.1142/s0217732320500145>
- [63] A. Maireche, "A model of modified Klien–Gordon equation with modified scalar-vector Yukawa potential", *Afr. Rev Phys.* **15**(0001), 1 (2020). <http://lamp.ictp.it/index.php/aphysrev/article/view/1777/618>
- [64] A. Maireche, "The relativistic treatment of hydrogen-like and neutral atoms subjected to the generalized perturbed Yukawa potential with centrifugal barrier in the symmetries of noncommutative quantum mechanics", *International Journal of Geometric Methods in Modern Physics*, **17**(5), 2050067 (2020). <https://doi.org/10.1142/S021988782050067X>
- [65] A. Maireche, "A Recent Study of Excited Energy Levels of Diatomics for Modified more General Exponential Screened Coulomb Potential: Extended Quantum Mechanics", *J. Nano- Electron. Phys.* **9**(3), 03021 (2017). [https://doi.org/10.21272/jnep.9\(3\).03021](https://doi.org/10.21272/jnep.9(3).03021)
- [66] A. Maireche, "A new study of energy levels of hydrogenic atoms and some molecules for new more general exponential screened coulomb potential", *Open Acc J Math Theor Phys.*, **1**(6), 232 (2018). <https://doi.org/10.15406/oajmtp.2018.01.00040>
- [67] A. Maireche, "A New Approach to the Approximate Analytic Solution of the Three-Dimensional Schrödinger Equation for Hydrogenic and Neutral Atoms in the Generalized Hellmann Potential Model", *Ukr. J. Phys.* **65**(11), 987 (2020). <https://doi.org/10.15407/ujpe65.11.987>
- [68] A. Maireche, "Effects of Two-Dimensional Noncommutative Theories on Bound States Schrödinger Diatomic Molecules under New Modified Kratzer-Type Interactions", *International Letters of Chemistry, Physics and Astronomy*, **76**, 1 (2017). <https://doi.org/10.18052/www.scipress.com/ILCPA.76.1>
- [69] A. Maireche, "Any L-states solutions of the modified Schrödinger equation with generalized Hellmann–Kratzer potential model in the symmetries of NRNCQM", *To Physics Journal*, **4**, 16 (2019). <https://www.purkh.com/articles/any-lstates-solutions-of-the-modified-schrdinger-equation-with-generalized-hellmannkratzer-potential-model-in-the-symmet.pdf>
- [70] L. Mezincescu, "Star Operation in Quantum Mechanics", (2000). <https://arxiv.org/abs/hep-th/0007046>
- [71] L. Gouba, "A comparative review of four formulations of noncommutative quantum mechanics", *Int. J. Mod. Phys. A*, **31**(19), 1630025 (2016). <https://doi.org/10.1142/s0217751x16300258>
- [72] F. Bopp, "La mécanique quantique est-elle une mécanique statistique classique particulière", *Ann. Inst. Henri Poincaré*, **15**(2), 81 (1956). [http://www.numdam.org/item/AIHP\\_1956\\_\\_15\\_2\\_81\\_0.pdf](http://www.numdam.org/item/AIHP_1956__15_2_81_0.pdf)
- [73] A. Maireche, "New Relativistic Bound States for Modified Pseudoharmonic Potential of Dirac Equation with Spin and Pseudo-Spin Symmetry in One-electron Atoms", *Afr. Rev Phys.* **12**(0018), 130 (2017). <http://lamp.ictp.it/index.php/aphysrev/article/view/1533/564>
- [74] A. Maireche, "New Relativistic Atomic Mass Spectra of Quark (u, d and s) for Extended Modified Cornell Potential in Nano and Plank's Scales *J. Nano- Electron. Phys.*, **8** (1), 01020 (2016). [https://doi.org/10.21272/jnep.8\(1\).01020](https://doi.org/10.21272/jnep.8(1).01020)
- [75] A. Maireche, "A New Relativistic Study for Interactions in One-electron atoms (Spin  $\frac{1}{2}$  Particles) with Modified Mie-type Potential *J. Nano-Electron. Phys.*, **8**(4), 04027 (2016). [https://doi.org/10.21272/jnep.8\(4\(1\)\).04027](https://doi.org/10.21272/jnep.8(4(1)).04027)
- [76] A. Maireche, "Investigations on the Relativistic Interactions in One-Electron Atoms with Modified Yukawa Potential for Spin 1/2 Particles", *International Frontier Science Letters*, **11**, 29 (2017). <https://doi.org/10.18052/www.scipress.com/IFSL.11.29>
- [77] A. Maireche, "On the interaction of an improved Schiöberg potential within the Yukawa tensor interaction under the background of deformed Dirac and Schrödinger equations", *Indian J Phys*, **96**(10), (2022). <https://doi.org/10.1007/s12648-022-02433-w>
- [78] A. Maireche, "New Approximate Solutions to a Spatially-Dependent Mass Dirac Equation for Modified Hylleraas Plus Eckart Potential with Improved Yukawa Potential as a Tensor in the DQM Framework", *Few-Body Syst*, **63**, 63 (2022). <https://doi.org/10.1007/s00601-022-01766-w>
- [79] A. Maireche, "Approximate Arbitrary k State Solutions of Dirac Equation with Improved Inversely Quadratic Yukawa Potential within Improved Coulomb-like Tensor Interaction in Deformation Quantum Mechanics Symmetries", *Few-Body Syst*, **63**, 54 (2022). <https://doi.org/10.1007/s00601-022-01755-zS>

- [80] A. Maireche, "Approximate k-state solutions of the deformed Dirac equation in spatially dependent mass for the improved Eckart potential including the improved Yukawa tensor interaction in ERQM symmetries", International Journal of Geometric Methods in Modern Physics **19**, No. 06, 2250085 (2022). <https://doi.org/10.1142/S0219887822500852>
- [81] A. Maireche, "Relativistic symmetries of the deformed Dirac equation through the improved Hulthén plus a class Yukawa potential including a Coulomb-like in deformed quantum mechanics", Journal of Physical Studies, **26**(2), 2001-1 (2022). <https://doi.org/10.30970/jps.26.2001>
- [82] I.S. Gradshteyn, and I.M. Ryzhik, "Table of Integrals, Series and Products, 7th. ed.; Elsevier, edited by Alan Jeffrey (the University of Newcastle upon Tyne, England) and Daniel Zwillinger (Rensselaer Polytechnic Institute USA) 2007.
- [83] K. Bencheikh, S. Medjedel, and G. Vignale, "Current reversals in rapidly rotating ultracold Fermi gases", Phys. Lett. A, **89**(6), 063620 (2014). <https://doi.org/10.1103/physreva.89.063620>
- [84] M. Abu-Shady, T.A. Abdel-Karim, and S.Y. Ezz-Alarab, "Masses and thermodynamic properties of heavy mesons in the non-relativistic quark model using the Nikiforov–Uvarov method", J. Egypt Math. Soc. **27**, 14 (2019). <https://doi.org/10.1186/s42787-019-0014-0>
- [85] R. Rani, S.B. Bhardwaj, and F. Chand, "Mass Spectra of Heavy and Light Mesons Using Asymptotic Iteration Method", Communications in Theoretical Physics, **70**(2), 179 (2018). <https://doi.org/10.1088/0253-6102/70/2/179>
- [86] A. Maireche, "A New Asymptotic Study to the 3-Dimensional Radial Schrodinger Equation under Modified Quark-antiquark Interaction Potential", J. Nanosci. Curr. Res. **4**(1), 1000131 (2019). <https://www.hilarispublisher.com/open-access/a-new-asymptotic-study-to-the-3dimensional-radial-schrödinger-equation-under-modified-quarkantiquark-interaction-potential.pdf>
- [87] A. Maireche, "Heavy-light mesons in the symmetries of extended nonrelativistic quark model", Yanbu Journal of Engineering and Science, **17**, 51 (2019). <https://doi.org/10.53370/001c.23732>
- [88] A. Maireche, "Analytical Expressions to Energy Eigenvalues of the Hydrogenic Atoms and the Heavy Light Mesons in the Framework of 3D-NCPS Symmetries Using the Generalized Bopp's Shift Method", Bulg. J. Phys. **49**(3), 239 (2022). <https://doi.org/10.55318/bgjp.2022.49.3.239>
- [89] A. Maireche, "The Impact of Deformed Space-Phase Parameters into HAs and HLM Systems with the Improved Hulthén Plus Hellmann Potentials Model in the Presence of Temperature-Dependent Confined Coulomb Potential Within the Framework of DSE". Rev. Mex. Fis., **68**, no. 5 050702 1 (2022), <https://doi.org/10.31349/RevMexFis.68.050702>.
- [90] A. Maireche, "The investigation of approximate solutions of Deformed Schrödinger Equations for the Hydrogenic Atoms, Heavy Quarkonium Systems ( $Q\bar{Q} = b\bar{b}, c\bar{c}$ ) and Diatomic molecule Bound-State Problem under Improved Exponential, Generalized, Anharmonic Cornell potential Model in NCPS symmetries", Lat. Am. J. Phys. Educ. **12**(2), 2304 (2022). [http://www.lajpe.org/jun22/16\\_2\\_04.pdf](http://www.lajpe.org/jun22/16_2_04.pdf)
- [91] A. Maireche, "Relativistic symmetries of bosonic particles and antiparticles in the background of the position-dependent mass for the improved deformed Hulthén plus deformed type-hyperbolic potential in 3D-EQM symmetries", East Eur. J. Phys. **4**, 201 (2022). <https://periodicals.karazin.ua/eejp/article/view/20865/19710>

**ВПЛИВ ДЕФОРМАЦІЇ ФАЗОВОГО ПРОСТОРУ НА СПЕКТРИ ВАЖКОГО КВАРКОНІУ В ПОКРАЩЕНОМУ ЕНЕРГЕТИЧНОМУ ПОТЕНЦІАЛІ ЗА СКІНЧЕНОЇ ТЕМПЕРАТУРНОЇ МОДЕЛІ РІВНЯННЯ ШРЕДІНГЕРА ЧЕРЕЗ МЕТОД УЗАГАЛЬНЕНОГО ЗСУВУ БОППА ТА СТАНДАРТНУ ТЕОРІЮ ЗБУРЕНЬ**

**Абдельмаджид Майреше**

*Факультет фізики, Університет Мсіла, Лабораторія РМС, Університет Мсіла, Алжир*

У цій роботі ми отримуємо розв'язання деформованого рівняння Шредінгера (DSE) з покращеним внутрішнім енергетичним потенціалом при кінцевій температурній моделі в 3-вимірній нерелятивістській некомутативній системі симетрії фазового простору (3D-NRNCPS), використовуючи узагальнений метод зсуву Боппа у випадку збуреної нерелятивістської квантової хромодинаміки (pNRQCD). Отримано модифіковані енергетичні спектри зв'язаного стану для важкої кварконієвої системи, такої як чармоній  $c\bar{c}$  і боттононій  $b\bar{b}$  при кінцевій температурі. Встановлено, що пертурбативні розв'язки дискретного спектру чутливі до дискретних атомних квантових чисел ( $j, l, s, m$ ) стану  $Q\bar{Q}$  ( $Q = c, b$ ), параметрів потенціалу внутрішньої енергії ( $T, \alpha_s(T), m_D(T), \beta, c$ ), які є екрануючою масою Дебая  $m_D(T)$ , поточною константою зв'язку  $\alpha_s(T)$ , критичною температурою  $\beta$ , вільним параметром  $c$  на додаток до параметрів некомутативності ( $\theta, \bar{\theta}$ ). Новий оператор Гамільтона в симетриях 3D-NRNCPS складається з відповідного оператора в комутативному фазовому просторі та трьох адитивних частин для спіно-орбітальної взаємодії, нової магнітної взаємодії та обертового терма Фермі. Отримані власні енергетичні значення використовуються для отримання мас-спектрів важких кварконієвих систем ( $c\bar{c}$  and  $b\bar{b}$ ). Загальна повна виродженість нових енергетичних рівнів покращеного потенціалу внутрішньої енергії змінилася і стала рівною новому значенню  $3n^2$  у симетриях 3D-NRNCPS замість значення  $n^2$  у симетриях 3D-NRQM. Наші нерелятивістські результати, отримані із DSE, будуть за можливості зіставлені з рівнянням Дірака у фізиці високих енергій.

**Ключові слова:** *рівняння Шредінгера; некомутативний фазовий простір; потенціал внутрішньої енергії при кінцевій температурі; метод зсуву Боппа, важкі кварконієві системи*

## BIANCHI TYPE V UNIVERSE WITH TIME VARYING COSMOLOGICAL CONSTANT AND QUADRATIC EQUATION OF STATE IN $f(R, T)$ THEORY OF GRAVITY<sup>†</sup>

Chandra Rekha Mahanta<sup>a, #</sup>, Shayanika Deka<sup>a, ‡</sup>,  Manash Pratim Das<sup>b, \*</sup>

<sup>a</sup>Department of Mathematics, Gauhati University, Guwahati-781014 (INDIA)

<sup>b</sup>Department of Mathematics, BBK College, Barpeta (INDIA)

\*Corresponding Author E-mail: [manashpratimdas2222@gmail.com](mailto:manashpratimdas2222@gmail.com)

<sup>#</sup>E-mail: [crmahanta@gauhati.ac.in](mailto:crmahanta@gauhati.ac.in), <sup>‡</sup>E-mail: [shayanikadeka.sd75@gmail.com](mailto:shayanikadeka.sd75@gmail.com)

Received December 14, 2022; revised January 14, 2023; accepted January 17, 2023

In recent years, modified theories of gravity have been extensively studied because of the discovery and confirmation of the current phase of accelerated expansion of the universe. The  $f(R, T)$  theory of gravity is one such theory, proposed by Harko *et al.* in 2011, in which  $R$  is the Ricci scalar and  $T$  is the trace of the stress-energy tensor. In this paper, we study Bianchi type V universe in  $f(R, T)$  theory of gravity with time varying cosmological constant and a quadratic equation of state  $p = \alpha\rho^2 - \rho$ , where  $\alpha \neq 0$  is a constant. We obtain exact solutions of the field equations for two cases: one with a volumetric expansion law and the other with an exponential expansion law. The physical features of the two models are discussed by examining the behavior of some important cosmological parameters such as the Hubble parameter, the deceleration parameter etc. We find that the models have initial singularity and the physical parameters diverge at the initial epoch. The model 1, corresponding to the volumetric expansion law does not resemble  $\Lambda$ CDM model while the model 2, corresponding to the exponential expansion law, resembles  $\Lambda$ CDM model. The energy conditions of the models are also examined and found to be consistent with recent cosmological observations.

**Keywords:** *Bianchi type V universe;  $f(R, T)$  theory of gravity; Equation of state;  $\Lambda$ CDM model*

**PACS:** 98.80.jk, 04.20.jb

### 1. INTRODUCTION

Various astrophysical and cosmological observations like type Ia supernovae [1-3], Cosmic Microwave Background (CMB) [4, 5], Large Scale Structure (LSS) [6, 7] and other improved measurements of supernovae confirms the discovery of the late-time cosmic acceleration although it is yet to be ascertained what led to the start of this acceleration. According to the recent Planck collaboration results [8], it is found that about 95% of the total constituent of the universe is mysterious. Within the framework of General Relativity, the observed cosmic acceleration can be attributed to an exotic component of the universe with large negative pressure which contributes nearly 68% of the total energy content of the universe. This unknown energy fluid, supposed to be responsible for the late-time cosmic acceleration, is given the name dark energy. In literature, several dark energy candidates like quintessence [9,10], k-essence [11], tachyon [12], phantom [13], Chaplygin gas [14], Holographic dark energy [15] etc. have been proposed and studied in various cosmological background. It is seen that even though the hypothetical dark energy can smoothly explain the accelerated expansion of the universe, many dark energy models encounter with problems when tested by some old red-shift objects [16, 17]. Therefore, the other way considered to explain the cosmic acceleration is modifications of Einstein's theory of gravitation. Some of the most studied modifications of Einstein's General theory of Relativity are the  $f(R)$  theory of gravity [18, 19],  $f(T)$  gravity [20],  $f(R, T)$  theory of gravity [21],  $f(G)$  gravity [22] etc. In the  $f(R, T)$  theory of gravity, the gravitational Lagrangian in the Einstein-Hilbert action is modified by replacing the Ricci scalar  $R$  by an arbitrary function  $f(R, T)$  of  $R$  and the trace  $T$  of the stress-energy tensor. Harko *et al.* [21] have derived the gravitational field equations of this theory in the metric formalism, as well as the equations of motion for test particles, which follow from the covariant divergence of the stress-energy tensor. They have also presented the field equations corresponding to the homogeneous and isotropic FRW metric and provided a number of specific cosmological models that correspond to some explicit forms of the function  $f(R, T)$  such as  $f(R, T) = R + 2f(T)$ ,  $f(R, T) = f_1(R) + f_2(T)$ ,  $f(R, T) = f_1(R) + f_2(R)f_3(T)$ . Since then many researchers have studied various isotropic and anisotropic cosmological models in different contexts within this framework of modified theory of gravity.

In literature, various homogeneous and anisotropic cosmological models such as the Bianchi type models are studied in the context of dark energy as well as in alternative or modified theories of gravity. Homogeneous and anisotropic models of the universe are becoming more and more popular because of the anomalies found in the observations like Cosmic Microwave Background (CMB) and Large-Scale Structure [23, 24]. Also, models that are spatially homogeneous and anisotropic are helpful in describing the evolution of the early stages of the universe. Bianchi type V models are significant because they include the space of constant negative curvature as a special case.

In this paper, we study a spatially homogeneous and anisotropic Bianchi type V universe with a time dependent cosmological constant  $\Lambda$  and a quadratic equation of state  $p = \alpha\rho^2 - \rho$  [25], where  $\alpha \neq 0$  is a constant within the

<sup>†</sup> Cite as: C.R. Mahanta, S. Deka, and M.P. Das, East Eur. J. Phys. 1, 44 (2023), <https://doi.org/10.26565/2312-4334-2023-1-04>

© C.R. Mahanta, S. Deka, M.P. Das, 2023

framework of  $f(R, T)$  theory of gravity. In Sect.2, we provide basic field equations of the  $f(R, T)$  theory of gravity for the functional form  $f(R, T) = R + 2f(T)$ . In Sect. 3, we obtain explicit field equations corresponding to Bianchi type V metric for  $f(R, T) = R + 2f(T) = R + 2\lambda T$ , where  $\lambda$  is a constant. The expressions for the directional scale factors  $A, B, C$  in terms of the average scale factor  $a$  are also obtained. In Sect. 4, we find exact solutions of the field equations for two cases: one with a volumetric expansion law and the other with an exponential expansion law. Evolutions of some relevant cosmological parameters are investigated in Sect. 5, and physical and geometrical properties of the models are discussed. We conclude the paper in Sect. 6.

## 2. BASIC FIELD EQUATIONS OF THE $f(R, T)$ THEORY OF GRAVITY

The gravitational Lagrangian in  $f(R, T)$  theory of gravity, proposed by Harko *et al.* [21], is given by an arbitrary function  $f(R, T)$  of the Ricci scalar  $R$  and of the trace  $T$  of the stress- energy tensor  $T_{ij}$ . The field equations of this theory are derived by varying the action

$$S = \frac{1}{16\pi} \int f(R, T) \sqrt{-g} d^4x + \int L_m \sqrt{-g} d^4x, \quad (1)$$

with respect to the metric tensor  $g^{ij}$ , where  $L_m$  is the matter Lagrangian density.

The stress-energy tensor of matter is defined as

$$T_{ij} = \frac{-2}{\sqrt{-g}} \frac{\delta(\sqrt{-g}L_m)}{\delta g^{ij}}. \quad (2)$$

Assuming the matter Lagrangian density  $L_m$  to depend only on the metric tensor components  $g_{ij}$ , and not on its derivatives,  $T_{ij}$  can be obtained as

$$T_{ij} = g_{ij}L_m - 2 \frac{\partial L_m}{\partial g^{ij}}. \quad (3)$$

Hence, the variation of (1) with respect to the metric tensor  $g^{ij}$  provides the field equations of the  $f(R, T)$  theory of gravity as

$$f_R(R, T)R_{ij} - \frac{1}{2}f(R, T)g_{ij} + (g_{ij}\nabla_k\nabla^k - \nabla_i\nabla_j)f_R(R, T) = 8\pi T_{ij} - f_T(R, T)T_{ij} - f_T(R, T)\Theta_{ij}, \quad (4)$$

where  $f_R(R, T) = \frac{\partial f(R, T)}{\partial R}$ ,  $f_T(R, T) = \frac{\partial f(R, T)}{\partial T}$ ,  $\nabla_i$  is the covariant derivative with respect to the symmetric connection  $\Gamma$  associated to the metric  $g$  and

$$\Theta_{ij} = -2T_{ij} + g_{ij}L_m - 2g^{lk} \frac{\partial^2 L_m}{\partial g^{ij} \partial g^{lk}}. \quad (5)$$

Since there is no unique definition of the matter Lagrangian density  $L_m$ , therefore, by assuming the stress-energy tensor of matter to be given by the stress-energy tensor of a perfect fluid of density  $\rho$  and pressure  $p$  in the form

$$T_{ij} = (\rho + p)u_i u_j - p g_{ij}, \quad (6)$$

where the four velocity  $u_i$  satisfies the conditions  $u^i \nabla_j u_i = 0$  and  $u^i u_i = 1$ , the matter Lagrangian density can be taken as  $L_m = -p$ . Then from Eq. (5), we obtain

$$\Theta_{ij} = -2T_{ij} - p g_{ij}. \quad (7)$$

And for the functional form

$$f(R, T) = R + 2f(T), \quad (8)$$

where  $f(T)$  is an arbitrary function of the trace  $T$  of the stress-energy tensor of matter, the gravitational field equations, from Eq (4) are obtained as

$$R_{ij} - \frac{1}{2}Rg_{ij} = 8\pi T_{ij} - 2f'(T)T_{ij} - 2f'(T)\Theta_{ij} + f(T)g_{ij}, \quad (9)$$

where the prime denotes differentiation with respect to the argument.

In view of Eq. (6), the Eq. (9) becomes

$$R_{ij} - \frac{1}{2}Rg_{ij} = 8\pi T_{ij} + 2f'(T)T_{ij} + [2pf'(T) + f(T)]g_{ij}. \quad (10)$$

## 3. METRIC AND FIELD EQUATIONS

We consider a spatially homogeneous and anisotropic Bianchi type V metric in the form

$$ds^2 = dt^2 - A^2 dx^2 - e^{2x}(B^2 dy^2 + C^2 dz^2), \quad (11)$$

where  $A, B, C$  are functions of the cosmic time  $t$  only.

Using comoving coordinates the field equations (10) for the metric (11) with a time dependent cosmological constant  $\Lambda$  and the functional,

$$f(R, T) = R + 2f(T) = R + 2\lambda T$$

where  $\lambda$  is a constant, are obtained as

$$\frac{\ddot{B}}{B} + \frac{\ddot{C}}{C} + \frac{\dot{B}\dot{C}}{BC} - \frac{1}{A^2} = -(8\pi + 3\lambda)p + \lambda\rho - \Lambda \tag{12}$$

$$\frac{\ddot{A}}{A} + \frac{\ddot{C}}{C} + \frac{\dot{A}\dot{C}}{AC} - \frac{1}{A^2} = -(8\pi + 3\lambda)p + \lambda\rho - \Lambda \tag{13}$$

$$\frac{\ddot{A}}{A} + \frac{\ddot{B}}{B} + \frac{\dot{A}\dot{B}}{AB} - \frac{1}{A^2} = -(8\pi + 3\lambda)p + \lambda\rho - \Lambda \tag{14}$$

$$\frac{\dot{A}\dot{B}}{AB} + \frac{\dot{B}\dot{C}}{BC} + \frac{\dot{C}\dot{A}}{CA} - \frac{3}{A^2} = (8\pi + 3\lambda)\rho - \lambda\rho - \Lambda \tag{15}$$

$$-2\frac{\dot{A}}{A} + \frac{\dot{B}}{B} + \frac{\dot{C}}{C} = 0 \tag{16}$$

where an overhead dot indicates differentiation with respect to the cosmic time  $t$ .

For the Bianchi type V metric given in Eq. (11), the various parameters of cosmological importance are: The spatial volume,

$$V = ABC \tag{17}$$

The average scale factor,

$$a = V^{\frac{1}{3}} = (ABC)^{\frac{1}{3}} \tag{18}$$

The mean Hubble parameter,

$$H = \frac{\dot{a}}{a} = \frac{1}{3}\left(\frac{\dot{A}}{A} + \frac{\dot{B}}{B} + \frac{\dot{C}}{C}\right) \tag{19}$$

The deceleration parameter,

$$q = -\frac{a\ddot{a}}{\dot{a}^2} \tag{20}$$

The expansion scalar,

$$\theta = 3H = \left(\frac{\dot{A}}{A} + \frac{\dot{B}}{B} + \frac{\dot{C}}{C}\right) \tag{21}$$

The shear scalar,

$$\sigma^2 = \frac{1}{2}\left(\sum_{i=1}^3 H_i^2 - 3H^2\right) \tag{22}$$

The anisotropy parameter,

$$A_m = \frac{1}{3}\sum_{i=1}^3 \left(\frac{H_i - H}{H}\right)^2 \tag{23}$$

where  $H_1 = \frac{\dot{A}}{A}, H_2 = \frac{\dot{B}}{B}, H_3 = \frac{\dot{C}}{C}$  are the directional Hubble parameters.

#### 4. SOLUTIONS OF THE FIELD EQUATIONS

From equation (16), on integration, we get

$$A^2 = BC \tag{24}$$

From (12), (13) and (14), we obtain

$$A = l_1 a \exp\left(m_1 \int \frac{dt}{a^3}\right) \tag{25}$$

$$B = l_2 a \exp\left(m_2 \int \frac{dt}{a^3}\right) \tag{26}$$

$$C = l_3 a \exp\left(m_3 \int \frac{dt}{a^3}\right) \tag{27}$$

where the constants satisfy the relations  $m_1 + m_2 + m_3 = 0$  and  $l_1 l_2 l_3 = 1$ .

Using (25), (26), (27) in Eq. (24), we get

$$l_1 = \exp\left(-m_1 \int \frac{dt}{a^3}\right)$$

Now, since  $l_1$  is a constant, so we may assume that  $m_1 = 0$  so that  $l_1 = 1$  and consequently  $l_2 l_3 = 1$  and  $m_2 + m_3 = 0$ . Without loss of generality, we take

$$l_2 = l_3^{-1} = c_1 \text{ and } m_2 = -m_3 = c_2$$

where  $c_1$  and  $c_2$  are non-zero constants.

Then from (25)-(27), we obtain the directional scale factors as

$$A = a \tag{28}$$

$$B = c_1 a \exp\left(c_2 \int \frac{dt}{a^3}\right) \tag{29}$$

$$C = \frac{1}{c_1} a \exp\left(-c_2 \int \frac{dt}{a^3}\right) \tag{30}$$

Now, to find exact solution of the field equations, we need one extra condition for which we consider a volumetric expansion law. We also find another exact solution by using the exponential expansion law.

For volumetric expansion law, we consider

$$V = V_0 t^{3n} \tag{31}$$

where  $V = ABC = a^3$ , and  $V_0$  and  $n$  are non-zero constants.

Then from (28), (29) and (30), we get

$$A = V_0^{\frac{1}{3}} t^n \tag{32}$$

$$B = c_1 V_0^{\frac{1}{3}} t^n \exp\left[-\frac{c_2 t^{-3n+1}}{V_0(3n-1)}\right] \tag{33}$$

$$C = \frac{1}{c_1} V_0^{\frac{1}{3}} t^n \exp\left[\frac{c_2 t^{-3n+1}}{V_0(3n-1)}\right] \tag{34}$$

For exponential expansion law, we consider

$$V = V_0 e^{3nt}$$

where  $V = ABC = a^3$ , and  $V_0$  and  $n$  are non-zero constants.

Then from (28), (29) and (30), we get

$$A = V_0^{\frac{1}{3}} e^{nt} \tag{35}$$

$$B = c_1 V_0^{\frac{1}{3}} e^{nt} \exp\left\{\frac{-c_2 e^{-3nt}}{3nV_0}\right\} \tag{36}$$

$$C = \frac{1}{c_1} V_0^{\frac{1}{3}} e^{nt} \exp\left\{\frac{c_2 e^{-3nt}}{3nV_0}\right\} \tag{37}$$

## 5. PHYSICAL AND GEOMETRICAL PROPERTIES OF THE MODELS

### Model 1

The average Hubble parameter  $H$ , the expansion scalar  $\theta$ , the deceleration parameter  $q$  and the shear scalar  $\sigma$  and the anisotropy parameter  $A_m$  for the model corresponding to the volumetric expansion law are obtained as

$$H = \frac{n}{t} \tag{38}$$

$$\theta = 3H = \frac{3n}{t} \tag{39}$$

$$q = -\frac{a\ddot{a}}{\dot{a}^2} = -1 + \frac{1}{n} \tag{40}$$

$$\sigma^2 = \frac{c_2^2}{V_0^2 t^{6n}} \tag{41}$$

$$A_m = \frac{2}{3} \frac{c_2^2}{V_0^2 n^2 t^{6n-2}} \tag{42}$$

From equation (40), we see that the cosmic expansion accelerates for  $n > 1$ .

Now, adding equations (14) and (15) and using quadratic equation of state

$p = \alpha\rho^2 - \rho$ , where  $\alpha \neq 0$  constant, we get

$$\rho^2 = \frac{1}{(4\pi+\lambda)\alpha} \left[ \frac{n}{t^2} - \frac{c_2^2}{V_0^2 t^{6n}} - \frac{1}{V_0^{\frac{2}{3}} t^{2n}} \right] \tag{43}$$

$$p = \frac{1}{(4\pi+\lambda)} \left[ \frac{n}{t^2} - \frac{c_2^2}{V_0^2 t^{6n}} - \frac{1}{V_0^{\frac{2}{3}} t^{2n}} \right] - \sqrt{\frac{1}{(4\pi+\lambda)\alpha} \left[ \frac{n}{t^2} - \frac{c_2^2}{V_0^2 t^{6n}} - \frac{1}{V_0^{\frac{2}{3}} t^{2n}} \right]} \tag{44}$$

Using  $p$  and  $\rho$  in (12), we obtain

$$\Lambda = \frac{(8\pi+3\lambda)}{(4\pi+\lambda)} \left[ \frac{c_2^2}{V_0^2 t^{6n}} + \frac{1}{V_0^{\frac{2}{3}} t^{2n}} - \frac{n}{t^2} \right] + 4(2\pi + \lambda) \sqrt{\frac{1}{(4\pi+\lambda)\alpha} \left[ \frac{n}{t^2} - \frac{c_2^2}{V_0^2 t^{6n}} - \frac{1}{V_0^{\frac{2}{3}} t^{2n}} \right]} - \frac{3n^2}{t^2} + \frac{2n}{t^2} - \frac{c_2^2}{V_0^2 t^{6n}} + \frac{1}{V_0^{\frac{2}{3}} t^{2n}} \tag{45}$$

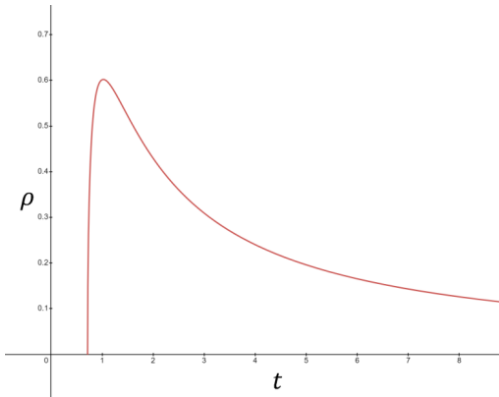


**Figure 1.** The plot of energy density  $\rho$  vs. cosmic time  $t$  graph with  $\alpha = 0.1, c_2 = 0.1, V_0 = 1, n = 1.5, \lambda = 1$

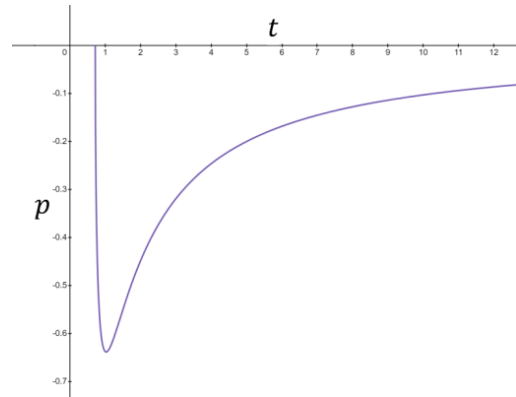


**Figure 2.** The plot of pressure  $p$  vs. cosmic time  $t$  graph with  $\alpha = 0.1, c_2 = 0.1, V_0 = 1, n = 1.5, \lambda = 1$

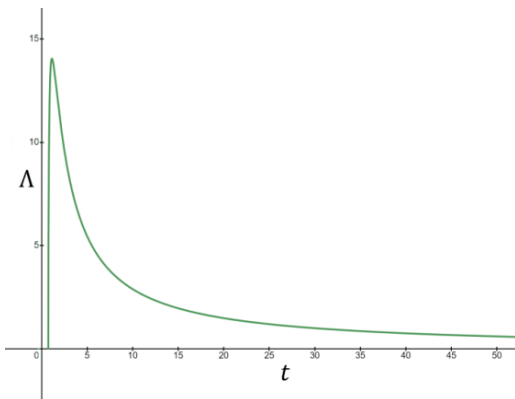


**Figure 3.** The plot of the cosmological constant  $\Lambda$  vs. cosmic time  $t$  graph with  $\alpha = 0.1, c_2 = 0.1, V_0 = 1, n = 1.5, \lambda = 1$

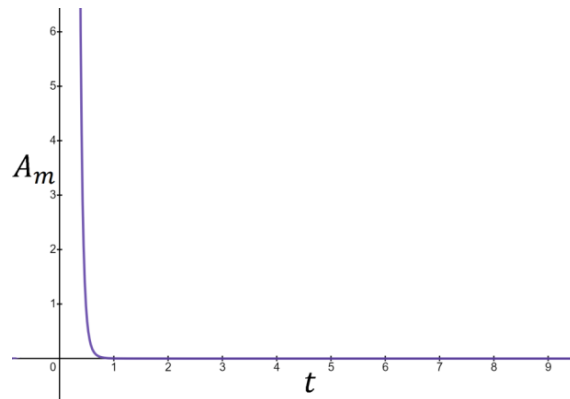


**Figure 4.** The plot of anisotropy parameter  $A_m$  vs. cosmic time  $t$  graph with  $c_2 = 0.1, V_0 = 1, n = 1.5$

From the graphs we observe that the energy density  $\rho$  is a decreasing function of cosmic time, pressure  $p$  is negative throughout the evolution of the universe and the cosmological constant  $\Lambda$  decreases rapidly and tend to zero. The figure 4 shows that the universe is highly anisotropic at its early stage and the anisotropy dies out in the course of evolution.

**The Cosmic Jerk Parameter.**

The cosmic jerk parameter is defined as

$$j(t) = \frac{1}{H^3} \frac{\ddot{a}}{a} \tag{46}$$

The equation (46) can be written in terms of the deceleration and the Hubble parameter as

$$j(t) = q + 2q^2 - \frac{\dot{q}}{H} \tag{47}$$

From equations (38) and (40), using (47), we get the cosmic jerk parameter for this model as

$$j(t) = \frac{(n-1)(n-2)}{n^2} \tag{48}$$

At late times, the value of the cosmic jerk parameter is 1 for  $\Lambda$ CDM model. For this model,  $j(t) = 1$  for  $n = \frac{2}{3}$ . But we have a restriction  $n > 1$ . Hence, this model does not resemble with  $\Lambda$ CDM model.

**Energy Conditions**

Weak Energy Condition (WEC), Null Energy Condition (NEC), Dominant Energy Condition (DEC) and Strong Energy Condition (SEC) are given by

WEC :  $\rho \geq 0$

NEC :  $\rho + p \geq 0$

DEC :  $\rho - p \geq 0$

SEC :  $\rho + 3p \geq 0$

For this model, we have

$$\rho + p = \frac{1}{(4\pi + \lambda)} \left[ \frac{n}{t^2} - \frac{c_2^2}{V_0^2 t^{6n}} - \frac{1}{V_0^{\frac{2}{3}} t^{2n}} \right]$$

$$\rho - p = 2 \sqrt{\frac{1}{(4\pi + \lambda)\alpha} \left[ \frac{n}{t^2} - \frac{c_2^2}{V_0^2 t^{6n}} - \frac{1}{V_0^{\frac{2}{3}} t^{2n}} \right]} - \frac{1}{(4\pi + \lambda)} \left[ \frac{n}{t^2} - \frac{c_2^2}{V_0^2 t^{6n}} - \frac{1}{V_0^{\frac{2}{3}} t^{2n}} \right]$$

$$\rho + 3p = \frac{3}{(4\pi + \lambda)} \left[ \frac{n}{t^2} - \frac{c_2^2}{V_0^2 t^{6n}} - \frac{1}{V_0^{\frac{2}{3}} t^{2n}} \right] - 2 \sqrt{\frac{1}{(4\pi + \lambda)\alpha} \left[ \frac{n}{t^2} - \frac{c_2^2}{V_0^2 t^{6n}} - \frac{1}{V_0^{\frac{2}{3}} t^{2n}} \right]}$$

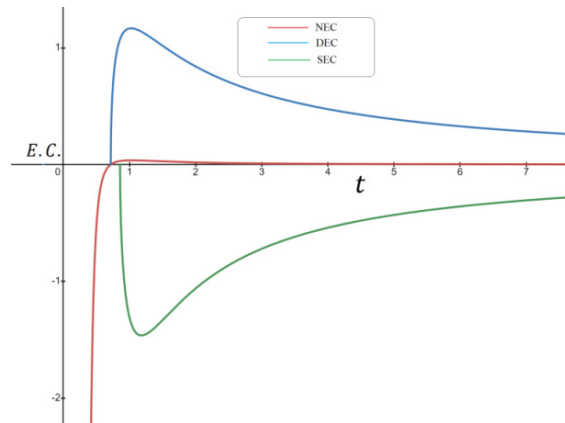


**Figure 5.** The plot of left hand sides of energy conditions vs. cosmic time  $t$  graph with  $\alpha = 0.1, c_2 = 0.1, V_0 = 1, n = 1.5, \lambda = 1$

From figure 1 and figure 5, we see that the WEC and DEC are satisfied. NEC is satisfied only at late times while the SEC is violated for this model.

**Model 2**

The average Hubble parameter  $H$ , the expansion scalar  $\theta$ , the deceleration parameter  $q$  and the shear scalar  $\sigma$  and the anisotropy parameter  $A_m$  for the model corresponding to the exponential expansion are obtained as

$$H = n \tag{49}$$

$$\theta = 3n \tag{50}$$

$$q = -\frac{a\ddot{a}}{\dot{a}^2} = -1 \tag{51}$$

$$\sigma^2 = \frac{c_2^2}{V_0^2 e^{6nt}} \tag{52}$$

$$A_m = \frac{2c_2^2}{3n^2 V_0^2 e^{6nt}} \tag{53}$$

From the expression for the deceleration parameter  $q$ , we see that the expansion of the universe is decelerating throughout the evolution and does not depend on  $n$ .

Now, adding (12) and (15) and using quadratic equation of state  $p = \alpha\rho^2 - \rho$ , where  $\alpha \neq 0$  is a constant, we get

$$\rho^2 = \frac{-1}{\alpha(4\pi+\lambda)} \left( \frac{c_2^2}{V_0^2 e^{6nt}} + \frac{1}{V_0^{\frac{2}{3}} e^{2nt}} \right) \tag{54}$$

$$p = \frac{-1}{4\pi+\lambda} \left( \frac{c_2^2}{V_0^2 e^{6nt}} + \frac{1}{V_0^{\frac{2}{3}} e^{2nt}} \right) - \sqrt{\frac{-1}{\alpha(4\pi+\lambda)} \left( \frac{c_2^2}{V_0^2 e^{6nt}} + \frac{1}{V_0^{\frac{2}{3}} e^{2nt}} \right)} \tag{55}$$

Using  $p$  and  $\rho$  in (12), we obtain

$$\Lambda = 2 \left( \frac{2\pi+\lambda}{4\pi+\lambda} \right) \frac{c_2^2}{V_0^2 e^{6nt}} + 4 \left( \frac{3\pi+\lambda}{4\pi+\lambda} \right) \frac{1}{V_0^{\frac{2}{3}} e^{2nt}} - 3n^2 + 4(2\pi + \lambda) \sqrt{\frac{-1}{\alpha(4\pi+\lambda)} \left( \frac{c_2^2}{V_0^2 e^{6nt}} + \frac{1}{V_0^{\frac{2}{3}} e^{2nt}} \right)} \tag{56}$$

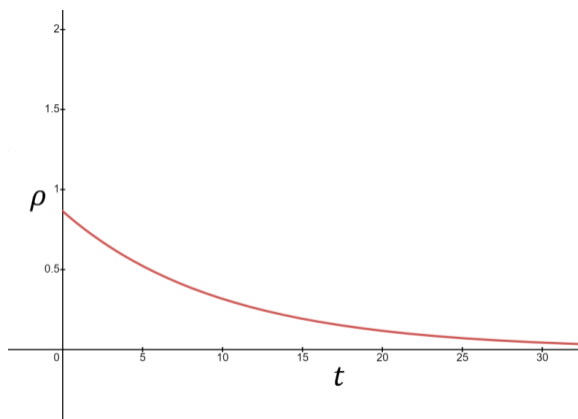


**Figure 6.** The plot of energy density  $\rho$  vs. cosmic time  $t$  graph with  $\alpha = -0.1, c_2 = 0.1, V_0 = 1, n = 0.1, \lambda = 1$

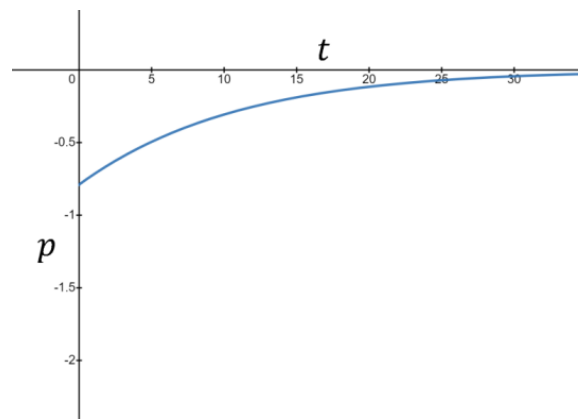


**Figure 7.** The plot of pressure  $p$  vs. cosmic time  $t$  graph with  $\alpha = -0.1, c_2 = 0.1, V_0 = 1, n = 0.1, \lambda = 1$

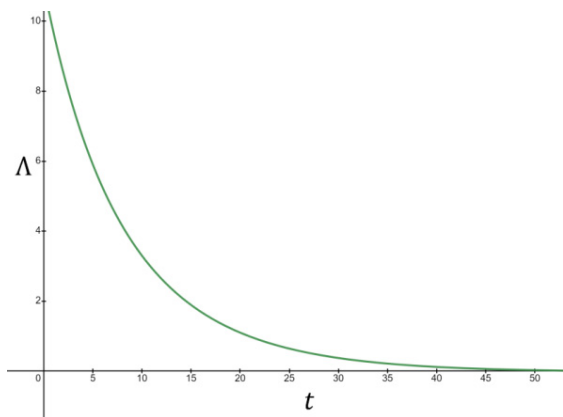


**Figure 8.** The plot of cosmological constant  $\Lambda$  vs. cosmic time  $t$  graph with  $\alpha = -0.1, c_2 = 0.1, V_0 = 1, n = 0.1, \lambda = 1$

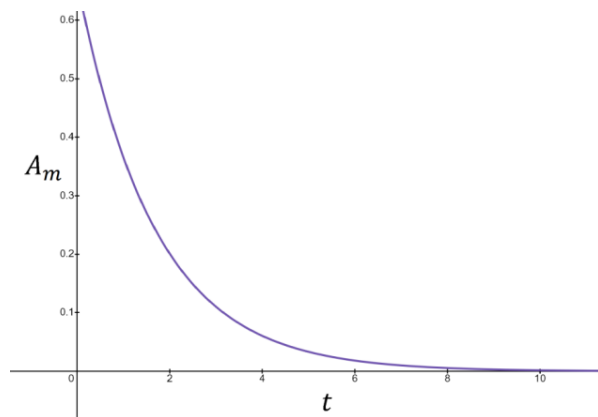


**Figure 9.** The plot of anisotropy parameter  $A_m$  vs. cosmic time  $t$  graph with  $c_2 = 0.1, n = 0.1, V_0 = 1$

From the figures 6, 7, 8 and 9, we see that the behavior of the energy density, pressure, cosmological constant and anisotropy parameter satisfies the present cosmological observations. However, in this case, the constant  $\alpha$  should assume negative values

**The Cosmic Jerk Parameter:**

From equations (49) and (51), using (47), we obtain the cosmic jerk parameter for this model as

$$j(t) = 1$$

This shows that this model resembles  $\Lambda$ CDM for any value of  $n$ .

**Energy Conditions**

For this model, the energy conditions are obtained as

$$\rho + p = -\frac{1}{4\pi + \lambda} \left( \frac{c_2^2}{V_0^2 e^{6nt}} + \frac{1}{V_0^{\frac{2}{3}} e^{2nt}} \right)$$

$$\rho - p = 2 \sqrt{\frac{-1}{\alpha(4\pi + \lambda)} \left( \frac{c_2^2}{V_0^2 e^{6nt}} + \frac{1}{V_0^{\frac{2}{3}} e^{2nt}} \right)} + \frac{1}{4\pi + \lambda} \left( \frac{c_2^2}{V_0^2 e^{6nt}} + \frac{1}{V_0^{\frac{2}{3}} e^{2nt}} \right)$$

$$\rho + 3p = -\frac{3}{4\pi + \lambda} \left( \frac{c_2^2}{V_0^2 e^{6nt}} + \frac{1}{V_0^{\frac{2}{3}} e^{2nt}} \right) - 2 \sqrt{\frac{-1}{\alpha(4\pi + \lambda)} \left( \frac{c_2^2}{V_0^2 e^{6nt}} + \frac{1}{V_0^{\frac{2}{3}} e^{2nt}} \right)}$$

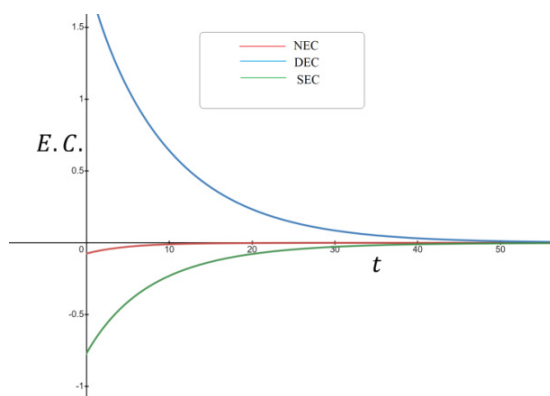


**Figure 10.** The plot of left-hand side of energy conditions vs. cosmic time  $t$  graph with  $\alpha = -0.1, c_2 = 0.1, V_0 = 1, n = 0.1, \lambda = 1$

From figures 6 and 10, we see that for this model, the WEC and DEC are satisfied and NEC and SEC are violated.

**6. CONCLUSION**

In this paper, we study a spatially homogeneous and anisotropic Bianchi type V universe with time varying cosmological constant and a quadratic equation of state in  $f(R, T)$  theory of gravity for the functional form  $(R, T) = R + 2\lambda T$ , where  $\lambda$  is a constant. We construct two cosmological models corresponding to a volumetric power law expansion (Model 1) and an exponential expansion (Model 2). We find that

- Both the models have initial singularity as the metric coefficients  $A, B$  and  $C$  vanish at the initial moment.
- The physical parameters  $H, \theta, \sigma^2$  for both the models diverge at the initial epoch and for large  $t$ , these parameters tend to 0. Also, the volume of the universe is zero at  $t = 0$  and increases exponentially with time  $t$ . Hence, both the models start with the big bang singularity at  $t = 0$  and then expand throughout the evolution.
- The energy density of the model 1 increases at the beginning but it decreases in the course of evolution and tends to 0 at late time. The energy density of the model 2 decreases from the evolution of the universe and tends to 0 as time goes on.
- For both the models, the cosmological constant is a decreasing function of the cosmic time and tends to 0 at late time.
- The model 1 exhibits accelerated expansion for  $n > 1$ , while for model 2, it happens for any values of  $n$ .
- The model 1 never approaches  $\Lambda$ CDM model while the model 2 resembles  $\Lambda$ CDM model for any values of  $n$ .
- The model 1 satisfies present cosmological observations for positive values of  $\alpha$  while the model 2 satisfies the same for negative values of  $\alpha$ .
- For both the models, the energy conditions WEC and DEC are satisfied and NEC and SEC are violated. The violation of SEC shows that the universe has anti-gravitating effect which results accelerating expansion of the universe.

**ORCID IDs**

Manash Pratim Das, <https://orcid.org/0000-0002-1179-8068>

**REFERENCES**

[1] S. Perlmutter, G. Aldering, M. Della Valle, S. Deustua, R.S. Ellis, S. Fabbro, and A. Fruchter, et al, "Discovery of supernovae explosion at half the age of the universe", Nature (London), **391**, 51 (1998). <https://doi.org/10.1038/34124>

[2] A.G. Riess, A.V. Filippenko, P. Challis, A. Clocchiatti, A. Diercks, P.M. Garnavich, R.L. Gilliland, et al, "Observational evidence from supernovae for an accelerating universe and a cosmological constant", Astron. J. **116**, 1009 (1998). <https://doi.org/10.1086/300499>

- [3] S. Perlmutter, G. Aldering, G. Goldhaber, R.A. Knop, P. Nugent, P.G. Castro, S. Deustua, et al, "Measurement of  $\Omega$  and  $\Lambda$  from 42 High-Red shift Supernovae", *Astrophys. J.* **517**, 565 (1999). <https://doi.org/10.1086/307221>
- [4] C.L. Bennett, M. Halpern, G. Hinshaw, N. Jarosik, A. Kogut, M. Limon, S.S. Meyer, et al, "First-Year Wilkinson Microwave Anisotropy Probe (WMAP)\* Observations: Preliminary Maps and Basic Results", *Astrophys. J. Suppl. Ser.* **148**, 1 (2003). <https://doi.org/10.1086/377253>
- [5] D.N. Spergel, L. Verde, H.V. Peiris, E. Komatsu, M.R.olta, C.L. Bennett, M. Halpern, et al, "First-Year Wilkinson Microwave Anisotropy Probe (WMAP)\* Observations: Determination of Cosmological Parameters", *Astrophys. J. Suppl. Ser.* **148**, 175 (2003). <https://doi.org/10.1086/377226>
- [6] Ed. Hawkins, S. Maddox, S. Cole, O. Lahav, D.S. Madgwick, P. Norberg, J.A. Peacock, et al, "The 2dF Galaxy Redshift Survey: correlation functions, peculiar velocities and the matter density of the Universe", *Mon. Not. Roy. Astron. Soc.* **346**, 78 (2003). <https://doi.org/10.1046/j.1365-2966.2003.07063.x>
- [7] K. Abazajian, J.K. Adelman-McCarthy, M.A. Agüeros, S.S. Allam, K.S.J. Anderson, S.F. Anderson, J. Annis, et al, "The Second Data Release of the Sloan Digital Sky Survey", *Astron. J.* **128**, 502 (2004). <https://doi.org/10.1086/421365>
- [8] N. Aghanim, et al, [Planck Collaboration], (2018). <https://doi.org/10.48550/arXiv.1807.06209>
- [9] T. Barreiro, E.J. Copeland, and N.J. Nunes, "Quintessence arising from exponential potentials", *Phys. Rev. D*, **61**, 127301 (2000). <https://doi.org/10.1103/PhysRevD.61.127301>
- [10] V. Sahni, and A.A. Starobinsky, "The Case for a Positive Cosmological Lambda-term", *Int. J. Mod. Phys. D*, **9**(4), 373 (2000). <https://doi.org/10.1142/S0218271800000542>
- [11] C. Armendariz-Picon, V. Mukhanov, and P.J. Steinhardt, "Essentials of k-essence", *Phys. Rev. D*, **63**, 103510 (2001). <https://doi.org/10.1103/PhysRevD.63.103510>
- [12] A. Sen, "Rolling Tachyon", *J. High Energy Phys.* **2002**, JHEP04 (2002). <https://doi.org/10.1088/1126-6708/2002/04/048>
- [13] R.R. Caldwell, M. Kamionkowski, and N.N. Weinberg, "Phantom Energy: Dark Energy with  $\omega < -1$  Causes a Cosmic Doomsday", *Phys. Rev. Lett.* **91**, 071301 (2003). <https://doi.org/10.1103/PhysRevLett.91.071301>
- [14] A. Kamenshchik, U. Moschella, and V. Pasquier, "An alternative to quintessence", *Phys. Lett. B*, **511**, 265 (2001). [https://doi.org/10.1016/S0370-2693\(01\)00571-8](https://doi.org/10.1016/S0370-2693(01)00571-8)
- [15] M. Li, "A Model of Holographic Dark Energy", *Phys. Lett. B*, **603**, 1 (2004). <https://doi.org/10.1016/j.physletb.2004.10.014>
- [16] A.C.S. Friaça, J.S. Alcaniz, and J.A.S. Lima, "An old quasar in a young dark energy-dominated universe?", *Mon. Not. Roy. Astron. Soc.* **362**, 1295 (2005). <https://doi.org/10.1111/j.1365-2966.2005.09401.x>
- [17] S. Wang, X.-D. Li, and M. Li "Revisit of cosmic age problem", *Phys. Rev. D*, **82**, 103006 (2010). <https://doi.org/10.1103/PhysRevD.82.103006>
- [18] S.M. Carroll, V. Duvvuri, M. Trodden, and M.S. Turner, "Is cosmic speed-up due to new gravitational physics?", *Phys. Rev. D*, **70**, 043528 (2004). <https://doi.org/10.1103/PhysRevD.70.043528>
- [19] S. Nojiri, and S.D. Odintsov, "Modified  $f(R)$  gravity consistent with realistic cosmology: From a matter dominated epoch to a dark energy universe", *Phys. Rev. D*, **74**, 086005 (2006). <https://doi.org/10.1103/PhysRevD.74.086005>
- [20] B. Li, T.P. Sotiriou, and J.D. Barrow, " $f(T)$  gravity and local Lorentz invariance", *Phys. Rev. D*, **83**(6), 064035 (2011). <https://doi.org/10.1103/PhysRevD.83.064035>
- [21] Harko T. *et al.*, " $f(R, T)$  gravity", *Phys. Rev. D*, **84**(2), 024020 (2011).
- [22] N.M. García, F.S.N. Lobo, J.P. Mimoso, and T. Harko, " $f(G)$  modified gravity and the energy Conditions", *Journal of Physics: Conference Series*, **314**, 012056 (2011). <https://doi.org/10.1088/1742-6596/314/1/012056>
- [23] C.J. Copi, D. Huterer, D.J. Schwarz, and G.D. Starkman, "Large-Angle Anomalies in the CMB", *Advances in Astronomy*, **2010**, 847541 (2010). <https://doi.org/10.1155/2010/847541>
- [24] I. Agullo, D. Kranas, and V. Sreenath, "Anomalies in the Cosmic Microwave Background and Their Non-Gaussian Origin in Loop Quantum Cosmology", *Front. Astron. Space Sci.* **8**, 703845 (2021). <https://doi.org/10.3389/fspas.2021.703845>
- [25] G.P. Singh, and B.K. Bishi, "Bianchi type-I transit Universe in  $f(R, T)$  modified gravity with quadratic equation of state and  $\Lambda$ ", *Astrophys. Space Sci.* **360**, 34 (2015). <https://doi.org/10.1007/s10509-015-2495-0>

### ВСЕСВІТ Б'ЯНЧІ ТИПУ V ЗІ ЗМІННОЮ В ЧАСІ КОСМОЛОГІЧНОЮ СТАЛОЮ ТА КВАДРАТИЧНИМ РІВНЯННЯМ СТАНУ В ТЕОРІЇ ГРАВІТАЦІЇ $f(R, T)$

Чандра Рекха Маханта<sup>a</sup>, Шаяніка Дека<sup>a</sup>, Манаш Пратім Дас<sup>b</sup>

<sup>a</sup>Факультет математики, Університет Гаухаті, Гувахаті-781014, Індія

<sup>b</sup>Факультет математики, коледж ВВК, Барнета, Індія

В останні роки модифіковані теорії гравітації широко вивчалися через відкриття та підтвердження поточної фази прискореного розширення Всесвіту. Теорія гравітації  $f(R, T)$  є однією з таких теорій, що запропонована Харко та ін. у 2011 році, де  $R$  є скаляром Річчі, а  $T$  є слідом тензора енергії напруги. У цій статті ми вивчаємо Всесвіт типу Б'янчі V в теорії гравітації  $f(R, T)$  із змінною в часі космологічною константою та квадратним рівнянням стану  $p = \alpha\rho^2 - \rho$ , де  $\alpha \neq 0$  є константою. Отримано точні розв'язки рівнянь поля для двох випадків: один з законом об'ємного розширення, а інший – з експоненціальним законом розширення. Фізичні характеристики двох моделей обговорюються шляхом вивчення поведінки деяких важливих космологічних параметрів, таких як параметр Хабла, параметр уповільнення тощо. Ми виявили, що моделі мають початкову сингулярність, а фізичні параметри розходяться в початкову епоху. Модель 1, що відповідає закону об'ємного розширення, не нагадує модель  $\Lambda$ CDM, а модель 2, яка відповідає закону експоненціального розширення, нагадує модель  $\Lambda$ CDM. Енергетичні умови моделей також досліджуються та виявляються узгодженими з нещодавніми космологічними спостереженнями.

**Ключові слова:** Всесвіт типу Б'янчі V; теорія гравітації  $f(R, T)$ ; рівняння стану; модель  $\Lambda$ CDM

## THEORETICAL INVESTIGATION OF MESON SPECTRUM USING EXACT QUANTIZATION RULE TECHNIQUE<sup>†</sup>

 Etido P. Inyang<sup>a\*</sup>,  Fina O. Faithpraise<sup>c</sup>, Joseph Amajama<sup>c</sup>,  Eddy S. William<sup>b</sup>, Effiong O. Obisung<sup>c</sup>,  Joseph E. Ntibi<sup>b</sup>

<sup>a</sup>Department of Physics, National Open University of Nigeria, Jabi, Abuja, Nigeria

<sup>b</sup>Theoretical Physics Group, Department of Physics, University of Calabar, P.M.B 1115, Calabar, Nigeria

<sup>c</sup>Department of Physics, University of Calabar, P.M.B 1115, Calabar, Nigeria

\*Corresponding author email: [etidophysics@gmail.com](mailto:etidophysics@gmail.com), [einyang@noun.edu.ng](mailto:einyang@noun.edu.ng)

Received December 7, 2022; revised January 1, 2023; accepted January 9, 2023

The energy eigenvalues with the Extended Cornell potential were obtained by analytically solving the radial Schrödinger equation using the Exact Quantization Rule technique. It was then used for computing the mass spectra of the heavy mesons like charmonium ( $c\bar{c}$ ) and bottomonium ( $b\bar{b}$ ) as well as heavy-light mesons such as bottom-charm ( $b\bar{c}$ ) and charm-Strange ( $c\bar{s}$ ) for various quantum states. Two exceptional cases such as the Coulomb and Cornell potentials, were taken into consideration when some of the potential parameters were set to zero. The current potential offers good outcomes when compared to experimental data and the work of other researchers with a maximum error of  $0.0065 \text{ GeV}$ .

**Keywords:** *Cornell potential; Schrödinger equation; Exact Quantization Rule; Mesons*

**PACS:** 12.39.Jh

### 1. INTRODUCTION

The development of the radial Schrödinger equation (SE) in quantum mechanics and its solutions plays a fundamental role in many fields of modern physics. The study of the behavior of quite a lot of physical problems in physics requires the solving of the SE. The solutions can be well-known only if we know the confining potential for a particular physical system [1-4]. The theory of quantum chromodynamics (QCD) which is described by the meson system is mediated by strong interactions [5]. The heavy mesons are the constituents of quark and antiquark such as charmonium and bottomonium that are considered as the non-relativistic system described by the SE [6]. In recent times, researchers have obtained the solutions of the SE and Klein-Gordon equation (KGE) with the quarkonium interaction potential model such as the Cornell or the Killingbeck potentials [7-9]. The Cornell potential is the sum of the Coulomb plus linear potentials. The Cornell potential and its extended form have been solved with SE with different analytical methods [10,11]. The exact solutions of the SE with some potentials are solvable for  $l = 0$ , but insolvable for any arbitrary angular momentum quantum number  $l \neq 0$ . In this case, several approximate techniques are employed in obtaining the solutions. Example of such techniques include, the asymptotic iteration method (AIM) [12], the Nikiforov-Uvarov functional analysis (NUFA) method [13-17] the Laplace transformation method [18], the Nikiforov-Uvarov (NU) method [19-24], the series expansion method (SEM) [25-27], analytical exact iterative method (AEIM) [28], WKB approximation method [29-31] and others [32,33].

Recently, the mass spectrum of the quarkonium system has been studied by researchers [34,35]. For instance, Vega and Flores [36] obtained the solution of the SE with the Cornell potential via the variational method and super symmetric quantum mechanics (SUSYQM). Ciftci and Kisoglu [37] addressed non-relativistic arbitrary  $l$ -states of quark-antiquark through the Asymptotic Iteration Method (AIM). An analytic solution of the N-dimensional radial SE with the mixture of vector and scalar potentials via the Laplace transformation method (LTM) was studied by [18]. Their results were employed to analyze the different properties of the heavy-light mesons. Also, Al-Jamel and Widyan [38] studied heavy quarkonium mass spectra in a Coulomb field plus quadratic potential by employing the Nikiforov-Uvarov (NU) method. In their work, the spin-averaged mass spectra of heavy quarkonia in a Coulomb plus quadratic potential is analyzed within the non-relativistic SE. In addition, Al-Oun et al. [39] examined heavy quarkonia characteristics in the general framework of a non-relativistic potential model consisting of a Coulomb plus quadratic potential. Furthermore, Omugbe et al. [29] solved the SE with Killingbeck potential plus an inversely quadratic potential model via the WKB method. They obtained the energy eigenvalues and the mass spectra of the heavy and heavy-light meson systems. In addition, Inyang et al. [40] obtained the KGE solutions for the Yukawa potential via the NU method. They obtained energy eigenvalues both in the relativistic and non-relativistic regimes, and the results were then applied to calculate heavy-meson masses of charmonium  $c\bar{c}$  and bottomonium  $b\bar{b}$ . Ibekwe et al. [41] solved the radial SE with  $b\bar{b}$  an exponential, generalized, harmonic

<sup>†</sup> **Cite as:** E.P. Inyang, F.O. Faithpraise, J. Amajama, E.S. William, E.O. Obisung, and J.E. Ntibi, East Eur. J. Phys. 1, 53 (2023), <https://doi.org/10.26565/2312-4334-2023-1-05>

© E.P. Inyang, F.O. Faithpraise, J. Amajama, E.S. William, E.O. Obisung, J.E. Ntibi, 2023

Cornell potential via the series expansion method. They applied the bound state eigenvalues to study the energy spectra for CO, NO, CH and N<sub>2</sub> diatomic molecules and the mass spectra of heavy quarkonium systems.

Therefore, in this present work, we aim at studying the SE with the extended Cornell potential via the Exact quantization rule (EQR) to obtain the mass spectra of heavy mesons such as charmonium ( $c\bar{c}$ ), bottomonium ( $b\bar{b}$ ) and the heavy–light mesons such as the charm-Strange ( $c\bar{s}$ ) and bottom-charm ( $b\bar{c}$ ). The extended Cornell potential (ECP) takes the form [29].

$$V(r) = \eta_0 r^2 + \eta_1 r - \frac{\eta_2}{r} + \frac{\eta_3}{r^2} \tag{1}$$

where  $\eta_0$ ,  $\eta_1$ ,  $\eta_2$  and  $\eta_3$  are potential strength parameters. The second term in Eq. (1) is a linear term for confinement feature and the third term is the Coulomb potential that describes the short distance between quarks. While the first and the last terms are quadratic and the inverse quadratic potentials.

It is important to note that if we set  $\eta_0 = \eta_1 = \eta_3 = 0$ , the (ECP) reduces to the Coulomb potential also, if we set  $\eta_0 = \eta_3 = 0$  the (ECP) reduces to the standard Cornell potential. The paper is organized as follows: in section 2, the brief EQR formalism is presented. Section 3, the analytical solution of the bound states of the SE is solved via the EQR. In section 4, we present the results of the mass spectrum of the mesons. Finally, in section 5, the study is concluded.

## 2. EXACT QUANTIZATION RULE FORMALISM

In this section, we give a brief review of exact quantization rule. The details can be found in [42,43]. It is a well known fact that, in one dimension, the SE is given as:

$$\frac{d^2\psi(x)}{dx^2} + \frac{2\mu}{\hbar^2} [E_{nl} - V(x)]\psi(x) = 0 \tag{2}$$

Equation (2) can be written in the following form:

$$\phi'(x) + \phi(x)^2 + k(x)^2 = 0 \tag{3}$$

with

$$k(x) = \sqrt{\frac{2\mu}{\hbar^2} [E_{nl} - V(x)]} \tag{4}$$

where  $\phi(x) = \psi'(x) / \psi(x)$  is the logarithmic derivative of the wave function,  $\mu$  is the reduced mass of the quarkonium particles,  $k(x)$  is the momentum, and  $V(x)$  is a piecewise continuous real potential function of  $x$ . The phase angle of the SE is the logarithmic derivative  $\phi(x)$ . From Eq. (3), as  $x$  increases across a node of wave function  $\psi(x)$ ,  $\phi(x)$  decreases to  $-\infty$ , jumps to  $+\infty$ , and then decreases again. We can generalize EQR to the three – dimensional radial SE with spherically symmetric potential by simply making the replacement  $x \rightarrow r$  and  $V(x) \rightarrow V_{eff}(r)$  [42,43].

$$\int_{r_a}^{r_b} k(r) dr = N\pi + \int_{r_a}^{r_b} \phi(r) \left[ \frac{dk(r)}{dr} \right] \left[ \frac{d\phi(r)}{dr} \right]^{-1} \tag{5}$$

$$k(r) = \sqrt{\frac{2\mu}{\hbar^2} [E_{nl} - V_{eff}(r)]} \tag{6}$$

where  $r_a$  and  $r_b$  are two turning points determined by  $E = V_{eff}(r)$ .  $N = n + 1$  is the number of the nodes of  $\phi(r)$  in the region  $E_{nl} = V_{eff}(r)$  and is larger by 1 than the  $n$  of the nodes of the wave function  $\psi(r)$ . The first term  $N\pi$  is the contribution from the nodes of the logarithmic derivatives of the wave function, and the second one is called the quantum correction. It was found that for all well-known exactly solvable quantum systems, this quantum correction is independent of the number of nodes of the wave function. This means that it is enough to consider the ground state in calculating the quantum correction ( $Q_c$ ), i.e.

$$Q_c = \int_{r_a}^{r_b} k'_o(r) \frac{\phi'_o}{\phi_o} dr \tag{7}$$

To determine the energy eigenvalues, we equate Eqs. (5) and (7).

### 3. APPROXIMATE SOLUTIONS OF THE SCHRÖDINGER EQUATION WITH EXTENDED CORNELL POTENTIAL

The SE for two particles interacting via potential  $V(r)$  is given by [44].

$$\frac{d^2 R(r)}{dr^2} + \frac{2\mu}{\hbar^2} \left[ E_{nl} - V(r) - \frac{l(l+1)\hbar^2}{2\mu r^2} \right] R(r) = 0, \quad (8)$$

where  $l, \mu, r$  and  $\hbar$  are the angular momentum quantum number, the reduced mass for the quarkonium particle, inter-particle distance and reduced plank constant respectively.

We substitute Eq. (1) into Eq. (8) and obtain

$$\frac{d^2 R(r)}{dr^2} + \frac{2\mu}{\hbar^2} \left[ E_{nl} - V_{eff}(r) \right] R(r) = 0, \quad (9)$$

where

$$V_{eff}(r) = \eta_0 r^2 + \eta_1 r - \frac{\eta_2}{r} + \frac{\eta_3}{r^2} + \frac{l(l+1)\hbar^2}{2\mu r^2}. \quad (10)$$

We transform the coordinate of Eq. (9) by setting

$$x = \frac{1}{r}. \quad (11)$$

Upon substituting Eq. (11) into Eq. (10) we have

$$V_{eff}(x) = \frac{\eta_0}{x^2} + \frac{\eta_1}{x} - \eta_2 x + \eta_3 x^2 + \frac{l(l+1)\hbar^2 x^2}{2\mu}. \quad (12)$$

To deal with the first and second terms of Eq. (12), we propose the following approximation scheme. We assume that there is a characteristic radius  $r_0$  of the meson. Then the scheme is based on the expansion of  $\frac{\eta_1}{x}$  and  $\frac{\eta_0}{x^2}$  in a power

series around  $r_0$ ; i.e. around  $\delta \equiv \frac{1}{r_0}$ , up to the second order. This is similar to Pekeris approximation, which helps to

deform the centrifugal term such that the modified potential can be solved by NU method [45].

Setting  $y = x - \delta$  and around  $y = 0$  it can be expanded into a series of powers as:

$$\frac{\eta_1}{x} = \frac{\eta_1}{y + \delta} = \frac{\eta_1}{\delta \left( 1 + \frac{y}{\delta} \right)} = \frac{\eta_1}{\delta} \left( 1 + \frac{y}{\delta} \right)^{-1}, \quad (13)$$

which yields

$$\frac{\eta_1}{x} = \eta_1 \left( \frac{3}{\delta} - \frac{3x}{\delta^2} + \frac{x^2}{\delta^3} \right). \quad (14)$$

Similarly,

$$\frac{\eta_0}{x^2} = \eta_0 \left( \frac{6}{\delta^2} - \frac{8x}{\delta^3} + \frac{3x^2}{\delta^4} \right). \quad (15)$$

We then substitute Eqs. (14) and (15) into Eq. (12) and obtain

$$V_{eff}(x) = \xi_1 + \xi_2 x + \xi_3 x^2, \quad (16)$$

where

$$\left. \begin{aligned} \xi_1 &= \frac{6\eta_0}{\delta^2} + \frac{3\eta_1}{\delta}, & \xi_2 &= \frac{3\eta_1}{\delta^2} - \frac{8}{\delta^3} - \eta_2 \\ \xi_3 &= \frac{l(l+1)\hbar^2}{2\mu} + \frac{3\eta_0}{\delta^4} + \frac{\eta_1}{\delta^3} + \eta_3 \end{aligned} \right\}. \quad (17)$$

The non-linear Riccati equation for ground state is written in terms of the new variable  $x$  as,

$$-x^2 \phi'(x) + \phi^2(x) = k(x), \tag{18}$$

where

$$k(x) = \sqrt{\frac{2\mu}{\hbar^2} [\xi_3 x^2 + \xi_2 x + \xi_1 - E]}. \tag{19}$$

We now apply the quantization rule to study the potential. To this end we first calculate the turning points  $x_a$  and  $x_b$ , which is determined by solving the content of the square bracket of Eq. (19), these yields:

$$\left. \begin{aligned} x_a &= \frac{-\xi_2 - \sqrt{\xi_2^2 - 4\xi_3(\xi_1 - E)}}{2\xi_3} \\ x_b &= \frac{-\xi_2 + \sqrt{\xi_2^2 - 4\xi_3(\xi_1 - E)}}{2\xi_3} \end{aligned} \right\} \tag{20}$$

From Eq. (20) we have

$$\left. \begin{aligned} x_a x_b &= \frac{\xi_1 - E}{\xi_3} \\ x_a + x_b &= -\frac{\xi_2}{\xi_3} \end{aligned} \right\} \tag{21}$$

Also, from Eq. (19) we have

$$k(x) = \sqrt{\frac{2\mu}{\hbar^2} \xi_3 \left( x^2 + \frac{\xi_2}{\xi_3} x + \frac{\xi_1 - E}{\xi_3} \right)} \tag{22}$$

Substituting Eq.(21) into Eq.(22) we obtain

$$k(x) = \sqrt{\frac{2\mu\xi_3}{\hbar^2} (x - x_a)(x - x_b)} \tag{23}$$

where  $k(x)$  is the momentum between the two turning points  $x_a$  and  $x_b$ .

From Eq.(18), since the logarithmic derivative  $\phi_0(x)$  for the ground state has one zero and no pole, therefore we assume the trial solution for the ground states

$$\phi_0(x) = A + Bx \tag{24}$$

Substituting Eq. (24) into Eq. (18) and then solving the non-linear Riccati equation, we obtain the ground state energy as

$$E_0 = \xi_1 - \frac{\hbar^2 A^2}{2\mu} \tag{25}$$

Also, we obtain  $A$  and  $B$  as follows

$$\left. \begin{aligned} A &= \frac{\mu\xi_2}{B\hbar^2} \\ B &= \frac{1}{2} + \sqrt{\frac{1}{4} - \frac{2\mu\xi_3}{\hbar^2}} \end{aligned} \right\} \tag{26}$$

Here we choose the positive sign in front of the square root for  $B$ . This is as a result of the logarithmic derivatives  $\phi_0(x)$  which decreases exponentially, which is required. We now calculate the quantum correction and obtain

$$\int_{r_a}^{r_b} \phi(r) \left[ \frac{dk(r)}{dr} \right] \left[ \frac{d\phi(r)}{dr} \right]^{-1} dr = - \int_{x_a}^{x_b} \frac{k_0'(x) \phi_0(x)}{x^2 \phi_0'(x)} dx \tag{27}$$

From Eq. (27) we have

$$\sqrt{\frac{2\mu\xi_3}{\hbar^2}} \int_{x_a}^{x_b} \left( \frac{\frac{A}{B} - \frac{x_a + x_b}{2}}{x\sqrt{(x-x_a)(x-x_b)}} + \frac{\frac{A}{B} \left( \frac{x_a + x_b}{2} \right)}{x^2 \sqrt{(x-x_a)(x-x_b)}} \right) dx \tag{27a}$$

We utilized the integrals given by Appendix A, and obtain

$$\pi \sqrt{\frac{2\mu\xi_3}{\hbar^2}} \left[ \frac{\frac{A}{B} - \frac{x_a + x_b}{2}}{\sqrt{1 + (x_a + x_b) + x_a x_b}} + \frac{\frac{A}{B} \left( \frac{x_a + x_b}{2} \right) \left( \sqrt{x_a x_b} - \frac{1}{2(x_a + x_b)} \right)}{\sqrt{x_a x_b}} \right] \tag{27b}$$

We substitute Eq. (21) into Eq.(27b) and obtain

$$\pi \sqrt{\frac{2\mu\xi_3}{\hbar^2}} \left[ \frac{\frac{A}{B} + \frac{\xi_2}{2\xi_3}}{\sqrt{\frac{\hbar^2}{2\mu\xi_3}} (A+B)} - \frac{A\xi_2}{2B\xi_3} \left( \frac{\sqrt{\frac{\hbar^2}{2\mu\xi_3}} A + \frac{\xi_3}{2\xi_2}}{\sqrt{\frac{\hbar^2}{2\mu\xi_3}} A} \right) \right] \tag{27c}$$

Inserting Eq. (27c) into Eq. (5) we obtain

$$\pi \sqrt{\frac{2\mu\xi_3}{\hbar^2}} \left[ \frac{\frac{A}{B} + \frac{\xi_2}{2\xi_3}}{\sqrt{\frac{\hbar^2}{2\mu\xi_3}} (A+B)} - \frac{A\xi_2}{2B\xi_3} \left( \frac{\sqrt{\frac{\hbar^2}{2\mu\xi_3}} A + \frac{\xi_3}{2\xi_2}}{\sqrt{\frac{\hbar^2}{2\mu\xi_3}} A} \right) \right] + N\pi \tag{27d}$$

Furthermore, the integral of Eq.(7) is obtain as

$$\int_{r_a}^{r_b} k(r)dr = -\int_{x_a}^{x_b} \frac{k(x)}{x^2} dx \tag{28}$$

From Eq. (28) we have

$$-\sqrt{\frac{2\mu\xi_3}{\hbar^2}} \int_{x_a}^{x_b} \frac{\sqrt{(x-x_a)(x-x_b)}}{x^2} dx \tag{28a}$$

Using Eq. (29), Eq. (28a) becomes

$$-\sqrt{\frac{2\mu\xi_3}{\hbar^2}} \left[ \frac{(x_a + x_b) - \sqrt{x_a x_b}}{2\sqrt{x_a x_b}} \right] \tag{28b}$$

We substitute Eq. (21) into Eq. (28b) and obtain

$$-\sqrt{\frac{2\mu\xi_3}{\hbar^2}} \left[ \frac{-\frac{\xi_2}{\xi_3} - \frac{\sqrt{\xi_1 - E}}{\xi_3}}{2\sqrt{\frac{\xi_1 - E}{\xi_3}}} \right] \tag{28c}$$

In order to obtain the integral of Eq.(28a), we used maple software to obtain the following useful integral, which is not available in integral table

$$\int_a^b \frac{\sqrt{(x-a)(b-x)}}{x^2} dx = \frac{(a+b) - \sqrt{ab}\pi}{2\sqrt{ab}} \tag{29}$$

By equating Eqs.(27d) and (28c) ,and substituting Eqs.(17) and (26) ,setting  $\hbar = 1$  we obtain the energy equation for extended Cornell potential as

$$E_{nl} = \frac{3\eta_1}{\delta} + \frac{6\eta_0}{\delta^2} - \frac{2\mu \left( \frac{3\eta_1}{\delta^2} + \frac{8\eta_0}{\delta^3} + \eta_2 \right)^2}{\left[ (2n+1) + \sqrt{1 + \frac{8\mu\eta_1}{\delta^3} + 4 \left( \left( l + \frac{1}{2} \right)^2 - \frac{1}{4} \right) - 8\mu\eta_3 + \frac{24\mu\eta_0}{\delta^4}} \right]^2} \tag{30}$$

### 3.1. Special case

In this subsection, we present some special cases of the energy eigenvalues of the ECP.

1. When we set  $\eta_0 = \eta_1 = \eta_3 = 0$  we obtain energy eigenvalues expression for Coulomb potential

$$E_{nl} = -\frac{\mu\eta_2^2}{2(n+l+1)^2} \tag{31}$$

2. When we set  $\eta_0 = \eta_3 = 0$  we obtain energy eigenvalues expression for Cornell potential

$$E_{nl} = \frac{3\eta_1}{\delta} - \frac{2\mu\left(\frac{3\eta_1}{\delta^2} + \eta_2\right)^2}{\left[(2n+1) + \sqrt{1 + \frac{8\mu\eta_1}{\delta^3} + 4\left(\left(l + \frac{1}{2}\right)^2 - \frac{1}{4}\right)}\right]^2} \tag{32}$$

The result of Eq. (32) is consistent with the result obtained in Eq. (30) in Ref. [9]

### 4. RESULTS

Using the relation in Ref. [46], we calculate the mass spectra of the heavy quarkonia such as charmonium and bottomonium, and heavy-light mesons.

$$M = 2m + E_{nl} \tag{33}$$

where  $m$  is quarkonium bare mass and  $E_{nl}$  is energy eigenvalues.

By substituting Eq. (30) into Eq. (33) we obtain the mass spectra for extended Cornell potential for heavy quarkonia as,

$$M = 2m + \frac{3\eta_1}{\delta} + \frac{6\eta_0}{\delta^2} - \frac{2\mu\left(\frac{3\eta_1}{\delta^2} + \frac{8\eta_0}{\delta^3} + \eta_2\right)^2}{\left[(2n+1) + \sqrt{1 + \frac{8\mu\eta_1}{\delta^3} + 4\left(\left(l + \frac{1}{2}\right)^2 - \frac{1}{4}\right) - 8\mu\eta_3 + \frac{24\mu\eta_0}{\delta^4}}\right]^2} \tag{34}$$

We also obtain the mass spectra of the special case of Eq. (32) for heavy-light mesons by substituting into Eq.(33)

$$M = m_s + m_c + \frac{3\eta_1}{\delta} - \frac{2\mu\left(\frac{3\eta_1}{\delta^2} + \eta_2\right)^2}{\left[(2n+1) + \sqrt{1 + \frac{8\mu\eta_1}{\delta^3} + 4\left(\left(l + \frac{1}{2}\right)^2 - \frac{1}{4}\right)}\right]^2} \tag{35}$$

We test the accuracy of the predicted results, by using the Chi square function defined by [47]

$$\chi^2 = \frac{1}{n} \sum_{i=1}^n \frac{(M_i^{\text{Exp.}} - M_i^{\text{Theo.}})^2}{\Delta_i} \tag{36}$$

where  $n$  runs over selected samples of mesons,  $M_i^{\text{Exp.}}$  is the experimental mass of mesons, while  $M_i^{\text{Theo.}}$  is the corresponding theoretical prediction. The  $\Delta_i$  quantity is experimental uncertainty of the masses. Intuitively,  $\Delta_i$  should be one. The tendency of overestimating Chi square value is that, it reflects some mean error.

We calculate mass spectra of charmonium and bottomonium for states from 1S to 1F, as presented in Tables 1 and 2. Also calculated the mass spectra of heavy-light mesons for states from 1S to 1D as presented in Tables 3 and 4. The free parameters of Eq. (34) were obtained by solving two algebraic equations of mass spectra in Eq. (34) for charmonium.

We followed the same procedure for bottomonium and obtained the free parameters of mass spectra. Equation (35) was fitted with experimental data of mass spectra of 1S, 2S to obtain the free parameters for bottom-charm ( $b\bar{c}$ ) and charm-strange ( $c\bar{s}$ ) heavy-light mesons.

For bottomonium  $b\bar{b}$ , charmonium  $c\bar{c}$  and strange systems we adopt the numerical values of  $m_b = 4.823 \text{ GeV}$ ,  $m_c = 1.209 \text{ GeV}$  and  $m_s = 0.419 \text{ GeV}$ , and the corresponding reduced mass are  $\mu_b = 2.4115 \text{ GeV}$ ,  $\mu_c = 0.6045 \text{ GeV}$

and  $\mu_s = 0.2095 \text{ GeV}$ , respectively [48-50]. We note that the theoretical prediction of the mass spectra of charmonium and bottomonium are in excellent agreement with experimental data and the work of other researchers like; Refs.[28,9,18,37,41] as shown in Tables 1 and 2. Also, the results for charm-strange meson presented in Table 4, are in excellent agreement with the work of other authors in Refs.[28,37] Furthermore, in Table 3, the mass spectra of the bottom-charm meson are very close to the ones obtained in Refs[28,18,37] with other methods and experimental data indicating an improvement compared to the other methods. The maximum error in comparison with experimental data is  $0.0065 \text{ GeV}$ .

**Table 1.** Mass spectra of charmonium in (GeV) ( $m_c = 1.209 \text{ GeV}$ ,  $\mu = 0.6045 \text{ GeV}$ ,  $\eta_1 = 0.001 \text{ GeV}$ ,  $\eta_2 = 14.94 \text{ GeV}$ ,  $\eta_0 = 0.02 \text{ GeV}$ ,  $\eta_3 = -15.04 \text{ GeV}$ ,  $\delta = 1.7 \text{ GeV}$ )

State	Present work	AEIM[28]	NU[9]	AIM[37]	LTM[18]	SEM[41]	Experiment[48,49]
1S	3.096	3.0954	3.095	3.096	3.0963	3.095922	3.097
2S	3.686	3.5673	3.685	3.686	3.5681	3.685893	3.686
1P	3.295	3.5677	3.258	3.214	3.5687	-	3.525
2P	3.802	4.0396	3.779	3.773	3.5687	3.756506	3.773
3S	4.040	4.0392	4.040	4.275	4.0400	4.322881	4.040
4S	4.269	4.5110	4.262	4.865	4.5119	4.989406	4.263
1D	3.583	4.0396	3.510	3.412	4.0407	-	3.770
2D	3.976	-	-	-	-	-	4.159
1F	3.862	-	-	-	-	-	-

**Table 2.** Mass spectra of bottomonium in (GeV) ( $m_b = 4.823 \text{ GeV}$ ,  $\mu = 2.4115 \text{ GeV}$ ,  $\eta_1 = 0.798 \text{ GeV}$ ,  $\eta_2 = 5.051 \text{ GeV}$ ,  $\eta_0 = 0.02 \text{ GeV}$ ,  $\eta_3 = -3.854 \text{ GeV}$ ,  $\delta = 1.5 \text{ GeV}$ )

State	Present work	AEIM[28]	NU[9]	AIM[37]	LTM[18]	SEM[41]	Experiment[48,49]
1S	9.460	9.74473	9.460	9.460	9.745	9.515194	9.460
2S	10.023	10.02315	10.022	10.023	10.023	10.01801	10.023
1P	9.661	10.02406	9.609	9.492	10.025	-	9.899
2P	10.138	10.30248	10.109	10.038	10.303	10.09446	10.260
3S	10.355	10.30158	10.360	10.585	10.302	10.44142	10.355
4S	10.567	10.58000	10.580	11.148	10.580	10.85777	10.580
1D	9.943	10.30248	9.846	9.551	10.303	-	10.164
2D	10.306	-	-	-	-	-	-
1F	10.209	-	-	-	-	-	-

**Table 3.** Mass spectra of bottom-charm ( $b\bar{c}$ ) in (GeV) ( $m_b = 4.823 \text{ GeV}$ ,  $m_c = 1.209 \text{ GeV}$ ,  $\eta_1 = 0.202 \text{ GeV}$ ,  $\eta_2 = 1.213 \text{ GeV}$ ,  $\delta = 0.371 \text{ GeV}$ )

State	Present work	AEIM[28]	LTM[18]	AIM[37]	Experiment[50]
1S	6.274	6.2774	6.2770	6.277	6.275
2S	6.845	7.0376	7.0372	6.814	6.842
3S	7.125	7.7978	7.7973	7.351	-
4S	7.283	7.0386	-	7.889	-
1P	6.519	7.7987	7.0381	6.340	-
2P	6.959	-	7.7983	6.851	-
1D	6.813	-	-	6.452	-

**Table 4.** Mass spectra of charm-strange ( $c\bar{s}$ ) meson in (GeV) ( $m_s = 0.419 \text{ GeV}$ ,  $m_c = 1.209 \text{ GeV}$ ,  $\eta_1 = 0.202 \text{ GeV}$ ,  $\eta_2 = 2.046 \text{ GeV}$ ,  $\delta = 0.561 \text{ GeV}$ )

State	Present work	AEIM [18]	AIM [37]	Experiment [48, 51]
1S	1.969	1.968	2.512	1.968[48]
2S	2.709	2.709	2.709	2.709[51]
3S	2.913	2.932	2.906	-
4S	2.998	-	3.102	-
1P	2.601	2.565	2.649	-
2P	2.877	-	2.860	-
1D	2.863	2.857	2.859	2.859[51]

**5. CONCLUSION**

In this study, we used the EQR technique to derive the approximate Schrödinger equation solutions for energy eigenvalues with extended Cornell potential. Consideration was given to two particular instances that lead to Cornell and Coulomb potentials. We use the current findings to determine the masses of heavy mesons like charmonium and

bottomonium as well as the heavy-light mesons such as bottom-charm and charm-strange for various quantum states. We noticed that the mass spectra of the meson systems reported in this current work are also consistent with those of other researchers and are enhanced. This research could be expanded to study the thermodynamic properties of the mesons.

#### Appendix A: Some Useful Standard Integrals

$$\int_{r_a}^{r_b} \frac{1}{\sqrt{(r-r_a)(r_b-r)}} dr = \pi \quad (\text{A1})$$

$$\int_{r_a}^{r_b} \frac{1}{(a+br)\sqrt{(r-r_a)(r_b-r)}} dr = \frac{\pi}{\sqrt{(a+br_b)(a+br_a)}} \quad (\text{A2})$$

$$\int_{r_a}^{r_b} \frac{1}{r\sqrt{(r-r_a)(r_b-r)}} dr = \frac{\pi}{2}(r_a+r_b) - \pi\sqrt{r_a r_b} \quad (\text{A3})$$

$$\int_{r_a}^{r_b} \frac{1}{r\sqrt{(r-r_a)(r_b-r)}} dr = \frac{\pi}{\sqrt{r_a r_b}} \quad (\text{A4})$$

#### Acknowledgement

Dr. Etido P. Inyang would like to thank C. O. Edet, Department of Physics, University of Cross River State, Nigeria for his encouragement, which lead to the successful completion of this work.

**Competing interests.** The authors declare that they have no competing interests.

**Funding.** Not applicable.

**Authors contributions.** EPI suggested the point research and the writing of the full manuscript. FOF obtain the numerical. ESW analyzed the results and reviewed it. FOF and EOO proofread and makes appropriate corrections in the manuscript. All authors read and approved the final manuscript.

#### ORCID IDs

© Etido P. Inyang, <https://orcid.org/0000-0002-5031-3297>; © Fina O. Faithpraise, <https://orcid.org/0000-0001-8222-2034>  
© Eddy S. William, <https://orcid.org/0000-0002-5247-5281>; © Joseph E. Ntibi, <https://orcid.org/0000-0002-7908-2840>

#### REFERENCES

- [1] E.P. Inyang, E.S. William, J.O. Obu, B.I. Ita, E.P. Inyang, and I.O. Akpan, Energy spectra and expectation values of selected diatomic molecules through the solutions of Klein-Gordon equation with Eckart-Hellmann potential model, *Molecular Physics*, **119**(23), e1956615 (2021) <https://doi.org/10.1080/00268976.2021.1956615>
- [2] E.P. Inyang, F. Ayedun, E.A. Ibanga, K.M. Lawal, I.B. Okon, E.S. William, O. Ekwevugbe, C.A. Onate, A.D. Antia, and E.O. Obisung, "Analytical Solutions of the N-Dimensional Schrödinger equation with modified screened Kratzer plus Inversely Quadratic Yukawa potential and Thermodynamic Properties of selected Diatomic Molecules", *Results in Physics*, **43**, 106075 (2022). <https://doi.org/10.1016/j.rinp.2022.106075>
- [3] M. Allosh, Y. Mustafa, N.K. Ahmed, and A.S. Mustafa, "Ground and Excited state mass spectra and properties of heavy-light mesons", *Few-Body Syst.* **62**, 26 (2021). <https://doi.org/10.1007/s00601-021-01608-1>
- [4] E. Omugbe, O.E. Osafire, I.B. Okon, E.S. Eyube, E.P. Inyang, U.S. Okorie, A. Jahanshir, and C.A. Onate, "Non-relativistic bound state solutions with  $l$ -deformed Kratzer-type potential using the super-symmetric WKB method: application to theoretic-information measures", *European Physical Journal D*, **76**, 72 (2022). <https://doi.org/10.1140/epjd/s10053-022-00395-6>
- [5] M. Abu-shady, C.O. Edet, and A.N. Ikot, "Non-relativistic Quark model under external magnetic and Aharanov-Bohm (AB) fields in the presence of Temperatur-Dependent confined Cornell potential", *Canadian Journal of Physics*, **99**(11), (2021) <https://doi.org/10.1139/cjp-2020-0101>
- [6] I.O. Akpan, E.P. Inyang, E.P. Inyang, and E.S. William, "Approximate solutions of the Schrödinger equation with Hulthen-Hellmann Potentials for a Quarkonium system", *Rev. Mex. Fis.* **67**, 483 (2021). <https://doi.org/10.31349/revmexfis.67.482>
- [7] R. Kumar, and F. Chand, "Asymptotic study to the N-dimensional Radial Schrodinder Equation for the quark-antiquark system", *Commun. in Theor. Phys.* **59**, 528 (2013). <https://doi.org/10.1088/0253-6102/59/5/02>
- [8] R. Kumar, R.M. Singh, S.B. Bahardivaj, R. Rani, and F. Chand, "Analytical solutions to the Schrodinger equation for generalized Cornell potential and its application to diatomic molecules and heavy mesons", *Mod. Phys. Lett. A*, **37**, 2250010 (2022). <https://doi.org/10.1142/S0217732322500109>
- [9] M. Abu-Shady, "N-dimensional Schrödinger equation at finite temperature using the Nikiforov-Uvarov method", *J. Egypt. Math. Soc.* **23**, 4 (2016). <https://doi.org/10.1016/j.joems.2016.06.006>
- [10] J.P. Prasanth, K. Sebastian, and V.M. Bannur, "Revisiting Cornell potential model of the Quark-Gluon plasma", *Physica A*, **558**, 124921 (2020). <https://doi.org/10.1016/j.physa.2020.124921>
- [11] E. Omugbe, O.E. Osafire, I.B. Okon, E.P. Inyang, E.S. William, and A. Jahanshir, "Any L-state energy of the spinless Salpeter equation under the Cornell potential by the WKB Approximation method: An Application to mass spectra of mesons", *Few-Body Systems*, **63**, 7 (2022). <https://doi.org/10.1007/s00601-021-01705-1>
- [12] C.O. Edet, S. Mahmoud, E.P. Inyang, N. Ali, S.A. Aljunid, R. Endut, A.N. Ikot, and M. Asjad, "Non-Relativistic Treatment of the 2D Electron System Interacting via Varshni-Shukla Potential Using the Asymptotic Iteration Method", *Mathematics*, **10**, 2824 (2022). <https://doi.org/10.3390/math10152824>

- [13] A.N. Ikot, U.S. Okorie, P.O. Amadi, C.O. Edet, G.J. Rampho, and R. Sever, "The Nikiforov-Uvarov –Functional Analysis (NUFA) Method: A new approach for solving exponential – Type potentials", *Few-Body System*, **62**, 9 (2021). <https://doi.org/10.1007/s00601-021-021-01593-5>
- [14] E.P. Inyang, E.S. William, J.E. Ntibi, J.A. Obu, P.C. Iwuji, and E.P. Inyang, "Approximate solutions of the Schrödinger equation with Hulthén plus screened Kratzer Potential using the Nikiforov–Uvarov – functional analysis (NUFA) method: an application to diatomic molecules", *Can. J. Phys.* **100**(10), 473 (2022). <https://doi.org/10.1139/cjp-2022-003>
- [15] E.P. Inyang, P.C. Iwuji, J.E. Ntibi, E. Omugbe, E.A. Ibanga, and E.S. William, "Quark-antiquark study with inversely quadratic Yukawa potential using Nikiforov-Uvarov-Functional analysis method", *East European Journal of Physics*, **2**, 51 (2022). <https://doi.org/10.26565/2312-4334-2022-2-05>
- [16] E.P. Inyang, E.S. William, E. Omugbe, E.P. Inyang, E.A. Ibanga, F. Ayedun, I.O. Akpan, and J.E. Ntibi, "Application of Eckart-Hellmann potential to study selected diatomic molecules using Nikiforov-Uvarov-Functional analysis method", *Revista Mexicana de Fisica*, **68**, 14 (2022). <https://doi.org/10.31349/RevMexFis.68.020401>
- [17] E.P. Inyang, E.P. Inyang, E.S. William, J.E. Ntibi, and E.A. Ibanga, "Bound State Solutions of the Schrödinger equation with Frost-Musulin potential using the Nikiforov-Uvarov-Functional Analysis (NUFA) method", *Bulg. J. Phys.* **49**(4), 329 (2022), <https://doi.org/10.55318/bgjp.2022.49.4.329>
- [18] M. Abu-Shady, T.A. Abdel-Karim, and E.M. Khokha, "Exact solution of the N-dimensional Radial Schrödinger Equation via Laplace Transformation method with the Generalized Cornell potential", *Journal of theoretical Physics*, **45**, 567-587 (2018).
- [19] E.S. William, E.P. Inyang, I.O. Akpan, J.A. Obu, A.N. Nwachukwu, and E.P. Inyang, "Ro-vibrational energies and expectation values of selected diatomic molecules via Varshni plus modified Kratzer potential model", *Indian Journal of Physics*, **96**, 3461 (2022). <https://doi.org/10.1007/s12648-022-02308-0>
- [20] E.P. Inyang, and E.O. Obisung, "The study of electronic states of NI and Scl molecules with screened Kratzer Potential", *East European Journal of Physics*, **3**, 32 (2022). <https://doi.org/10.26565/2312-4334-2022-3-04>
- [21] E.S. William, E.P. Inyang, J.E. Ntibi, J.A. Obu, and E. P. Inyang, "Solutions of the Non-relativistic Equation Interacting with the Varshni-Hellmann potential model with some selected Diatomic molecules", *Jordan Journal of Physics*, **15**, 193 (2022). <https://doi.org/10.47011/15.2.8>
- [22] P.O. Okoi, C.O. Edet, T.O. Magu, and E.P. Inyang, "Eigensolution and Expectation values of the Hulthén and Generalized Inverse Quadratic Yukawa potential", *Jordan Journal of Physics*, **15**, 148 (2022). <https://doi.org/10.47011/15.2.4>
- [23] E.P. Inyang, A.N. Ikot, E.P. Inyang, I.O. Akpan, J.E. Ntibi, E. Omugbe, and E.S. William, "Analytic study of thermal properties and masses of heavy mesons with quarkonium potential", *Result in Physics*, **39**, 105754 (2022). <https://doi.org/10.1016/j.rinp.2022.105754>
- [24] E.P. Inyang, E.O. Obisung, E.S. William, and I.B. Okon, "Non-Relativistic study of mass spectra and thermal properties of a quarkonium system with Eckart-Hellmann potential", *East European Journal of Physics*, **3**, 114 (2022). <https://doi.org/10.26565/2312-4334-2022-3-14>
- [25] E.P. Inyang, E.P. Inyang, I.O. Akpan, J.E. Ntibi, and E.S. William, "Analytical solutions of the Schrödinger equation with class of Yukawa potential for a quarkonium system via series expansion method", *European Journal of Applied Physics*, **2**, 26 (2020). <http://dx.doi.org/10.24018/ejphysics.2020.2.6.26>
- [26] E.P. Inyang, P.C. Iwuji, J.E. Ntibi, E.S. William, and E.A. Ibanga, "Solutions of the Schrodinger equation with Hulthen –screened Kratzer potential: Application to diatomic molecules", *East European Journal of Physics*, **1**, 11 (2022). <https://doi.org/10.26565/2312-4334-2022-2-02>
- [27] E.P. Inyang, E.P. Inyang, J.E. Ntibi, and E.S. William, "Analytical solutions of Schrodinger equation with Kratzer-screened Coulomb potential for a Quarkonium system. *Bulletin of Pure and Applied Sciences*", **40**, 24 (2021). <https://doi.org/10.5958/2320-3218.2021.0002.6>
- [28] E.M. Khokha, M. Abushady, and T.A. Abdel-Karim, "Quarkonium Masses in the N-dimensional Space Using the Analytical Exact Iteration Method", <https://doi.org/10.48550/arXiv.1612.08206>
- [29] E. Omugbe, O.E. Osafire, and M.C. Onyeajh, "Mass spectrum of mesons via WKB Approximation method", *Advances in High Energy Physics*, **2020**, 5901464 (2020). <https://doi.org/10.1155/2020/5901464>
- [30] E. Omugbe, O.E. Osafire, E.P. Inyang, and A. Jahanshir, "Bound state solutions of the hyper-radial Klein-Gordon equation under the Deng-Fan potential by WKB and SWKB methods", *Physica Scripta*, **96**(12), 125408 (2021). <https://doi.org/10.1088/1402-4896/ac38d4>
- [31] E. Omugbe, "Non-relativistic energy spectrum of the Deng-Fan Oscillator via the WKB Approximation method", *Asian Journal of Physical and Chemical Sciences*, **8**, 26 (2020). <https://doi.org/10.9734/ajopacs/2020/v8i130107>
- [32] M. Abu-Shady, and E.P. Inyang, "Heavy-Light Meson masses in the Framework of Trigonometric Rosen-Morse Potential using the Generalized Fractional Derivative", *East Eur. J. Phys.* **4**, 80 (2022). <https://doi.org/10.26565/23124334-2022-4-06>
- [33] E.E. Ibekwe, J.B. Emah, E.P. Inyang, and A.O. Akpan, "MASS Spectrum of Heavy Quarkonium for Combined Potentials (Modified Kratzer Plus Screened Coulomb Potential)", *Iran J. Sci. Technol. Trans. Sci.* **46**, 1741 (2022). <https://doi.org/10.1007/s40995-022-01377-4>
- [34] M. Abu-Shady, and S.Y. Ezz-Alarab, "Trigonometric Rosen–Morse Potential as a Quark–Antiquark Interaction Potential for Meson Properties in the Non-relativistic Quark Model Using EAIM", *Few-Body Systems*, **60**, 66 (2019). <https://doi.org/10.1007/s00601-019-1531-y>
- [35] E.P. Inyang, E.P. Inyang, E.S. William, and E.E. Ibekwe, "Study on the applicability of Varshni potential to predict the mass-spectra of the Quark-Antiquark systems in a non-relativistic framework", *Jordan Journal of Physics*, **14**, 345 (2021). <https://doi.org/10.47011/14.4.8>
- [36] A. Vega, and J. Flores, "Heavy quarkonium properties from Cornell potential using variational method and supersymmetric quantum mechanics", *Pramana-J. Phys.* **87**, 73 (2016). <http://doi.org/10.1007/s12043-016-1278-7>
- [37] H. Ciftci, and H.F. Kisoglu, "Nonrelativistic-Arbitrary l-states of quarkonium through Asymptotic Iteration method", *Advances in High Energy Physics*, **2018**, 4549705 (2018). <http://doi.org/10.1155/2018/4549705>
- [38] A. Al-Jamel, and H. Widyan, "Heavy Quarkonium Mass Spectra in A Coulomb Field Plus Quadratic Potential Using Nikiforov-Uvarov Method", *Appl. Phys. Research*, **4**, (2012). <https://doi.org/10.5539/apr.v4n3p94>

- [39] A. Al-Oun, A. Al-Jamel, and H. Widyan, "Various Properties of Heavy Quarkonia from Flavor-Independent Coulomb Plus Quadratic Potential", *Jordan J. Phys.* **8**, 203 (2015). <https://journals.yu.edu/jjp/JJPIssues/Vol8No4pdf2015/2.pdf>
- [40] E.P. Inyang, E.P. Inyang, J.E. Ntibi, E.E. Ibekwe, and E. S. William, "Approximate solutions of D-dimensional Klein-Gordon equation with Yukawa potential via Nikiforov-Uvarov method", *Indian Journal of Physics*, **95**(12), 2733 (2021) <https://doi.org/10.1007/s12648-020-01933-x>
- [41] E.E. Ibekwe, U.S. Okorie, J.B. Emah, E.P. Inyang, and S.A. Ekong, "Mass spectrum of heavy quarkonium for screened Kratzer potential(SKP) using series expansion method", *Eur. Phys. J. Plus*, **87**, 136 (2021). <https://doi.org/10.1140/epjp/s13360-021-01090-y>
- [42] Z.Q. Ma, and B.W. Xu, "Quantum correction in exact quantization rules", *Europhys. Lett.* **69**, 685 (2005). <https://doi.org/10.1209/epl/i2004-10418-8>
- [43] Z.Q. Ma, and B.W. Xu, "Quantum correction in exact quantization rules", *Int. J. Mod. Phys. E*, **14**, 599 (2005) <https://doi.org/10.1209/epl/i2004-10418-8>
- [44] E.S. William, E.P. Inyang, and E.A. Thompson, "Arbitrary  $l$ -solutions of the Schrödinger equation interacting with Hulthén-Hellmann potential model", *Revista Mexicana Fisica*, **66**, 730 (2020). <https://doi.org/10.31349/RevMexFis.66.730>
- [45] E.P. Inyang, E.O. Obisung, P.C. Iwuji, J.E. Ntibi, J. Amajama, and E.S. William, "Masses and thermal properties of a charmonium and Bottomonium mesons", *J. Nig. Soc. Phys. Sci.* **4**, 884 (2022). <https://doi.org/10.46481/jnsps.2022.884>
- [46] E.P. Inyang, E.P. Inyang, I.O. Akpan, J.E. Ntibi, and E.S. William, "Masses and thermodynamic properties of a Quarkonium system", *Canadian Journal Physics*, **99**, 990 (2021). <https://doi.org/10.1139/cjp-2020-0578>
- [47] M.S. Ali, G.S. Hassan, A.M. Abdelmonem, S.K. Elshamdy, F. Elmasry, and A.M. Yasser, "The spectrum of charmed quarkonium in non-relativistic quark model using matrix Numerov's method", *Journal of Radiation Research and Applied Sciences*, **13**(1), 233 (2020). <https://doi.org/10.1080/16878507.2020.1723949>
- [48] R. Olive, D.E. Groom, and T.G. Trippe, Particle Data Group, *Chin. Phys. C*, **38**, 60 (2014). <https://doi.org/10.1088/1674-1137/38/9/090001>
- [49] M. Tanabashi, C.D. Carone, T.G. Trippe, and C.G. Wohl, "Particle Data Group", *Phys. Rev. D*, **98**, 546 (2018).
- [50] C. Patrignani, "Review of particle physics", *Chin. Phys. C*, **40**, 100 (2016). <http://hdl.handle.net/20.500.12386/25063>
- [51] S. Godfrey, and K. Moats,  $D_{s1}^*(2860)$  mesons as excited D-wave  $c\bar{s}$  states, *Phys. Rev. D*, **92**, 119903 (2015). <https://doi.org/10.1103/PhysRevD.92.119903>

#### ТЕОРЕТИЧНЕ ДОСЛІДЖЕННЯ СПЕКТРУ МЕЗОНІВ ЗА МЕТОДИКОЮ ПРАВИЛА ТОЧНОГО КВАНТУВАННЯ

Етідо П. Ін'янґ<sup>а</sup>, Фіна О. Фейтпрайз<sup>с</sup>, Джозеф Амаджама<sup>с</sup>, Едді С. Вільям<sup>б</sup>, Еффіонґ О. Обісунґ<sup>с</sup>, Джозеф Е. Нтібі<sup>б</sup>

<sup>а</sup>Фізичний факультет, Національний відкритий університет Нігерії, Джабі, Абуджа, Нігерія

<sup>б</sup>Група теоретичної фізики, фізичний факультет, Університет Калабара, Р.М.В 1115, Калабар, Нігерія

<sup>с</sup>Фізичний факультет, Університет Калабара, Р.М.В 1115, Калабар, Нігерія

Шляхом аналітичного розв'язання радіального рівняння Шредінґера за допомогою техніки точного правила квантування були отримані власні значення енергії з розширеним потенціалом Корнелла. Потім його використовували для обчислення мас-спектрів важких мезонів, таких як чармоній ( $c\bar{c}$ ) і боттоній ( $b\bar{b}$ ), а також важких і легких мезонів, таких як bottom-charm ( $b\bar{c}$ ) і charm-strange ( $c\bar{s}$ ) для різних квантових станів. Були взяті до уваги, два виняткових випадки, такі як потенціали Кулона та Корнелла, коли деякі з параметрів потенціалу були встановлені на нуль. Поточний потенціал забезпечує хороші результати в порівнянні з експериментальними даними та роботою інших дослідників з максимальною похибкою у  $0.0065 \text{ GeV}$ .

**Ключові слова:** потенціал Корнелла; рівняння Шредінґера; Правило точного квантування; Мезони

## THE FRACTIONAL SCHRÖDINGER EQUATION WITH THE GENERALIZED WOODS-SAXON POTENTIAL<sup>†</sup>

✉ Mohamed Abu-Shady<sup>a,‡</sup>, ✉ Etido P. Inyang<sup>b,\*</sup>

<sup>a</sup>Department of Mathematics and computer science, Faculty of Science, Menoufia University, Egypt

<sup>b</sup>Department of Physics, National Open University of Nigeria, Jabi, Abuja, Nigeria

\*Corresponding Author e-mail: [etidophysics@gmail.com](mailto:etidophysics@gmail.com); [einyang@noun.edu.ng](mailto:einyang@noun.edu.ng); <sup>‡</sup>E-mail: [dr.abushady@gmail.com](mailto:dr.abushady@gmail.com)

Received January 28, 2023; accepted February 7, 2023

The bound state energy eigenvalues and the corresponding eigenfunctions of the generalized Woods-Saxon potential reported in [Phys. Rev. C, **72**, 027001 (2005)] is extended to the fractional forms using the generalized fractional derivative and the fractional Nikiforov-Uvarov (NU) technique. Analytical solutions of bound states of the Schrödinger equation for the present potential are obtained in the terms of fractional Jacobi polynomials. It is demonstrated that the classical results are a special case of the present results at  $\alpha = \beta = 1$ . Therefore, the present results play important role in molecular chemistry and nuclear physics.

**Keywords:** *generalized Fractional derivative; Schrödinger equation; Nikiforov-Uvarov method; Woods-Saxon potential*

**PACS:** 21.60.Cs, 03.65.Ge, 02.30.Gp, 24.10.Ht

### 1. INTRODUCTION

The fractional calculus (FC) has numerous applications in all connected fields of science and engineering [1]. However, the use of this extremely powerful tool in many studies is still in its infancy. Fractional calculus has recently expanded its scope to include the dynamics of the complicated real world, and new concepts are now being put to the test on actual data. Although FC has been around for a while and is used in numerous scientific and technical sectors, the FC still has a crucial role to play in promoting applications. Many theoretical FC researchers are likewise unfamiliar with the application-related aspects. Because FC is not universal and has specific applications, we should understand this and provide examples of some significant FC applications that have been successful in the past to serve as a model for future FC application research. The FC has grown throughout decades in numerous disciplines of mathematics, but until recently they had little use in physics and other mathematically focused sciences.

There are now more and more physics study fields that use FC, which indicates that the situation is starting to change [2,3]. Scholars in physics and its related fields have recently become interested in the applications of FC to the Schrödinger equation (SE). For instance, Laskin [4] explored the fractional SE that contains the quantum Riesz fractional operator and the Caputo fractional derivative (FD). In order to solve the local fractional SE for the harmonic oscillator potential, the Hulthen potential (HP), and the Woods-Saxon potential (WSP), Karayer et al. [5] deduced the conformable fractional form of the NU technique. By utilizing the fractional version of the NU technique, Karayer et al. [6] have investigated the analytical solutions of the local Klein-Gordon problem for the generalized HP. The applications of FC in complicated and nonlinear physics were also presented by Baleanu et al. [7]. Another development was the study in [9-12] of the energy spectrum of heavy quarkonium in the context of fractional SE with an extended Cornell potential model in different systems. To examine the fractional version of Newtonian mechanics, conformable FD and integral have been used by Chung [13]. The fractional parameter (FP)  $0 < \alpha \leq 1$  is connected to the space-roughness time's properties through the FC and its use in quantum physics. Additionally, the nature of wave equation solutions for different values of the FP indicates the fundamental behavior of the quantum mechanical systems [14].

Abu-Shady and Kaabar, recently introduced the generalized fractional derivative in [15,16] that gives advantageous results more than the classical definitions. In addition, the definition gives good results in applying to different models such as in Refs. [17-19].

The WSP is a short-range potential and is used to study the nuclear structure within the shell model [20]. This potential has been presented in many forms to investigate the elastic and quasi-elastic scattering of nuclear particles. The usual ( $q = 1$ ) and the  $q$ -deformed WS potentials have been applied in nuclear calculations [21]. The helium model and the nonlinear scalar theory of mesons both use it to explore the behavior of valence electrons in metallic systems [22].

The WSP and its various modifications have been crucial in microscopic physics in determining the energy level spacing, particle number dependence of energy quantities, and universal properties of electron distributions in atoms, nuclei, and atomic clusters because they can be used to describe the interaction of a neutron with a single heavy-ion nucleus as well as for the optical potential model [23]. We are motivated to consider the solutions of the fractional SE for the generalized WSP using the generalized fractional (GF) NU method. This work is generalized to the work reported in [24] in the fractional model.

<sup>†</sup> Cite as: M. Abu-Shady, and E.P. Inyang, East Eur. J. Phys. **1**, 63 (2023), <https://doi.org/10.26565/2312-4334-2023-1-06>

© M. Abu-Shady, E.P. Inyang, 2023

The following is how the paper is set up: The GF-NU approach is briefly presented in Section 2. In Section 3, the GF-NU technique is applied on the fractional Schrödinger equation. The results are discussed in Section 4. The overview and conclusion are offered in Section 5.

**2. THE GENERALIZED FRACTIONAL NU METHOD**

This section provides a brief explanation of the GF-NU technique for solving the generalized fractional differential equation that has the following equation (see Refs. [6, 15] for more information).

$$D^\alpha \left[ D^\alpha \Psi(s) \right] + \frac{\bar{\tau}(s)}{\sigma(s)} D^\alpha \Psi(s) + \frac{\tilde{\sigma}(s)}{\sigma^2(s)} \Psi(s) = 0, \tag{1}$$

where  $\sigma(s)$  and  $\tilde{\sigma}(s)$  are polynomials of maximum second degree of  $\alpha$  and  $2\alpha$ , respectively, and  $\bar{\tau}(s)$  has a maximum degree of  $\alpha$  where

$$D^\alpha \Psi(s) = I s^{1-\alpha} \Psi'(s), \tag{2}$$

$$D^\alpha \left[ D^\alpha \Psi(s) \right] = I^2 \left[ (1-\alpha) s^{1-2\alpha} \Psi'(s) + s^{2-2\alpha} \Psi''(s) \right]. \tag{3}$$

where

$$I = \frac{\Gamma(\beta)}{\Gamma(\beta - \alpha + 1)}, \tag{4}$$

where  $0 < \alpha \leq 1$  and  $0 < \beta \leq 1$ . Substituting by Eqs. (2) and (3) into Eq. (1), we obtain

$$\Psi''(s) + \frac{\bar{\tau}_f(s)}{\sigma_f(s)} \Psi'(s) + \frac{\tilde{\sigma}_f(s)}{\sigma_f^2(s)} \Psi(s) = 0, \tag{5}$$

where

$$\bar{\tau}_f(s) = (1-\alpha) s^{-\alpha} \sigma(s) + I^{-2} \bar{\tau}(s), \sigma_f(s) = s^{1-\alpha} \sigma(s), \tilde{\sigma}_f(s) = I^{-2} \tilde{\sigma}(s). \tag{6}$$

If one works with the transformation, one may use the separation of variables to determine the specific solution of Eq. (5).

$$\Psi(s) = \Phi(s) \chi(s), \tag{7}$$

it is reduced to the following hypergeometric equation.

$$\sigma_f(s) \chi''(s) + \tau_f(s) \chi'(s) + \lambda \chi(s) = 0, \tag{8}$$

where

$$\sigma_f(s) = \pi_f(s) \frac{\Phi(s)}{\Phi'(s)}, \tag{9}$$

$$\tau_f(s) = \bar{\tau}_f(s) + 2\pi_f(s); \quad \tau_f'(s) < 0, \tag{10}$$

and

$$\lambda = \lambda_n = -n\tau_f'(s) - \frac{n(n-1)}{2} \sigma_f''(s), n = 0, 1, 2, \dots \tag{11}$$

$\chi(s) = \chi_n(s)$  It has the following form and is an n-degree polynomial that satisfies the hypergeometric equation.

$$\chi_n(s) = \frac{B_n}{\rho_n} \frac{d^n}{ds^n} (\sigma_f'(s) \rho(s)), \tag{12}$$

where  $B_n$  is a normalization constant and  $\rho(s)$  is a weight function which satisfies the following equation

$$\frac{d}{ds} \omega(s) = \frac{\tau(s)}{\sigma_f(s)} \omega(s); \quad \omega(s) = \sigma_f(s) \rho(s) \tag{13}$$

$$\pi_f(s) = \frac{\sigma_f'(s) - \bar{\tau}_f(s)}{2} \pm \sqrt{\left( \frac{\sigma_f'(s) - \bar{\tau}_f(s)}{2} \right)^2 - \tilde{\sigma}_f(s) + K \sigma_f(s)}, \tag{14}$$

and

$$\lambda = K + \pi_f'(s), \tag{15}$$

the  $\pi_f(s)$  is a first-degree polynomial. If the expressions beneath the square root are squares of expressions, it is feasible to determine the values of K in Eq. (14). If its discriminant is zero.

### 3. THE GENERALIZED FRACTIONAL OF SCHRÖDINGER EQUATION

The generalized WSP takes the form [24]

$$V(r) = -\frac{V_0}{1 + qe^{2\beta r}} - \frac{ce^{2\beta r}}{(1 + qe^{2\beta r})^2} \tag{16}$$

where  $V_0$  is the potential depth,  $q$  is a real parameter, and  $c$  is the surface thickness. This is often modified to reflect the experimental ionization energy values.

By substituting by Eq. (14), we can write Schrodinger equation [24]

$$\left[ \frac{d^2}{dr^2} + \frac{2\mu}{\hbar^2} \left( E + \frac{V_0}{1 + qe^{2\beta r}} + \frac{ce^{2\beta r}}{(1 + qe^{2\beta r})^2} \right) \right] R(r) = 0. \tag{17}$$

By assuming  $x = -e^{2\beta r}$ , Eq. (17) takes the following form

$$\left[ \frac{d^2}{dx^2} + \frac{2\mu}{\hbar^2} \left( E + \frac{V_0}{1 + qe^{2\beta r}} + \frac{ce^{2\beta r}}{(1 + qe^{2\beta r})^2} \right) \right] R(r) = 0. \tag{18}$$

We introduce the following dimensional parameters:  
where

$$\varepsilon = -\frac{\mu E}{2\hbar^2 \beta_1^2}, \quad \beta = \frac{mV_0}{2\hbar^2 \beta_1^2}, \quad \gamma = \frac{\mu C}{2\hbar^2 \beta_1^2} \tag{19}$$

The following equation is obtained

$$\left[ \frac{d^2}{dx^2} + \frac{1 - qx}{x(1 - qx)} \frac{d}{dx} + \frac{1}{s^2(1 - qs)^2} (-\varepsilon q^2 x^2 + (2\varepsilon q - \beta q - \gamma)x + \beta - \varepsilon) \right] R(x) = 0. \tag{20}$$

To transfer Eq. (20) to the fractional form as in Eq. (1)

$$\left[ D^\alpha \left[ D^\alpha R(x) \right] + \frac{1 - qx^\alpha}{x^\alpha (1 - qx^\alpha)} D^\alpha R(x) + \frac{1}{x^{2\alpha} (1 - qx^\alpha)^2} (-\varepsilon q^2 x^{2\alpha} + (2\varepsilon q - \beta q - \gamma)x^\alpha + \beta - \varepsilon) \right] R(x) = 0. \tag{21}$$

Substituting by Eqs. (2) and (3) into (21), we obtain

$$R''(x) + \frac{\bar{\tau}_f(x)}{\sigma_f(x)} R'(x) + \frac{\tilde{\sigma}_f(x)}{\sigma_f^2(x)} R(x) = 0, \tag{22}$$

where

$$\bar{\tau}_f(s) = (1 - \alpha)(1 - qx^\alpha) + I^{-2}(1 - qx^\alpha), \tag{23}$$

$$\sigma_f(s) = x(1 - qx^\alpha), \tag{24}$$

$$\tilde{\sigma}_f(s) = I^{-2}(-\varepsilon q^2 x^{2\alpha} + (2\varepsilon q - \beta q - \gamma)x^\alpha + \beta - \varepsilon). \tag{25}$$

Using Eq. (14)

$$\pi_f = \frac{(-2 + I^{-2})qx^\alpha + \alpha - I^{-2}}{2} \pm \frac{1}{2} \sqrt{(A_1 - 4qw)x^{2\alpha} + 4(A_2 + w)x^\alpha + A_3}, \tag{26}$$

where

$$A_1 = (-2 + I^{-2})q^2 + 4I^{-2}\varepsilon q^2, \tag{27}$$

$$A_2 = \frac{1}{2}(-2 + I^{-2})(\alpha - I^{-2})q - I^{-2}(2\varepsilon q - \beta q - \gamma), \tag{28}$$

$$A_3 = 4(\alpha - I^{-2})q + 4(\varepsilon - \beta). \tag{29}$$

The quantity  $w$  is selected so that the discriminant of the function under the square roots equals zero, giving the function a double zero. Hence, In addition,  $k = wx^{\alpha-1}$  that defined in the following equation

$$w_{\pm} = \frac{-(8A_2 + 4A_3q) \pm \sqrt{(8A_2 + 4A_3q)^2 - 16(A_2^2 - 4A_1A_3)}}{8}. \tag{30}$$

So, we can write Eq. (26) as follows

$$\pi_f = \frac{(-2 + I^{-2})qx^\alpha + \alpha - I^{-2}}{2} \pm \frac{1}{2} \left[ \frac{\sqrt{(A_1 - 4qw_+)x^\alpha + 2\sqrt{(\varepsilon - \beta) + (\alpha - I^{-2})^2}}}{\sqrt{(A_1 - 4qw_-)x^\alpha - 2\sqrt{(\varepsilon - \beta) + (\alpha - I^{-2})^2}}} \right] \tag{31}$$

By using Eq. (8), we write and select a negative sign as in Ref. [24]

$$\tau_f(s) = (1 - \alpha)(1 - qx^\alpha) + I^{-2}(1 - qx^\alpha) + (-2 + I^{-2})qx^\alpha + \alpha - I^{-2} - \left[ \sqrt{(A_1 - 4qw_-)x^\alpha - 2\sqrt{(\varepsilon - \beta) + (\alpha - I^{-2})^2}} \right] \tag{32}$$

using Eqs. 11 and 15, we can write

$$\lambda_n = n(1 - \alpha)\alpha qx^{\alpha-1} + nI^{-2}\alpha qx^{\alpha-1} - n(-2 + I^{-2})\alpha qx^{\alpha-1} + \alpha n\sqrt{(A_1 - 4qw_-)x^{\alpha-1}} + \frac{n(n-1)}{2}(1 + \alpha)\alpha qx^{\alpha-1} \tag{33}$$

$$\lambda = w_-x^{\alpha-1} + \frac{1}{2}(-2 + I^{-2})\alpha qx^{\alpha-1} - \frac{1}{2} \left[ \alpha\sqrt{(A_1 - 4qw_-)x^{\alpha-1}} \right], \tag{34}$$

by using the  $\lambda_n = \lambda$ , we obtain the energy eigenvalue in the fractional form

$$w_- + \frac{1}{2}(-2 + I^{-2})\alpha q - \frac{1}{2} \left[ \alpha\sqrt{(A_1 - 4qw_-)x^{\alpha-1}} \right] = n(1 - \alpha)\alpha q + nI^{-2}\alpha q - n(-2 + I^{-2})q + \alpha n\sqrt{(A_1 - 4qw_-)} + \frac{n(n-1)}{2}(1 + \alpha)\alpha q. \tag{35}$$

**The special case at**  $\alpha = \beta = 1, \Rightarrow I = 1,$

$$\varepsilon_{nq} = \frac{1}{16} \left[ \sqrt{1 + \frac{4\gamma}{q}} + (1 + 2n) \right]^2 + \frac{\beta^2}{\left[ \sqrt{1 + \frac{4\gamma}{q}} + (1 + 2n) \right]^2} + \frac{\beta}{2} \tag{36}$$

Eq. (36) is compatible with Ref. [24].

Let us now find the corresponding eigenfunctions as in Ref. [24]. It is necessary to identify the hypergeometric function that solves the differential equation in order to determine the polynomial solutions of the hypergeometric function

$\rho(x)$  satisfying the equation  $[\sigma_f \rho]' = \tau_f \sigma_f$ . Thus,  $\rho(x)$  is calculated as

$$\rho(x) = \frac{x^{A_1}}{(1 - qx^\alpha)^{\frac{A_1 + \beta_1}{\alpha q}}} \tag{37}$$

By using the following relation

$$y_n(x) = \frac{B_n}{\rho(x)} \frac{d^n}{dx^n} (\sigma_f(x)^n \rho(x)) \tag{38}$$

where  $B_n$  is a normalization constant, we obtain

$$y_n(x) = \frac{B_n}{x^{A_{11}}} (1 - qx^\alpha)^{-\frac{A_{11}q + B_{11}}{\alpha q}} \frac{d^n}{dx^n} \left( x^{n+A_{11}} (1 - qx^\alpha)^{n - \frac{A_{11}q + B_{11}}{\alpha q}} \right) \tag{39}$$

where

$$A_{11} = 2\sqrt{(\varepsilon - \beta) + (\alpha - I^{-2})^2} \tag{40}$$

$$B_{11} = 2\alpha q - I^{-2}q + (-2 + I^{-2})q - \sqrt{(A_{11} - 4qw)} \tag{41}$$

By using the relation  $\frac{\Phi'(x)}{\Phi(x)} = \frac{\pi_f(x)}{\sigma_f(x)}$  we can obtain

$$\Phi(x) = \frac{x^C}{(1 - qx^\alpha)^{\frac{Cq+D}{\alpha q}}} \tag{42}$$

where

$$C = \frac{1}{2}(\alpha - I^{-2}) + \sqrt{(\varepsilon - \beta) + (\alpha - I^{-2})^2} \tag{43}$$

$$D = \frac{1}{2}(-2 + I^{-2})q - \frac{1}{2}\sqrt{(A_{11} - 4qw)} \tag{44}$$

Thus, we can write final form the corresponding wave function  $R(x) = y_n(x)\Phi(x)$  as follows

$$\begin{aligned} R(x) &= A_n x^{-(C+A_{11})} (1 - qx^\alpha)^{-\frac{A_{11}q + B_{11} + Cq + D}{\alpha q}} \frac{d^n}{dx^n} \left( x^{n+A_{11}} (1 - qx^\alpha)^{n - \frac{A_{11}q + B_{11}}{\alpha q}} \right) \\ &= A_n x^{-(C+A_{11})} (1 - qx^\alpha)^{-\frac{A_{11}q + B_{11} + Cq + D}{\alpha q}} P_n^{(A_{11}, \frac{A_{11}q + B_{11}}{\alpha q})} (1 - qx^\alpha) \end{aligned} \tag{45}$$

where  $A_n$  is the normalization constant and  $P_n^{(A_{11}, \frac{A_{11}q + B_{11}}{\alpha q})}$  is the orthogonal Jacobi polynomials.

At  $\alpha = \beta = 1$  and  $q = 1$ , we obtain the special of classical case with compatible with Ref. [24].

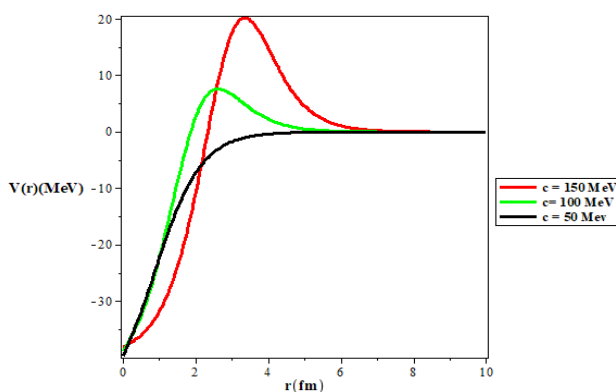


**Figure 1.** Variation of the generalized Woods-Saxon potential as a function of  $r$

In Fig. 1, the variation of the generalized WSP is plotted where the empirical values are taken from Perey *et al.* [25] as  $r_0 = 1.285$  fm and  $a = 0.65$  fm. Moreover, the WSP parameter is investigated at  $V_0 \approx 40.5 + 0.13 A$  MeV. Here,  $A$  is the atomic mass number of target nucleus. We note that the potential shifts to higher values by increasing parameter  $c$ .

#### 4. SUMMARY AND CONCLUSION

We have adopted a generalized WSP to obtain the solutions of the fractional SE using the GF-NU method. Analytical solutions are obtained for the eigenvalues and eigenfunctions in the fractional forms. The results of Ref. [24] are obtained as a special case at  $\alpha = \beta = 1$ . The present results are not considered in the recent works. Therefore, the present results play an important role in molecular physics and nuclear physics. We hope to extend this work to hot and dense media, mass spectra of heavy and heavy-light mesons, and/or the present of magnetic field as future works as in Refs. [26-40].

## ORCID IDs

© Mohamed Abu-Shady, <https://orcid.org/0000-0001-7077-7884>; © Etido P. Inyang, <https://orcid.org/0000-0002-5031-3297>

## REFERENCES

- [1] R. Hilfer, *Applications of fractional calculus in physics*, (World Scientific, 2010).
- [2] J. Banerjee, U. Ghosh, S. Sarkar, S. Das, and Pramana, *J. Phys.* **88**, 70 (2017). <https://doi.org/10.1007/s12043-017-1368-1>
- [3] M. Nouzid, M. Merad, and D. Baleanu, *Few-Body Syst.* **57**, 265 (2016). <https://arxiv.org/ftp/arxiv/papers/2103/2103.14064.pdf>
- [4] N. Laskin, *Phys. Rev. E*, **62**, 3135 (2000). <https://doi.org/10.1103/PhysRevE.62.3135>
- [5] N. Laskin, *Phys. Lett. A*, **268**, 298 (2000). [https://doi.org/10.1016/S0375-9601\(00\)00201-2](https://doi.org/10.1016/S0375-9601(00)00201-2)
- [6] H. Karayer, D. Demirhan, and F. Buyukkilic, *Commun. Theor. Phys.* **66**, 12 (2016). <https://doi.org/10.1088/0253-6102/66/1/012>
- [7] H. Karayer, D. Demirhan, and F. Buyukkilic, *Adv. Theor. Math. Phys.* **19**, 701 (2015). <https://arxiv.org/pdf/1703.03234.pdf>
- [8] D. Baleanu, K. Diethelm, E. Scalas, and J.J. Trujillo, *Fractional Calculus Models and Numerical Methods*, (World Scientific, 2012).
- [9] A. Al-Jamel, *Int. J. Mod. Phys. A*, **34**, 1950054 (2019). <https://doi.org/10.1142/S0217751X19500544>
- [10] M. Abu-Shady, *Inter. J. Modern Phys. A*, **34**, 31, 1950201 (2019). <https://doi.org/10.1142/S0217751X19502014>
- [11] M. Abu-Shady, and Sh. Y. Ezz-Alarab. *Few-Body Systems*, **62**, 13, (2021). <https://doi.org/10.1007/s00601-021-01591-7>
- [12] M. Abu-shady; Azar I. Ahmadov; He M. Fath-Allah; Vatan H. Badalov, *Journal of Theoretical and Applied Physics*, **16**(3), 1 (2022). <https://doi.org/10.30495/jtap.162225>
- [13] W.S. Chung, *J. Comput. Appl. Math.* **290**, 150 (2015). <https://doi.org/10.1016/j.cam.2015.04.049>
- [14] T. Tas, U. Ghosh, S. Sarkar, and S. Das, *J. Math. Phys.* **59**, 022111 (2018). <https://doi.org/10.1063/1.4999262>
- [15] M. Abu-Shady, and M.K.A. Kaabar, *Mathematical Problems in Engineering*, **2021**, (2021). <https://doi.org/10.1155/2021/9444803>
- [16] M. Abu-Shady, and M.K.A. Kaabar, *Computational and Mathematical Methods in Medicine*, **2022**, 2138775 (2022). <https://doi.org/10.1155/2022/2138775>
- [17] M. Abu-Shady, and E.P. Inyang, *East Eur. J. Phys.* **4**, 80-86 (2022). <https://periodicals.karazin.ua/eejp/article/view/20419>
- [18] M. Abu-Shady, and E.M. Khokha, *Molecular Physics*, **120**:24 (2022), <https://doi.org/10.1080/00268976.2022.2140720>
- [19] M. Abu-Shady et al. "Fractional Effective Quark-Antiquark Interaction in Symplectic Quantum Mechanics", (2022). <https://doi.org/10.48550/arXiv.2209.12083>
- [20] R.D. Woods, and D.S. Saxon, *Phys. Rev.* **95**, 577 (1954). <https://doi.org/10.1103/PhysRev.95.577>
- [21] N. Wang, and W. Scheid, *Phys. Rev. C*, **78**, 014607 (2008). <https://doi.org/10.1103/PhysRevC.78.014607>
- [22] S. Ikhdaïr, and R. Sever, *Open Physics*, **8**(4), 52-666 (2010). <https://doi.org/10.2478/s11534-009-0118-5>
- [23] S. Ikhdaïr, B.J. Falaye, and M. Hamzavi, *Chinese Phys. Lett.* **30**, 020305 (2013). <https://doi.org/10.1088/0256-307X/30/2/020305>
- [24] C. Berkdemir, A. Berkdemir, and R. Sever, *Phys. Rev. C*, **72**(2), 027001 (2005). <https://doi.org/10.1103/PhysRevC.72.027001>
- [25] C.M. Perey, F.G. Perey, J.K. Dickens, and R.J. Silva, *Phys. Rev.* **175**, 1460 (1968). <https://doi.org/10.1103/PhysRev.175.1460>
- [26] M. Abu-Shady, and A.N. Ikot, *Eur. Phys. J. Plus*, **134**, 321 (2019). <https://doi.org/10.1140/epjp/i2019-12685-y>
- [27] M. Abu-Shady, T.A. Abdel-Karim, and E.M. Khokha, *Advances in High Energy Physics*, **2018**, 7356843 (2018). <https://doi.org/10.1155/2018/7356843>
- [28] M. Abu-Shady, H.M. Mansour, and A.I. Ahmadov, *Advances in High Energy Physics*, **2019**, 4785615 (2019). <https://doi.org/10.1155/2019/4785615>
- [29] S.B. Doma, M. Abu-Shady, F.N. El-Gammal, and A. Amer, *Molecular Physics*, **114**, 11 1787 (2016). <https://doi.org/10.1080/00268976.2016.1154198>
- [30] E.P. Inyang, and E.O. Obisung, *East Eur. J. Phys.* **3**, 32 (2022). <https://doi.org/10.26565/2312-4334-2022-3-04>
- [31] E.P. Inyang, P.C. Iwuji, J.E. Ntibi, E. Omugbe, E.A. Ibanga, and E.S. William, *East Eur. J. Phys.* **2**, 51 (2022). <https://doi.org/10.26565/2312-4334-2022-2-05>
- [32] E.P. Inyang, P.C. Iwuji, J.E. Ntibi, E.S. William, and E.A. Ibanga, *East Eur. J. Phys.* **2**, 12 (2022). <https://doi.org/10.26565/2312-4334-2022-2-02>
- [33] E.P. Inyang, E.O. Obisung, P.C. Iwuji, J.E. Ntibi, J. Amajama, and E.S. William, *J. Nig. Soc. Phys. Sci.* **4** (2022) <https://doi.org/884.10.46481/jnsps.2022.884>
- [34] E.P. Inyang, E.O. Obisung, E.S. William, and I.B. Okon, *East Eur. J. Phys.* **3**, 114 (2022). <https://doi.org/10.26565/2312-4334-2022-3-14>
- [35] E.P. Inyang, E.O. Obisung, J. Amajama, D.E. Basse, E.S. William, and I.B. Okon, *Eurasian Physical Technical Journal*, **19**, (4 (42)), (2022) 78-87. <https://doi.org/10.31489/2022No4/78-87>
- [36] E.P. Inyang, E.P. Inyang, I.O. Akpan, J.E. Ntibi, and E.S. William, *Canadian J. Phys.* (2021). <https://doi.org/10.1139/cjp-2020-0578>
- [37] E.P. Inyang, J. Ntibi, E.A. Ibanga, F. Ayedun, E.P. Inyang, and E.S. William, *AIP Conference Proceedings*, **2679**, 030003 (2023). <https://doi.org/10.1063/5.0112829>
- [38] E.E. Ibekwe, J.B. Emah, E.P. Inyang, and A.O. Akpan, *Iran J. Sci. Technol Trans Sci.* (2022). <https://doi.org/10.1007/s40995-022-01377-4>
- [39] F. Ayedun, E.P. Inyang, E.A. Ibanga, and K.M. Lawal. *East Eur. J. Phys.* **4**, 87 (2022). <https://doi.org/10.26565/2312-4334-2022-4-06>
- [40] E.E. Ibekwe, E.P. Inyang, J.B. Emah, J.B. Akpan, and O.J. Yawo, *Sri Lankan Journal of Physics*, **23**(2), 63-76 (2022). <https://doi.org/10.4038/sljp.v23i2.8119>

## ДРОБОВЕ РІВНЯННЯ ШРЕДІНГЕРА З УЗАГАЛЬНЕНИМ ПОТЕНЦІАЛОМ ВУДСА-САКСОНА

Мохамед Абу-Шаду<sup>а</sup>, Етідо П. Інянг<sup>б</sup><sup>а</sup>Кафедра математики та інформатики, факультет природничих наук, Університет Менуфія, Єгипет<sup>б</sup>Фізичний факультет, Національний відкритий університет Нігерії, Джабі, Абуджа, Нігерія

Власні значення енергії зв'язаного стану та відповідні власні функції узагальненого потенціалу Вудса-Саксона, наведені в [Phys. Rev. C, 72, 027001 (2005)] поширюється на дробові форми з використанням узагальненої дробової похідної та дробової методики Нікіфорова-Уварова (NU). Отримано аналітичні розв'язки зв'язаних станів рівняння Шредінгера для наявного потенціалу в термінах дробових поліномів Якобі. Продемонстровано, що класичні результати є окремим випадком сучасних результатів при  $\alpha = \beta = 1$ , тому ці результати відіграють важливу роль у молекулярній хімії та ядерній фізиці.

**Ключові слова:** узагальнена дробова похідна; рівняння Шредінгера; Метод Нікіфорова-Уварова; потенціал Вудса-Саксона

## NUCLEAR ENERGY LEVELS IN $^{44}\text{Ca}$ USING FPD6PN INTERACTION<sup>†</sup>

 Maryam K. Hassan\*,  Firas Z. Majeed

University of Baghdad, College of Science, Department of Physics, Baghdad, Iraq

\*Corresponding Author e-mail: [mariam.kameel1204a@sc.uobaghdad.edu.iq](mailto:mariam.kameel1204a@sc.uobaghdad.edu.iq)

Received November 13, 2022; revised January 10, 2023; accepted January 16, 2023

Nuclear energy levels; Inelastic electron scattering C4 form factors for nucleons that were present outside closed core for the isobars  $^{44}\text{Ca}$  nuclei, which occupied low levels fp-LS shell ( $1f_{7/2}, 1f_{5/2}, 2p_{3/2}, 2p_{1/2}$ ), within shell model calculations had been studied. The interaction has been used to calculate the nuclear energy levels which is fpd6pn with fp shell model space. The results are compared with each other and with available experimental data its agreement with some results is clear. All inscriptions are given in diagrammatic notation., the wave vectors and analysis are modeled in the so-called diagrammatic notation. The potential of oscillator is utilized to construct single particle vector, considering  $^{40}\text{Ca}_{20}$  as a core. For the form factors the residual interaction M3Y has been adopted to include the inert core to the calculations. The OXFORD BEUNES AIRES SHELL MODEL CODE is utilized to accomplish the results for all tested nuclei.

**Keywords:** Nuclear energy levels; Calcium isotope 44; Nuclear reaction; Diagrammatic notations FPD6pn; OXBASH

**PACS:** 21.10.-k, 21.60.Cs

### 1. INTRODUCTION

Many studies had been performed to understand the nuclear properties and the internal structure of nuclei. Due to the complex nature of nuclei, there is no unified theory to describe the nuclear behaviors, properties and structures [1]. The shell theory has many benefits and properties such as the model independence of suggested, the applied physical N-N potential, beside the traditional Hamiltonian related to different categories of eigenvectors, and for plenty of nuclei. The shell theory stays valid to supplies the main theoretical methods for realizing all measurable of nuclei [1].

Excitation energies, binding energies, and spectroscopic factors were calculated in the LS shell ( $1f_{5/2}, 2p_{3/2}, 2p_{1/2}$ ) space so acquired effective N-N matrix elements [2]. Interactions between PN had been inspired to measure for the presence of a orbits distance at  $N=32$  in isotopes rich neutron localized in the nearby of magic nucleus  $^{48}\text{Ca}$  [3]. Filled pf-LS shell model inspections of  $A=48$  nuclei were executed [4], modified Kuo-Brown (KB) [10] to KB1 and KB3G. The isobaric chains  $A=50$ ,  $A=51$  and  $A=52$  studied [5] using KB3G and FPD6 and their released version KB3G [6].

The shell theory introduced an important method for such research. In this hypothesis, realistic potentials are founded and the basis vectors are denoted by exact quantum numbers of angular momentum (J), isospin (T) and parity ( $\pi$ ) [7]. A plenty of researches [8] were done to detect the distribution of eigen functions constructs the framework of the shell model [9]. Independently by Maria Mayer, and by Jensen, Haxel, and Suess) in the 1950s, the nuclear shell theory has regarded a major theory in the understanding of nuclear structure [10]. Extreme single-particle motion in spherical symmetry, only the addition of strong spin-orbit term was invoked to permit redesign of a wide range of results for isotopes near the nuclear magic numbers [11].

Calculations had been accomplished in model space of full fp- LS shell contains  $1f_{7/2}, 1f_{5/2}, 2p_{3/2}, 2p_{1/2}$  subshell and considering  $^{40}\text{Ca}$  as a core. The number of particles which can be excited to higher configurations is not restricted. Thus, apart from testing the suitability of GXPF1A interaction in explaining the experimental data, a comparison of results with that of him results would also throw light on the role of intruder  $g_{9/2}$  orbital, appropriate choice of core, and the effect of truncation on the particles to be excited [12]. Nuclear energy levels; total angular momenta and even-even parity for nucleons that were present outside closed and no core for ( $^{42}\text{Ca}$ ,  $^{44}\text{Ca}$ ,  $^{46}\text{Ca}$  and  $^{48}\text{Ca}$ ), which occupied fp-shell ( $1f_{7/2}, 1f_{5/2}, 2p_{3/2}, 2p_{1/2}$ ), within shell model calculations had been interested.

Four interactions had been assigned to calculate the nuclear energy spectrum of  $^{42}\text{Ca}$ ,  $^{44}\text{Ca}$ ,  $^{46}\text{Ca}$  and  $^{48}\text{Ca}$ . The results of the FPD6, GXPF1 and KB3G interactions are compared with each other and with available experimental data, its agreement with some results is clear, the results are compared with GOGNY-P2 (fp, fpg and fpgd model space) interaction. The technique of frozen orbitals and restricted occupations were adopted (applied) in the framework of full space calculation, when GOGNY-P2 interaction had been used as an effective full space two body interaction [13]. Code OXBASH had been utilized to generate model space wave vectors and in the same time receive the comparable model space effective interaction that are selected for this study. The aim of this thesis is to reproduce the nuclear energy levels of ( $^{44}\text{Ca}$ ) isotope, utilizing FPD6pn as a model space effective interaction to generate model space vectors, the calculations is performed by using OXBASH code [14]. The calculated energy levels for the isotopes under study with different set of effective interactions will be compared with the available experimental data.

### 2. THEORY

#### 2.1. Interacting Particles in One and Two Active Orbits

The two particles wave function can be written as a product of a spin and an isospin dependent part as [15]:

<sup>†</sup> Cite as: M.K. Hassan, and F.Z. Majeed, East Eur. J. Phys. 1, 69 (2023), <https://doi.org/10.26565/2312-4334-2023-1-07>

© M.K. Hassan, F.Z. Majeed, 2023

$$\Phi_{JM T T_z}(1,2) = \Phi_{JM}(j(1)j(2))\Theta_{T T_z}(t(1)t(2)). \tag{1}$$

where  $j + j = J$  and  $t + t = T$  with  $T = 0$  or  $1$  since  $t = 1/2$ .

A diagrammatic notation for the spin part of Eq. (1) has been introduced and one can write as [15]:

$$\Phi_{JM}(j(1)j(2)) = \sum_{mm'} \langle jmjm' | JM \rangle \phi_{jm}(1)\phi_{jm'}(2) \equiv \begin{array}{c} j(1) \quad j(2) \\ \triangle \\ JM \end{array} \tag{2}$$

where  $\Phi_{jm}(1)$  and  $\Phi_{jm}(2)$  are the single-particle States for particles 1 and 2 with their angular momenta  $j$  has been coupled to a total  $J$ . The coupling yields:

$$P_{12}\Phi_{JM}(j(1)j(2)) = (-1)^{J-2j}\Phi_{JM}(j(1)j(2)) = -(-1)^J\Phi_{JM}(j(1)j(2)) \tag{3}$$

when  $P_{12}$ : interchanges operator. So, the isospin dependent part as [15]:

$$\Theta_{T T_z}(t(1)t(2)) = \sum_{t_z t'_z} \langle t t_z t t'_z | T T_z \rangle \theta_{t t_z}(1)\theta_{t t'_z}(2) \equiv \begin{array}{c} t(1) \quad t(2) \\ \triangle \\ T T_z \end{array} \tag{4}$$

Condensed the notation to include spin and isospin as,  $\rho \equiv (j, t)$  and  $\Gamma \equiv (J, T)$ . So, Eq. (1) can be rewritten as:

$$\Phi_{\Gamma}(1,2) = \begin{array}{c} \rho(1) \quad \rho(2) \\ \triangle \\ j \end{array} \begin{array}{c} \rho(1) \quad \rho(2) \\ \triangle \\ T \end{array} \equiv \begin{array}{c} \rho(1) \quad \rho(2) \\ \triangle \\ \Gamma \end{array}, \tag{5}$$

Anti-symmetry of a wave function is referred to by a circular arc and one obtains for two particles in two different orbits  $\rho$  and  $\lambda$

$$\Phi_{\Gamma}^{as}(1, 2) \equiv \begin{array}{c} \rho \quad \lambda \\ \triangle \\ \Gamma \end{array} \tag{6}$$

For two particles in the same orbit the notation can be further formed as

$$\Phi_{\Gamma}^{as}(1, 2) \equiv \begin{array}{c} \rho^2 \\ \triangle \\ \Gamma \end{array} \tag{7}$$

One can be extended easily to wave functions of more than two particles in one Orbit  $\rho$  as

$$\Phi_{\Gamma}^{as}(1, 2, \dots, n) \equiv \begin{array}{c} \rho^n \\ \triangle \\ \Gamma \end{array} \tag{8}$$

### 2.2. Coefficients of Fractional Parentage

The  $n$ -particle function with all particles in one orbit  $\rho$  is given as [14]:

$$\Phi_{\Gamma}(1, 2, \dots, n) = \begin{array}{c} \rho^{n-1} \\ \triangle \\ \Gamma \end{array} \tag{9}$$

The group  $\rho^{n-1}$  is coupled to  $J_{\epsilon}, T_{\epsilon}, X_{\epsilon}$  with  $x_{\epsilon}$  denoting all further quantum numbers needed to specify the state  $|\rho^{n-1}\rangle_{\epsilon}$  uniquely. When the operator  $P_{ij}$  interchanges all coordinates of particles  $i$  and  $j$ , then one obtains for  $i, j \leq n-1$  due to the anti-symmetry:

$$P_{ij} \begin{array}{c} \rho^{n-1} \\ \triangle \\ \Gamma \end{array} = \begin{array}{c} \rho^{n-1} \\ \triangle \\ \Gamma \end{array} = - \begin{array}{c} \rho^{n-1} \\ \triangle \\ \Gamma \end{array} \tag{10}$$

The result of the permutation  $P_{ij}$  for  $i$  or  $j$  equal to  $n$ , however, cannot in general be represented by a simple expression in terms of the original function as in Eq. (10).

$$\Phi_{\Gamma}^{\alpha S}(1, 2, \dots, n) \equiv \text{Diagram} \quad (11)$$

The wave function of eq. (9) due to anti symmetrization. Also, one can write:

$$\text{Diagram} = \sum \langle \rho^n \Gamma | \rho^{n-1} \epsilon \rangle \quad (12)$$

where  $\langle \rho^n \Gamma | \rho^{n-1} \epsilon \rangle$  represented “coefficients of fractional parentage” or c.f.p. The normalization and orthogonality lead to the states  $|\rho^n\rangle_{\Gamma x}$  be denoted by  $x$  as:

$$\sum_{\Gamma' x'} \langle \rho^n \Gamma x | \rho^{n-1} \Gamma' x' \rangle \langle \rho^n \Gamma x'' | \rho^{n-1} \Gamma' x' \rangle = \delta_{xx''}. \quad (13)$$

The simple reordering depending on equation (12), if the particle numbered  $k$  is willing to decouple, then:

$$\Phi_{\Gamma}^{\alpha S}(1, 2, \dots, k, \dots, n) = (-1)^{n-k} \Phi_{\Gamma}^{\alpha S}(1, 2, \dots, n, k). \quad (14)$$

In the completely antisymmetric wave function leads to the expansion [15].

$$\text{Diagram} = (-1)^{n-k} \sum_{\epsilon} \langle \rho^n \Gamma | \rho^{n-1} \epsilon \rangle \text{Diagram} \quad (15)$$

It is beneficial to discuss in detail the derivation of c.f.p. for the relatively simple case of three identical particles (maximum isospin) in one orbit with  $j \leq 7/2$ . It is only for  $j \leq 7/2$  that three particles couple in an unique way to a given total spin  $J$ . The coupling of three single-particle wave functions to an non-antisymmetrized function of total spin  $J$  can be obtained by using the same diagrammatic representation as given in details in [15].

### 2.3. The Reduced Matrix Elements of the Longitudinal Operator ( $\eta = Co$ )

The longitudinal form factor describes the spatial distribution of the charge (the transition charge densities), so the longitudinal scattering might be considered as a result of the interactions of the incident electrons with the charge distribution of the nucleus [18]. The longitudinal form factor operator is defined as [18]:

$$\hat{T}_{JM_z}^{Co}(q) = \int d\vec{r} j_J(qr) Y_{JM}(\Omega_r) \hat{\rho}(\vec{r}, t_z) \quad (16)$$

where  $j_J(qr)$  is the spherical Bessel basis,  $Y_{JM}(\Omega_r)$  is the spherical harmonic and  $\hat{\rho}(\vec{r}, t_z)$  is the nucleon charge density operator. From equations (2-29) and (2-30), one obtains:

$$\hat{T}_{JM_z}^L(q) = e(t_z) j_J(qr) Y_{JM}(\Omega_r) \quad (17)$$

### 2.4. Core polarization effects

Microscopic theory will include the discarded space as a first order perturbation that is particle hole state (p-h), and using mixing interaction in order to calculate these effects as a residual interaction, For Nuclei of  $A > 40$ ,  $Z, N \geq 20$ , the fpLS shell model space is the suitable space [18], with a core of <sup>40</sup>Ca is assumed. The electron scattering operator  $\hat{T}_{\Lambda}^{\eta}$  reduced matrix elements is formed by two parts, the former "Model space" matrix elements, and the latter is for the "Core-polarization" matrix elements [18].

$$\langle \Gamma_f | \hat{T}_{\Lambda}^{\eta} | \Gamma_i \rangle = \langle \Gamma_f | \hat{T}_{\Lambda}^{\eta} | \Gamma_i \rangle_{MS} + \langle \Gamma_f | \delta \hat{T}_{\Lambda}^{\eta} | \Gamma_i \rangle_{CP}. \quad (18)$$

## 3. RESULTS AND DISCUSSION

Microscopic models have been introduced to constitute nuclear energy states. The model with mixed multi-nucleon conformations is one of the most important models. In the adopted method, the systems <sup>40</sup>Ca and <sup>32</sup>S are considered a non-active core with extractive baryons (neutrons only) that are named the LS shell. Calculations of the shell model are carried out within a model-space in which the nucleons are free to occupy a few orbits and are able to reproduce the measured static moments and transition strengths [16,19].

The shell theory is a major part of the nuclear theory and an essential theoretical topic for the micro scale calculations of nucleus build-up. The essential assumption in the shell model is that every particle plays separately in a potential average, including a dominant non-central spin-orbit part, and consists of the baryons themselves [19]. After this, the baryons allied into classes, the "shells," distant from each other. By this approach, the nucleus is divided into an inert core made up of filled LS shells plus a certain number of valence nucleons called the valence bodies [16,20]. Energy level values in this work are calculated by the shell model calculations that are performed via the computer code OXBASH [14].

The calcium elements that existed in the human's bone structure are very important. It's very important to study the calcium isotopes. Some of the experimental properties of  $^{42}\text{Ca}$ ,  $^{44}\text{Ca}$ ,  $^{46}\text{Ca}$  and  $^{48}\text{Ca}$  isotopes shown in Table.

**Table.** Experimental properties of some Ca isotopes [17]

	$^{42}\text{Ca}$	$^{44}\text{Ca}$	$^{46}\text{Ca}$	$^{48}\text{Ca}$
J $\pi$	0 <sup>+</sup>	0 <sup>+</sup>	0 <sup>+</sup>	0 <sup>+</sup>
M (micro-u)	41958617.828	43955481.543	45953687.988	47952522.904
M <sub>ex</sub> (MeV)	-38.547245	-41.468675	-43.139361	-44.224629
B/A (MeV)	8.616563	8.658175	8.668979	8.666686
S <sub>p</sub> (MeV)	10.27667	12.18226	13.81269	15.80162
S <sub>2p</sub> (MeV)	18.08529	21.62394	25.04405	29.02964
S <sub>n</sub> (MeV)	11.48067	11.13117	10.3985	9.95153
S <sub>2n</sub> (MeV)	19.84349	19.06406	17.81332	17.2279
Q <sub>α</sub> (MeV)	-6.25734	-8.8537	-11.1416	-13.97629
E <sub>β</sub> (MeV)	-6.426092	-3.65269	-1.378143	0.279213
Q <sub>β-n</sub> (MeV)	-17.97615	-13.35189	-10.13878	-7.95935
Q <sub>2β</sub> (MeV)	-13.44257	-3.92011	0.98844	4.26808
Q <sub>4β</sub> (MeV)	-45.277	-28.108	-13.66779	-1.40261

#### 4. INELASTIC LONGITUDINAL FORM FACTOR IN $^{44}\text{Ca}$ FOR THE TRANSITION (0<sup>+</sup>2 → 4<sup>+</sup>2) AT E<sub>x</sub>=1.561 MEV

Inelastic longitudinal (C4) form factors were calculated by using M3Y-P1. Fig. 1 represents the calculated form factors using (M3Y-P1) as a residual interaction in the first peak the results overestimate the data at all  $q \geq 1.2$  till  $2.2 \text{ fm}^{-1}$  while the calculations underestimate the data at the second peak. The form factor for C4 transition in  $^{44}\text{Ca}$  with an excitation energy  $E_x=1.561 \text{ MeV}$  is displayed in Fig. 1, where the total contributions are due to the core polarization effect. The data are well explained for the first lobe, and also up to  $q=3 \text{ fm}^{-1}$ . Higher  $q$  values are estimated. The values of  $|F(q)|^2$  are in between  $10^{-4}$  and downward with the maximum at  $q = 1.8 \text{ fm}^{-1}$ .

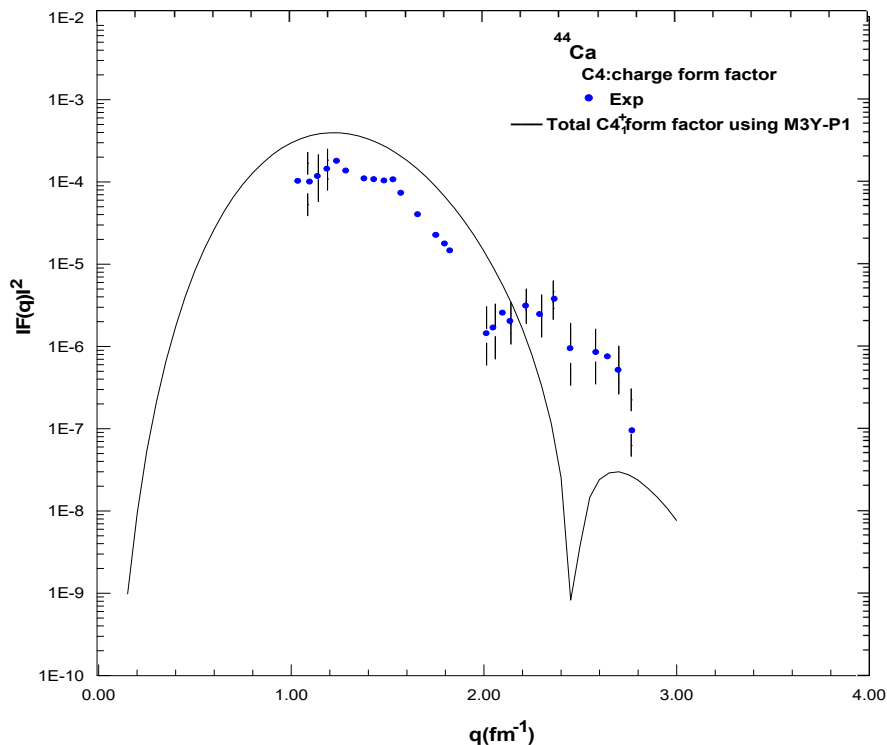


**Figure 1.** Inelastic longitudinal C4 form factors for the  $4_1^+$  ( $E_x=1.561 \text{ MeV}$ ) (The value of  $E_x$  is theoretical) state in  $^{44}\text{Ca}$  using M3Y-P1 as a residual interaction.

### 5. CONCLUSIONS

From Figure 2 which represents the energy level scheme for  $^{44}\text{Ca}$ , it is clear that there are clear differences between the calculated and experimental results in general. The calculated results reveals that there are an energy gap between  $J_k^\pi = 0_1^+$  and  $J_k^\pi = 4_2^+$  by the value of  $\Delta E = 3\text{MeV}$  but this state has a well defined value as compared with the experimental one and the state  $J_k^\pi = 2_2^+$  has a fair agreement with the experiment but the higher the states the wider the difference with the laboratory states. The function of energy levels density will be very useful to identify the energy spectrum and study the distribution of states between 1 to 10 MeV besides the number of every state and their values, nuclear shell theory is based on some dependable not sure realistic and a wide range of fitting parameters are not well reproduced to generate the static and dynamic nuclear properties and they need to be readjusted to meet the experimental results table 1 tabulates some nuclear properties for some even Ca isotopes.

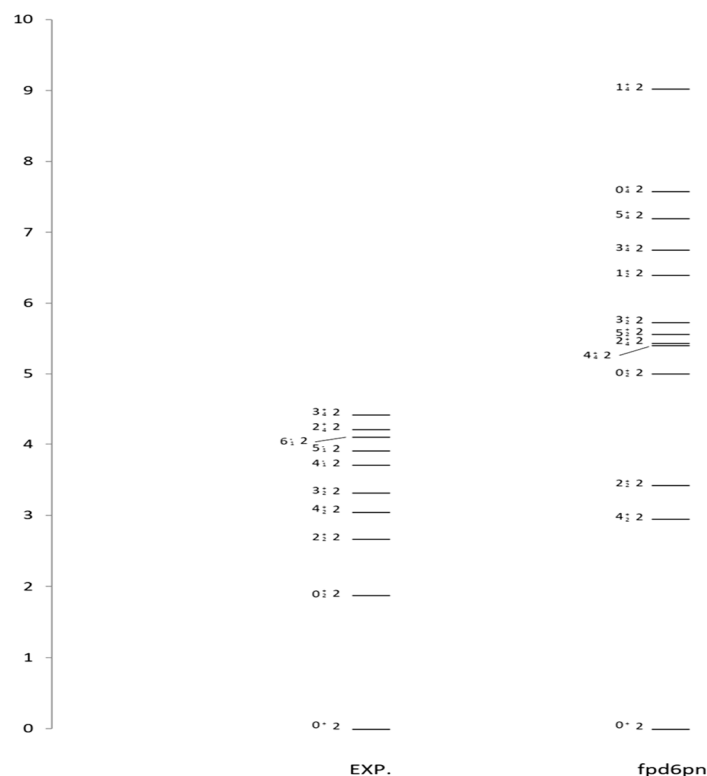


**Figure 2.** The energy levels scheme of  $^{44}\text{Ca}$  by using fpd6pn interactions with closed core  $^{40}\text{Ca}$  for  $(J_K^\pi T)$ , positive parity, ten orders

### Acknowledgement

Special appreciation to Dr. B.A. Brown for production energy levels files from OXBASH code for this work.

### ORCID IDs

©Maryam K. Hassan, <https://orcid.org/0000-0003-2060-4672>; ©Firas Z. Majeed, <https://orcid.org/0000-0001-6527-3913>

### REFERENCES

- [1] M. Honma, T. Otsuka, B.A. Brown and T. Minzusaki, "Effective interaction for pf-shell nuclei", Phys. Rev. C, **65**, 061301(R) (2002). <https://doi.org/10.1103/PhysRevC.65.061301>
- [2] H. Crannell, R. Helm, H. Kendall, J. Oeser, and M. Yearian, "Electron-Scattering Study of Nuclear Levels in Cobalt, Nickel, Lead, and Bismuth", Phys. Rev. **123**(3), 923 (1961). <https://doi.org/10.1103/PhysRev.123.923>
- [3] J.I. Prisciandaro, P.F. Mantica, B.A. Brown, D.W. Anthony, M.W. Cooper, A. Garcia, D.E. Groh, A. Komives, W. Kumarasiri, P.A. Lofy, A.M. Oros-Peusquens, S.L. Tabor, and M. Wiedeking, Phys. Lett. B, **510**, 17-23 (2001). [https://doi.org/10.1016/S0370-2693\(01\)00565-2](https://doi.org/10.1016/S0370-2693(01)00565-2)
- [4] E. Caurier, and A. P. Zuker, Phys. Rev. C, **50**, 225 (1994). <https://doi.org/10.1103/PhysRevC.50.225>
- [5] A. Poves, J. Sánchez-Solano, E. Caurier, and F. Nowacki, Nucl. Phys. A, **694**, 157 (2001). [https://doi.org/10.1016/S0375-9474\(01\)00967-8](https://doi.org/10.1016/S0375-9474(01)00967-8)
- [6] W.A. Richter, M.G. Van Der Merwe, R.E. Julies, and B.A. Brown, Nucl. Phys. A, **532**, 325 (1991). [https://doi.org/10.1016/0375-9474\(91\)90007-S](https://doi.org/10.1016/0375-9474(91)90007-S)
- [7] V. Zelevinsky, B.A. Brown, N. Frazier, and M. Horoi, Phys. Rep. **276**, 8 (1996). [https://doi.org/10.1016/S0370-1573\(96\)00007-5](https://doi.org/10.1016/S0370-1573(96)00007-5)
- [8] R.R. Whitehead, A. Watt, D. Kelvin, and A. Conkie, Phys. Lett. B, **76**, 149 (1978). [https://doi.org/10.1016/0370-2693\(78\)90262-9](https://doi.org/10.1016/0370-2693(78)90262-9)
- [9] B.A. Brown, and G. Bertsch, Phys. Lett. B, **148**, 5 (1984). [https://doi.org/10.1016/0370-2693\(84\)91598-3](https://doi.org/10.1016/0370-2693(84)91598-3)
- [10] J. Suhonen, *From Nucleons to Nucleus Concepts of Microscopic Nuclear Theory*, (Springer, Finland, 2006).

- [11] R.D. Lawson, *Theory of the Nuclear Shell Model*, (Clarendon Press, Oxford, New York, 1980).
- [12] L. Coraggio, A. Covello, N. Itaco, and T.T.S. Kuo, *Prog. Part. Nucl. Phys.* **62**, 135 (2009). <https://doi.org/10.1016/j.pnpnp.2008.06.001>
- [13] F.Z. Majeed, and S.S. Mashaan, *Indian Journal of Natural Sciences*, **9**, 50 (2018).
- [14] B.A. Brown et al, OXBASH code, MSUNSL Report 524 (1988).
- [15] P.J. Brussaard, and P.W.M. Glademans, *Shell-model Applications in Nuclear Spectroscopy*, (North-Holland Publishing Company, Amsterdam, 1977).
- [16] H. Sagawa, X.R. Zhou, and X.Z. Zhang, “Evolution of Deformations in Medium-Mass Nuclei”, *Phys. Rev. C*, **72**, 054311 (2005). <https://doi.org/10.1103/PhysRevC.72.054311>
- [17] G. Audi, F.G. Kondev, Meng Wang, W.J. Huang, and S. Naimi, “The NUBASE2016 Evaluation of Nuclear Properties”, *Chinese Phys. C*, **41**, 030001 (2017). <https://doi.org/10.1088/1674-1137/41/3/030001>
- [18] A.A. Al-Rahmani, and S.F. Kazem, “Elastic Electron-Nucleus Scattering Form Factors of Selected Medium Mass Nuclei”, *NeuroQuantology*, **18**(8), 49-58 (2020). <https://www.neuroquantology.com/data-cms/articles/20201001121608pmNQ20204.pdf>
- [19] A.H. Ali, “Investigation of the Quadrupole Moment and Form Factors of Some Ca Isotopes”, *Baghdad Science Journal*, **17**(2), 0502 (2020). <https://orcid.org/0000-0002-1525-1406>
- [20] L. Wang, J. Liu, R. Wang, M. Lyu, C. Xu, and Z. Ren, “Global analysis of nuclear cluster structure from the elastic and inclusive electron scattering”, *Phys. Rev. C*, **103**, 054307 (2021). <https://doi.org/10.1103/PhysRevC.103.054307>

### РІВНІ ЯДЕРНОЇ ЕНЕРГІЇ У $^{44}\text{Ca}$ ЗА ВИКОРИСТАННЯ FPD6PN ВЗАЄМОДІЇ

Мар'ям К. Хассан, Фірас З. Маджид

Багдадський університет, Науковий коледж, факультет фізики, Багдад, Ірак

У рамках розрахунків оболонки моделі були вивчені рівні ядерної енергії, формфактори  $S_4$  непружного розсіювання електронів для нуклонів, які були присутні за межами закритого ядра для ізобар ядер  $^{44}\text{Ca}$ , і які займали низькі рівні оболонки  $f_7$ -LS ( $1f_7/2, 1f_5/2, 2p_3/2, 2p_1/2$ ). Для розрахунку рівнів ядерної енергії була використана взаємодія, яка є  $fpd_6pn$  з простором моделі оболонки  $f_7$ . Результати порівнюються один з одним, і з наявними експериментальними даними чітко збігається з деякими результатами. Хвильові вектори та аналіз моделюються у так званому діаграмному записі. Для побудови одно часткового вектора використовується потенціал осцилятора, розглядаючи  $^{40}\text{Ca}_{20}$  у якості ядра. Для форм-факторів було прийнято залишкову взаємодію МЗУ, щоб включити до розрахунків інертне ядро. Для отримання результатів для усіх перевірених ядер використовується код моделі оболонки OXFORD BEUNES AIRES.

**Ключові слова:** ядерні енергетичні рівні; ізотоп кальцію 44; ядерна реакція; діаграмний запис FPD6pn; OXBASH

## THEORETICAL STUDY OF PROTON HALO STRUCTURE AND ELASTIC ELECTRON SCATTERING FORM FACTOR FOR $^{23}\text{Al}$ AND $^{27}\text{P}$ NUCLEI BY USING FULL CORRELATION FUNCTIONS (TENSOR FORCE AND SHORT RANGE)<sup>†</sup>

✉ **Abeer A.M. Hussein\***, ✉ **Ghaith N. Flaiyh**

*Department of Physics, College of Science, University of Baghdad, Baghdad, Iraq*

*\*Corresponding Author e-mail: [Abeer.Ali1104a@sc.uobaghdad.edu.iq](mailto:Abeer.Ali1104a@sc.uobaghdad.edu.iq)*

Received November 13, 2022; revised December 12, 2022; accepted December 15, 2022

The study of proton-rich nuclei's form factors, root-mean-square radius (*rms*), and nuclear density distributions is the focus of this work for nuclei ( $^{23}\text{Al}$  and  $^{27}\text{P}$ ), use two body charge density distributions (2BCDD's). With the effects of the strong tensor force and short range, the nucleon distribution function of the two oscillating harmonic particles in a two-frequency shell model operates with two different parameters: *bc* for the inner (core) orbits and *bv* for the outer (halo) orbitals. This work demonstrated the existence of proton halo nuclei for the nuclei ( $^{23}\text{Al}$  and  $^{27}\text{P}$ ) in the shell ( $2s_{1/2}$ ), and the computed proton, neutron, and matter density distributions for these nuclei both displayed the long tail of the performance. Using the Borne approximation of the plane wave, the elastic form factor of the electron scattering from the alien nucleus was calculated, this form factor is dependent on the difference in the proton density distribution of the last proton in the nucleus. The Fortran 95 power station program was used to calculate the neutrons, protons, matter density, elastic electron scattering form factor, and *rms* radii. The calculated outcomes for these exotic nuclei agree well with the experimental data.

**Keywords:** *Exotic nuclei; Form Factor; Proton-rich; Root mean square (rms) radii*

**PACS:** 21.10.Ft, 21.10.Gv, 21.45.Bc, 21.60.n, 21.65.f

### 1. INTRODUCTION

The nuclear halo is a threshold effect with low separation energy. There are two different kinds of exotic halo nuclei: proton halo [1] and neutron halo [2,3]. Neutron halo nuclei have recently undergone extensive experimental and theoretical study [4,5]. However, studies on proton halos are very rare. Although the proton separation energy in some light nuclei such as  $^8\text{B}$  and  $^{17}\text{F}$  is very low [4,6-7].

Emil Ryberg and others examined the impact of finite-range corrections for S-wave proton halo nuclei on the halo effective field theory [8]. Dellagiaco et al. [9] provided a straightforward phenomenological technique for creating dynamical short-range and tensor correlations. Da Providencia and Shakin [10] developed a similar correlation operator for explaining short-range correlation effects, as did Malecki and Picchi [11]. Luay F. Sultan [12] used the binary cluster model within the single-particle wave functions of Gaussian and harmonic oscillator potentials to investigate the ground state density distributions of proton-rich  $^{23}\text{Al}$  and  $^{27}\text{P}$  halo nuclei. The radial wave functions of the calculated Woods–Saxon potentials for  $^8\text{B}$ ,  $^{17}\text{F}$ ,  $^{17}\text{Ne}$ ,  $^{23}\text{Al}$ , and  $^{27}\text{P}$  have been used before Rafah I. Noori [13].

Using a coherent density fluctuation model and 2pF to study one- and two-proton halo nuclei for  $^{23}\text{Al}$ ,  $^{26}\text{P}$ , and  $^{28}\text{S}$  nuclei is presented by Maha Taha Yassin [14]. The two-frequency shell model and the binary cluster model are used to investigate the ground state densities of unstable proton-rich  $^9\text{C}$ ,  $^{12}\text{N}$ , and  $^{23}\text{Al}$  exotic nuclei [15].

In this study, we will use the two-body charge density distributions (2BCDD's) in the ground state for the proton-rich nuclei for ( $^{23}\text{Al}$  and  $^{27}\text{P}$ ) with full correlations (tensor force and short range) with we used two different oscillator size parameters *bc* and *bv* and we calculated of *rms* radii, density distributions for (protons, neutrons, and matter) and form factors for these exotic nuclei.

### 2. THEORY

The operator has been used to define the nucleon density of a point-like particle nucleus [16]:

$$\hat{\rho}^{(1)}(\vec{r}) = \sum_{i=1}^A \delta\left(\vec{r} - \vec{r}_i\right). \quad (1)$$

This operator can be transformed into a two-body density form ( $\hat{\rho}^{(1)}(\vec{r}) \Rightarrow \hat{\rho}^{(2)}(\vec{r})$ ) as [17]:

$$\sum_{i=1}^A \delta\left(\vec{r} - \vec{r}_i\right) \equiv \frac{1}{2(A-1)} \sum_{i \neq j} \left\{ \delta\left(\vec{r} - \vec{r}_i\right) + \delta\left(\vec{r} - \vec{r}_j\right) \right\}. \quad (2)$$

Another relevant transformation is that of the coordinates of the two particles, which may be expressed, ( $\vec{r}_i$  and  $\vec{r}_j$ )

in terms -of- that relative  $\vec{r}_{ij}$  and center -of- mass  $\vec{R}_{ij}$  coordinates [18]:

<sup>†</sup> Cite as: A.A.M. Hussein, and G.N. Flaiyh, East Eur. J. Phys. 1, 82 (2023), <https://doi.org/10.26565/2312-4334-2023-1-08>  
© A.A.M. Hussein, G.N. Flaiyh, 2023

$$\vec{r}_{ij} = \frac{1}{\sqrt{2}}(\vec{r}_i - \vec{r}_j), \tag{3-a}$$

$$\vec{R}_{ij} = \frac{1}{\sqrt{2}}(\vec{r}_i + \vec{r}_j), \tag{3-b}$$

Subtracting and adding (3-a) and (3-b) can be obtain:

$$\vec{r}_i = \frac{1}{\sqrt{2}}(\vec{R}_{ij} + \vec{r}_{ij}), \tag{3-c}$$

$$\vec{r}_j = \frac{1}{\sqrt{2}}(\vec{R}_{ij} - \vec{r}_{ij}). \tag{3-d}$$

Using eqs. (3-c) and (3-d) in Eq (2), we obtain:

$$\hat{\rho}^{(2)}(\vec{r}) = \frac{1}{2(A-1)} \sum_{i \neq j} \left\{ \delta \left[ \vec{r} - \frac{1}{\sqrt{2}}(\vec{R}_{ij} + \vec{r}_{ij}) \right] + \delta \left[ \vec{r} - \frac{1}{\sqrt{2}}(\vec{R}_{ij} - \vec{r}_{ij}) \right] \right\} \tag{4}$$

Using the identity  $\delta(a\vec{r}) = \frac{1}{|a^3|} \delta(\vec{r})$  (for three –dimension), where ( $a$ ) is a constant. For closed shell nuclei with  $N=Z$ , the two-body charge density operator can be deduced from Eq. (4) as:

$$\hat{\rho}_{ch}^{(2)}(\vec{r}) = \frac{1}{2} \hat{\rho}^{(2)}(\vec{r})$$

i.e.

$$\hat{\rho}_{ch}^{(2)}(\vec{r}) = \frac{\sqrt{2}}{(A-1)} \sum_{i \neq j} \left\{ \delta \left[ \sqrt{2} \vec{r} - \vec{R}_{ij} - \vec{r}_{ij} \right] + \delta \left[ \sqrt{2} \vec{r} - \vec{R}_{ij} + \vec{r}_{ij} \right] \right\}. \tag{5}$$

The operator from Equation (5) can be folded with the two-body correlation functions  $\tilde{f}_{ij}$  to yield an efficient two-body charge density operator.

$$\hat{\rho}_{eff}^{(2)}(\vec{r}) = \frac{\sqrt{2}}{(A-1)} \sum_{i \neq j} \tilde{f}_{ij} \left\{ \delta \left[ \sqrt{2} \vec{r} - \vec{R}_{ij} - \vec{r}_{ij} \right] + \delta \left[ \sqrt{2} \vec{r} - \vec{R}_{ij} + \vec{r}_{ij} \right] \right\} \tilde{f}_{ij}, \tag{6}$$

where the from  $\tilde{f}_{ij}$  is given by [18]

$$\tilde{f}_{ij} = f(r_{ij}) \Delta_1 + f(r_{ij}) \{ 1 + \alpha(A) P_{ij} \} \Delta_2. \tag{7}$$

It is clear that eq. (7) contains two kinds of correlations:

- The first term of equation (7)'s two-body short range correlations, which is expressed as  $f(r_{ij})$ . Here  $\Delta_1$  With the exception of  $^3S_1$  and  $^3D_1$  states, is a projection operator onto the space of all two-body wave functions. Short-range correlations should be observed as important functions of particle separation, which diminish the two-body wave function at short distances where the repulsive core forces the particles apart and heal to unity at a lengthy distance where the interactions are very weak. The two-body short-range correlation is given by [18]:

$$f(r_{ij}) = \begin{cases} 0 & \text{for } r_{ij} \leq r_c \\ 1 - \exp\{-\mu(r_{ij} - r_c)^2\} & \text{for } r_{ij} > r_c \end{cases} \tag{8}$$

where  $r_c$  ( $fm$ ) is the radius of a suitable hard core and,  $\mu = 25 fm^{-2}$  [20] correlation parameter.

- The strong tensor component in the nucleon-nucleon force induces the longer range two body tensor correlations that are shown in the second term of equation (7).

$$\tilde{f}_{ij} = f(r_{ij}) \{ 1 + \alpha(A) P_{ij} \} \Delta_2, \tag{9}$$

into triplet  $^3S_1 - ^3D_1$  channels, where

$$\Delta_2 = \sum_{lSgT} | (lS) gT \rangle \langle (lS) gT |. \tag{10}$$

This projection operator only affects the  ${}^3S_1$  and  ${}^3D_1$  states. The typical tensor operator,  $P_{ij}$ , is known as [18]:

$$P_{ij} = \frac{3}{r_{ij}^2} (\vec{\sigma}_i \cdot \vec{r}_{ij}) (\vec{\sigma}_j \cdot \vec{r}_{ij}) - \vec{\sigma}_i \cdot \vec{\sigma}_j. \quad (11)$$

While  $\alpha$  ( $A$ ) can be defined as the strength of tensor correlation and it is non-zero just in the  ${}^3S_1$  and  ${}^3D_1$  channel. Where the relative orbital angular momentum ( $\ell$ ) and total spin ( $S$ ) of two particles are coupled to the channel spin ( $g$ ) a projection operator onto triplet coupled states of  ${}^3S_1$  and  ${}^3D_1$ . In Eq. (7) the radial part is easily included as it only modifies the radial integrals involving  $r_{12}$ . Acting the operator of Eq. (6) into triplet  ${}^3S_1$  state

$$\tilde{f}_{12} |{}^3S_1\rangle = f(r_{12}) \{ 1 + \alpha(A) P_{12} \} |{}^3S_1\rangle \Delta_2, \quad (12)$$

and acting the operator  $\tilde{f}_{12}$  into triplet  ${}^3D_1$ , we get

$$\tilde{f}_{12} |{}^3D_1\rangle = f(r_{12}) \{ 1 + \alpha(A) P_{12} \} |{}^3D_1\rangle \Delta_2. \quad (13)$$

It makes sense to parameterize the core and halo densities independently in the case of exotic nuclei. Consequently, the following is how the halo nuclei's ground-state matter density distribution can be expressed [19]:

$$\rho_m(r) = \rho_{(p+n)}^{core}(r) + \rho_n^{valence}(r). \quad (14)$$

The normalization condition of the above ground state densities is given by:

$$g = 4\pi \int_0^\infty \rho^g(r) r^2 dr, \quad (15)$$

here  $\rho^g(r)$  represents one of the following densities: nucleon, charge, core, halo densities. The *rms* radii of corresponding above densities are given by [20]:

$$\langle r^2 \rangle_g^{1/2} = \frac{4\pi}{g} \int_0^\infty \rho^g(r) r^4 dr, \quad (16)$$

where  $g$  is (proton, neutron or matter).

The PWBA was used to study the elastic electron scattering form factors from emitted by the nuclei under study. The charge form factor in PWBA is [21]:

$$F(q) = \frac{4\pi}{qZ} \int_0^\infty \rho_o(r) \text{Sin}(qr) r dr F_{fs}(q) F_{cm}(q), \quad (17)$$

where the nucleon finite size correction  $F_{fs}(q)$  is defined [22]:

$$F_{fs}(q) = e^{-0.43q^2/4}, \quad (18)$$

where the free nucleon form factor  $F_{fs}(q)$  for protons and neutrons is consider to be the same. According to [23], the center of mass correction  $F_{cm}(q)$  is as follows:

$$F_{cm}(q) = e^{q^2 b^2 / 4A}, \quad (19)$$

where  $b$ : The harmonic-oscillator size parameter and  $A$ : The nuclear mass number.

As a result, when the shell model wave function is, removes  $F_{cm}(q)$  eliminates the spurious state caused by the center of mass's motion. The form factor  $F(q)$  comprising the impact of two-body correlation functions may now be calculated by entering the ground state ( $r$ ) of equation (6) into equation (14).

### 3. RESULTS AND DISCUSSION

The density distributions for (protons, neutrons, and matter) of the ground state of ( ${}^{23}\text{Al}$  and  ${}^{27}\text{P}$ ) nuclei and *rms* radii with the form factors  $F(q)$  were studied by the two body charge density distributions (2BCDD's) with effect short-range and tensor force by using the two body oscillator model (core +1p) shell model with used parameters (bc), (bv), and by relying on equations 6, 7, and 11.

Table 1, summarizes some of the characteristics of halo nuclei [24,25]. The average radius of neutrons and protons was calculated based on equations 6, 7, and 16, where we got the results shown in Table 2, when the full correlation ( $r_c=0.5\text{ fm}$ ,  $\alpha=0.1$ ) and without correlation ( $r_c=0$ ,  $\alpha=0$ ). It is found that the proton *rms* radius is larger than the neutron *rms* radius.

**Table 1.** Some properties of  $^{23}\text{Al}$  and  $^{27}\text{P}$  nuclei

Exotic nucleus	$J^\pi, T$ [25]	Nuclei core	$J^\pi, T$ [25]	Half life time ( $T_{1/2}$ ) [24]	Separation energy (Mev)[24]
$^{23}\text{Al}$	$1/2^+, 3/2$	$^{22}\text{Mg}$	$0^+, 1$	470 ms	0.141
$^{27}\text{P}$	$1/2^+, 3/2$	$^{26}\text{Si}$	$0^+, 1$	260 ms	0.870

**Table 2.** The calculated neutrons and protons *rms* radii for nuclei ( $^{23}\text{Al}$  and  $^{27}\text{P}$ )

Exotic nuclei $^{23}\text{Al}$			
Proton size parameter	$b_p=2\text{ fm}$	Neutron size parameter	$b_n=1.75\text{ fm}$
$\langle r_p^2 \rangle_{r_c=0.5, \alpha=0.1}^{1/2}$	3.195974	$\langle r_n^2 \rangle_{r_c=0.5, \alpha=0.1}^{1/2}$	2.669840
$\langle r_p^2 \rangle_{r_c=0, \alpha=0}^{1/2}$	3.203143	$\langle r_n^2 \rangle_{r_c=0, \alpha=0}^{1/2}$	2.667579
$\langle r_p^2 \rangle_{\text{exp}}^{1/2}$ [25]	$3.1 \pm 0.25$	$\langle r_n^2 \rangle_{\text{exp}}^{1/2}$ [25]	$2.634 \pm 0.23$
$\langle r_p^2 \rangle_{FC's}^{1/2}$	-0.0071	$\langle r_n^2 \rangle_{FC's}^{1/2}$	-0.0022
Exotic nuclei $^{27}\text{P}$			
Proton size parameter	$b_p=2.05\text{ fm}$	Neutron size parameter	$b_n=1.73\text{ fm}$
$\langle r_p^2 \rangle_{r_c=0.5, \alpha=0.1}^{1/2}$	3.395257	$\langle r_n^2 \rangle_{r_c=0.5, \alpha=0.1}^{1/2}$	2.744588
$\langle r_p^2 \rangle_{r_c=0, \alpha=0}^{1/2}$	3.405219	$\langle r_n^2 \rangle_{r_c=0, \alpha=0}^{1/2}$	2.745390
$\langle r_p^2 \rangle_{\text{exp}}^{1/2}$ [25]	$3.22 \pm 0.163$	$\langle r_n^2 \rangle_{\text{exp}}^{1/2}$ [25]	$2.754 \pm 0.14$
$\langle r_p^2 \rangle_{FC's}^{1/2}$	-0.0099	$\langle r_n^2 \rangle_{FC's}^{1/2}$	-0.0008

Table 3, shows the calculated *rms* radii for core nuclei ( $^{22}\text{Mg}$  and  $^{26}\text{Si}$ ) with oscillator size parameter ( $b_c = 2.85, 187$ ) for  $^{22}\text{Mg}$  and  $^{26}\text{Si}$  respectively, and exotic nuclei ( $^{23}\text{Al}$  and  $^{27}\text{P}$ ) with oscillator size parameter ( $b_m = 1.87, 2.015$ ) for  $^{23}\text{Al}$  and  $^{27}\text{P}$  respectively with effects of the short-range ( $r_c = 0.5\text{ fm}$ ) and the tensor force ( $\alpha = 0.1$ ).

**Table 3.** The calculated core, valance and matter radii *rms* with experimental data for  $^{23}\text{Al}$  and  $^{27}\text{P}$  nuclei

Halo nuclei	Core nuclei	$b_c$	$b_v$	$b_m$	<i>rms</i> matter radii for core nuclei $\langle r^2 \rangle_c^{1/2}$ (fm)		<i>rms</i> matter radii for halo nuclei $\langle r^2 \rangle_h^{1/2}$ (fm)	
					Calculated results	Experimental Data	Calculated results	Experimental Data
$^{23}\text{Al}$	$^{22}\text{Mg}$	1.85	3.85	1.87	2.872617	$2.78 \pm 0.26$ [26]	2.911843	$2.905 \pm 0.25$ [26]
$^{27}\text{P}$	$^{26}\text{Si}$	1.87	3.5	1.912	3.025680	$2.88 \pm 0.06$ [27]	3.028345	$3.02 \pm 0.155$ [27]

The calculated results are in good agreement with the indicated experimental data [26,27]. The correlation short range force with root mean square radii  $\langle r^2 \rangle^{1/2}$ . We note an increase in *rms* values with an increase in short-range force by relying on equations (7, 8), as we showed in Table 4. Table 5, show correlation tensor force with *rms* radii  $\langle r^2 \rangle^{1/2}$ . It is found to decrease *rms* values with increased tensor force by relying on equations (7, 9), and 11.

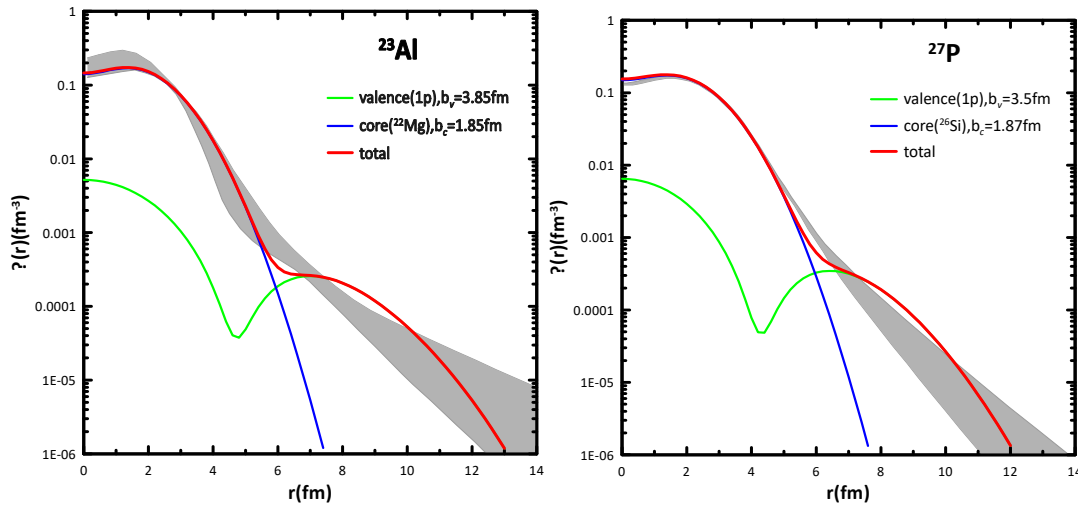
**Table 4.** The calculated of the *rms* radii with different values for the short-range correlations for  $^{23}\text{Al}$  and  $^{27}\text{P}$  nuclei

$r_c$ (fm)	$\langle r^2 \rangle^{1/2}$ for $^{23}\text{AL}$ nuclei	$\langle r^2 \rangle^{1/2}$ for $^{27}\text{P}$ nuclei
0.3	2.898914	3.01684
0.35	2.899032	3.016960
0.4	2.900136	3.017976
0.45	2.903780	3.021325
0.5	2.911843	3.028711
0.55	2.923239	3.039108

**Table 5.** The calculated of the *rms* radii with different values for the tensor force correlations for  $^{23}\text{Al}$  and  $^{27}\text{P}$  nuclei

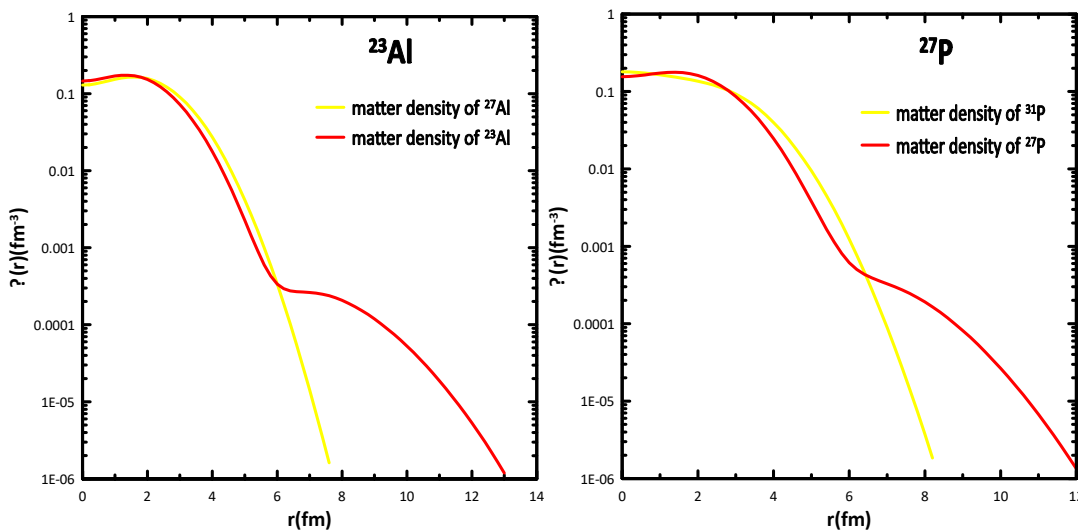
$\alpha$	$\langle r^2 \rangle^{1/2}$ for $^{23}\text{Al}$ nuclei	$\langle r^2 \rangle^{1/2}$ for $^{27}\text{P}$ nuclei
0.07	2.916419	3.032756
0.075	2.915664	3.032097
0.08	2.914908	3.031432
0.085	2.914147	3.030761
0.09	2.913382	3.030083
0.095	2.912615	3.029400
0.1	2.911843	3.028711

Figure 1 shows the relation between the two-body nucleon density distributions (2BNDD's) (in  $\text{fm}^{-3}$ ) of the ground state and  $r$  (in  $\text{fm}$ ) for  $^{23}\text{Al}$  and  $^{27}\text{P}$  nuclei. The blue curve represents 2BNDD's for the core nuclei  $^{22}\text{Mg}$  and  $^{26}\text{Si}$  (proton + neutron) with oscillator size parameter ( $b_c = 2.85, 1.87$ ) respectively. The green curve represents 2BNDD's for valence (one proton) for  $^{23}\text{Al}$  and  $^{27}\text{P}$  nuclei with oscillator size parameter ( $b_v = 3.85, 3.5$ ) respectively, while the red solid curve represents the total calculation for the core nucleons and the valence one proton, and the shaded curve represents the experimental of nucleon densities of  $^{23}\text{Al}$  and  $^{27}\text{P}$  respectively [25,26]. Figure 1 shows that the computed matter density distributions show a long tail for all of these nuclei and shows that the halo phenomenon and the long tail in  $^{23}\text{Al}$  and  $^{27}\text{P}$  are connected to the outer one proton for nucleon densities but not to the core nucleons, which is consistent with the experimental data.



**Figure 1.** Core, halo and matter density distribution of ( $^{23}\text{Al}$  and  $^{27}\text{P}$ ).

Figure 2 illustrates a comparison of the matter density distributions of halo ( $^{23}\text{Al}$  and  $^{27}\text{P}$ ) (red line) with the matter density distributions of the stable nuclei ( $^{27}\text{Al}$  and  $^{31}\text{P}$ ) (yellow line) by using 2BCDD's with the effect of short-range and tensor force, we shown along tail is clearly in the matter distribution of the halo nuclei.



**Figure 2.** Comparison of matter density distribution of exotic nuclei ( $^{23}\text{Al}$  and  $^{27}\text{P}$ ) with that of stable nuclei ( $^{27}\text{Al}$  and  $^{31}\text{P}$ ).

Figure 3: The neutron (blue curves), proton (brown curves), and matter (red curves) show densities of  $^{23}\text{Al}$  and  $^{27}\text{P}$ , respectively. The proton diffuseness is also larger than the neutron diffuseness in these nuclei. There is a large density difference between the proton and neutron in  $^{23}\text{Al}$  and  $^{27}\text{P}$ . The usual performance of the halo nucleus (i.e., the long tail) is apparent in the proton density distributions (brown curves), as indicated by these figures. For  $^{23}\text{Al}$  and  $^{27}\text{P}$ , the difference between the *rms* radii of the proton and the neutron is ( $r_p - r_n = 0.52613, 0.65066 \text{ fm}$ ). This difference is also supported by the halo structure of these alien cores.

It is seen from the Figure 4 a plotted for the elastic form factor versus  $q$  (in  $\text{fm}^{-1}$ ) for  $^{23}\text{Al}$  and  $^{27}\text{P}$  calculated with PWBA. The blue solid curve represents the form factor for 2BCDD's with ( $F_{fs} \neq 0, F_{cm} \neq 0$ ) and oscillator size parameter ( $b_m = 1.87 \text{ fm}$  for  $^{23}\text{Al}$  and  $b_m = 1.912 \text{ fm}$  for  $^{27}\text{P}$ ), the red curve represents the form factor for 2BCDD's with correlation and oscillator size parameter ( $b_m = 1.87 \text{ fm}$  for  $^{23}\text{Al}$  and  $b_m = 1.912 \text{ fm}$  for  $^{27}\text{P}$ ), ( $F_{fs} = 0, F_{cm} = 0$ ) i.e the finite nucleon size and the center of mass corrections doesn't take into account. The filled circle represents the experimental elastic form factors of  $^{27}\text{Al}$  and  $^{31}\text{P}$  [28]. The form factor is determined by the detailed properties of a single proton halo as well as the difference, which is determined by the mass number and the size parameter  $b_m$ . We obtain good agreement at the momentum for  $q < 3.6$ , and we note that the behavior of the theoretical results for halo nuclei ( $^{23}\text{Al}$  and  $^{27}\text{P}$ ) matches the practical results for stable nuclei ( $^{27}\text{Al}$  and  $^{31}\text{P}$ ).

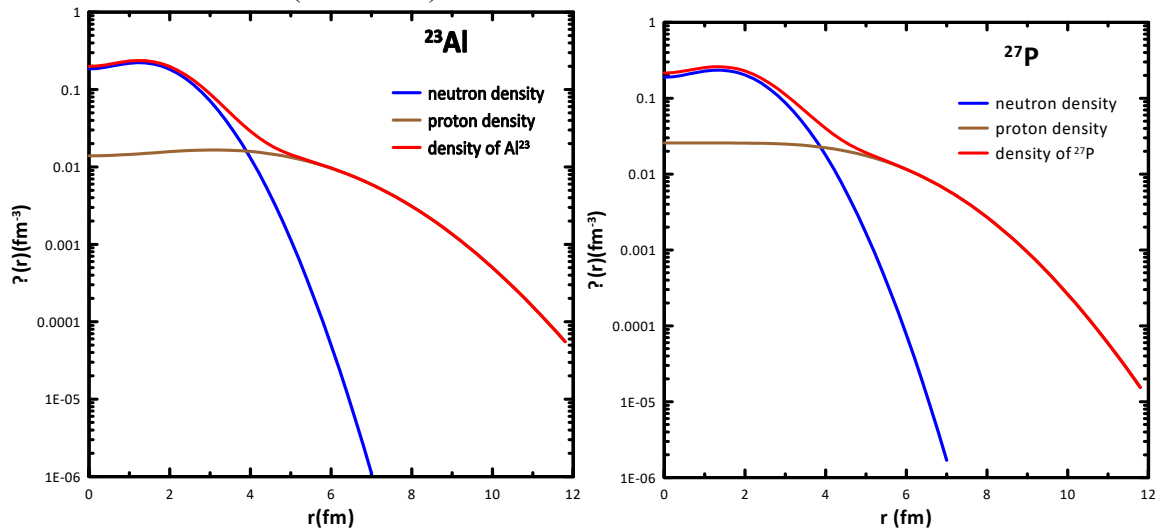


Figure 3. Comparison of proton, neutron and matter densities for  $^{23}\text{Al}$  and  $^{27}\text{P}$  halo

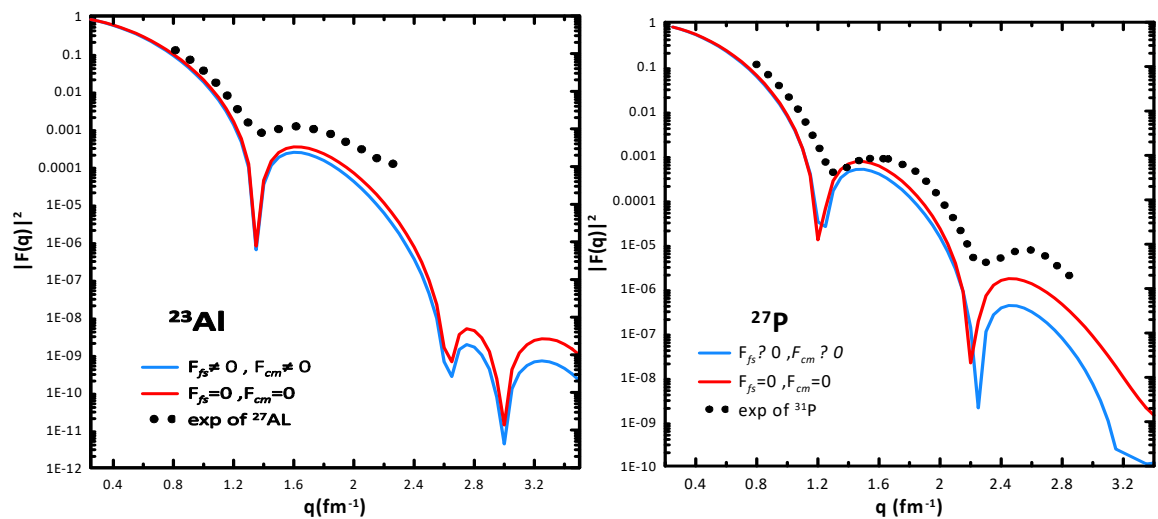


Figure 4. The form factors for  $^{23}\text{Al}$  and  $^{27}\text{P}$  nuclei with experimental data [28].

#### 4. CONCLUSIONS

In this work, halo nuclei are known to have a valence of a proton, the halo of a proton occupies a  $2s_{1/2}$  orbital. The measured material density of our halo nuclei showed a long-tailed behavior using the two-body nucleus density distribution framework with two different oscillator size parameters  $b_c$  and  $b_v$ , with tensor force effects (Increasing its effect, the *rms* radii increases) and the short range (the increase its effect, the *rms* radii decreases), which are consistent with the experimental data. The large variation in charge form factors between unstable nuclei ( $^{23}\text{Al}$  and  $^{27}\text{P}$ ) and stable isotopes ( $^{27}\text{Al}$  and  $^{31}\text{P}$ ) is due to the same charge distribution of the protons.

## ORCID IDs

Abbeer A.M. Hussein, <https://orcid.org/0000-0003-0068-1347>; Ghaith N. Flaiyh, <https://orcid.org/0000-0001-9918-4484>

## REFERENCES

- [1] B.A. Brown, and P.G. Hansen, Phys. Lett. B, **381**, 391, (1996). [https://doi.org/10.1016/0370-2693\(96\)00634-X](https://doi.org/10.1016/0370-2693(96)00634-X)
- [2] P.G. Hansen, and B. Jonson, Europhys. Lett. **4**, 409 (1987). <https://doi.org/10.1209/0295-5075/4/4/005>
- [3] J. Meng, and P. Ring, Phys. Rev. Lett. **80**, 460 (1998). <https://doi.org/10.1103/PhysRevLett.80.460>
- [4] I. Tanihata, T. Kobayashi, O. Yamakawa, S. Shimoura, K. Ekuni, K. Sugimoto, N. Takahashi, et al., Phys. Lett. B, **206**, 592, (1988). [https://doi.org/10.1016/0370-2693\(88\)90702-2](https://doi.org/10.1016/0370-2693(88)90702-2)
- [5] I.J. Thompson, S. Al-khalili, J.A. Tostevin, and J.M. Bang, Phys. Rev. C, **47**, 1364 (1993). <https://doi.org/10.1103/PhysRevC.47.R1364>
- [6] W. Schwab et al., Z. Phys. A, **350**, 283 (1995). <https://doi.org/10.1007/BF01291183>
- [7] A. Ozawa, et al., Phys. Lett. B, **334**, 18 (1994). [https://doi.org/10.1016/0370-2693\(94\)90585-1](https://doi.org/10.1016/0370-2693(94)90585-1)
- [8] E. Ryberg, C. Forss'ena, H.-W. Hammer, and L. Platter, "Range corrections in proton halo nuclei", Nucl. Phys. **367**, 13 (2016). <https://doi.org/10.1016/j.aop.2016.01.008>
- [9] F. Dellagiacomma, G. Orlandiniand, and M. Traini, "Dynamical correlations in finite nuclei: A simple method to study tensor effects", Nucl. Phys. A, **393**, 1, 95-108 (1983).
- [10] J. Da Providencia, and C. M. Shakin, "Some aspects of short-range correlation in nuclei", Ann. Phys. **30**(1), 95-118 (1964).
- [11] A. Malecki and P. Picchi, "Elastic electron scattering from  $^4\text{He}$ ", Phys. Rev. Lett. **21**(19), 1395-1398 (1968). <https://doi.org/10.1103/PhysRevLett.21.1395>
- [12] L.F. Sultan, and A.N. Abdullah, "Study of the Proton Halo Structure of Nuclei  $^{23}\text{Al}$  and  $^{27}\text{P}$  Using the Binary Cluster Model", Iraqi Journal of Physics, **19**(48), 21 (2021). <https://ijp.uobaghdad.edu.iq/index.php/physics/article/view/581>
- [13] R.I. Noori, and A.R. Ridha, "Density Distributions and Elastic Electron Scattering Form Factors of Proton-rich  $^8\text{B}$ ,  $^{17}\text{F}$ ,  $^{17}\text{Ne}$ ,  $^{23}\text{Al}$  and  $^{27}\text{P}$  Nuclei", Iraqi Journal of Science, **60**(6), 1286-1296 (2019). <https://doi.org/10.24996/ij.s.2019.60.6.12>
- [14] M.T. Yaseen, and A.M. Ali, "Charge Density Distributions, Momentum Density Distribution, and Elastic Form Factors of Exotic One- And Two-Proton Halo Nuclei", Journal of Critical Reviews, **7**(15), (2020). <https://www.jcreview.com/admin/Uploads/Files/61f278fc50d2d4.61077221.pdf>
- [15] A.K. Hamoudi, G.N. Flaiyh, and A.N. Abdullah, Iraqi Journal of Science, **56**(1A), 147 (2015). <https://www.iasj.net/iasj/download/e5ff2f1a46127a57>
- [16] A.N. Antonov, P.E. Hodgson, and I.Z. Petkov, *Nucleon Momentum and Density Distributions in Nuclei*, (Clarendon Press, Oxford, 1988, pp. 97-102.
- [17] S. Gartenhaus, and C. Schwartz, Phys. Rev. **108**(2), 482 (1957). <https://doi.org/10.1103/PhysRev.108.482>
- [18] J. Fiasi, A. Hamoudi, J.M. Irvine, and F. Yazici, J. Phys. G: Nucl. Phys. **14**, 27 (1988). <https://doi.org/10.1088/0305-4616/14/10/002>
- [19] A.N. Abdullah, Int. J. Mod. Phys. E, **29**, 2050015 (2020). <https://doi.org/10.1142/S0218301320500159>
- [20] T.T.S. Kuo, and G.E. Brown, Nucl. Phys. A, **85**, 40-86 (1966). [https://doi.org/10.1016/0029-5582\(66\)90131-3](https://doi.org/10.1016/0029-5582(66)90131-3)
- [21] A.N. Antonov, M.K. Gaidarov, D.N. Kadrev, P.E. Hodgson, and E.M.D. Guerr, Int. J. Mod. Phys. E, **13**, 759 (2004). <https://doi.org/10.1142/S0218301304002430>
- [22] T. de Forest, Jr., and J.D. Walecka, "Electron scattering and nuclear structure", Adv. Phys. **15**(1), 1 (1966). <https://doi.org/10.1080/00018736600101254>
- [23] J.D. Walecka, *Electron Scattering for Nuclear and Nucleon Structure*, (Cambridge University Press, Cambridge, 2001), pp. 14-16.
- [24] G. Audi, F.G. Kondev, M. Wang, W.J. Huang, and S. Naimi, Chin. Phys. C, **41**, 030001 (2017). <http://dx.doi.org/10.1088/1674-1137/41/3/030001>
- [25] H.Y. Zhang, W.Q. Shen, Z.Z. Ren, Y.G. Ma, W.Z. Jiang, Z.Y. Zhu, X.Z. Cai, et al. Nuclear Physics A, **707**, 303–324 (2002). [https://doi.org/10.1016/S0375-9474\(02\)01007-2](https://doi.org/10.1016/S0375-9474(02)01007-2)
- [26] Y.L. Zhao, Z.Y. Ma, B.Q. Chen, and W.Q. Shen, "Halo structure of nucleus  $^{23}\text{Al}$ ", Chinese Physics Letters, **20**(1), 53-55 (2003). <http://dx.doi.org/10.1088/0256-307X/20/1/316>
- [27] A.N. Abdullah, "Systematic Study of the Nuclear Structure for Some Exotic Nuclei Using Skyrme–Hartree–Fock Method", Iran. J. Sci. Technol. Trans. Sci. **44**, 283 (2020). <https://doi.org/10.1007/s40995-019-00799-x>
- [28] H. De Vries, and C.W. Jager, "Nuclear charge-density-distribution parameters from elastic electron scattering", Atomic Data and Nuclear Data Tables, **36**(3), 495-536 (1987). [https://doi.org/10.1016/0092-640X\(87\)90013-1](https://doi.org/10.1016/0092-640X(87)90013-1)

**ТЕОРЕТИЧНЕ ДОСЛІДЖЕННЯ СТРУКТУРИ ПРОТОННОГО ГАЛО ТА ФОРМ-ФАКТОРА ПРУЖНОГО РОЗСІЯННЯ ЕЛЕКТРОНІВ ДЛЯ ЯДЕР  $^{23}\text{Al}$  ТА  $^{27}\text{P}$  ЗА ВИКОРИСТАННЯ ПОВНИХ КОРЕЛЯЦІЙНИХ ФУНКЦІЙ (ТЕНЗОРНА СИЛА І КОРОТКОДІЯ)**

Абір А.М. Хусейн, Гейт Н. Флей

*Факультет фізики, Науковий коледж, Багдадський університет, Багдад, Ірак*

Дослідження форм-факторів ядер, багатих на протони, середньоквадратичного радіуса (середньоквадратичного значення) і розподілу ядерної щільності є центром цієї роботи для ядер ( $^{23}\text{Al}$  і  $^{27}\text{P}$ ), використовуються два розподіли щільності заряду (2BCDD). З ефектами сильної тензорної сили та короткодії функція розподілу нуклонів двох осцилюючих гармонійних частинок у двочастотній моделі оболонки працює з двома різними параметрами:  $b_s$  для внутрішніх (ядерних) орбіт і  $b_v$  для зовнішніх (гало) орбіталей. Ця робота продемонструвала існування ядер протонного гало для ядер ( $^{23}\text{Al}$  і  $^{27}\text{P}$ ) в оболонці ( $2s_{1/2}$ ), а обчислені розподіли густини протонів, нейтронів і речовини для цих ядер показали довгий хвіст продуктивності. Використовуючи борнівське наближення плоскої хвилі, було розраховано пружний форм-фактор розсіювання електрона від чужорідного ядра, цей форм-фактор залежить від різниці в розподілі густини протонів останнього протона в ядрі. Для розрахунку нейтронів, протонів, щільності речовини, форм-фактора пружного розсіювання електронів і середньоквадратичних радіусів використовувалася програма PowerStation Fortran 95. Розраховані результати для цих екзотичних ядер добре узгоджуються з експериментальними даними.

**Ключові слова:** екзотичні ядра; форм-фактор; багатопротонні ядра; середньоквадратичні радіуси